GEOCHEMICAL AND GEOCHRONOLOGICAL STUDIES IN THE STORA LE - MARSTRAND BELT OF ORUST, S. W. SWEDEN

by

John Stephen Daly

Thesis submitted to the University of Keele

for the degree of Doctor of Philosophy

December, 1978.

ORIGINAL COPY IS TIGHTLY BOUND AND TEXT IS CLOSE TO THE EDGE OF THE PAGE

CONTAINS PULLOUTS

ABSTRACT

The Stora Le - Marstrand belt in Orust consists of a basement complex of semi-pelitic and psammitic para-gneisses with minor tholeiitic amphibolite bodies which exhibit widespread migmatite development in two stages. Several intrusive bodies cut the basement complex between the two migmatisations; these include the Hälleviksstrand amphibolite and the Assmunderöd-Myckleby augen granite. A suite of granite sheets followed by basic dykes and finally pegmatites cut the complex after the second migmatisation.

The geochemistry of the para-gneisses offers some support to the geological evidence for a sedimentary origin. The migmatitic para-gneisses grade into areas of nebulite which may originate by closed-system anatexis and localised collection of the resulting melt. The disequilibrium of the Rb-Sr isotopic systems of these rocks is probably due to the effects of the later period of migmatisation and partly to secondary recrystallisation of muscovite.

Rb-Sr whole-rock emplacement ages for the Hällevikstrand amphibolite (1432 $\pm$ 92 m.y.) and the Assmunderöd-Myckleby augen granite (1379 $\pm$ 46 m.y.) provide a younger age limit for the first migmatisation, which they cut, and an older age limit for the second migmatisation and subsequent events. The low initial $^{87}Sr/^{86}Sr$ ratio (0.7032 $\pm$ 5) of the amphibolite implies a primitive (e.g. upper mantle) source , while that of the augen granite (0.713 $\pm$ 3) indicates a crustal source.

Geochemical variation in the younger granites suite is probably the result of differentiation of a basaltic or tonalitic magma, implying an upper mantle source. It is likely that metamorphic disturbance rather than variation in initial $^{87}Sr/^{86}Sr$ ratio has been responsible for the non-equilibrated Rb-Sr isotopic systems in these rocks.

The geochemical data for the basic (and minor acidic) dyke suite is consistent with fractionation of a tholeiitic magma. Relatively

narrow deformed dykes record isotopic equilibration ca. 1060 m.y. ago. This Sveconorwegian age is interpreted as the age of the first post-dyke metamorphism and it implies that the important regional post-dyke deformation is Sveconorwegian in age. A temperature of 590°C is estimated for this metamorphism using garnet-biotite geothermometry.

Muscovites from two bodies of deformed granitic pegmatite give a Rb-Sr age of ca. 950 m.y.

Acknowledgements

I wish to thank the past and present Heads of Department, Professor F. W. Cope and Professor G. Kelling for the provision of facilities in the Department of Geology at Keele.

I am particularly grateful to Dr. R. G. Park who supervised this research, for his interest and encouragement and for critically reading a draft of this thesis.

I acknowledge a University of Keele Research Studentship and an award from the Daniel Pidgeon Fund of the Geological Society of London.

I am indebted to Drs. A. I. Bailey, A. Crane, B. S. Moorlock and R. C. Standley for provision of samples from their collections and for access to field notes and thin sections.

The geochronological work, carried out at the Department of Earth Sciences, University of Leeds, was supervised by Dr. R. A. Cliff, whom I thank for his guidance and constructive criticism. The geochronology laboratories at Leeds are supported in part by N.E.R.C. grant GR/2725. Many others formerly and presently at Leeds, particularly Dr. C. J. Hawkesworth and A. Gledhill,helped with analytical problems and Drs. M. Bickle and J. C. Roddick generously allowed the use of their computer programs. I am very grateful to Peter and Gila Croker for having me to stay with them while working in Leeds.

The mineral analyses were performed with the kind assistance of F. C. Wilkinson at the Department of Geology, University of Manchester and Professor J. Zussmann is thanked for provision of facilities.

I made many new friends during my short visits to Sweden. Gull-Britt and Mats Niklasson took me in out of the rain at the end of the first field season. I stayed with, and was amply fed by them on my second visit. Without their help and the use of their boat many of the samples from western Orust could not have been collected. C. H. Olsson AB of Ellos is thanked for transporting samples to England and Eric Andersson and Mona Stromberg kindly provided accommodation in Goteborg.

I thank many friends and colleagues at Keele, too numerous to mention all individually, for their help with all kinds of problems, especially Bernard Besly, Richard Bevins and Mark Avison for much needed logistic support. I owe a particular debt of gratitude to Graham Lees for help with computing and geochemical analysis. I thank him for his patience, his interest in my work and for listening to several drafts of the manuscript.

The technical staff at Keele, under the direction of Mike Stead contributed significantly to the research and to the preparation of this thesis. David Emley helped with analytical and computing problems. Marion Cooke and John Pepper photographed the diagrams and David Kelsall helped with the photomicrographs and did the photographic printing.

My wife, Hilary, supported me financially and morally in the last three months of the work, coped patiently with my unusual and unpredictable hours in the laboratory and helped to compile the references.

Finally, I wish to express my sincere thanks to Mrs. J. Dawson who carefully and efficiently typed a difficult and frequently illegible manuscript.

Table of Contents

CHAPTER 1. Introduction.

1.1 The Sveconorwegian Province.

The "Sveconorwegian Province" (Fig. 1.1) of southern Norway and south-western Sweden was recognised by Magnusson (1960) on the basis of K-Ar ages, the majority of which group in the 1050-850 m.y. range (Magnusson, 1960, Neumann, 1960, Skiöld, 1976). This K-Ar province has an equivalent in the North American Grenville Province and in both areas the spread of similar K-Ar ages may be attributed to post-orogenic uplift and cooling (Harper, 1967, Wynne-Edwards and Hasan, 1972).

The "Schistosity Zone" (or Sveconorwegian "front") (Fig. 1.1) (Magnusson, 1965), a 500 Km. linear belt of subvertical shearing and mylonitisation, separates the Sveconorwegian Province from the older (ca. 1700 m.y.) Svecofennian Province to the east. To the north-west the Sveconorwegian Province is bounded by the Caledonian front.

The Swedish sector of the Sveconorwegian Province has been sub-divided on lithological and tectonic grounds by (Magnusson et al. (1960) and Gorbatschev (1975)). The main subdivisions (Fig. 1.1) are:

1. The "Pregothian" belt (Magnusson et al., op. cit., Lundegårdh, 1974), a migmatite terrain dominated by tonalitic to granodioritic gneisses and subordinate supracrustal rocks.
2. The "Åmål" or "Gothian" belt (Magnusson et al., op. cit., Gorbatschev, 1975), is dominated by granitoid plutonic rocks (Åmål-Kroppefjäll complex) and includes at least two groups of supracrustal rocks - the Åmål formation (Magnusson et al., op. cit.) and the Kappebo formation (Gorbatschev, 1977). The granitoid rocks were formerly regarded as a single differentiated group (Larsson, 1947, 1956, Lundegårdh, 1951, 1953, 1958) but recently sub-divided by Gorbatschev (op. cit.) into three groups (in decreasing order of age): Åmål (I), Åmål (II) and Hästefjorden.
3. The Dal Group (Larsson, 1956, Lundberg, 1973), a supracrustal

Fig. 1.1 Sketch map to show the location of the Orust area within the Sveconorwegian province of southern Sweden and southern Norway. The Sveconorwegian province (K-Ar ages ca. 1000 m.y.) is separated from the Svecofennian province (K-Ar ages ca. 1700 m.y.) by the Schistosity Zone (SZ) or Sveconorwegian front to the east and bounded by the Caledonian front to the north-west. The principal tectonic and lithological components of the Sveconorwegian province are also shown.

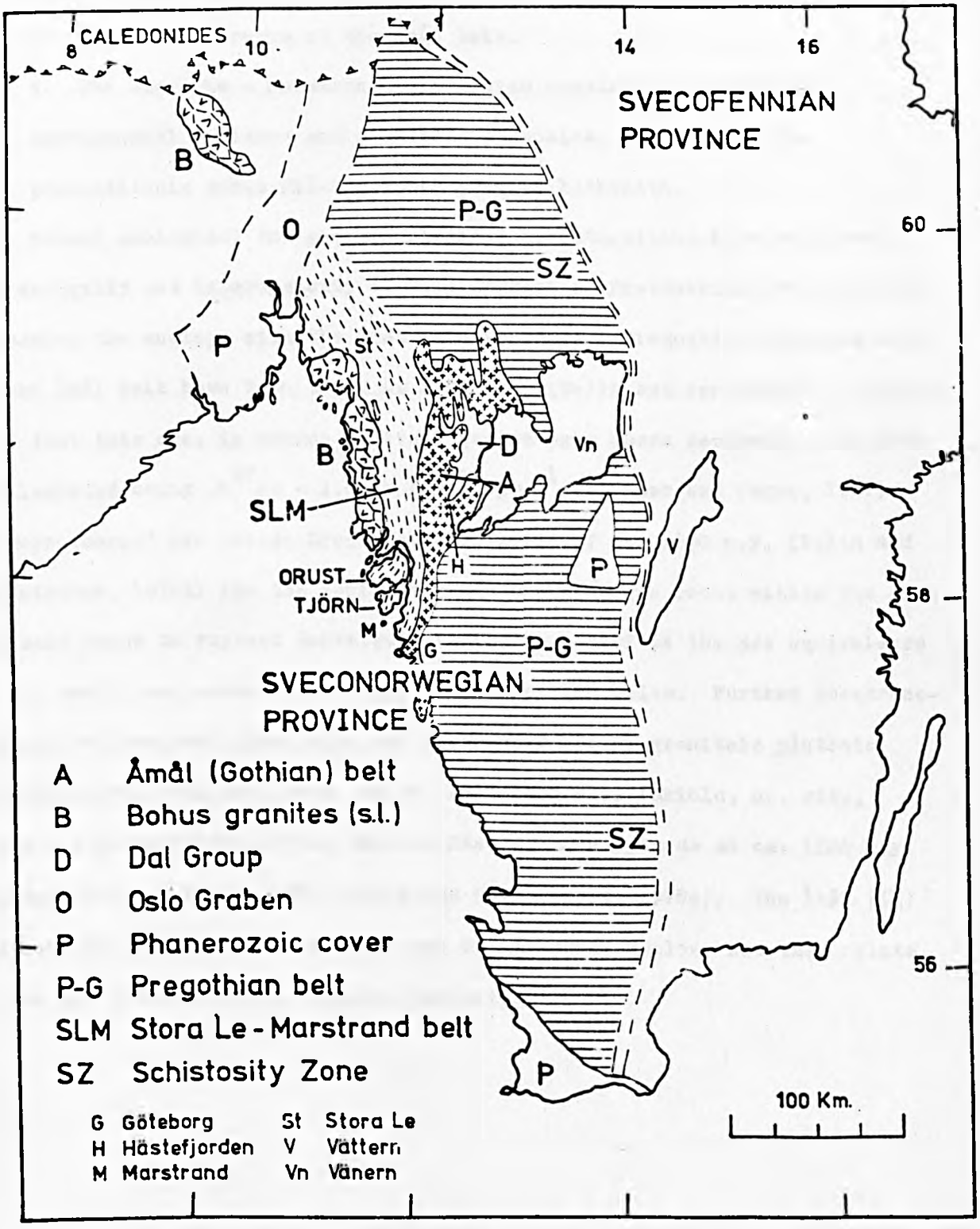
CALEDONIDES
8
10
14
16
SVECOFENNIAN
PROVINCE
B
O
P-G
SZ
60
P
St
B
D
Vn
A
SLM
ORUST
TJÖRN
M
H
P
V
58
G
P-G
SVECONORWEGIAN
PROVINCE
SZ
P
56
100 Km.
A Åmål (Gothian) belt
B Bohus granites (s.l.)
D Dal Group
O Oslo Graben
P Phanerozoic cover
P-G Pregothian belt
SLM Stora Le - Marstrand belt
SZ Schistosity Zone
G Göteborg
H Hästefjorden
M Marstrand
St Stora Le
V Vättern
Vn Vänern

sequence of coarse clastic sediments, slates and spilites, deformed in the Sveconorwegian orogeny (Skiöld, op. cit.) and unconformably overlying the youngest (Hästefjorden) division of the plutonic rocks of the Åmål belt.

4. The Stora Le - Marstrand belt, which consists of migmatised supracrustal gneisses and granitoid plutonics, intruded by the post-tectonic Bohus-Flå-Iddefjord granite batholith.

Recent geological and geochronological investigations have confirmed the antiquity and heterogeneity of this segment of Precambrian crust further extending the analogy with the Grenville Province. Pregothian gneisses east of the Åmål belt have been dated at 1700 m.y. (Welin and Gorbatschev, 1976a). Note that this age, in common with all quoted ages where necessary, has been recalculated using $\lambda^{87}Rb = 1.42 \times 10^{-11}\ yr^{-1}$ (Steiger and Jager, 1977). An "errorchron" age (sensu Brooks et al., 1972) of ca. 1650 m.y. (Welin and Gorbatschev, 1976b) for the earliest granitoid plutonic rocks within the Åmål (I) belt tends to support Gorbatschev's (1975) belief in the age equivalence of the early components of the Åmål and Pregothian belts. Further geochronological studies have identified two later episodes of granitoid plutonic activity within the Åmål belt, at ca. 1375-1450 m.y. (Skiöld, op. cit., Welin and Gorbatschev, 1978a) and the Hästefjorden episode at ca. 1200 m.y. (Gorbatschev and Welin, 1975, Welin and Gorbatschev, 1976c). The Åmål (II) plutonic rocks have not been dated and it is as yet unclear how they relate to the ca. 1375-1450 m.y. magmatic activity.

1.2 Sveconorwegian events.

Following Kratz et al. (1968) the term "Sveconorwegian" will be used in a chronological sense in this work to describe tectonic and igneous events occurring between ca. 1200 m.y. and ca. 900 m.y. This corresponds to the period of the Grenville Orogeny (Wynne-Edwards, 1972). In Norway the early Sveconorwegian (ca. 1200-1150 m.y.) involved amphibolite facies metamorphism and alkaline magmatism (O'Nions and Baadsgaard, 1971, O'Nions and Heier, 1972, Versteeve, 1975) with higher grade metamorphism occurring later (1000-950 m.y.) at least in south-west Norway (Versteeve, 1975).

In Sweden, however, the earliest dated Sveconorwegian events are (1) the emplacement of alkaline intrusives within the Schistosity Zone with an Rb-Sr whole-rock isochron age of 1185 $\pm$ 37 m.y. (Klingspor, 1976) and (2) the Hästefjorden granites at ca. 1200 m.y. (Gorbatschev and Welin, 1975, Welin and Gorbatschev, 1976c). The Hästefjorden intrusive episode was followed by sedimentation of the Dal Group and greenschist facies metamorphism and deformation. Slates from the Dal Group give a Rb-Sr whole-rock isochron age of 1028 $\pm$ 39 m.y. (Skiöld, op. cit.).

From this time onwards, cooling of the Sveconorwegian Province through K-Ar blocking temperatures had begun. Post-tectonic granitic intrusives, not recorded in the Grenville Province, occur in both Norway and Sweden and have been dated in the interval 950-850 m.y. (Brueckner, 1972, Killeen and Heier, 1975, Pedersen and Falkum, 1975, Priem et al., 1973, Skiöld, op. cit., Versteeve, 1975, Welin and Blomqvist, 1964).

1.3 The Stora Le - Marstrand belt.

This westernmost segment of the Sveconorwegian Province outcrops from Marstrand, west of Göteborg, in the south, to Stora Le in the north and continues northward into Norway as the Ostfold "Series". The dominant lithologies comprise a generally migmatised suite of quartzo-feldspathic gneisses with minor metapelites, calc-silicates and metabasic rocks (Magnusson, 1965, Larsson, 1956) intruded by a variety of deformed and metamorphosed granitoid and basic plutonic rocks. The post-tectonic Bohus granite (Asklund, 1947, Skiöld, op. cit.) intrudes the Swedish sector of the belt and a Rb-Sr isochron age of 891 $\pm$ 34 m.y. obtained for it (Skiöld, ibid.) sets a younger limit on the development of the Stora Le - Marstrand rocks.

The relationship between the Stora Le - Marstrand belt and the rest of the Sveconorwegian Province is a major stratigraphic problem. Magnusson (1960, 1965) considered these rocks to be older than the Åmål (Gothian) belt but younger than the Pregothian. There is, however, some evidence that the main migmatisation event affecting the Stora Le - Marstrand supracrustals (Park et al., in press) may be as old as the earliest events in the rest of the Sveconorwegian Province. Pedersen (quoted in Hageskov, 1978) has obtained an age of ca. 1900 m.y. from migmatitic gneisses in the Norwegian continuation of the Stora Le - Marstrand belt. Welin and Gorbatschev (1978b) quote a four point Rb-Sr isochron age of 1674 $\pm$ 113 m.y. and a reference line of ca. 1580 m.y. for a tonalite-granodiorite which intrudes the Stora Le - Marstrand rocks on Tjörn. However, the isotopic systems depart considerably from equilibrium and no firm conclusions can be drawn about the age.

1.4 Location of the Orust area.

The island of Orust and the adjacent areas of Skaftölandet and Dragsmark, within which the rocks discussed in this thesis are found, is situated off the west coast of Sweden, 50 Km. north of Göteborg, and together with the islands of Tjörn and Marstrand (Fig. 1.1) forms the best exposed area within the Stora Le - Marstrand belt. Relevant geographical details, place names and sampling localities referred to in this thesis may be found in the enclosed fold-out map (referred to subsequently as the Map).

1.5 Previous work in the Orust area.

Lindstrom (1902) described the geology of the Orust area in the account of the Uddevalla map sheet (1:100,000). Bergström (1963) described the petrography of the Stora Le - Marstrand rocks on nearby Tjörn accompanied by a map on a scale of 1:50,000. Much of his petrographic detail is relevant to the present work since a number of his rock types continue northwards into Orust. Berthelsen and Murthy (1970) discussed the structural evolution of part of north-eastern Orust and published a map on a scale of 1:20,000.

Recently Park et al. (in press) have described in detail the structure and geological history of a ca.45 Km.^{2} area in western Orust which they mapped on a scale of 1:10,000. The present work is based upon the structural chronology established by Park et al. and on the author's reconnaissance mapping over much of Orust, Dragsmark and Skaftölandet.

1.6 Lithological nomenclature.

The rock types distinguished by Park et al. (op. cit.) occur over much of the Orust area and their terminology is used in this thesis with minor amendments to include lithologies not seen in western Orust. A tripartite division of the lithologies is made as follows:

1. The basement complex. This comprises the "gneisses and migmatites", the "older amphibolites" and most of the "older granites" of Park et al. (op. cit.). In addition a localised development of migmatised leucocratic gneiss and three calc-silicate occurrences are included.

2. Pre-dyke intrusive rocks. In addition to the "younger granites" and "Hälleviksstrand amphibolite" of Park et al. (op. cit.) this group includes the Assmunderöd-Myckleby augen granites of north-eastern Orust (Berthelsen and Murthy, 1970), their extension southwards to the augen granites of Tjörn (Bergstrom, 1963), the Källviken augen granite and the "grey granites" of Park et al. (op. cit.).

3. "Dyke suite" is used in the same sense as in Park et al. (op. cit.)

1.7 General geological relationships.

The geological history of the area, summarised in Table 1.1 (from Daly et al., in press), is based on detailed mapping in western Orust (Park et al., op. cit.) together with the work of Berthelsen and Murthy (op. cit.) and supplemented by reconnaissance mapping over much of the Orust area by the author.

The geology of the area is summarised on the Map. The most common rock type is a medium-grained, banded, migmatitic para-gneiss with well developed stromatic and locally schlieren and nebulitic structures (Mehnert, 1968). The palaeosome comprises psammitic to semi-pelitic gneisses and minor amphibolites (the "older amphibolites") whose margins are generally concordant with the migmatitic banding and S1 foliation.

Oldest

DEFORMATION	METAMORPHISM	MIGMATISATION	IGNEOUS INTRUSION	
			W. ORUST	E. ORUST
	high amphibolite facies	early granitoid leucosome	older amphibolites	
intense regional deformation (D1)		?		
shearing (E. Orust)	?	?	Hälleviksstrand amphibolite grey granites	Assmunderöd-Myckleby augen granites
		later granitoid leucosome		
regional folding (D2)				
shears and faults	cooling			
			younger granite sheets basic to acidic dykes pegmatites	
foliation in dykes, shearing (D3)	amphibolite facies			
regional and local folding (D4-6)				
shears and faults	cooling			

Youngest

Table 1.1

A second development of migmatitic leucosome, often pegmatitic, is discordant to the first and at many localities it may be shown to be later than the D1 deformation which folds the earlier migmatitic banding. Intrusions of a mafic to ultramafic amphibolite (the Hällevіksstrand amphibolite) in western Orust and of a suite of augen granites (the Assmunderöd-Myckleby augen granites) in eastern and southern Orust occurred in the time interval between the two episodes of migmatisation. The Kallviken augen granite in Skaftölandet and Dragsmark may also be of this age.

In places, e.g. near Stocken and Kungsviken the migmatisation process has apparently been more intense and schlieren and nebulitic structures are developed. It is often unclear, however, to which episode of migmatisation any particular leucosome development belongs. Locally cross-cutting relationships in cogenetic leucosomes are to be expected and may only reflect small scale variations in degree of mobilisation and ductility contrasts between leucosome and palaeosome. Stictolithic structures (Mehnert, op. cit.), the problem of whose origin has not been considered in this thesis, occur widely on Flatön and in Skaftölandet.

D2 folding affects all of the preceding rocks but is most clearly identified as a second deformation in western and northern Orust.

In the Källviken area, close to the Källviken augen granite, a small area of coarse-grained leucocratic gneiss also exhibits two generations of migmatitic leucosome, but its relationship with the surrounding exposures of typical Stora Le - Marstrand para-gneisses is unclear.

Following the D2 folding episode there is some evidence (Park et al., op. cit.) for cooling of the complex prior to the emplacement of two independant suites of minor intrusive rocks. The first (the younger granites) comprises dykes and sills of tonalitic to alkali-granitic but dominantly of granodioritic composition and is followed by dykes and sills of the mainly basic dyke suite. Both suites of minor intrusive rocks occur throughout the

area but there is a marked concentration of both types in western Orust. Both suites cut across F2 folds and the Assmunderöd-Myckleby augen granites, but only the younger granites are observed to cut the Hälleviksstrand amphibolite. In all cases where contacts are seen members of the dyke suite cut across the younger granites. An heterogeneous group of muscovite-granite and quartz-feldspar pegmatites cut across D2 structures but contacts with the other intrusive rocks are rarely seen. One of these cuts across a member of the dyke suite. A few narrow and undeformed pegmatite sheets may be related to the post-tectonic Bohus granite (Magnusson, 1960, 1965), but the majority are affected by post-dyke deformation and may be earlier.

Two regionally important phases of deformation affected the complex following the emplacement of the dyke suite. The first, D3, is best recognised in the dykes as a planar mineral fabric expressed by the alignment of biotite and hornblende. S3 is also developed in the younger granites and a number of F3 folds have been recognised by Park et al. (op. cit.). D4 deformation is represented by the widespread development of flat-lying F4 folds within one or more low-angle shear zones within which the relative transport direction is upwards towards the north or north-west. One such zone extends from northern Härmanö, off the coast of western Orust, to the vicinity of Henan in the north-east. In eastern Orust the F4 structures may be traced continuously from Henån in the north to Varekil in the south. Elsewhere in central Orust exposure is incomplete and discrete boundaries to the D4 shear zones cannot be identified. In the area mapped by Park et al. (op. cit.) a discrete zone of D4 shearing has been identified in northern Härmanö. Belts of D4 shearing, expressed as F4 folds, are also seen on Flatön and in Skaftölandet.

Two further folding episodes have been recognised in western Orust by Park et al. (op. cit.) but no attempt has been made in this work to correlate these regionally.

1.8 Aims of research and organisation of thesis.

The principal aims of this research were as follows:

1. to extend the geological investigations of Park et al. (op. cit.) into a wider area of the Stora Le - Marstrand belt.

2. to assess the possibilities of radiometric dating following which it was decided to use Rb-Sr whole rock methods to attempt to date the principal igneous events, to investigate the effects of the metamorphic events on the Rb-Sr systematics and to place a limiting age on the Sveconorwegian activity using both whole rock and mineral Rb-Sr studies.

3. to investigate the petrochemical evolution of the varied lithologies in the area in the light of whole rock geochemical studies.

4. to examine the local and regional variation, within the basic members of the dyke suite, of certain trace elements generally held to be immobile under conditions of amphibolite facies metamorphism.

5. to attempt to estimate the temperature of metamorphism, using the partitioning of Mg and Fe between garnet and biotite in the basic dykes, in a terrain where low-variance assemblages and metamorphic index minerals are rare.

In Chapter 2, analytical techniques and methods of research are discussed. The lithological subdivisions (Section 1.6) form the basis of Chapters 3-5 and in these chapters the geology and petrography, whole-rock geochemistry and geochronology of each group of rocks is discussed. Chapter 6 contains a brief discussion of the mineral geochemistry and geothermometry of the basic dykes. The principal conclusions are given in Chapter 7.

Sample descriptions, sample localities, whole-rock and mineral geochemical data and the results of two replicate whole-rock sampling experiments are given in Appendices A-E.

CHAPTER 2. Methods of research and analytical techniques.

2.1 Field studies and sampling.

A total of fifteen weeks fieldwork was undertaken in the Orust area, of which six were spent in collection of samples for analysis and detailed examination of the geology of the sampling sites. In addition, reconnaissance geological mapping of an area of ca. 200 $Km.^2$ in Orust and adjacent parts of Dragsmark and Skaftölandet was undertaken (see Map).

The rock type and number of the analysed samples are as follows: gneisses (total of 30 including 13 nebulitic migmatites), older amphibolites (7), pegmatitic (second generation) leucosomes (7), the Hälleviksstrand amphibolite (6), the Assmunderöd-Myckleby augen granite (11), the younger granites (23) and the dyke suite (71).

Samples prefixed "SJ" in Appendices A to E were collected by the author, primarily for geochronology. As far as possible samples were collected as single blocks and the majority weighed between 5 Kg. and 10 Kg. Samples prefixed as follows: "GP" (mainly younger granites), "SA" (one sample of older amphibolite) and "SB" (mainly gneisses) were collected by R. G. Park, A. Crane and A. I. Bailey respectively. Samples prefixed "S" (gneisses) and "RCS" (dyke suite) were supplied in powder form by B. S. P. Moorlock and R. C. Standley.

2.2 Sample preparation.

Weathered material was removed and the samples were washed, rinsed in distilled water and dried in air. After initial breaking with a sledge-hammer and removal of a reference hand specimen the samples were reduced to small blocks (ca. 3 cm. across) in a Denbigh rock splitter and in each case the entire sample was passed through a Sturtevant rock crusher. At this stage the rock chips (usually less than 0.5 cm. in length) were

homogenised mechanically and subdivided using an automatic sample splitter. Larger samples (ca. 10 Kg.) were homogenised by repeated mixing and cone-and-quartering. Samples were further subdivided by the cone-and-quarter method and ca. 150 gm. was crushed in a Tema ring mill. Approximately 50 gm. of this material was further crushed in a ball mill, specifically to reduce the grain size of biotite present. All but the very biotite-rich samples tested passed -180 mesh.

Two samples (basic dyke SJ 632 (see Chapter 5) and pegmatitic leucosome SJ 522 (see Chapter 3)) were selected for replicate sampling. Nine samples of each (weighing ca. 150 gm.) were split off at the rock chip stage of crushing and prepared as indicated above. No special precautions were taken and thus the samples may be used to assess overall analytical uncertainties, which take into account the possible inhomogeneity of the sample during preparation of the rock powder. The analytical results of these sampling experiments are presented in Appendix A (Tables 1 and 2).

Samples were prepared for electron-microprobe analysis by lapping down rock chips mounted on glass slides. The surface was polished using a Kent polisher with diamond abrasives in the size range 6 - 0.25 . Using this method, it was found that bevelling of the sample was unavoidable due to the difficulty of holding the thin glass slide in the polisher so that it was coplanar with the polishing surface. It was found that better results could be obtained by first polishing the rock chip, mounting the polished face onto a glass slide, lapping down the reverse side and transferring to the final slide.

2.3 Whole rock geochemistry.

Major and trace element data were determined at Keele in an automatic Phillips PW 1212 X-ray fluorescence spectrometer. Instrumental drift was monitored by sequential analysis of a standard rock (KUM-1), resident in

the machine (as a glass disc or powder pellet, as appropriate) for the entire period of analysis. Major elements were also determined on a Unicam SP 1900 atomic absorption spectrophotometer equipped with an emission mode facility (for Na_2O and K_2O).

X.R.F.S. major element data were reduced to mean (peak minus background) counts on a Digital PDP-8S computer and the data was further processed using a series of Fortran programs, written by the author, on a CDC-7600 computer at Manchester, accessed at Keele. Trace element data were processed on a Digital PDP-8S computer, using programs in Focal, written by J. P. Sedgley and on a Digico M16E, using programs in Basic, written by G. J. Lees and D. Emley.

Major and trace element data were stored in character files on an ICL 1906A computer, linked to the CDC-7600 at Manchester. Many of the tables in Appendices A-E were obtained from these files.

Binary plots in the style of Fig. 4.6 were produced offline to the CDC-7600 at Manchester on a Calcomp graph plotter using the statistical package SPSS from the Vogelback Computer Centre, Northwestern University. Routine statistical calculations were also made using SPSS. The ternary diagrams were traced from line-printer plots using a series of programs written by the author, based on the program "Triplot" by G. J. Lees.

The analytical uncertainties in X.R.F.S. (major and trace element) analyses may be assessed from the data on the two replicate sampling experiments, presented in Appendix A (Tables 1 and 2). Error bars on binary plots and triangles shown on ternary diagrams were calculated (2σ) from this data.

2.3.1 Major elements.

Whole-rock powders were dried at ca. 110°C overnight and the loss on ignition (L.O.I.) at 1000°C was determined. Samples were prepared for X-ray fluorescence spectrometry (X.R.F.S.) by fusion of the ignited powders, diluted with five parts of $LiBO_2$. No heavy absorber was added. Operating

conditions are given in Appendix A (Table 3).

Calibrations were made by analysing between seven and fifteen well characterised international standards, prepared by the same method as for the unknowns. The data of Flanagan (1973) was used for calibration after recalculation on an oxidised volatile-free basis. Thus iron was determined as Fe_2O_3. No separate determination of FeO was made.

An attempt was made to derive empirical corrections for matrix effects in the samples. Following the method of Norrish and Hutton (1969) a series of multicomponent mixtures of the nine oxides (above) and Na_2O was quantitatively prepared and analysed. However, the results of this experiment were not satisfactory; the expected linear relationship between mass absorption coefficient and atomic number did not hold. It was concluded that two sources of uncertainty, (1) non-stoichiometry in starting materials and (2) incomplete loss of volatiles during ignition (Mn and Ca were weighed as carbonates) were responsible.

The calibrations were obtained by least squares linear regression (assuming zero error in concentration) and good linear relationships were found for most elements using the uncorrected data. This together with the high flux:rock ratio (5:1), which might be expected to have reduced the matrix effects, suggests that the failure to apply mass absorption corrections may not be serious. Thus the uncorrected data (for nine oxides) are presented as partial analyses of ignited samples in Appendices A-D. L.O.I. and Na_2O, the latter determined separately on pressed powder pellets, using international and interlaboratory standards for calibration, are also given. The data are also presented as normalised analyses, recalculated to 100% including Na_2O and L.O.I. as components.

Twenty-nine samples of the basic dyke suite were also analysed by atomic absorption spectrometry (A.A.S.) (SiO_2, Al_2O_3, Fe_2O_3, MnO, MgO and CaO) and flame emission spectrometry (F.E.S.) (K_2O and Na_2O) following the method of Yule and Swanson (1969). TiO_2 was determined photometrically on these rocks as a peroxide complex in a Unicam SP 500 Spectrophotometer.

The results are presented in Appendix D2.

2.3.2 Trace elements.

The trace elements Ce, Cr, Ga, La, Nb, Ni, Sc, Rb, Sr, Y and Zr were determined using pressed powder pellets by X.R.F.S. Calibrations were obtained by a spiking technique similar to that of Leake et al. (1969) using, as spiking matrices, rocks of similar composition to the unknowns. Differences in mass absorption between the spiking matrix and the unknowns were corrected using the ($MoK\alpha_C$) method of Reynolds (1963). The $MoK\alpha_C$ peak was measured "in run" for Rb, Sr, Y and Zr and the $MoK\alpha_C$ data were abstracted for correction of the remaining elements, measured using the Cr and W tubes. La and Ce were analysed for a small number of rocks only and mass absorption corrections were calculated using the ratio of peak minus background to background counts. Detection limits and operating conditions for each of the analysed trace elements are given in Appendix A, Table 4.

2.4 Isotope geochemistry.

2.4.1 Whole rock analyses.

Sr was separated by standard cation exchange techniques. $^{87}Sr/^{86}Sr$ ratio was measured as unspiked Sr, on single Ta filaments, in a VG Micromass 30 (MM 30) mass spectrometer at the University of Leeds. $^{87}Sr/^{86}Sr$ ratios were normalised using $^{88}Sr/^{86}Sr = 8.37521$. Total chemical blank Sr was routinely less than 6 ng. Correction was made for any Rb contaminant detected (usually at the early stage only) in the Sr mass spectrometer runs using $^{87}Rb/^{85}Rb = 0.3815$. The mean value of $^{87}Sr/^{86}Sr$ for NBS standard SRM 987, obtained over the period of this work, was 0.71031 ± 4 (see Appendix A, Table 5). Tabulated errors (everywhere 2σ unless stated otherwise) for $^{87}Sr/^{86}Sr$ analyses are based on "in run" statistics but a realistic minimum standard deviation of 8.0×10^{-5} (2σ) was assigned to the data in

all regression treatments.

Rb/Sr ratios and Rb and Sr contents were determined using standard techniques (Pankhurst and O'Nions, 1973, modified by M. Bickle) in a Phillips PW 1212 X.R.F. spectrometer. Estimated (2σ) errors are as follows: Rb and Sr contents, $\pm$ 5%; Rb/Sr and $^{87}Rb/^{86}Sr$ ratios, $\pm$ 2%. Rb/Sr data for one of the replicate sampling experiments is given in Appendix A, Table 6. The accuracy of the Rb/Sr data may be assessed from the values obtained for international standards (Appendix A, Table 7).

Isochron calculations were performed using a computer program written by J. C. Roddick which uses a combination of York (1969) and McIntyre et al. (1966) regression treatments. Following Steiger and Jager (1977), $\lambda Rb = 1.42 \times 10^{-11}$ yr.$^{-1}$ and all quoted ages have been recalculated where necessary using this value. All quoted errors in ages and initial ratios are 2σ. For each of the regressions quoted the value of the mean square of weighted deviates (MSWD) is given. This index is a measure of the scatter of the data points about the fitted line (see Brooks et al. 1972). Generally values of MSWD greater than 2.5 indicate errors in excess of that expected from analytical uncertainties alone (i.e. "geological errors"), in which case the regression line is termed an "errorchron". It is important to realise that the boundary condition (MSWD = 2.5) may rise to higher values when small numbers of samples are involved.

2.4.2 Mineral isotopic analyses.

Hand picked muscovite and plagioclase samples were cut up with a pair of scissors and crushed by hand in an agate pestle and mortar, respectively. Aliquots were weighed accurately and a mixed Rb and Sr isotopic spike added quantitatively for isotope dilution analysis of Rb and Sr contents and $^{87}Rb/^{86}Sr$. Rb and Sr were separated using standard ion exchange techniques. Rb was determined using standard techniques on an MS5 mass spectrometer. Sr was analysed on the MM30 and correction for any Rb contaminant was made using the $^{87}Rb/^{85}Rb$ ratio measured in the Rb run. The ages and errors were calculated using the short Basic program "Pegage", written by the

author, for a Digico M16E computer.

2.5 Mineral compositions.

Mineral analyses were obtained using EDS (energy-dispersive spectrometry) electron-microprobe analysis at the University of Manchester. The method and treatment of analytical errors are described by Dunham and Wilkinson (1977).

2.6 REE analyses.

REE analyses were obtained on a commercial basis from the Universities Research Reactor, Risley. The analytical technique is a modification of the method of Graber et al. (1970) and involves radiochemical group separation and thermal-neutron activation. REE data were normalised using the mean values for 22 chondrites of Herrmann (1974) (Appendix A, Table 8).

CHAPTER 3. The basement complex.

3.1 Introduction.

The Stora Le - Marstrand rocks of the Orust area are dominated by a suite of migmatised semi-pelitic, psammitic and basic gneisses. The semi-pelitic and psammitic gneisses (together referred to as para-gneisses), the basic gneisses and their migmatitic leucosomes are collectively termed the 'basement complex'. Park et al. (op. cit.) have described the field occurrence, structure and petrography of the components of the basement complex outcropping in western Orust and Bergström (1963) includes detailed petrographic descriptions of similar rocks on Tjörn to the south of Orust. Berthelsen and Murthy (op. cit.) briefly described the rocks of the basement complex in north-eastern Orust. Rock types representing the basement complex are found throughout the investigated area and there is little variation in the lithological composition of the gneisses on a regional scale. However, in the western part of the area mapped by Park et al. (op. cit.), psammitic gneisses dominate over the more typical semi-pelitic compositions, which elsewhere account for 80-90% of the basement complex.

On outcrop scale, variations in the palaeosome are more evident. The principal variation is in the proportion of psammite which may be present in the form of bands or pods up to several metres in length and varying in width from a few cm. to ca. 2 m.

Regional and local variations in the style and extent of migmatisation are also apparent. Both concordant and discordant leucosomes have been recognised and at least two groups of leucosomes are separated in time by the earliest recognised phase of deformation (D1 of Park et al. op. cit.) and by the emplacement of granitic and basic intrusions (Chapter 4).

A further product of migmatisation is the development, on various scales from outcrop to mappable units up to ca. 5 sq. Km. in area, of areas of nebulite (sensu Mehnert, 1968) or diatexite (sensu M. Brown, 1973) in which the distinction between leucosome and palaeosome can no longer be made and within which xenoliths of gneiss occur.

3.2 Geology and petrography.

3.2.1 Gneisses with minor development of leucosome.

Grey medium-grained psammitic gneisses with minor development of migmatitic banding (up to 10% of outcrop area) occur throughout the area as bands or pods within more thoroughly migmatised rocks of semi-pelitic composition (Plate 3.1). Park et al. (op. cit.) distinguished an area dominated by psammitic gneisses in the western part of their map of western Orust (Fig. 3.1) but elsewhere semi-pelitic migmatites are more important.

The psammites (mean grain size ca. 2 mm.) contain quartz (50-60%), plagioclase An10-35 (20-30%), micas (5-20%, dominantly biotite) and microcline (0-10%). Accessories include garnet, opaque ores, epidote (s.l.), apatite, sphene and zircon. Sometimes heavy mineral banding is apparent. In places, e.g. in western Härmanö, the psammites show a marked compositional banding expressed by the variation in quartz-feldspar ratio and in the abundance of heavy minerals and micas. There are rare occurrences of narrow flinty bands (a few cm. in width) approaching quartzite (80% quartz) in composition. Park et al. (op. cit.) have recorded "grading" and Bergström (1963) has described "banded sediments" and "graded bedding" on St. Äggelös off the island of Tjörn to the south of Orust.

A further suggestion of a sedimentary origin for these rocks is found in four occurrences of calc-silicate bands (Plate 3.2). These occur within bands or enclaves of psammite in the migmatised semi-pelite and vary in thickness from 2 cm. to 10 cm. Similar rocks are also found on Tjörn (Bergström, 1963) and in north-western parts of Skaftölandet (R. G. Park and A. Crane, pers. comm.). Some compositional banding is apparent within these calc-silicates and they are generally differentiated into a dark central zone containing hornblende, rare clinopyroxene and garnet and an outer zone dominated by quartz, plagioclase and zoisite.

Plate 3.1 Photograph to illustrate the migmatised psammitic and semipelitic para-gneisses of the basement complex. Locality: Stocken (41, 57). The (10 cm. to 20 cm. wide) folded band of psammite sits within a more thoroughly migmatised semi-pelite. Concordant first generation leucosome in both lithologies has a stromatic (layered) structure. At top the contact of the psammite and semi-pelite is cut by a small body (10 cm. wide) of second generation leucosome. Hammer head measures 16 cm.

Plate 3.2 Photograph to illustrate a 5 cm. wide compositionally-zoned band of calc-silicate within a 10 cm. wide band of migmatised psammite. The main lithology is a heavily migmatised semi-pelitic gneiss, which grades into an inhomogeneous nebulite. At hammer head a narrow (10 cm. to 15 cm. wide) dyke of younger granite (Section 4.2.5) cuts the migmatitic gneiss. Locality Fiskeback (44, 58). Hammer head measures 16 cm.

3.2.2 Migmatitic gneisses and leucosomes.

Concordant migmatitic banding occurs in all of the migmatised rocks of the basement complex. In the psammites the palaeosome is readily discernible: 2 cm.-15 cm. wide bands of unmigmatised gneiss are separated by 1 mm.-5 mm. wide leucosomes. Closely-spaced concordant leucosomes are developed in semi-pelitic rocks which are usually more coarse-grained than the psammites and have a higher mica content, generally 25-35%.

Modal mineralogical compositions are difficult to estimate in these semi-pelitic gneisses due to their banded nature. Palaeosomes are not always discernible and every gradation occurs from regular alternations of leucosome and discrete semi-pelitic or psammitic palaeosome to thoroughly migmatised gneisses (nebulites or diatexites) in which a distinction between leucosome and palaeosome cannot be made and which locally contain xenoliths of semi-pelitic gneiss, amphibolite or psammite.

A discordant, usually pegmatitic, leucosome (Plate 3.3) occurs locally throughout the area and is considered to be later than the main (pre-D1) migmatisation on these grounds:

1. In places, throughout the area, pegmatitic leucosomes are discordant to F1 folds which fold the earlier migmatitic banding.
2. In eastern Orust a second generation of leucosome follows a set of dextral shears (Plate 3.4) which buckle and sometimes offset the earlier leucosomes.
3. The Hällevikstrand amphibolite (Park et al., op cit. and Chapter 4) and the Assmunderöd-Myckleby augen granite (Berthelsen and Murthy, op. cit. and Chapter 4) cut the main migmatitic banding but are themselves cut by migmatitic leucosome.
4. Grey granite (Park et al., op. cit. and Chapter 4) cuts the Hällevikstrand amphibolite and is in turn cut by a leucosome which displays diktyonitic structure (Mehnert, op. cit.).

Plate 3.3 Photograph to illustrate the discordant pegmatitic leucosome of the second migmatisation. Locality: Stocken (41, 57). At centre a large pegmatitic leucosome (1 m. across) cuts across the migmatitic banding of the early (pre-D1) migmatisation. At hammer a 10-20 cm. band of psammite with minor concordant stromatic banding. At right a heavily migmatised semi-pelite with smaller (15-20 cm. across) pods of pegmatitic leucosome with pinch-and swell structure. At top left minor amounts of leucosome cut a small (few sq. m.) discordant body of grey granite (Section 4.2.2) which cuts the first generation leucosome. Hammer measures 80 cm. x 16 cm.

Plate 3.4 Photograph to illustrate second generation leucosome cutting dextral shears which displace the earlier concordant leucosome. Locality: north of Varekil on Rte. 160 (59, 48). Pencil measures 15 cm.

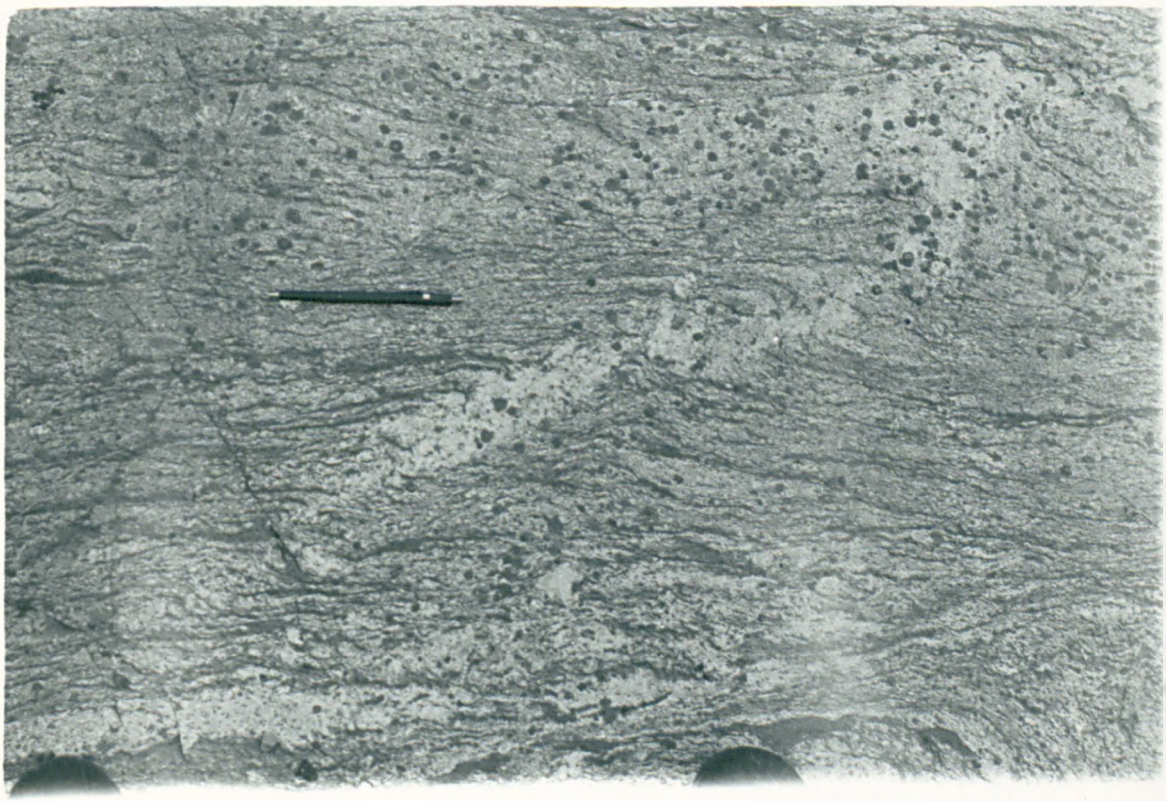

5. Nebulitic migmatite (Section 3.2.2.2), e.g. in the area north of Hällevikstrand (the Hällevikstrand granite), is locally cut by a pegmatitic leucosome which displays stictolithic structure.

In many places, especially in western Orust, where F2 folds are positively identified (Park et al., op. cit.) these fold both generations of leucosome. If the chronological equivalence of the second-generation leucosome in eastern and western Orust is correct then the migmatised shears in eastern Orust (2 above and Plate 3.4) represent a phase of deformation between D1 and D2. Where they occur, members of the younger granite suite (Park et al., op. cit. and Chapter 4) cut both generations of leucosome. These rocks never show migmatisation, nor do members of the dyke suite (Park et al., op. cit. and Chapter 5) which cut them.

While these observations clearly identify events which separate the emplacement of migmatitic leucosome and so provide convenient chronological markers, it is not known if migmatisation ceased between D1 and D2. It is possible that it was continuous (see description of Assmunderöd-Myckleby augen granite, Section 4.2). For convenience of description the products of the two generations of migmatisation will be referred to as first and second generation leucosomes.

In the following sections the different morphological expressions of migmatite are described in turn. The concordant and nebulitic leucosomes belong to the first generation. Both of these are cut by discordant second generation leucosome.

3.2.2.1 Concordant leucosomes.

Concordant leucosomes are medium to coarse-grained and white to cream in colour. Although considerably modified by up to six phases of deformation (Park et al., op. cit.) they frequently display stromatic and opthalmitic structures (Mehnert, op. cit.). The former are more common and the leucosome thickness varies from less than 0.5 cm. to ca. 3 cm. Concordant

leucosomes are illustrated in Plates 3.1, (3.2), 3.3 and 3.4.

The majority have trondhjemitic to granodioritic compositions with quartz (25-35%), plagioclase ca. An30 (20-30%), micas (15-30%), microcline (up to 10%) with accessory garnet, zircon, sphene and apatite. They show considerable departure from textural equilibrium. In particular, muscovite and microcline are clearly late and overgrow earlier textures and mineral fabrics. A border-zone rich in micas varies in thickness but may be up to half as thick (up to 4 mm.) as some of the more narrow leucosomes. The micas in these selvedges are clearly of two generations (Plate 3.1.M). Biotite is always earlier and defines a planar (S1) mineral fabric which is cross-cut by coarse-grained muscovite. Both micas may be up to 4 mm. across.

Similarly, microcline is often out of equilibrium with the rest of the leucosome. It occurs as small (0.05 mm.) patchy inclusions in large (up to 0.5 cm.) probably anti-perthitic plagioclase porphyroblasts (Plate 3.2.M) and also as a subordinate component of the leucosome matrix where it may enclose plagioclase and quartz.

Plagioclase porphyroblasts frequently show heavy sericitisation and may contain abundant inclusions of epidote (s.l.) and quartz.

3.2.2.2 Nebulitic migmatites (Diatexites).

These coarse-grained mesocratic rocks vary in composition from granodioritic to adamellitic. They apparently represent an extreme development of the main D1 migmatisation and in many places grade imperceptibly into banded rocks as biotite schlieren give way to discrete biotite-rich palaeosomes. They frequently contain xenoliths of migmatised psammite, semi-pelite or amphibolite and also unmigmatised psammite. They are affected by the second migmatisation in the form of pegmatitic and locally stictolithic leucosomes and are cut by members of the younger granite suite.

The nebulitic migmatites occur throughout the area but are most abundant along the northern coast of Orust, in southern Orust near Varekil, and in the west near Hällevikstrand (referred to as the Hällevikstrand

Plate 3.1.M Photomicrograph to illustrate muscovite overgrowing biotite in the mica selvedge to a granodioritic leucosome in sample SJ 512. High relief grains associated with biotite right of centre are sphene.
X 55. XN.

Plate 3.2.M Photomicrograph to illustrate (probable) patch anti-perphite developed in a granodioritic leucosome in a migmatised semipelite (not analysed).
X 155. XN.

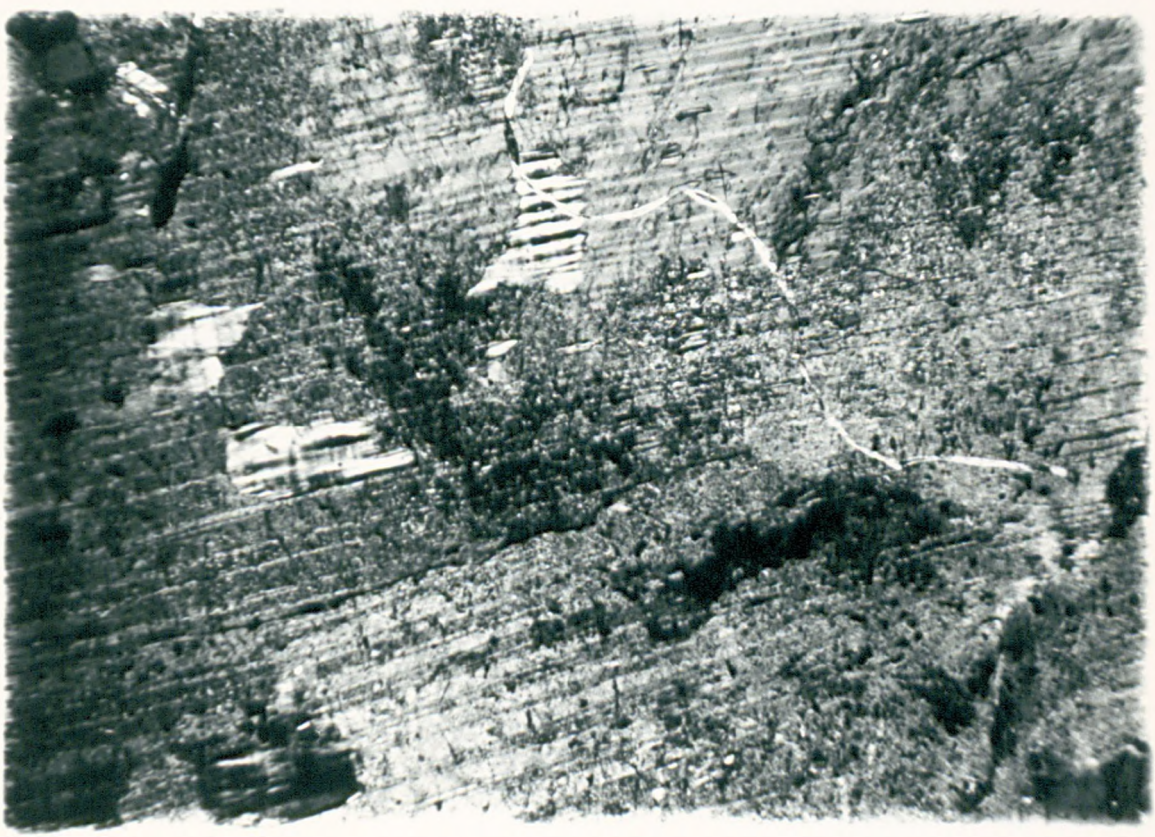

granite).

The field aspect of these rocks reflects their bulk composition. The homogeneous nebulitic varieties tend to be more leucocratic and are adamellitic in composition. They contain quartz (20-40%), plagioclase ca. An20-25 (20-40%), microcline (20-40%), with plagioclase and microcline generally in equal proportions, and micas (generally up to 20%). Accessories include garnet, apatite, zircon, sphene, pyrite and tourmaline.

The inhomogeneous nebulites are generally granodioritic and sometimes grade into migmatite with schlieren structure. They contain quartz (30-50%), plagioclase ca. An30 (20-40%), biotite (10-20%), muscovite (generally 10-20% micas together are usually less than 30%), microcline (usually less than 10%) and accessory garnet, sphene, pyrite, apatite and zircon.

In both the homogeneous and inhomogeneous nebulites porphyroblastic microcline (up to 5 mm. across) is later than plagioclase, which it encloses but microcline in the matrix exhibits a granoblastic texture, apparently in equilibrium with quartz, plagioclase and biotite. Locally, euhedral biotite is mantled by quartz and both are enclosed in plagioclase.

Replacement textures are common: chlorite often replaces garnet and biotite; and fine-grained muscovite, which replaces plagioclase and biotite, may make up 40% of the mode in thoroughly altered varieties. This fine-grained muscovite (Plate 3.3.M) overgrows any tectonic fabric that may be present. Pyrite (up to 4 mm.) also overgrows the biotite fabric (if present) and is often surrounded by clots of fine-grained muscovite.

In one example a narrow (2 mm. wide) zone of extreme shearing is defined by a fabric consisting of bands of sericitic muscovite overgrown by fibrolitic and prismatic sillimanite (Plate 3.4.M). This is the only occurrence of an alumino-silicate in more than 300 thin sections examined. No alumino-silicate was recognised in the field. Sillimanite has been recorded in migmatitic gneisses in the Norwegian continuation of the Stora Le -

Plate 3.3.M Photomicrograph to illustrate development of fine-grained muscovite in a coarse-grained biotite rich nebulitic migmatite (sample SJ 930).
X 55. XN.

Plate 3.4.M Photomicrograph to illustrate prismatic sillimanite developing in a narrow (2 mm. wide) zone of extreme shearing which cuts a nebulitic migmatite (not analysed). The age of this shearing is not known.
X 55. XN.

Marstrand belt in the Moss area of south-eastern Norway. (Hageskov, pers. comm.)

3.2.2.3 Discordant leucosomes.

Discordant, often pegmatitic leucosomes, occur sporadically throughout the area but there is a marked concentration in the western part where they commonly cut the psammites and grey granite bodies (Chapter 4). They are generally more coarse-grained and more leucocratic than the concordant leucosomes and sometimes the alkali feldspar is pink in colour. They occur as pods up to 2 m. across and, especially in the psammites, often exhibit pinch-and-swell structure (Plate 3.3) (Ramberg, 1955) in which the "pinch" part may be parallel to and indistinguishable from the concordant leucosomes. Occasionally they contain xenoliths of the adjacent palaeosome producing schollen structure and in one body cutting the Hällevikstrand amphibolite (Chapter 4) a xenolith of psammite contained earlier concordant leucosome. Stictolithic structure, consisting of flecks of biotite or biotite and garnet within the leucosome, is found in bodies of discordant leucosome cutting nebulitic migmatites (Section 3.2.2.2) near Hällevikstrand (the Hällevikstrand granite) and is a common feature of the migmatites on Flatön and in Skaftölandet (Plate 3.5).

Petrographically the discordant leucosomes form two groups. The first is apparently restricted to the para-gneisses and is adamellitic to alkali-granitic in composition. This group contains quartz (30-50%), microcline (up to 40%), plagioclase ca. An5-10 (usually less than 10%) and minor amounts of muscovite and biotite with accessory epidote (s.l.) and zircon. At least some of this epidote and mica is a late alteration feature and some fills late veins.

The second group is restricted to the older amphibolites and Hällevikstrand amphibolite and is trondhjemitic to granodioritic in composition. These leucosomes contain quartz (10-70% but usually 20-45%), plagioclase ca. An15-20 (45-60%) and biotite (0-20%) with accessory muscovite,

Plate 3.5 Photograph to illustrate stictolithic (fleck) structure in the second generation discordant leucosome. Locality: Kristineberg (43, 59). The flecks are composed of biotite, frequently chloritised, and minor garnet. Hammer head measures 16 cm.

Plate 3.6 Photograph to illustrate agmatic (breccia) structure and at right, near concordant contact with migmatised psammite, a minor development of diktyonitic (net-like) structure in leucosome cutting an older amphibolite body. Locality: Malö (45, 54). Hammer measures 80 cm. x 16 cm.

sphene, epidote (s.l.) and zircon.

3.2.3 Older amphibolites.

These rocks occur throughout the area as pods, bands and more massive bodies and range in composition from basic to ultrabasic. They are usually restricted in size to less than ca. 500 $m.^2$ but there are a number of larger bodies up to 300 m. in width which may be followed for over 1 Km. e.g. in western Orust (Park et al., op. cit.), near Kungsviken in northern Orust and near Harlycke in the south.

The older amphibolites are a petrographically heterogeneous group exhibiting considerable variation in grain size and texture. Both medium and coarse-grained varieties occur and the colour varies from green to black to grey. Mafic varieties contain hornblende (40-80%), plagioclase ca. An30-60 (0-25%), biotite (up to 30%) and minor amounts of garnet and quartz. Rarely garnet makes up to 40% of the mode in which case hornblende is greatly diminished in quantity.

Textural equilibrium is rarely observed in the older amphibolites and is usually restricted to ultramafic varieties which are dominated by polygonal hornblendes. A variety of mineral-replacement reactions is a common feature. Zoisite or clinozoisite replaces biotite, chlorite replaces biotite and garnet, and plagioclase may be heavily sericitised. In one example clinopyroxene makes up 20% of the mode and overgrows hornblende.

On a mesoscopic scale relict igneous textures are common. Relict ophitic or sub-ophitic textures and remnants of plagioclase phenocrysts are sometimes visible on weathered surfaces although these are often less apparent in thin section. Compositional banding in some rocks suggests plutonic magmatic crystallisation although this feature may also arise by degradation of migmatitic banding during deformation.

The older amphibolites are generally concordant with the compositional banding in the para-gneisses and are affected by both episodes of migmatisation. Locally, however, some migmatised amphibolites are discordant to the

compositional banding in the gneisses and are sometimes discordant to the earlier migmatitic leucosome. Thus at least some members of the group represent the earliest recognisable intrusions into the para-gneisses.

One of the larger bodies at Harlycke, which is concordant with the migmatitic banding in the surrounding semi-pelitic gneisses, contained several 10 cm.-15 cm. wide fine-grained grey bands of intermediate composition. These bands have a sharp base and top and are laterally persistent for ca. 50 m. Their appearance and composition are consistent with a volcanic or volcani-clastic origin.

Migmatitic leucosomes affecting the older amphibolites generally take two forms. The earlier leucosome forms agmatic and diktyonitic structures and is usually restricted to thicknesses of a few cm. or less (Plate 3.6). These leucosomes are often modified to a pseudo-stromatic structure in highly strained amphibolites (Plate 3.7). The later leucosome, often pegmatitic, exhibits agmatic and schollen structures and occurs as pods or bands from a few cm. to ca. 2 m. in width. The two sets of leucosome are not always present and a singular development may take either of the two forms. The leucosomes of both types have granodioritic to trondhjemitic compositions and some are unusually enriched in quartz (up to 70%).

3.2.4 Migmatised leucocratic gneiss at Källviken.

These rocks occur within a narrow (500 m. wide) belt of grey semi-pelitic para-gneisses, similar to those occurring elsewhere in the area, and which here form a septum within the intrusive Källviken augen granite (Chapter 4 and Map). They are coarse-grained, banded leucocratic rocks of adamellitic to alkali-granitic composition cut by a single generation of coarse, often pegmatitic, leucosome, often with a well developed stictolithic structure defined by hornblende crystals up to 1.5 cm. in length or by hornblende-biotite clots of similar size (Plate 3.8). These discordant leucosomes are up to 15 cm. in width and may persist for up to one metre in length.

Plate 3.7 Photograph to illustrate pseudo-stromatic (layered) structure, apparently developed by D1 flattening of agmatic structure in a (5 m. wide) band of older amphibolite. Small amounts of second generation leucosome cut the D1 fabric and at right are in turn cut by a narrow (2 cm. - 5 cm.) dyke of younger granite (Section 4.2.5). Locality: Stocken (41, 57). Hammer measures 80 cm. x 16 cm.

Plate 3.8 Photograph to illustrate the migmatised leucocratic gneiss at Källviken (46, 60), cut by discrete pods and diffuse patches of stictolithic (fleck) leucosome. The palaeosome is banded with garnet, biotite and hornblende concentrated in narrow (few mm. wide zones). At bottom right an opthalmitic (augen) migmatite structure is developed. Clinometer measures 10 cm. x 6 cm.

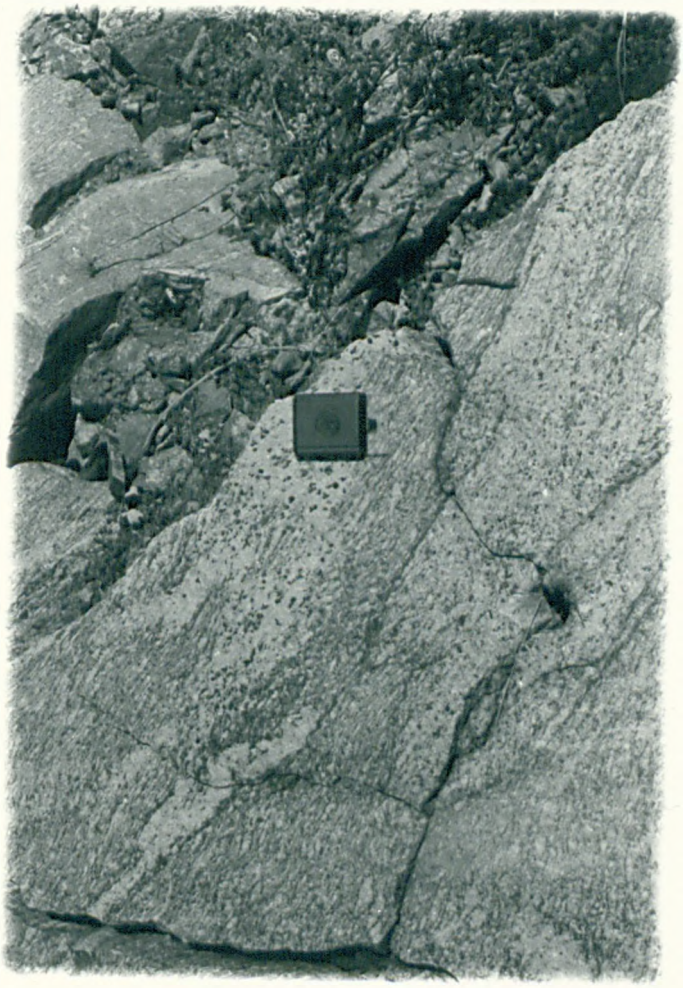

The palaeosome contains quartz (30-40%), microcline and untwinned alkali feldspar (25-40%), plagioclase ca. An15-20, sometimes anti-perthitic (up to 20% but usually less than 10%) and garnet (up to 10%). Green biotite (5-10%), green hornblende and sphene, with the latter extensively developed as inclusions in garnet, together make up as much as 15% of the mode in some examples. Apatite and allanite/epidote intergrowths occur in accessory amounts. Epidote, sphene, sericite and chlorite occur in discrete crush zones which vary in width from a few mm. to 5 cm. Cataclastic textures are also sporadically developed in the palaeosome outside these discrete zones.

The palaeosome is banded on a 2-5 mm. scale with mafic minerals - garnet, biotite and minor hornblende concentrated in narrow zones, parallel to a strong planar biotite fabric, which separates impersistent quartzo-feldspathic bands. Locally this banded lithology grades into an inhomogeneous migmatite which displays opthalmitic structure (Plate 3.8). Differentiation of the quartzo-feldspathic and mafic components in these ways is quite distinct from the development of the larger, more coarse-grained discordant leucosomes and may represent the pre-D1 concordant migmatisation seen elsewhere in the area.

The discordant leucosome occurs as discrete bands and pods sometimes with a narrow (ca. 5 mm.) biotite selvedge and also as patches with indistinct margins which grade into the banded gneiss. The discordant leucosome tends to be biotite and garnet-free and has a stictolithic structure defined by flecks of hornblende or hornblende with minor biotite. The leucosomes are often pegmatitic and thus the modal mineralogical composition is difficult to assess. Plagioclase (often anti-perthitic) is less calcic (up to ca. An15) and is generally more abundant than in the palaeosome and is apparently subordinate to microcline. Quartz is present in similar amounts and the mafic minerals, dominated by hornblende are diminished relative to the palaeosome.

Sericitised plagioclase, microcline, hornblende and quartz, all of similar size (ca. 1 mm.-2 mm.) define a granoblastic texture but microcline and anti-perthitic plagioclase both occur as porphyroblasts up to 1.5 cm. in length. Both contain rounded inclusions of quartz and green biotite. Porphyroblastic microcline includes equant (less than 1 mm.) grains of heavily sericitised plagioclase.

Grey migmatised semi-pelite, typical of much of the basement complex in the Orust area outcrops within a few hundred metres of this isolated occurrence of leucocratic gneiss. No contacts between the two lithologies are seen. However, it seems reasonable to correlate the two generations of leucosome in the leucocratic gneiss with the two generations of leucosome which affect the para-gneisses.

3.3 Geochemistry of the basement complex.

3.3.1 Gneisses.

3.3.1.1 Sampling.

Thirty samples of gneiss covering the compositional range psammite to semipelite, have been analysed for major and selected trace elements. All but two of the samples (GP19 and SJ521) contain more than ten per cent by volume of migmatitic leucosome. Thirteen samples are nebulitic migmatites (the "Hällevikstrand granite", Section 3.2.2.2), of which ten (Fig. 3.10) were collected for geochronology and are discussed further in Section 3.4.

The majority (25) of the samples are located within the area mapped by Park et al. (op. cit.) (Figs. 3.1, 3.10 and Map). Three samples (S10, S40, S41), supplied in powder form by B. S. P. Moorlock, were collected in the course of mapping of the Källviken augen granite (unpublished, see Chapter 4). Sample SJ953 was collected at Slussen in eastern Orust (Map) close to the contact with the Assmunderöd-Myckleby augen granite (Chapter 4). The

Fig. 3.1 Geological map of western Orust taken from Park et al. (op. cit.), on which is shown the locations of samples of the basement complex:- gneisses (•), nebulitic migmatites (the Hällevikstrand granite) (o), older amphibolites (•) and pegmatitic (second generation) leucosome (△).
The boxed area is shown on Fig. 3.10. On this and subsequent diagrams sample numbers without an alpha prefix refer to the "SJ" samples.
Inset shows the location of the Orust area and the main tectonic and lithological divisions of part of the Sveconorwegian province. A = Åmål belt, B = Bohus granite, D = Dal Group, SLM = Stora Le - Marstrand belt, P = Pregothian belt.

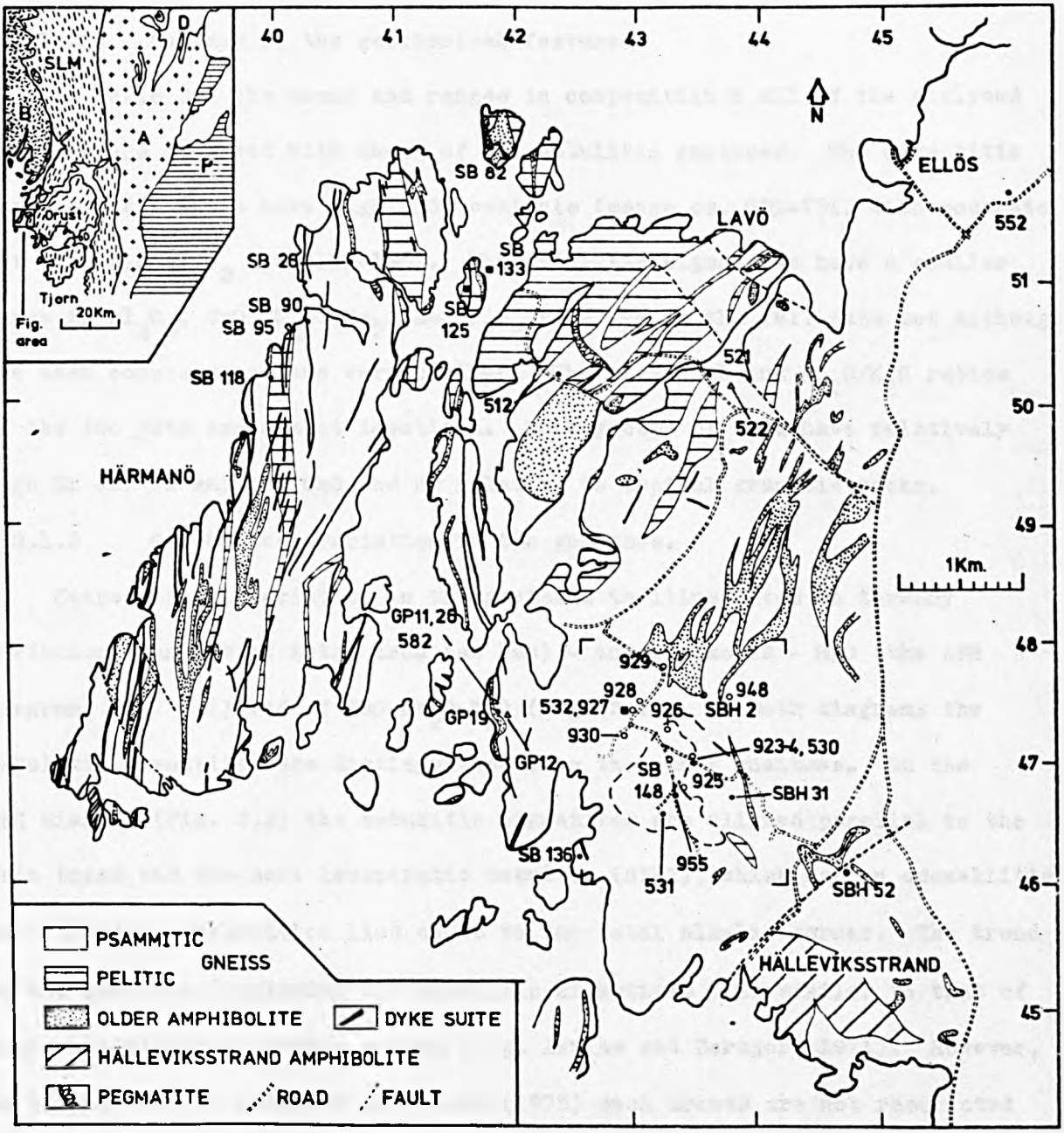
SLM
B
A
P
D
Orust
Tjorn
Fig. area
20Km.
40
41
42
43
44
45
N
ELLÖS
LAVÖ
552
51
50
49
48
47
46
45
SB 82
SB 133
SB 26
SB 90
SB 95
SB 125
SB 118
521
512
522
HÄRMANÖ
1Km.
GP11,26
582
929
928
948
SBH 2
GP19
532,927
926
930
923-4, 530
GP12
SB 148
925
SBH 31
SB 136
955
531
SBH 52
HÄLLEVIKSSTRAND
PSAMMITIC GNEISS
PELITIC
OLDER AMPHIBOLITE
DYKE SUITE
HÄLLEVIKSSTRAND AMPHIBOLITE
PEGMATITE
ROAD
FAULT

samples are briefly described in Appendix B1.

The geochemistry of the gneisses is summarised in Table 3.1 and average compositions of some sedimentary and granitic rocks are included for comparison. The full data set is presented in Appendix B2.

3.3.1.2 Summary of the geochemical features.

In Table 3.1 the means and ranges in composition of all of the analysed gneisses are compared with those of the nebulitic gneisses. The migmatitic gneisses as a whole have high SiO_2 contents (range ca. 65%-75%) with moderate but variable Al_2O_3 (ca. 11%-18%). The nebulitic migmatites have a smaller range in Al_2O_3, CaO, K_2O, Na_2O and P_2O_5 relative to the full data set although the mean compositions are very similar. The mean K/Rb and Na_2O/K_2O ratios of the two sets are almost identical. Both groups of data have relatively high Cr and Ni and low CaO and Sr relative to typical granitic rocks.

3.3.1.3 Geochemical variation in the gneisses.

Compositional variation in the gneisses is illustrated on ternary variation diagrams of total iron (as FeO) - total alkalis - MgO (the AFM diagram, Fig. 3.2) and of $CaO-Na_2O-K_2O$ (Fig. 3.3). On both diagrams the nebulitic migmatites are distinguished from the other gneisses. On the AFM diagram (Fig. 3.2) the nebulitic migmatites are aligned parallel to the main trend and the most leucocratic nebulite (SEH2), which has an adamellitic mineralogical composition lies close to the total alkalis corner. The trend of the gneisses (including the nebulitic migmatites) is similar to that of many calc-alkaline igneous suites (e.g. Irvine and Barager, 1971). However, as pointed out by Robinson and Leake (1975) such trends are not restricted to igneous rocks and are observed in many sedimentary and metasedimentary sequences - e.g. Moine metasediments (Butler, 1965), Welsh Ordovician greywackes (Bjorlykke , 1971) etc. Indeed the trend merely illustrates the restricted variation in Fe and Mg and the relatively larger variation in total alkalis. Consequently it is not reasonable to use AFM variations to discriminate between igneous and sedimentary affinities.

Table 3.1

Summary of geochemical data: gneisses.

	(a)		(b)		(1)	(2)	(3)	(4)
	mean	range	mean	range				
(Wt. %)								
SiO_2	70.9	65.1 - 78.2	71.1	65.1 - 76.4	66.7	69.2	66.9	73.9
TiO_2	0.59	0.19 - 1.47	0.62	0.19 - 1.47	0.6	0.5	0.6	0.2
Al_2O_3	13.86	10.72 - 18.35	13.55	11.38 - 15.73	13.5	13.7	15.7	13.8
Fe_2O_3*	4.28	1.39 - 7.61	4.37	1.39 - 7.61	5.5	4.9	3.8	2.0
MnO	0.07	0.02 - 0.19	0.08	0.03 - 0.18	0.1			0.1
MgO	1.74	0.52 - 3.07	1.91	0.52 - 3.07	2.1	1.6	1.6	0.3
CaO	1.47	0.68 - 4.25	1.17	0.68 - 2.22	2.5	1.8	3.6	0.7
Na_2O	2.60	1.17 - 4.13	2.49	1.73 - 3.51	2.9	3.1	3.8	3.5
K_2O	3.16	0.95 - 4.72	3.43	2.00 - 4.72	2.0	2.0	3.1	5.1
P_2O_5	0.09	0.05 - 0.26	0.08	0.07 - 0.11	0.2			0.1
(ppm.)								
Cr	88	28 - 166	95	28 - 163			30	
Ga	22	10 - 40	17	10 - 29			18	
Nb	29	11 - 58	20	11 - 44				
Ni	47	20 - 142	39	22 - 83		50	15	
Sc	18	7 - 51	16	8 - 27				
Rb	125	69 - 251	136	86 - 251	80	75	12	
Sr	169	114 - 275	152	114 - 215	200	190	440	
Y	41	21 - 78	44	30 - 64		20	30	
Zr	297	144 - 464	315	144 - 435		370	140	
ratios								
K/Rb	215	112 - 335	220	112 - 335	208	221	212	
Na_2O/K_2O	0.82	0.35 - 1.97	0.79	0.45 - 1.76	1.45	1.55	1.25	0.68

* total iron as Fe_2O_3

Notes (a) all gneiss samples (including nebulitic migmatities), (n = 30)
(b) nebulitic migmatites only (n = 13)
(1) average greywacke (Wedepohl, 1968)
(2) average Phanerozoic greywacke (Condie, 1976)
(3) average granodiorite (Nockolds, 1954)
(4) average alkali granite (Nockolds, 1954)

Fig. 3.2 Ternary variation diagram of total iron (as FeO) - total alkalis - MgO (the AFM diagram) for the gneisses (•) and nebulitic migmatites (○). 1 = average greywacke, 2 = average Phanerozoic greywacke, 3 = average granodiorite, 4 = average alkali granite (see Table 3.1). Triangle on this and on all subsequent ternary plots indicates approximate (2σ) analytical uncertainty.
The trend in the data illustrates the relatively larger variation in total alkalis and smaller variation in total iron and MgO.

Fig. 3.3 Ternary variation diagram of CaO-Na_2O-K_2O for the gneisses and nebulitic migmatites. Symbols as for Fig. 3.2. Samples SJ 521 and GP 19 contain less than 10% migmatitic leucosome, but it is not known if their composition is typical of the palaeosome in the more thoroughly migmatised gneisses or of the gneisses before migmatisation.

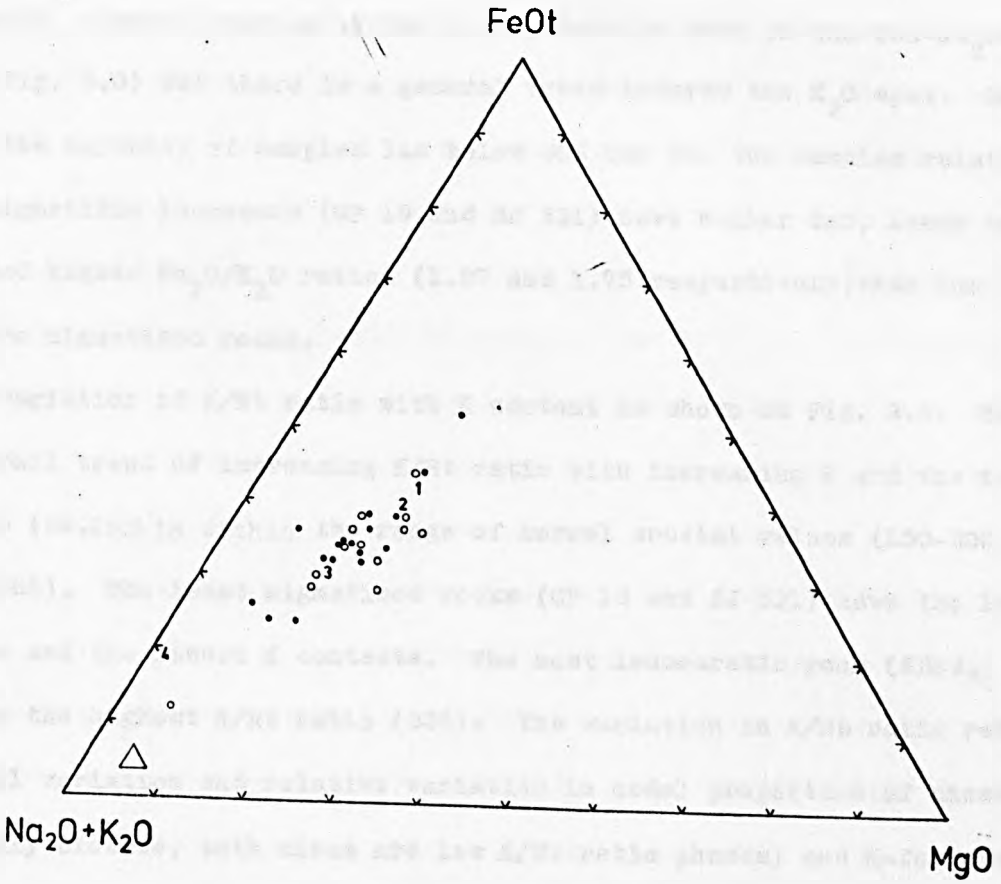
FeOt
Na_2O+K_2O
MgO
1
2
3
4

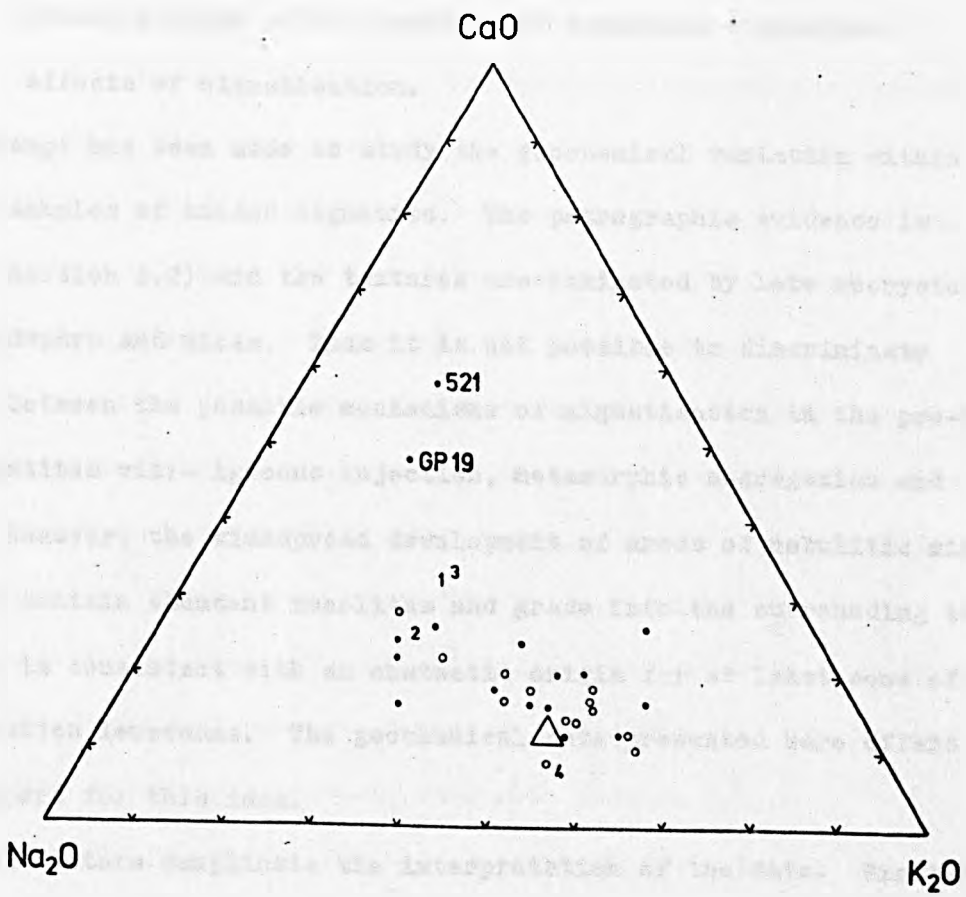
CaO
Na_2O
K_2O
521
GP19
1
3
2
4

Overall, a broad scatter of the data points is seen on the $CaO-Na_2O-K_2O$ diagram (Fig. 3.3) but there is a general trend towards the K_2O apex. On Fig. 3.3 the majority of samples lie below 30% CaO but two samples relatively free of migmatitic leucosome (GP 19 and SJ 521) have higher CaO, lower total alkalis and higher Na_2O/K_2O ratios (1.97 and 1.75 respectively)than the other, more migmatised rocks.

The variation of K/Rb ratio with K content is shown on Fig. 3.4. There is an overall trend of increasing K/Rb ratio with increasing K and the mean K/Rb ratio (ca.220) is within the range of normal crustal values (150-300, Taylor, 1965). The least migmatised rocks (GP 19 and SJ 521) have the lowest K/Rb ratio and the lowest K contents. The most leucocratic rock (SBH2, see above) has the highest K/Rb ratio (335). The variation in K/Rb ratio reflects the overall variation and relative variation in modal proportion of micas (principally biotite, both micas are low K/Rb ratio phases) and K-feldspar. The micas accommodate the larger (relative to K^+) Rb^+ion more readily than does alkali feldspar.

3.3.1.4 Interpretation of the geochemical variation - possible effects of migmatisation.

No attempt has been made to study the geochemical variation within individual samples of banded migmatite. The petrographic evidence is equivocal (Section 3.2) and the textures are dominated by late recrystallisation of feldspars and micas. Thus it is not possible to discriminate definitely between the possible mechanisms of migmatisation in the pre-D1 banded migmatites viz:- igneous injection, metamorphic segregation and anatexis. However, the widespread development of areas of nebulitic migmatite, (Map) which contain abundant xenoliths and grade into the surrounding banded migmatites, is consistent with an anatectic origin for at least some of the first generation leucosome. The geochemical data presented here offers limited support for this idea.

Several factors complicate the interpretation of the data. Firstly, the

least migmatised rocks are not necessarily equivalent in composition to the palaeosome portions of the migmatites analysed. No small scale sampling of the palaeosome was undertaken to test this possibility or to examine the range of palaeosome composition. Since no information is available on the composition of the gneisses before migmatisation the bulk geochemical effects of the migmatisation are difficult to assess. The fact that the nebulitic migmatites are so similar to the average composition of the gneisses as a whole (Table 3.1) lends some support to the view, but does not prove that the migmatisation took place in a closed system.

Secondly, two migmatisation events have affected the nebulitic migmatites (Section 3.2.2.2). Many of the analysed samples contain small (few cm.) blebs of stictolithic leucosome which is correlated with the second generation migmatisation. Other samples of the nebulitic migmatite, although free of actual bodies of this leucosome, were collected within tens of cm. of such material. The estimated volumetric proportion of second generation leucosome within or adjacent to the samples of nebulitic migmatite is 5%-10%. Only one generation of leucosome was recognised in the other gneiss samples.

Thirdly, the gneisses (including the nebulitic migmatites) contain variable amounts of muscovite, much of it very fine-grained, which considerably post-dates the biotite fabric where present (Section 3.2 and Plate 3.3.M). In addition, there has been considerable recrystallisation of alkali feldspar apparently at the expense of plagioclase.

The contributions of the second migmatisation and the late muscovite crystallisation to the geochemical variation in the nebulitic migmatites are not known and any such geochemical effects would, in any case, be difficult to distinguish from those of the main (pre-D1) migmatisation. It is possible, for example, that the trend of increasing K/Rb with increasing K (Fig. 3.4), may, at least in part, be due to redistribution of alkalis during either of these secondary processes. (see also Section 3.4).

It is possible to account for the geochemical variation in the gneisses

Fig. 3.4 Binary plot of K/Rb vs. K for the gneisses (•) and nebulitic migmatites (∘). GP 19 and 521 have less than 10% migmatitic leucosome, SBH 2 is the most leucocratic of the nebulitic migmatites. Error bars on this and on all subsequent binary plots represent the approximate (2σ) analytical uncertainty.

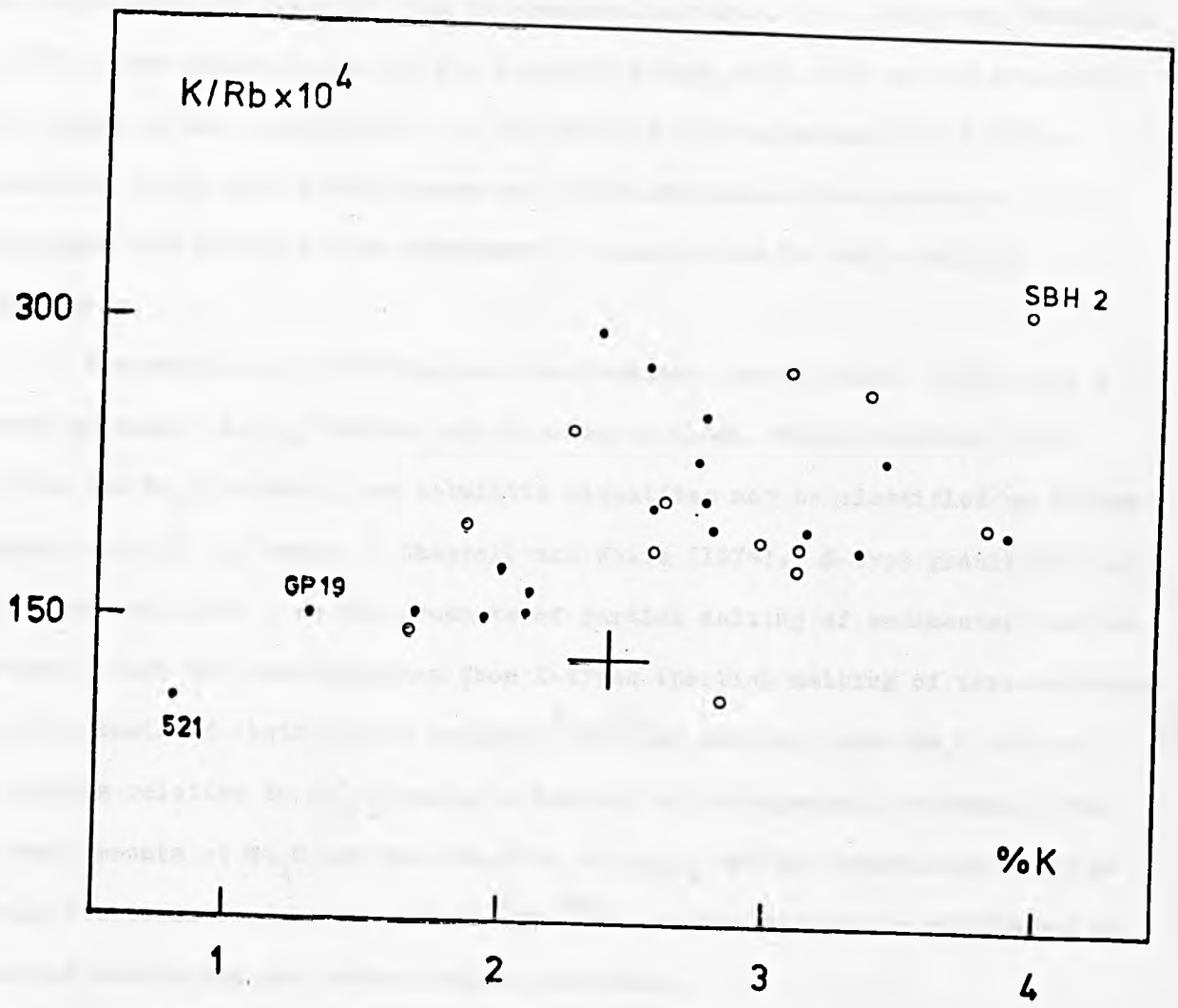
K/Rb x 10^4
300
150
SBH 2
GP19
521
%K
1
2
3
4

in terms of the degree of mixing (or perhaps better, unmixing) of palaeosome and leucosome. The geochemical data are consistent with anatexis culminating in the development of localised areas of nebulitic migmatite (Map) with the main control on the geochemical variation being the extent of separation of the melt from the residual material (cf. White and Chappell, 1977). The variation in Ca, Na, K and Rb (Figs. 3.3, 3.4) may be explained in terms of the fractionation of the alkalis (in the order: Na, K, Rb). relative to Ca into a melt phase and their subsequent incorporation in K-feldspar and in the albite component of plagioclase in the resulting leucosome.

The nebulitic migmatites are peraluminous (sensu Shand, 1953) with a mean molecular $Al_2O_3/(CaO+Na_2O+K_2O)$ ratio of 1.36. Thus, together with their low Na_2O content, the nebulitic migmatites may be classified as S-type granitoids in the sense of Chappell and White (1974). S-type granitoids are interpreted (ibid.) as the products of partial melting of sedimentary source rocks. They are distinguished from I-types (partial melting of igneous rocks) on the basis of their higher initial $^{87}Sr/^{86}Sr$ ratios, lower Na_2O and CaO contents relative to Al_2O_3 and on a variety of petrographic criteria. The lower amounts of Na_2O and CaO relative to Al_2O_3 and the fractionation of Rb relative to Sr (and hence higher $^{87}Sr/^{86}Sr$) in the S-types is attributed to marine weathering and sedimentation processes.

This idealised division of granitoid rocks may be applicable in certain circumstances but an obvious objection arises in the case of juvenile granites (with low $^{87}Sr/^{86}Sr$) produced by melting of rapidly buried volcani-clastic sediments e.g. products of andesitic volcanism on an Andean-type continental margin (e.g. Flood and Shaw, 1977). Thus the above criteria must not be used in isolation to characterise the parent rocks of granitoids as sedimentary or igneous.

3.3.1.5 Origin of the gneisses.

A large number of chemical criteria have been proposed to distinguish between igneous and sedimentary parents of metamorphic gneisses (e.g. Shaw, 1972, De la Roche, 1965, van de Kamp et al., 1976). In view of the limited number of samples, the degree of migmatisation and the complicated petrographic variation, this problem was not investigated in detail. The rationale behind many of the methods rests on the mobile behaviour of certain elements, e.g. alkalis and Sr and their depletion during marine weathering and deposition cycles. In view of their relative mobility these are the very elements least suitable for the application of discriminant techniques to metamorphosed rocks. The problem is illustrated on Fig. 3.5 which is a $MgO-K_2O-Na_2O$ variation diagram from Sighinolfi and Gorgoni (1978, after De la Roche, 1965). The data scatter close to the greywacke field. The variation in MgO relative to alkalis reflects the modal variation in biotite and the considerable spread parallel to the K_2O-Na_2O join reflects the variation in relative proportion of micas and feldspars. The failure of the nebulitic migmatites to follow De la Roche's igneous trend is not significant. Variations in Na_2O/K_2O ratio are consistent with the petrographic evidence (above). In general, the recrystallisation of feldspars and micas and the development of migmatitic leucosome are bound to produce a scatter approximately at right angles to the igneous trend.

The average composition of the gneisses (including the nebulites, Table 3.1) is close to some estimated averages for greywackes (Table 3.1) but both of these are, in turn, within the range of granitoid rocks (cf. average granodiorite and alkali granite, Table 3.1) for many elements. Total iron and MgO in the gneisses resemble the greywacke values but the average Na_2O/K_2O ratio (ca. 0.8) of the gneisses is more typical of granitic rocks. The low average Sr and CaO and high Cr and Ni values tend to favour a sedimentary origin (cf. van de Kamp et al., op. cit.) but none of these observations nor any combination of them ought to be used to decide

Fig. 3.5 Ternary variation diagram of MgO-K_2O-Na_2O for the gneisses and nebulitic migmatites. Symbols as for Fig. 3.2. In addition (after Sighinolfi and Gorgoni, 1978, from De la Roche, 1965), A = shales, B = greywackes, C = arkoses, IT = igneous trend.

Fig. 3.6 AFM diagram for the older amphibolites. Dashed line (from Irvine and Barager, 1971) distinguishes between tholeiitic (on the FeOt side) and calc-alkaline rock types. The older amphibolites lie on a trend parallel to the MgO-FeOt join. Together with their high Y/Nb ratio (ca. 3.9), this suggests a tholeiitic affinity for these rocks.

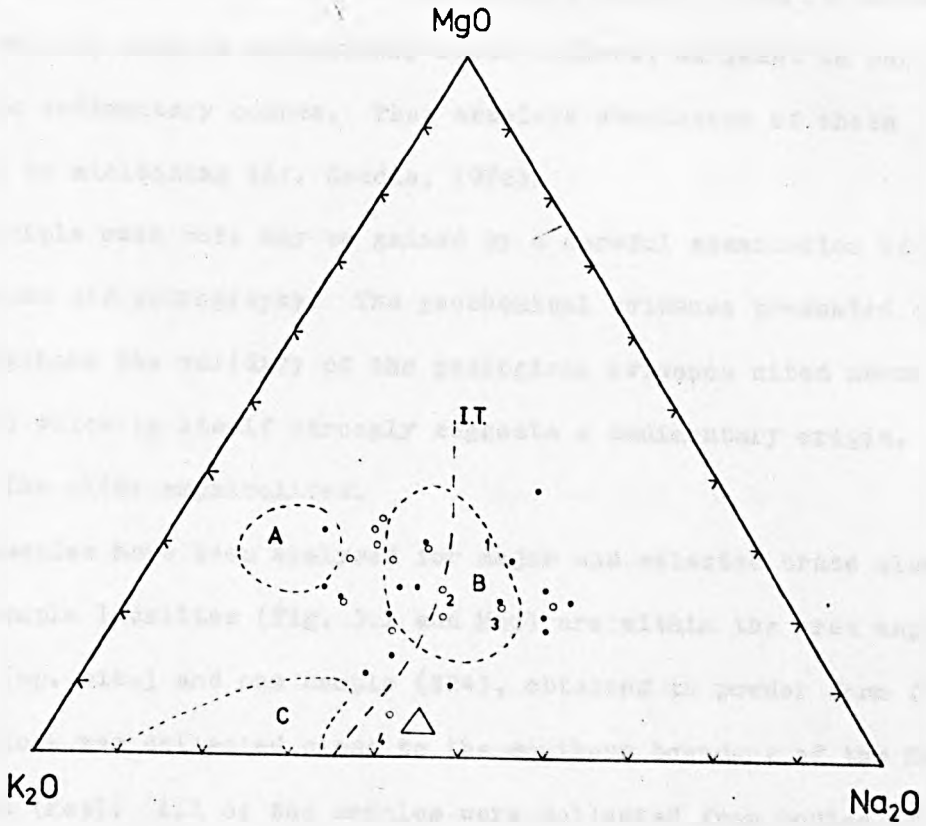
MgO
I.T.
A
B
C
1
2
3
K2O
Na2O

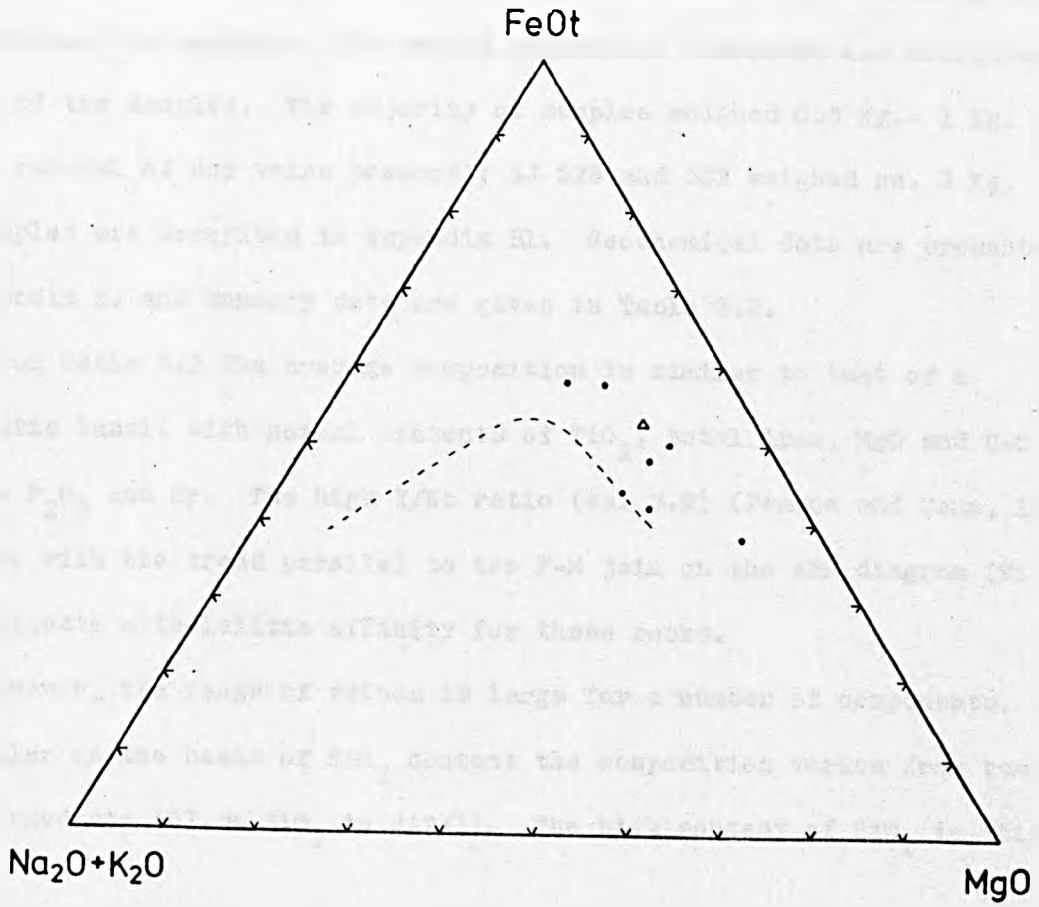
FeOt
Na2O+K2O
MgO

unequivocally the original nature of the present rocks. Clearly contents of Fe, Mg, Cr, Ni, etc. in sedimentary rocks reflect, at least in part, the nature of the sedimentary source. Thus absolute abundances of these elements may be misleading (cf. Condie, 1976).

In principle much more may be gained by a careful examination of the field relations and petrography. The geochemical evidence presented here merely strengthens the validity of the geological evidence cited above (Section 3.2) which by itself strongly suggests a sedimentary origin.

3.3.2 The older amphibolites.

Seven samples have been analysed for major and selected trace elements. Six of the sample localites (Fig. 3.1 and Map) are within the area mapped by Park et al. (op. cit.) and one sample (S24), obtained in powder form from B. S.P. Moorlock was collected close to the southern boundary of the Källviken augen granite (Map). All of the samples were collected from bodies of amphibolite affected by the first migmatisation and any leucosome veins present were excluded by removal of the veins and the adjacent 1 cm.- 2 cm. margin of amphibolite. Only material with less than 5% leucosome by volume was selected for analysis. No second generation leucosome was recognised in any of the samples. The majority of samples weighed 0.5 Kg.- 1 Kg. (after removal of any veins present); SJ 528 and 532 weighed ca. 3 Kg. The samples are described in Appendix B1. Geochemical data are presented in Appendix B2 and summary data are given in Table 3.2.

From Table 3.2 the average composition is similar to that of a tholeiitic basalt with normal contents of TiO_2, total iron, MgO and CaO and low P_2O_5 and Sr. The high Y/Nb ratio (ca. 3.9) (Pearce and Cann, 1973) together with the trend parallel to the F-M join on the AFM diagram (Fig. 3.6) suggests a tholeiitic affinity for these rocks.

However, the range of values is large for a number of components. In particular on the basis of SiO_2 content the composition varies from basic to intermediate (57.3% SiO_2 in SA2/1). The high content of SiO_2 in this

Table 3.2

Summary geochemical data: older amphibolites (seven samples).

	mean	range
	(wt. %)	
SiO_2	50.9	47.3 - 53.1
TiO_2	1.0	0.4 - 2.1
Al_2O_3	15.3	13.2 - 16.9
Fe_2O_3*	11.3	8.2 - 15.8
MnO	0.2	0.1 - 0.3
MgO	7.7	4.7 - 10.5
CaO	9.3	4.8 - 12.6
Na_2O	1.5	0.2 - 2.6
K_2O	1.5	0.4 - 3.4
P_2O_5	0.1	0.05 - 0.27
	(ppm.)	
Cr	216	69 - 463
Nb	ca. 7	BDL** - 13
Ni	65	18 - 120
Sc	45	32 - 54
Rb	67	9 - 92
Sr	150	115 - 194
Y	27	17 - 52
Zr	99	33 - 341
	ratios	
K/Rb	201	132 - 360
Y/Nb	ca. 3.9	

Notes * total iron as Fe_2O_3

** BDL = below detection limit (ca. 5-6 ppm.)

Fig. 3.7 Binary plots for the older amphibolites. Clockwise from top right:- TiO_2, P_2O_5, Y vs. Zr; CaO, TiO_2, total iron as Fe_2O_3, Al_2O_3 and SiO_2 vs. MgO.

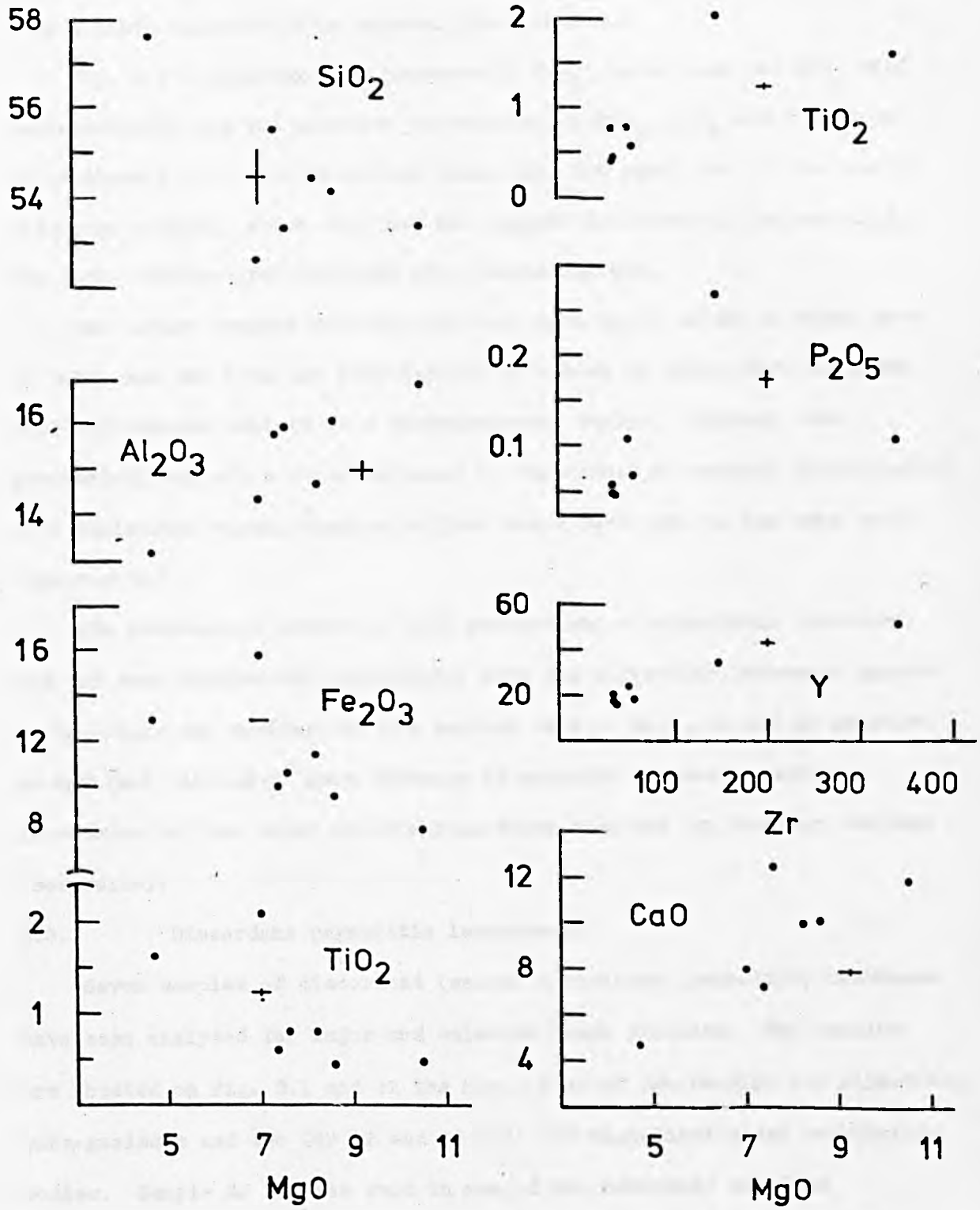
58
56
54
SiO2
2
1
0
TiO2
16
14
Al2O3
0.2
0.1
P2O5
16
12
8
2
1
Fe2O3
TiO2
60
20
Y
100
200
300
400
Zr
12
8
4
CaO
5
7
9
11
MgO
5
7
9
11
MgO

sheared rock may result from incomplete separation of the migmatitic leucosome during preparation of the sample. However, its high total iron, low MgO and high Nb, Y and Zr would be consistent with derivation from a basic composition by crystal fractionation.

Fig. 3.7 illustrates the increase in TiO_2, total iron and SiO_2 with decreasing MgO and the positive correlation of TiO_2, P_2O_5 and Y with Zr. Nb is close to or below detection limit (ca. 5-6 ppm.) for all but one of the rocks - SA2/1, which also has the highest Zr content. CaO and Al_2O_3 are both scattered but decrease with decreasing MgO.

The bodies sampled were for the most part small (a few m. wide) pods or bands and the data are insufficient in number to prove that the older amphibolites are members of a consanguineous series. However, the geochemical variation observed could be the result of crystal fractionation of a tholeiitic magma, similar to that which gave rise to the dyke suite (Chapter 5).

The geochemical effect of both generations of migmatitic leucosome has not been studied but interaction with the migmatitic leucosome present in the rocks may account for the scatter in K_2O, Na_2O, Rb and Sr relative to MgO (not plotted). Some exchange of material between pegmatitic leucosomes and the older amphibolites which they cut is, however, evident (see below).

3.3.3 Discordant pegmatitic leucosomes.

Seven samples of discordant (second generation) pegmatitic leucosome have been analysed for major and selected trace elements. The samples are located on Fig. 3.1 and on the Map. Five of the samples cut migmatitic para-gneisses and two (GP 12 and SJ 562) cut migmatised older amphibolite bodies. Sample SJ 522 was used in one of the replicate sampling experiments (Chapter 2), the results of which are given in Appendix A. The samples are described in Appendix B1 and the data are presented in Appendix B2. Summary geochemical data are given in Table 3.3 and the data are plotted on a CaO-Na_2O-K_2O diagram in Fig. 3.8.

Table 3.3

Summary geochemical data: discordant pegmatitic leucosomes. Group (a) (5 samples) cut the migmatitic para-gneisses. Group (b) (2 samples) cut the older amphibolites.

	(a)		(b)	
	mean	range	mean	GP 12	SJ 562
(wt. %)					
SiO_2	72.1	70.7 - 74.4	78.52	76.21	80.83
TiO_2	0.11	0.07 - 0.26	0.07	0.1	0.04
Al_2O_3	15.6	13.5 - 17.0	12.7	14.5	10.9
Fe_2O_3*	0.4	0.1 - 1.6	0.3	0.22	0.37
MnO	0.01	0.01 - 0.01	0.01	0.01	0.01
MgO	0.4	0.3 - 0.7	0.7	0.3	1.0
CaO	0.9	0.6 - 1.3	2.1	1.7	2.5
Na_2O	3.4	2.9 - 4.3	4.2	5.1	3.2
K_2O	6.1	4.5 - 7.5	0.9	1.2	0.6
P_2O_5	0.1	0.07 - 0.13	0.04	0.05	0.02
(ppm.)					
Ga	10	8 - 12	8	9	6
Nb	9	6 - 14	12	10	23
Rb	111	45 - 157	34	22	45
Sr	184	99 - 276	284	261	306
Y	25	15 - 39	3	2	3
Zr	70	6 - 167	15	12	18
ratios					
K/Rb	583	237 - 1383	283	449	116
Na_2O/K_2O	0.6	0.3 - 0.9	4.7	4.3	5.1

Notes * = total iron as Fe_2O_3

Fig. 3.8 Ternary variation diagram of CaO - Na_2O - K_2O for the second generation pegmatitic leucosome, which cut the migmatitic para-gneisses (•) and the older amphibolites (▲).

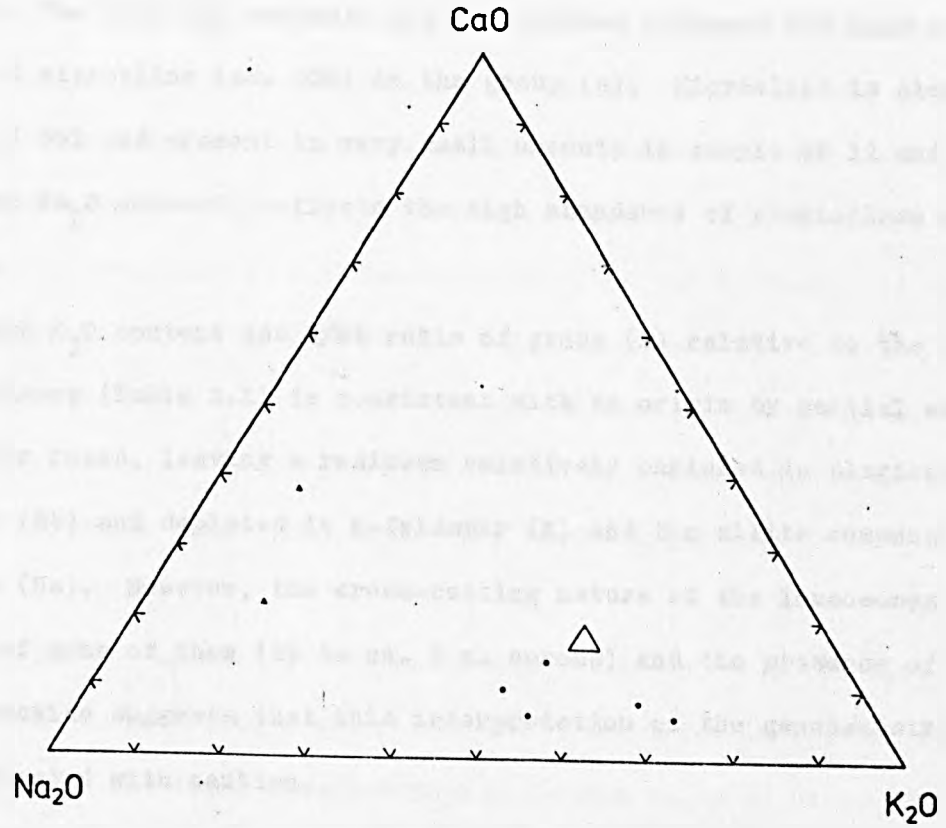
CaO
Na_2O
K_2O

There are distinct geochemical differences between the pegmatitic leucosomes cutting the gneisses (a) and the two samples which cut the older amphibolites (b). Group (a) leucosomes are characterised by high K_2O, low CaO, low Na_2O/K_2O and moderate to high K/Rb ratios. The two samples of group (b) have low K_2O, high CaO, and higher Na_2O/K_2O and lower K/Rb ratios than group (a). In addition Y is close to detection limit in (b), while group (a) have normal "granitic" contents of Y.

The geochemistry of the leucosomes may be explained in terms of the mineralogy. The high K_2O contents and K/Rb ratios reflects the high modal abundance of microcline (ca. 35%) in the group (a). Microcline is absent in sample SJ 562 and present in very small amounts in sample GP 12 and the high CaO and Na_2O content reflects the high abundance of plagioclase in both rocks.

The high K_2O content and K/Rb ratio of group (a) relative to the values for the gneisses (Table 3.1) is consistent with an origin by partial melting of the latter rocks, leaving a residuum relatively enriched in plagioclase (Ca) and biotite (Rb) and depleted in K-feldspar (K) and the albite component of plagioclase (Na). However, the cross-cutting nature of the leucosomes, the large size of some of them (up to ca. 2 m. across) and the presence of vein-filling muscovite suggests that this interpretation of the geochemistry should be treated with caution.

It is also possible to argue for a local derivation of the group (b) leucosomes by partial melting of amphibolite. Equilibration with residual hornblende would account for the low Y content (Lambert and Holland, 1974) and the high Na_2O/K_2O ratio (Wyllie, 1977) and is a reasonable interpretation for the two relatively small pods of group (b) leucosome analysed. However, much larger leucosomes, often as large as the older amphibolite bodies they cut, have similar mineralogical compositions to those analysed. Thus the mode of origin suggested for the two analysed samples may not be generally applicable. Furthermore, it is not known to what extent either group of leucosomes may have been modified by sub-solidus exchange with their respective host rocks.

3.4 Geochronology of the basement complex.

3.4.1 Introduction.

Few of the lithologies formed during the earliest recognisable geological events are suitable for application of the Rb-Sr method. The palaeosome of the gneisses is compositionally heterogeneous and the larger leucosomes, in which isotopic equilibrium might be expected are small in size and have a complex post-emplacement history of deformation and recrystallisation. In spite of their heterogeneous nature (see above) the nebulitic migmatites (Section 3.2.2) represent the largest bodies that might be expected to have reached isotopic equilibrium during the main episode of migmatisation. Second generation leucosome cuts the nebulites but is volumetrically small (10% at outcrop at most). The nebulites were sampled from an area north of Hälleviksstrand (the "Hällevikstrand granite") part of which was mapped by Park et al. (op. cit.) as a discrete body of granite. Samples outside this area represent a similar lithology but in which the proportion of inhomogeneous nebulite is greater and where the nebulites frequently grade into discretely banded migmatites.

3.4.2 Sampling.

Ten whole-rock samples of nebulitic migmatite (Appendix B1) were collected from an area (ca. 2 $Km.^2$) near Hällevikstrand in western Orust (Figs. 3.1, 3.10 and Map). Samples were collected so as to be as nearly homogeneous as possible. Heterogeneities arise as follows: from the presence of inclusions of psammite and biotite schlieren (925, 926, 927, 929); and from the presence of small (up to 2 cm. across) patches and impersistent bands of leucosome, which is sometimes stictolithic (Section 3.2.2.2) (925, 926, 927, 928, 929, 930). All samples weighed ca. 5 Kg. Sample 948 was collected by A. I. Bailey. The samples are described in Appendix B1.

3.4.3 Isotopic data and interpretation.

All ten samples have been analysed for Rb/Sr and $^{87}Sr/^{86}Sr$. The data are presented in Table 3.4 and plotted on a Nicolaysen diagram in Fig. 3.9.

Table 3.4

Rb-Sr analytical data: Hälleviksstrand granite

Sample	Rb (ppm)*1	Sr (ppm)*1	Rb/Sr*2	$^{87}Rb/^{86}Sr$ *2	$^{87}Sr/^{86}Sr$*3
923	129	153	0.841	2.440	0.76468 ± 3
924	154	115	1.331	3.880	0.78567 ± 3
925	157	140	1.116	3.250	0.77390 ± 5
926	117	127	0.917	2.667	0.76784 ± 2
927	86	171	0.499	1.450	0.74753 ± 8
928	112	202	0.554	1.607	0.74265 ± 3
929	84	119	0.711	2.064	0.74964 ± 3
930	185	127	1.454	4.240	0.79323 ± 6
948	167	126	1.332	3.881	0.78533 ± 6
955	104	144	0.723	2.101	0.76041 ± 4

*1 Errors in Rb and Sr contents estimated at ± 5% (2σ)

*2 Errors in Rb/Sr and $^{87}Rb/^{86}Sr$ estimated at ± 2% (2σ)

*3 $^{87}Sr/^{86}Sr$ values are normalised to $^{88}Sr/^{86}Sr = 8.37521$

Quoted errors are 2σ based on "in run" statistics.

Fig. 3.9

Nicolaysen diagram (a plot of $^{87}Sr/^{86}Sr$ vs. $^{87}Rb/^{86}Sr$) for ten samples of the Hälleviksstrand granite (Table 3.4). The data are poorly correlated (MSWD = 104.1). The best fit line (not plotted) corresponds to an "age" of 1298 $\pm$ 28 m.y. and an initial $^{87}Sr/^{86}Sr$ ratio of 0.7166 $\pm$ 9. No geological age significance may be attached to this line. The overall scatter of the data may be the result of (1) incomplete equilibration during the main (pre-D1) migmatisation or (2) disturbance of the isotopic systems during the second (post-D1, pre-D2) migmatisation, or (3) disturbance during later metamorphism. The dashed line was fitted to six points (924, 925, 928, 929, 930, 948) and is one of a number of co-linearities on the diagram. The corresponding age (1338 $\pm$ 41 m.y. (MSWD = 3.38)) is consistent with partial equilibration during (2) above. However, it is not possible to distinguish between (1)-(3) as explanations for the open system behaviour in the Hällevikstrand granite and the isotopic data do not place any precise constraint on the age of either migmatisation.

Fig. 3.10

Locations of the ten samples of the Hällevikstrand granite (plotted on Fig. 3.9) analysed for Rb-Sr geochronology. The dashed line encloses an area of "granite", mapped by Park et al. (op. cit.). Within this area the development of nebulitic migmatite is continuous. In the surrounding area the nebulitic migmatite grades into banded migmatites. The boundary shown is gradational.
The figured area is located on Fig. 3.1.

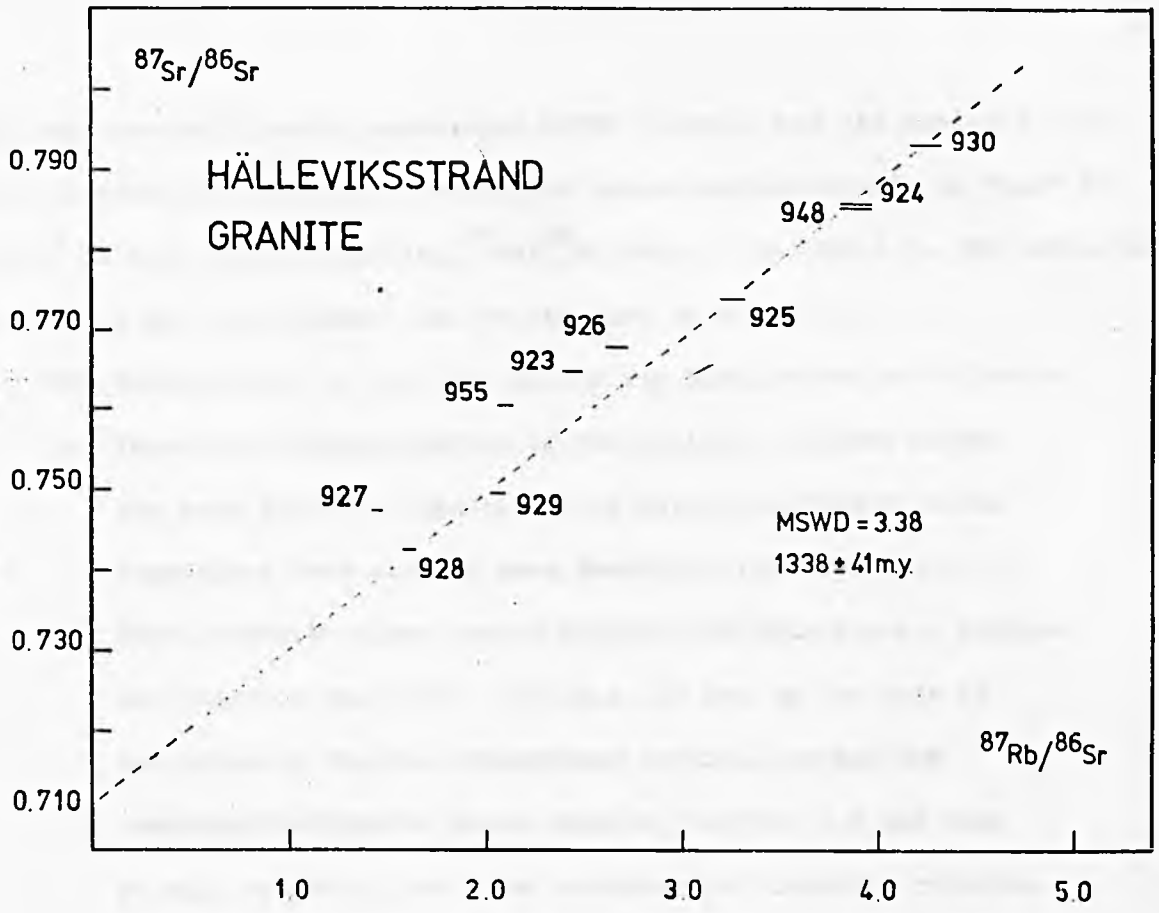
$^{87}Sr/^{86}Sr$
HÄLLEVIKSSTRAND
GRANITE
0.790
0.770
0.750
0.730
0.710
930
924
948
925
926
923
955
927
929
928
MSWD = 3.38
1338 ± 41m.y.
$^{87}Rb/^{86}Sr$
1.0
2.0
3.0
4.0
5.0

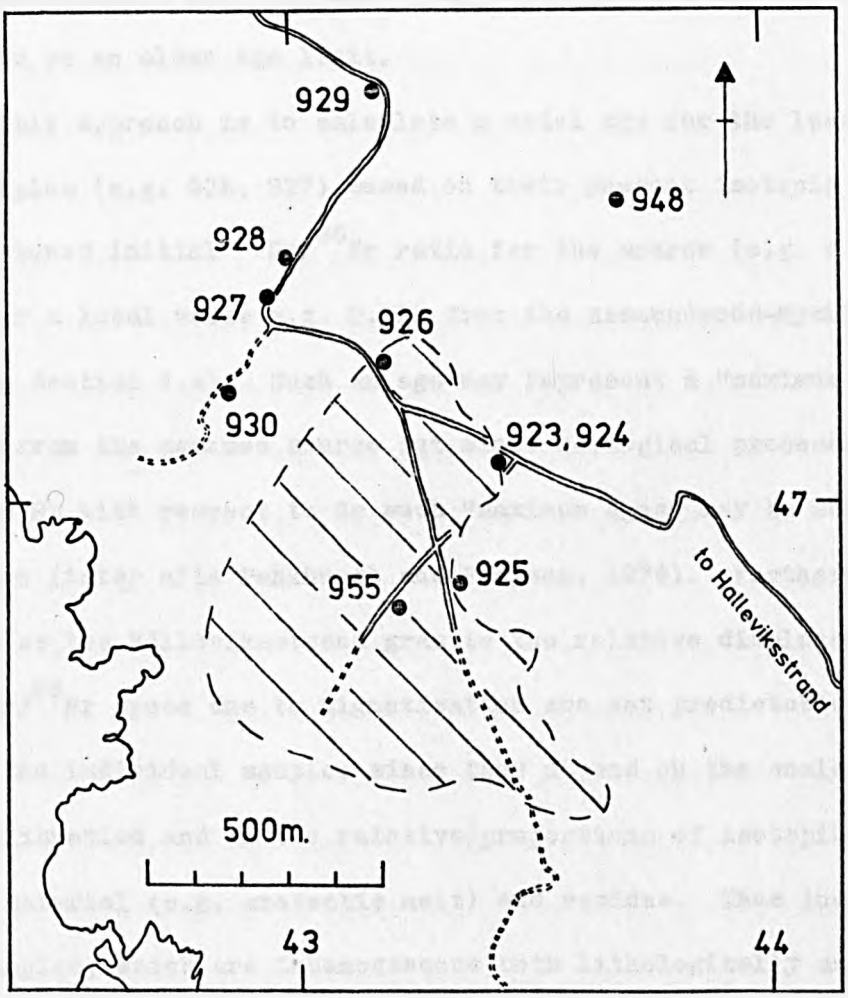
929
948
928
927
926
930
923, 924
47
955
925
to Hallevikssstrand
500m.
43
44

The data are only poorly correlated (MSWD = 104.1) and the best-fit line (not plotted) to the broad envelope of points corresponds to an "age" of 1298 ± 28 m.y. with an initial $^{87}Sr/^{86}Sr$ ratio of 0.7166 ± 9. No definite geological age significance can be attached to this line.

The wild scatter of the data points may have arisen as follows:-

1. Incomplete homogenisation of the isotopic systems during the main (pre-D1) migmatisation: heterogeneities in these migmatites have already been described (Section 3.2.2.2). This mechanism alone cannot explain the data since a younger age limit of ca. 1350 - 1450 m.y. is set by the ages of intrusion of the Hällevikstrand amphibolite and the Assmunderöd-Myckleby augen granite (Section 4.4 and Daly et al., op. cit.) and thus considerable clockwise rotation of the data points in $^{87}Rb/^{86}Sr$ - $^{87}Sr/^{86}Sr$ space during later events is implied. This and the observed scatter of the data points does not allow any useful constraint to be placed on an older age limit.

One possible approach is to calculate a model age for the least radiogenic samples (e.g. 928, 927) based on their present isotopic composition and an assumed initial $^{87}Sr/^{86}Sr$ ratio for the source (e.g. a mantle value, 0.702 or a local value e.g. 0.713 from the Assmunderöd-Myckleby augen granite, Section 4.4). Such an age may represent a "maximum age" of derivation from the assumed source but since geological processes tend to fractionate Rb with respect to Sr such "maximum ages" may be subject to underestimation (inter alia Pankhurst and Pidgeon, 1976). Furthermore, in such a system as the Hällevikstrand granite the relative displacements in Rb/Sr and $^{87}Sr/^{86}Sr$ space due to migmatisation are not predictable with reference to the individual samples since they depend on the scale of isotopic equilibration and on the relative proportions of isotopically equilibrated material (e.g. anatectic melt) and residue. Thus individual whole rock samples, which are inhomogeneous both lithologically and

isotopically may have moved toward either higher or lower model ages.

2. Disturbance of the isotopic systems during the second (post-D1, pre-D2) migmatisation. This event has an older age limit of ca. 1450 m.y. to 1350 m.y. and a younger age limit of ca. 1060 m.y. (post-dyke (Sveconorwegian) metamorphism, Chapter 5). Six samples (924, 925, 928, 929, 930, 948) define an "errorchron" (MSWD = 3.38) corresponding to an "age" of 1338 $\pm$ 41 m.y. and an initial $^{87}Sr/^{86}Sr$ ratio of 0.711 $\pm$ 1. Isotopic equilibrium at this time would be consistent with the geological and geochemical evidence (e.g. Fig. 3.4) but the latter is open to question (see above).

3. Disturbance of the isotopic systems during later metamorphism (e.g. during the Sveconorwegian). Porphyroblastic growth of microcline of uncertain age and post-tectonic crystallisation of fine-grained muscovite (both phases have high Rb/Sr ratios) have previously been noted (Section 3.2.2.2, Plate 3.3.M, Appendix B1). The modal proportion of muscovite is, however, not generally correlated with position on the Nicolaysen diagram (Fig. 3.9) except in the case of 930 which has the highest modal abundance and the highest Rb/Sr ratio (and hence highest $^{87}Rb/^{86}Sr$).

It is not possible, on the present evidence, to discriminate between these possible mechanisms, nor to decide upon their relative importance. The present data is not in conflict with Pedersen's evidence (quoted in Hageskov, op. cit.) for an age of ca. 1900 m.y. for migmatitic gneisses in the Norwegian sector of the Stora Le - Marstrand belt nor with the apparently less reliable data of Welin and Gorbatschev (1978b) which suggests a younger age limit for the migmatitic gneisses of ca. 1500 -

1600 m.y. However, it can in no way be said to substantiate the conclusions of either worker. Their data is discussed above in Section 1.3.

CHAPTER 4. The pre-dyke intrusive rocks.

4.1 Introduction.

In this chapter are discussed a variety of rocks which intrude the basement complex (Chapter 3) after the D1 deformation and the first migmatisation and before the emplacement of the dyke suite (Chapter 5). These intrusives span the period of the second migmatisation and the later D2 deformation. The compositional range from basic to granitic is represented and the intrusions take a variety of forms and sizes.

Basic compositions are subordinate and are confined to two small bodies, one ca. 1 $Km.^2$ in area (the Hällviksstrand amphibolite) at Hällviksstrand in western Orust and the other much smaller at Henån in north-eastern Orust (see Map). The Hällviksstrand amphibolite is cut by small bodies of grey granite (Park et al., op. cit.) which occur throughout the area. Both are cut by second generation migmatitic leucosome (Section 3.2.2) and were subsequently deformed during the D2 deformation.

The largest of the pre-dyke intrusive rocks are augen granites which form a belt extending from north-eastern Orust through southern Orust into Tjorn. This belt is referred to as the Assmunderöd-Myckleby augen granite (see Map). Another large body, assumed to be of the same age, occurs north of Orust in the Skaftölandet - Dragsmark area (the Källviken augen granite). Both augen granites are locally affected by minor migmatitic leucosome, correlated with the second migmatisation.

The above rocks (with the possible exception of the Källviken augen granite) are post-dated by members of the younger granites suite (Park et al., op. cit.). These rocks are not migmatised and take the form of narrow (usually less than 5 m. wide) sheets which cut the older intrusive rocks and the D2 fold structures. They occur throughout the Orust area with an apparent concentration in the west.

In this chapter geochemical and geochronological data are presented for the Hällviksstrand amphibolite, the Assmunderöd-Myckleby augen granite and the younger granites.

4.2 Geology and petrography.

4.2.1 The Hällevikstrand amphibolite.

The Hällevikstrand amphibolite is a composite intrusive body of basic to intermediate composition. It forms an outcrop ca. 1 Km.^{2} in area at Hällevikstrand on the west coast of Orust (Figs. 4.1, 4.13 and Map). The intrusion cuts the pre-D1 migmatitic banding and the D1 mineral fabric in the para-gneisses and older amphibolites and is itself cut by grey granite (Section 4.2.2) and by the second generation migmatitic leucosome (Plate 4.1 and Section 3.2.2). Inclusions of mafic to ultramafic amphibolite, similar to the older amphibolites, are common (Plate 4.2). In addition the body is deformed by F2 folding with a locally developed axial-planar hornblende-biotite mineral fabric and subsequently cut by sheets of the younger granites suite (Plates 4.1 and 4.2). Thus the emplacement of the Hällevikstrand amphibolite is an important chronological marker.

The amphibolite is petrographically variable. The mean grain size varies from 2 mm. to 4 mm. but some porphyroblastic hornblendes are up to 6 mm. in length. There is a gradational relationship between a dark green ultramafic hornblendite which occurs in the western part of the body and the more common grey-green mafic amphibolite. A mesocratic variety has a clotted appearance due to the presence of biotite and hornblende porphyroblasts.

In addition to polygonal hornblende, which may make up more than 95% of the mode, the medium to coarse-grained ultramafic portions of the body contain small amounts of opaque ores, quartz and sericitised plagioclase, and of interstitial calcite and chlorite.

The mafic amphibolite is generally less coarse-grained and contains hornblende (40-80%), plagioclase ca. An 30 (including fine-grained epidote and sericite, up to 20%) and quartz (up to 10%). Opaque ores, sphene, apatite and allanite occur in accessory amounts. Poikiloblastic hornblende encloses rounded grains of opaque ore, sphene, quartz and epidote and in some cases hornblende has grown later than biotite. Hornblende and biotite

Plate 4.1 Photograph to illustrate a heavily migmatised part of the Hällevikssstrand amphibolite. Locality: west coast of Orust, south of Hällevikssstrand (44, 44). The smaller blebs of leucosome (second generation) have basified margins. Hammer head rests on a narrow (3 cm. wide) dyke of leucocratic younger granite. Hammer measures 80 cm. x 16 cm.

Plate 4.2 Photograph to illustrate the more typical lithology of the Hällevikssstrand amphibolite from which the analysed samples were collected. The amphibolite has disrupted a small (20 cm. long) xenolith of ultramafic amphibolite, possibly an "older amphibolite". Large (30 cm. across) leucocratic body at bottom right is a folded leucosome in the core of an F2 fold. The associated axial planar (S2) hornblende-biotite fabric in the amphibolite is seen at top right. At Clinometer a narrow dyke of younger granite (4 cm. wide) cuts the Hallevikssstrand amphibolite, the amphibolite xenoliths and the migmatitic leucosome. Clinometer measures 10 cm. x 6 cm.

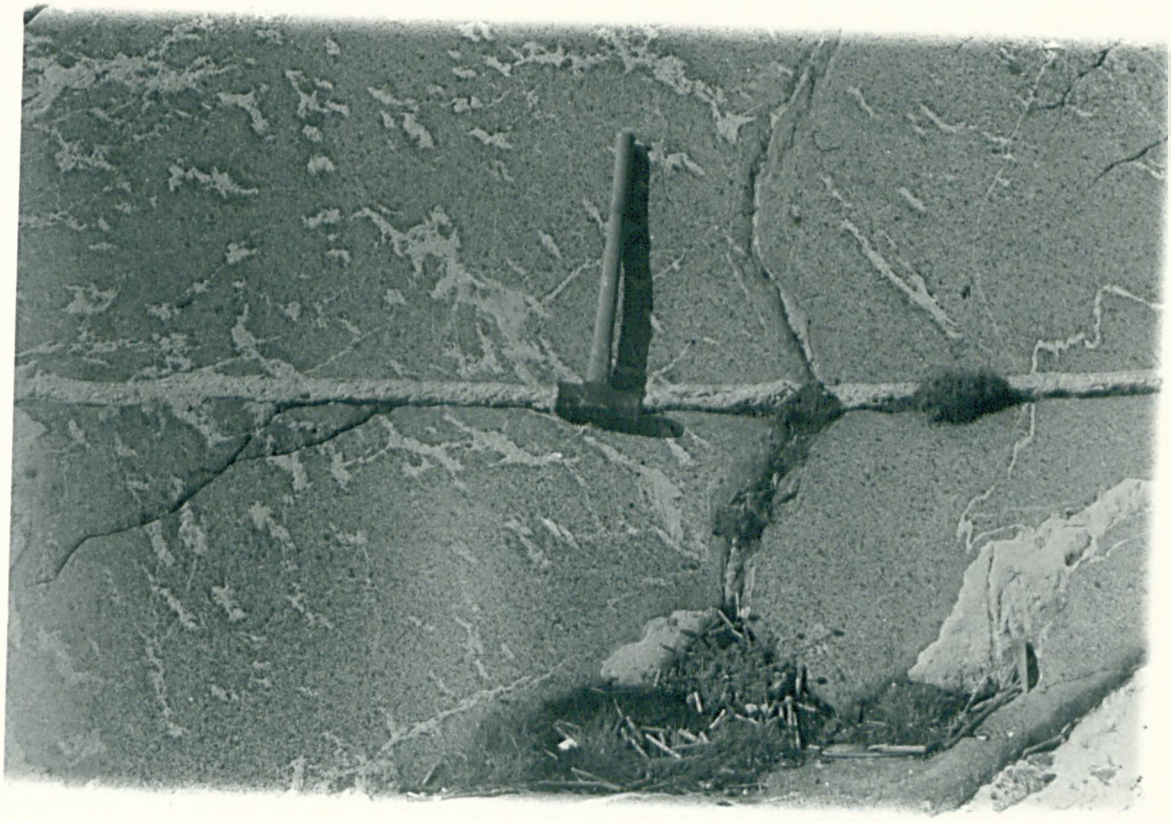

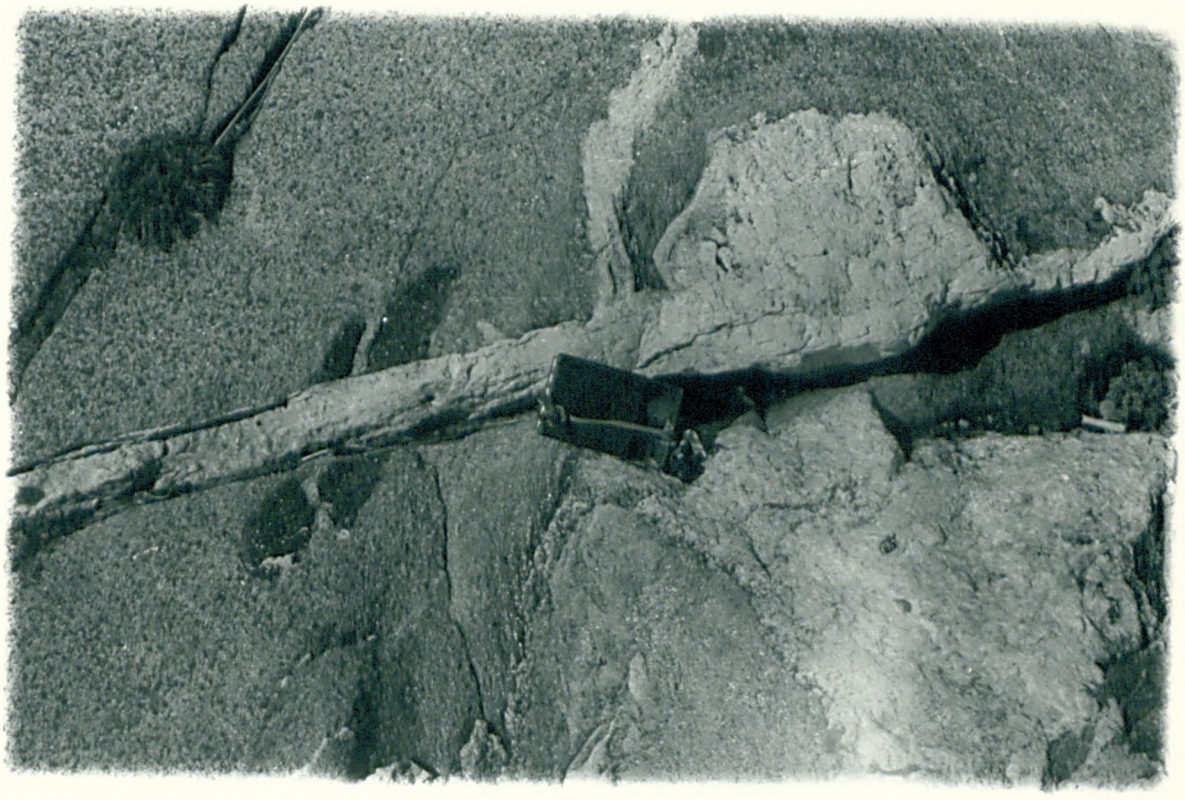

occurring in textural equilibrium define the syn-D2 mineral fabric. Together with plagioclase (ca. An 30) the assemblage implies an amphibolite grade metamorphism (Winkler, 1974).

Epidote group minerals vary considerably in their mode of occurrence and modal abundance. An earlier generation of epidote encloses grains of allanite and these composite grains are overgrown by biotite. This generation of epidote is pre-D2 in age. A more common variety, best developed where the hornblende-biotite fabric is absent and whose age is consequently uncertain, is probably related to the post-dyke (Sveconorwegian) metamorphism or to later retrogression. Commonly epidote replaces plagioclase and in extreme cases, in the mesocratic portions of the body, the replacement is almost complete, and biotite, epidote and quartz make up the bulk of the rock. Locally epidote and sometimes chlorite replace biotite.

The second generation migmatitic leucosome cuts the body (Plate 4.1) and occurs as blebs and pods varying in size from ca. 1 cm. to ca. 5 cm. and is similar in composition to the pegmatitic leucosomes which cut the older amphibolites. The plagioclase composition (ca. An 10) is considerably more albitic than that of the host rock (ca. An 30). Some examples have basified margins enriched in hornblende and biotite relative to the host (Plate 4.1). Larger irregular bodies of leucocratic granite (s.l.), a few m. in length, also cut the amphibolite (Plate 4.2) but their relationship to the discrete leucosomes is ambiguous. In places these larger bodies appear to feed smaller offshoots of migmatitic leucosome but elsewhere they cross-cut them. Some of these large bodies contain xenoliths of migmatitic para-gneiss. Both kinds of granitic material are folded by the D2 deformation and subsequently the amphibolite was cut by sheets of the younger granites suite (Plates 4.1 and 4.2).

Finally, a number of veinlets, usually 1 mm. or less in width, cut the amphibolite. These are undeformed and their precise age is not known. They contain quartz, clinozoisite and plagioclase in varying proportions.

In addition a small amount of pyrite was identified in one vein. These veins, together with the second generation migmatitic leucosome are investigated further in Section 4.4 where their effects on the Rb-Sr systematics are considered.

4.2.2 The grey granites.

The grey granites vary in composition from tonalitic to granodioritic and take a variety of forms. They occur as narrow (few cm. wide) sheets and larger (several metres wide) irregular bodies. They cut the pre-D1 migmatitic leucosome in the para-gneisses and also cut and agmatise the Hällevikssstrand amphibolite (Section 4.2.1). In many places they are concordant to the migmatitic banding and are difficult to distinguish from unmigmatised psammite. The grey granites are in turn cut by the second generation leucosome in the form of narrow (few mm. wide) diktyonitic veins and by larger (up to several m. wide) bodies of pegmatitic leucosome.

The grey granites occur sporadically throughout the Orust area. In the west where they have been described by Park et al. (op. cit.) they frequently contain large (up to 50 cm. long) xenoliths of the country rocks they intrude (e.g. angular blocks of psammite and older amphibolite). They also contain smaller (few cm.) biotite-rich inclusions with diffuse margins.

The rocks are medium-grained (ca. 1 mm. average grain size) and contain quartz (20-30%), plagioclase ca. An 15 (55-65%) and micas (10-15% with biotite in excess of muscovite. Microcline and garnet occur in small amounts and accessories include apatite, zircon, allanite and opaque ores. Epidote, sericite, calcite and chlorite occur as alteration products.

4.2.3 The Assmunderöd-Myckleby augen granite.

A belt of coarse-grained grey-red gneissose augen granites, which vary in composition from granitic to granodioritic, extends from north-eastern Orust southwards to the island of Tjörn (see Map). The term "Assmunderöd-Myckleby augen granite" is used in reference to the entire outcrop of augen granite on Orust (ca. 80 $Km.^2$) and is adapted from Berthelsen and Murthy (1970). In an account of the structure, including a brief description of

the petrography, these authors distinguished a northern body (Assmunderöd) which is separated from the northern (Myckleby) part of the main body of augen granite by a septum of migmatitic para-gneiss. Bergström (1963) described the continuation of the augen granites on Tjörn to the south.

The augen granites are petrographically heterogeneous but they are considered together because the field evidence suggests that they were emplaced penecontemporaneously. The western contact of the augen granites and the country rocks has been mapped from the area covered by Berthelsen and Murthy (op. cit., and see Map and Fig. 4.15) southwards to Varekil where the north-western boundary has been displaced sinistrally along a zone of shearing. West of Varekil the contact runs east-west to the vicinity of Tvet where it swings southwards towards Tjörn. The eastern contact has been mapped from Slussen to Varekil. Boundaries between the compositional types of augen granite appear to be gradational and have not been mapped in detail. Some of the petrographic and lithological variation is indicated on the Map. Berthelsen and Murthy (op. cit.) mapped a leucocratic augen-free muscovite-biotite alkali granite at the margin of the Assmunderöd body. Xenoliths of similar composition occur in a matrix of "normal" biotite-rich augen granite at Kleya, near the centre of the body (Plate 4.3). If this may be taken to imply relative age of emplacement it is the only such evidence observed over the entire augen granite outcrop.

Bulk mineralogical variation in the augen granites is largely controlled by the relative proportions of plagioclase and K-feldspar (usually microcline). The augen granites contain quartz (30-40%), feldspars (50-60%) and biotite (up to 15%). The majority of samples have K-feldspar and plagioclase in approximately equal proportions. Muscovite is a minor constituent where present and in many cases it replaces biotite. Garnet, sphene, apatite, zircon, epidote/allanite intergrowths and opaque ores occur as accessories. Sericite and chlorite occur as alteration products. Fluorite occurs interstitially to microcline and quartz in one example. Hornblende and minor biotite together make up 15% of the mode in a coarse-grained variety of the granite

Plate 4.3 Photograph to illustrate a xenolith of garnet-bearing leucocratic granite in biotite rich augen granite Assmunderöd body at Kleya (6, 59). Hammer measures 80 cm. x 16 cm.

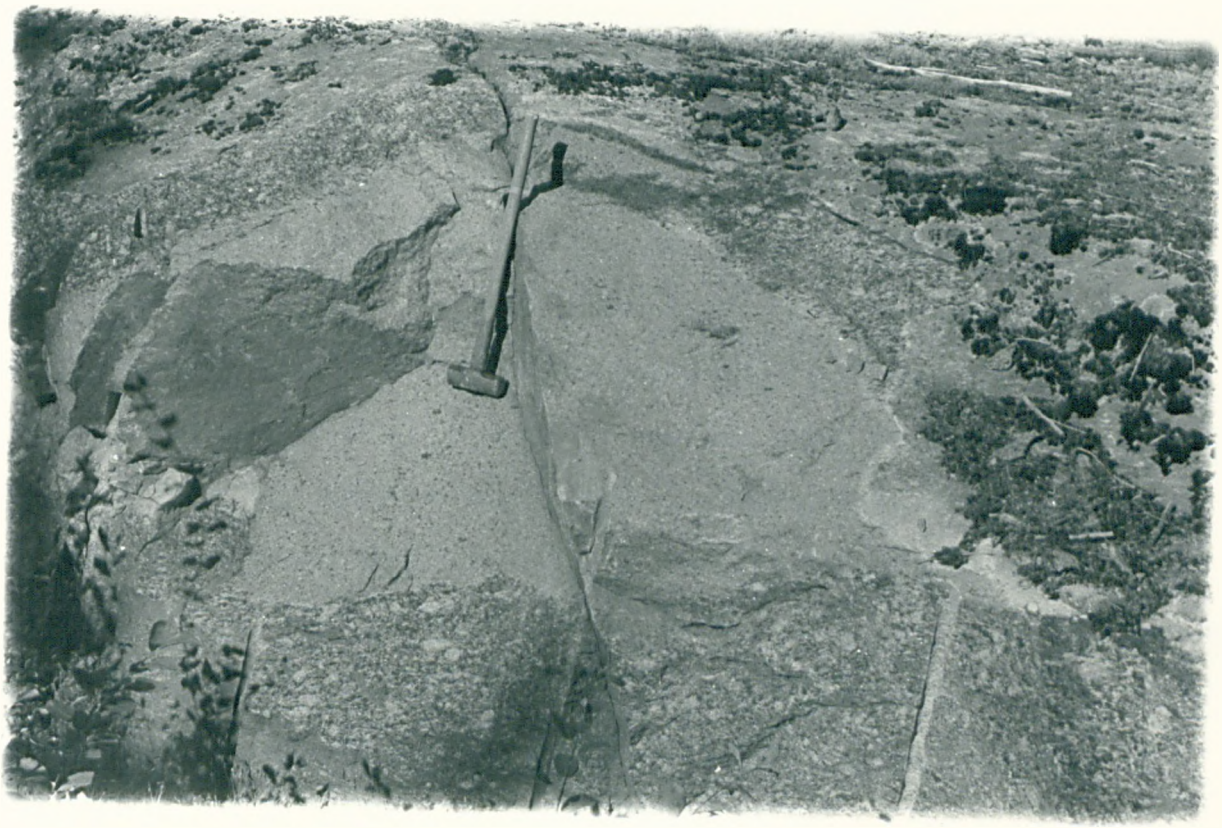

which outcrops over a ca. 3 Km.^{2} area west of Varekil. This augen-free rock grades into the surrounding biotite-bearing augen granites.

The augen composition is variable. The dominant type consists of aggregates (glomeroblasts) of quartz, plagioclase and K-feldspar. Glomeroblasts of quartz + plagioclase and quartz + K-feldspar also occur. Single-crystal augen of microcline occur sporadically. In places where deformation is least intense (e.g. near Lagmansholmen in south Orust), microcline augen have albite rims. Albite commonly rims sericitised plagioclase in the glomeroblastic augen and in some cases microcline replaces plagioclase. Myrmekite is locally abundant.

The augen vary in colour from light grey to brick-red as determined by the colour of the K-feldspar. There is some geographical variation in colour. Over most of the outcrop the augen granite is pink to red in colour but over a large area between Myckleby and Varekil grey colours predominate. Reddening of the K-feldspar develops within short distances (a few cm.) of purely grey varieties and the controlling process is not known. The larger augen (greater than 3 cm. across) and the mono-crystalline variety tend to be red as do the strongly lineated and sheared augen rocks.

The augen are set in a biotite matrix and there is considerable variation in their shape and size. The augen shape is mainly controlled by the biotite foliation but lineated augen rocks also occur. The augen vary in size from 0.5 cm. to 4 cm. across the foliation but may be up to 10 cm. measured along the lineation. Some augen have a porphyroclastic or glomeroclastic origin and mortar textures are developed.

In addition to rare inclusions of leucocratic granite (Plate 4.3) the augen granites contain xenoliths of psammitic, semi-pelitic and mafic gneiss which vary in size from a few cm. to several metres (Plate 4.4). In places, such xenoliths make up 40% of the outcrop area. Many of the larger bodies resemble the country rocks and are locally migmatised. Microcline porphyroblasts occur in some examples (Plate 4.5). Many of the xenoliths show clear evidence of assimilation and ablation and there is a depletion in

Plate 4.4 Photograph to illustrate xenoliths in the Assmunderöd-Myckleby augen granite. Locality: Rasson (56, 44). Narrow (few cm. wide) xenoliths of psammite and biotite rich pelite extend for several metres parallel to the biotite foliation in the augen granite. At lower left a wider (30 cm. wide) body of migmatised interbanded psammite-semipelite occurs. Microcline porphyroblasts develop preferentially in the more pelitic bands.
Hammer measures 80 cm. x 16 cm.

Plate 4.5 As Plate 4.4., same locality. Closer view of a semi-pelitic xenolith with microcline porphyroblasts undergoing assimilation into the granite. Augen in the granite occur up to 3 cm. across.
Hammer measures 80 cm. x 16 cm.

semi-pelitic compositions relative to the country rocks perhaps reflecting the relative ease of assimilation of the pelite component in the magma. Unmigmatised silicic and mafic inclusions also occur and the mafic variety grade in size down to biotite schlieren.

The relative age of emplacement of the augen granite is difficult to assess in the field. Generally the contacts with the migmatitic gneisses are conformable and on outcrop scale they are controlled by the effects of the D4 deformation. In consequence, flat-lying or variably-dipping interleaved contacts are common (Plate 4.6) and at least some of the lineation observed is parallel to F4 fold axes. However, in a number of places (e.g. at Slussen, Ödsmål and Lagmansholmen) the augen granite clearly cuts the migmatitic banding in the gneisses and a concordant biotite fabric whose age is not known precisely.

The augen granites are cut by at least three generations of later granites. Discrete fine-grained leucocratic sheets, up to 10 cm. across, cut across the augen foliation but are penetrated by biotite growing parallel to the main foliation. These minor sheets may represent late-stage sheets of aplitic material associated with the emplacement of the augen granite magma. Secondly, the augen granite is affected by local developments of migmatitic leucosome correlated with the second generation leucosome in the gneisses (Section 3.2.2). This takes the form of concordant (1 cm. to 3 cm. wide) pegmatite sheets with marked biotite selvedges and also of patches of leucogranite which are locally discordant to the foliation. Bergström (1963) describes similar material which cuts shears in the augen granite on Tjörn. Thirdly, the augen granite and the biotite foliation are cut by sheets of younger granite (Section 4.2.5). The augen granite is also cut by members of the dyke suite (Chapter 5).

With reference to the structural scheme of Park et al. (op. cit.) in western Orust the relative age of the biotite foliation in the augen granite is not known precisely and there is some evidence for a composite origin (above). The main biotite foliation is earlier than the younger granites

Plate 4.6 Photograph to illustrate flat lying contacts of the marginal medium-grained facies of the Assmunderöd-Myckleby augen granite (A) with screens of migmatic para-gneiss (B) and older amphibolite (C). It is not possible to demonstrate that the interleaving is due to F4 folding or parallel injection of the granite. Locality: Slussen (62, 61). Boat's mast is ca. 5 m. high.

Plate 4.7 Photograph to illustrate development of (recrystallised) microcline porphyroblasts in migmatised pelitic bands close to the contact with the Assmunderöd-Myckleby augen granite at Varekil (60, 46). The porphyroblasts overgrow the migmatic banding and are affected by a biotite fabric (probably of D2 age). The crenulations are the result of D4 deformation. Scale bar is 5 cm.


A
B
A
A
B
A
C
B

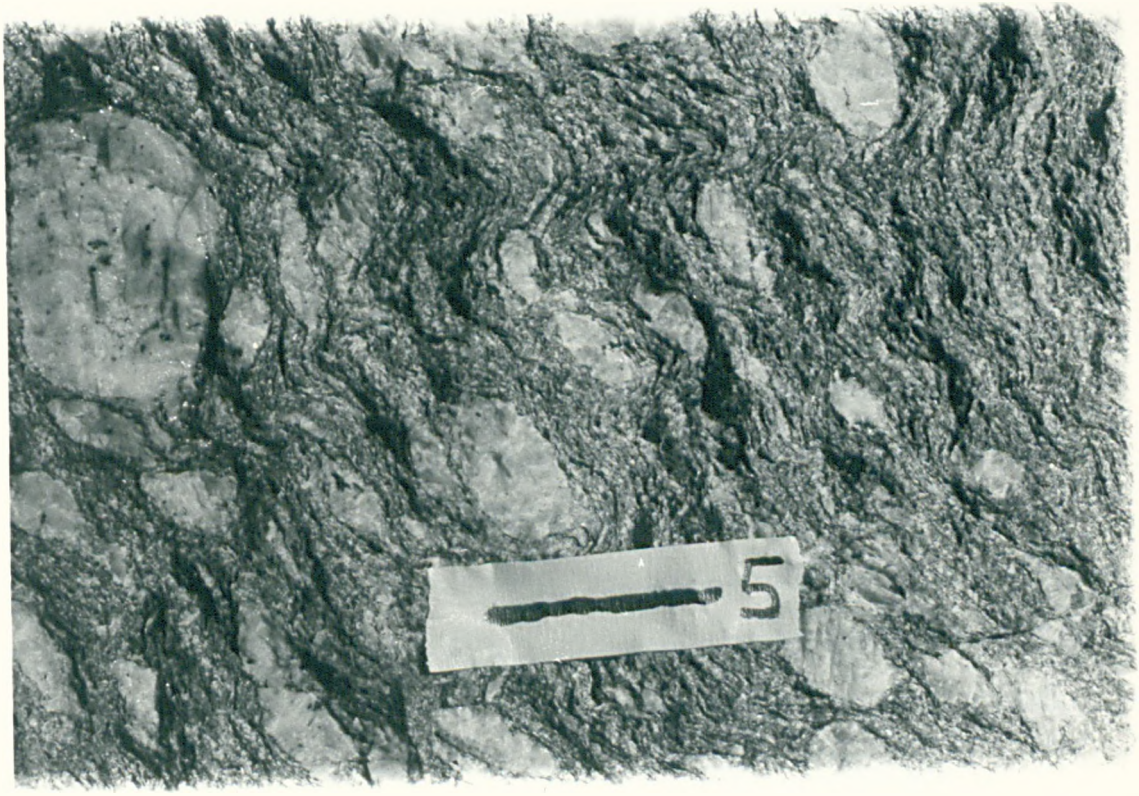
5

(post-D2) and later than the concordant migmatitic banding (pre-D1). The presence of second generation leucosome locally discordant to the foliation suggests that it may be of D1 age. Alternatively it may represent a phase of deformation between D1 and D2 - similar in age to shears in the country rocks which pre-date the second leucosome (Section 3.2.2).

4.2.3.1 Geological evidence for the origin of the Assmunderöd-Myckleby augen granite.

The problem of the origin of the augen granite is complicated by the deformation, extensive metamorphic recrystallisation and the variation in size, shape and composition of the augen. The presence of clearly intrusive contacts and abundant xenoliths suggests a magmatic origin. The augen may have arisen, at least in part, as K-feldspar phenocrysts. Some of the original igneous texture may be preserved in the albite-rimmed microcline augen in some of the least deformed rocks. The glomeroblastic augen and the variation in augen composition may have a largely metamorphic origin.

An alternative origin is suggested by resemblance of much of the augen granite to opthalmitic or pseudo-opthalmitic migmatite structure (Mehnert, op. cit.). If this observation has any genetic significance it implies an emplacement process similar to that argued by Berthelsen and Murthy (op. cit.) viz. - diapiric mobilisation of "basement" (ibid.) or migmatised Stora Le - Marstrand para-gneisses. It is possible that some of the glomeroblastic augen represent pockets of partial melt set in a matrix of residual garnet and biotite.

The variation in composition of the augen does not rule out this possibility and may have arisen in at least two ways: (1) from variation in the initial composition before melting (inter alia Kilinc, 1972) and (2) during subsequent metamorphic recrystallisation. Some of the inclusions may represent residual material after partial melting of the source rocks while others, especially the larger examples, probably represent country rocks incorporated close to the level of emplacement.

It is difficult to distinguish between the two origins outlined above

and the problem is discussed further in Section 4.3.2.

Outside the main body of augen granite (e.g. at Varekil) there are local developments of augen granite usually less than 1 Km.^{2} in area. These patchy developments contain psammitic xenoliths and are at least in part derived by overgrowth of the migmatitic banding in the semi-pelitic gneisses by K-feldspar porphyroblasts. K-feldspar porphyroblasts also locally overgrow the migmatitic banding in the gneisses at the margins of the augen granite (e.g. at Varekil (Plate 4.7) and Svanvik), where they preferentially develop in migmatised semi-pelitic bands. Some of these rocks resemble concordant intrusions of augen granite. These examples probably represent local alkali metasomatism or simply isochemical segregation of K-feldspar and do not necessarily have any bearing on the origin of the main development of augen granite.

4.2.4 The Källviken augen granite.

This body of red gneissose augen granite extends over an area of ca. 20 Km.^{2} centred on Källviken in south-western Bokenäs (Map). The body has been mapped by B. S. P. Moorlock from whom the boundaries on the Map are taken (pers. comm.). In spite of considerable re-mapping of the body, little definitive information on the age of emplacement is available. The contacts with the migmatitic gneisses are often concordant and sometimes faulted. In places the margins are sheared and the strong deformation, reddening and growth of K-feldspar porphyroblasts in the adjacent paragneisses results in locally gradational contacts. No xenoliths of paragneiss have been found in the augen granite but numerous large (50 m. to several Km. long) screens of country rock occur one of which is partly composed of leucocratic gneiss (see Section 3.2.4).

The augen granite is coarse-grained (augen up to 5 cm. long) and commonly strongly deformed. The mineralogy and textures are similar in

many respects to the Assmunderöd-Myckleby augen granite. However, alteration and recrystallisation are much more common. Biotite is strongly chloritised and plagioclase is often heavily sericitised. Reddening of both feldspars is common and brick-red microcline is present at most localities. Epidote is more common than in the Assmunderöd-Myckleby augen granite and in addition to its presence as a localised alteration product of plagioclase, it occurs as veins (a few mm. wide) in zones of intense crushing and alteration.

Biotite defines the augen structure and foliation throughout the body but the fabric is of uncertain age relative to the main fabric in the migmatitic para-gneisses.

Near Källviken, narrow zones (a few cm. wide) of near vertical shearing, which displace the biotite foliation in a transition zone between augen granite and migmatitic para-gneiss, are cut by bands of coarse pegmatitic leucosome. The shears are similar to those described in eastern Orust (Section 3.2.2) and consequently the leucosome is correlated with the second generation migmatisation. No migmatisation has been seen within the augen granite proper. No younger granites or members of the dyke suite have been observed to cut the augen granite, but both of these occur only rarely in the surrounding para-gneisses. Although the evidence is much less satisfactory than for the Assmunderöd-Myckleby augen granite the relative age is probably the same and certainly there is no evidence which conflicts with this view.

4.2.5 The younger granites.

Dykes and sills of the younger granites suite post-date the D2 deformation and cut both generations of migmatitic leucosome in the gneisses (Plate 4.8). They also cut the Hällevikstrand amphibolite (Plates 4.1 and 4.2) and the Assmunderöd-Myckleby augen granite. The younger granites are in turn cut by members of the dyke suite (Chapter 5).

The sheets of younger granite vary in width from a few cm. to five

Plate 4.8 Photograph to illustrate a composite younger granite dyke. At left the dyke cuts a large (several m. long) body of second generation pegmatitic leucosome.
Locality: Pilgrimmen (41, 50).
Hammer is 80 cm. long.

Plate 4.9 Photograph to illustrate the (1 cm. to 5 cm. wide) leucocratic pegmatitic margin to a medium-grained younger granite dyke which cuts the migmatitic banding in the para-gneisses.
Locality: Pilgrimmen (41, 49).
Crow bar measures 40 cm.

metres. The majority are 1 m. to 2 m. thick and typically may be followed for several tens of metres. One body in south-eastern Härmanö extends for 1.5 Km. (see Park et al., op. cit.). Some of the granite sheets are composite (Plate 4.8) and subtle colour-banding is a common feature. The composition varies from tonalite to alkali granite but the majority are granodiorites. Similar minor intrusions of granite are recorded on Tjörn by Bergström (op. cit.) and in north-eastern Orust by Berthelsen and Murthy (op. cit.). The younger granites have been found throughout the investigated area (Map) but there appears to be a greater concentration in western Orust within the area mapped by Park et al. (op. cit.). However, the regional distribution of such small bodies as these is difficult to assess and the apparent concentration in western Orust may result at least in part from better exposure there.

The tonalitic rocks are medium-grained (ca. 1 mm. average grain size), dark grey in colour and contain quartz (20-30%), plagioclase ca. An 10-20 (40-50%), biotite and muscovite (together 15-20%). Accessories are apatite, sphene, zircon, opaque ores and garnet. The last mineral occurs as skeletal grains with euhedral or subhedral outlines (Plate 4.1.M) and is possibly of igneous origin. Plagioclase is typically sericitised and sometimes replaced by epidote and muscovite. Biotite and garnet are chloritised in some examples.

The majority of the more leucocratic rocks vary in composition from granodiorite to adamellite. A small number of alkali granites also occur. The granodiorites contain quartz (25-35%), plagioclase An 20-30 (35-55%), K-feldspar (5-15%), biotite and muscovite (together ca. 20%). Generally biotite exceeds muscovite in amount and chlorite, replacing biotite, may comprise up to 15% of the mode. Epidote occurs in minor amounts in association with biotite and, together with sericite and muscovite, locally replaces plagioclase. Apatite, sphene, garnet and zircon occur in accessory amounts.

Granular textures are typical of these medium-grained rocks (mean grain size 1 mm. to 3 mm.). The extent of modification of the igneous textures by the first deformation in these rocks (D3) is variable. Randomly oriented

Plate 4.1.M Photomicrograph to illustrate skeletal garnet with euhedral outline in sample GP 3 (tonalite). Plagioclase, quartz and biotite are also present. X 55. XN.

Plate 4.2.M Photomicrograph to illustrate anhedral garnet containing inclusions quartz and sphene (centre of garnet grain). Plagioclase porphyroblast occurs at top right, plagioclase, quartz and muscovite are present in the matrix. X 55. XN.

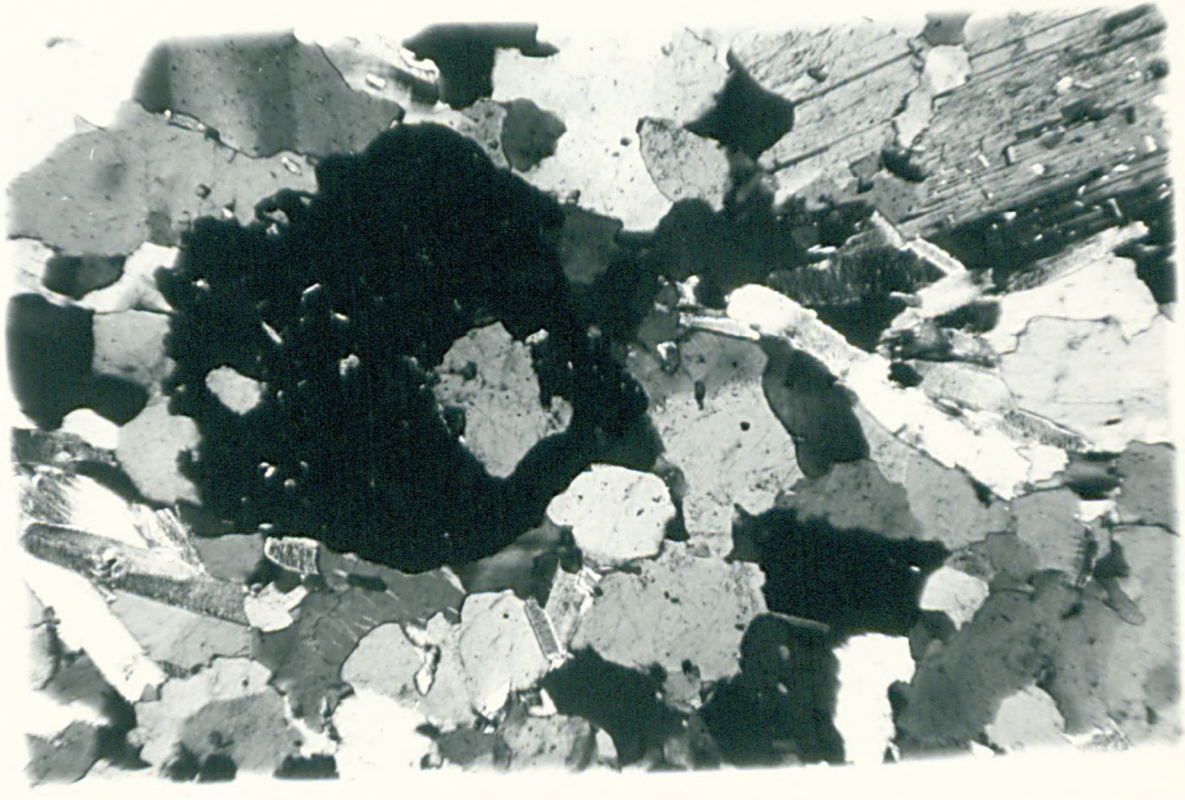

muscovite and biotite, which may have a magmatic origin are both locally overgrown by the syn-D3 mica fabric. Some rocks are thoroughly recrystallised during D3 and others are further modified by post-D3 cataclasis. Garnet in these rocks is anhedral and typically contains numerous inclusions of biotite, quartz and sphene (Plate 4.2.M). Some of the granodiorites have bimodal grain size distribution with large (up to 1 cm.) plagioclases (phenocrysts?), sometimes normally, sometimes complexly zoned (Plate 4.3.M), set in a granular matrix of quartz, K-feldspar, plagioclase and micas. Locally K-feldspar replaces plagioclase and in one example isolated megacrysts of K-feldspar (up to 2 cm. in length), with cataclastic margins, overgrow the syn-D3 biotite fabric. Myrmekite is locally developed in these rocks.

Some of the more leucocratic adamellitic to alkali-granitic rocks have pegmatitic margins (Plate 4.9) sometimes containing large (several cm. long) megacrysts of K-feldspar aligned perpendicular to the contacts. Some leucogranites have patchy developments of pegmatite while others have margin-parallel pegmatitic centres usually a few cm. in width. These pegmatitic alkali-rich portions of the younger granite sheets generally have lower mica contents than the darker rocks and muscovite exceeds biotite in amount.

Plate 4.3.M Photomicrograph to illustrate zoned plagioclase in a sample (SJ 920) of granodiorite from the Roparen younger granite sheet X 55. XN.

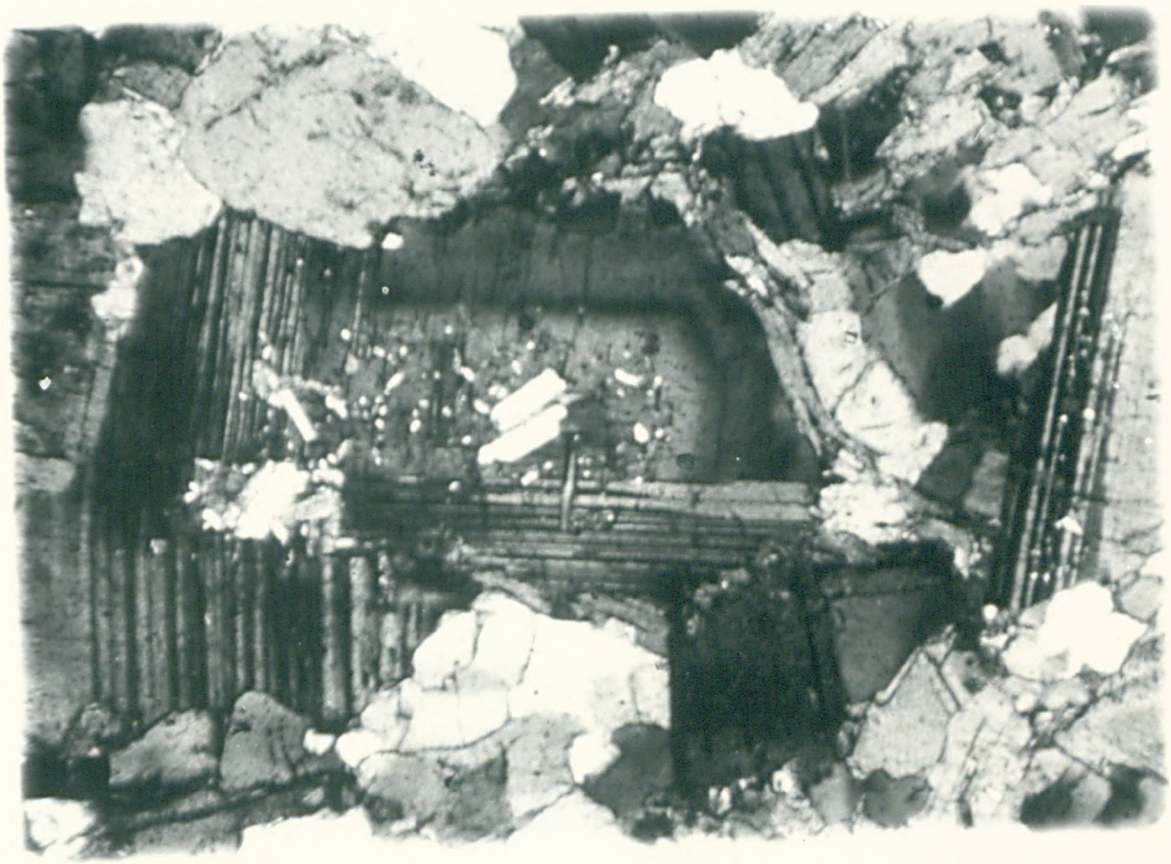

Fig. 4.1 Geological map of western Orust taken from Park et al. (op. cit.), showing the locations of samples of the Hällevikssstrand amphibolite (□) and the younger granites suite (•). The boxed area is shown on Fig. 4.13.
Inset shows the location of the Orust area and the main tectonic and lithological divisions of part of the Sveconorwegian province. A = Åmål belt, B = Bohus granite, D = Dal Group, SLM = Stora Le - Marstrand belt, P = Pregothian belt.

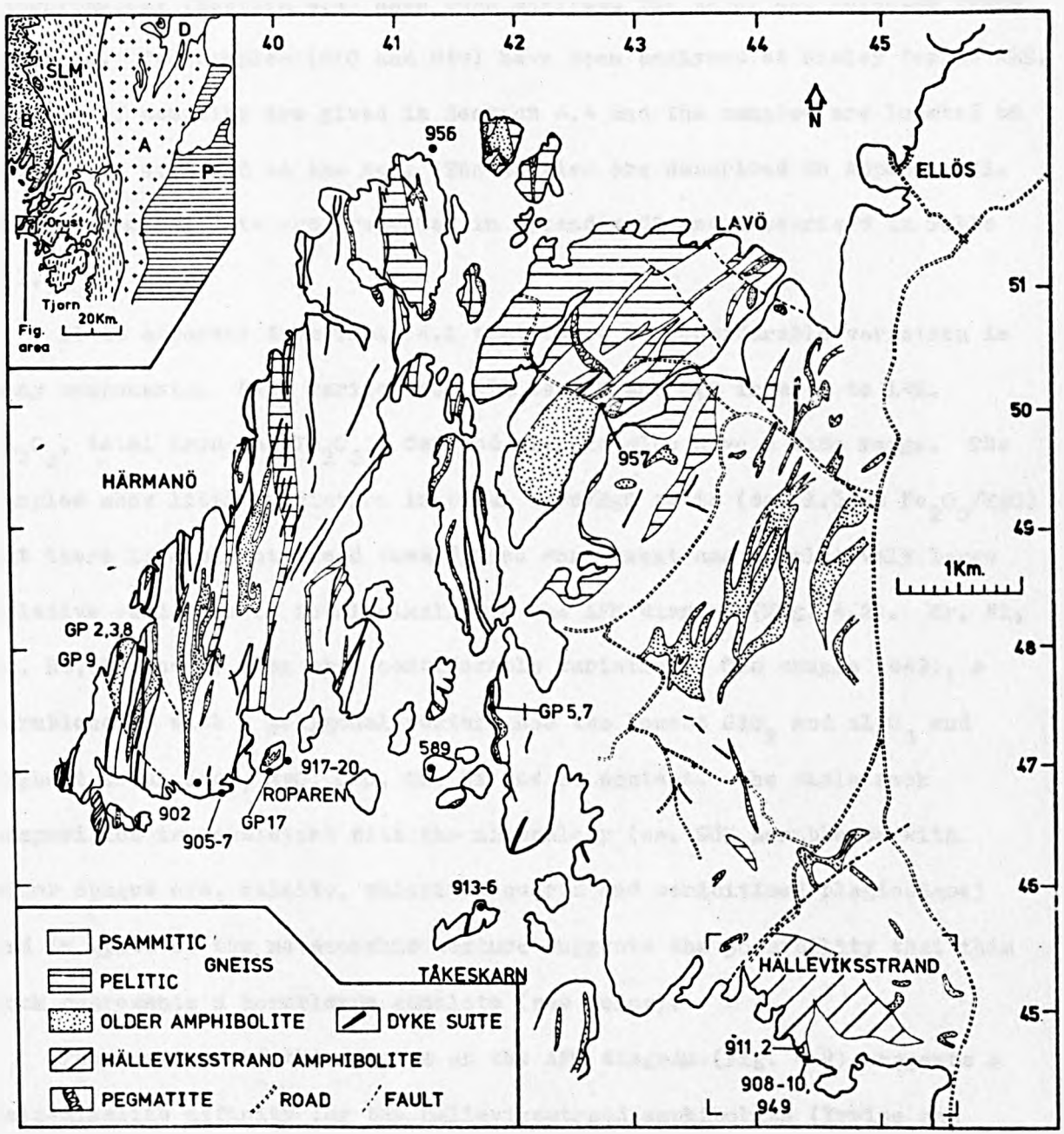
D
SLM
B
A
P
Orust
Tjorn
20Km.
Fig. area
40
41
42
43
44
45
N
956
ELLÖS
LAVÖ
51
50
957
HÄRMANÖ
49
1Km.
GP 2,3,8
GP 9
48
GP 5,7
589
917-20
ROPAREN
902
GP17
905-7
47
913-6
46
PSAMMITIC GNEISS
PELITIC
OLDER AMPHIBOLITE
DYKE SUITE
HÄLLEVIKSSTRAND AMPHIBOLITE
PEGMATITE
ROAD
FAULT
TÅKESKARN
HÄLLEVIKSSTRAND
911,2
908-10,
949
45

4.3 Geochemistry of the pre-dyke intrusive rocks.

4.3.1 The Hälleviksstrand amphibolite: geochemical data.

Six samples of the Hällevikssstrand amphibolite, collected for geochronology (Section 4.4) have been analysed for major and selected trace elements. Two samples (910 and 949) have been analysed at Risley for 14 REE. Details of sampling are given in Section 4.4 and the samples are located on Figs. 4.1, 4.13 and on the Map. The samples are described in Appendix C1. The geochemical data are presented in Appendix C2 and summarised in Table 4.1.

It is apparent from Table 4.1 that there is considerable variation in many components. SiO_2 varies from 47% to 57% and MgO from 4% to 14%. Al_2O_3, total iron (as Fe_2O_3), CaO and alkalis also have a wide range. The samples show little variation in total iron/MgO ratio (ca. 1.5 as Fe_2O_3/MgO) but there is a slight trend toward iron enrichment and a relatively large relative variation in total alkalis on the AFM diagram (Fig. 4.2). Cr, Ni, Sc, Rb, Sr and Zr also show considerable variation. One sample (949), a hornblendite with a polygonal texture, has the lowest SiO_2 and Al_2O_3 and highest total iron, MgO, CaO, Cr, Ni and Sc content. The whole rock composition is consistent with the mineralogy (ca. 95% hornblende with minor opaque ore, calcite, chlorite, quartz and sericitised plagioclase) and in spite of the metamorphic texture suggests the possibility that this rock represents a hornblende cumulate (see below).

The position of the samples on the AFM diagram (Fig. 4.2) suggests a calc-alkaline affinity for the Hällevikssstrand amphibolite (Irvine and Barager, 1971). However, it is not known to what extent the geochemistry (e.g. the increase in total alkalis) has been affected by the presence of second generation migmatitic leucosome or minor quartz-plagioclase-clinozoisite veins. In order to minimise any such geochemical effects, any veins present, including the surrounding 2 cm. margin of amphibolite, were removed. In addition large leucosomes and heavily migmatised areas (e.g. Plate 4.1)

Table 4.1

Summary geochemical data: Hällevikstrand amphibolite (six samples).

	mean	range
(wt. %)		
SiO_2	52.3	47.4 — 57.0
TiO_2	1.2	0.8 — 1.7
Al_2O_3	14.7	9.5 — 17.3
Fe_2O_3 *1	10.1	8.2 — 13.3
MnO	0.15	0.12 — 0.19
MgO	7.8	4.4 — 13.3
CaO	8.3	6.1 — 11.9
Na_2O	2.2	0.7 — 3.1
K_2O	1.9	0.5 — 2.9
P_2O_5	0.31	0.11 — 0.74
(ppm.)		
Cr	308	96 — 670
Ga	19	15 — 22
Nb	11	BDL*2 — 18
Ni	142	56 — 258
Sc	35	17 — 76
Rb	69	17 — 114
Sr	560	120 — 820
Y	30	14 — 49
Zr	164	75 — 392
ratios		
K/Rb	237	179 — 268
Y/Nb	2.55	1.4 — 6.0

Notes: *1 total iron as Fe_2O_3

*2 BDL = below detection limit

Fig. 4.2 AFM diagram for the Hällevikstrand amphibolite. The dashed line distinguishes between tholeiitic and calc-alkaline rock types (Irvine and Barager, op. cit.).

Fig. 4.3 REE data for two samples of the Hällevikstrand amphibolite, normalised to the mean of 22 chondrites (Herrmann, 1974, see Appendix A). Samples 910 and 949 are within (2σ) analytical uncertainty.

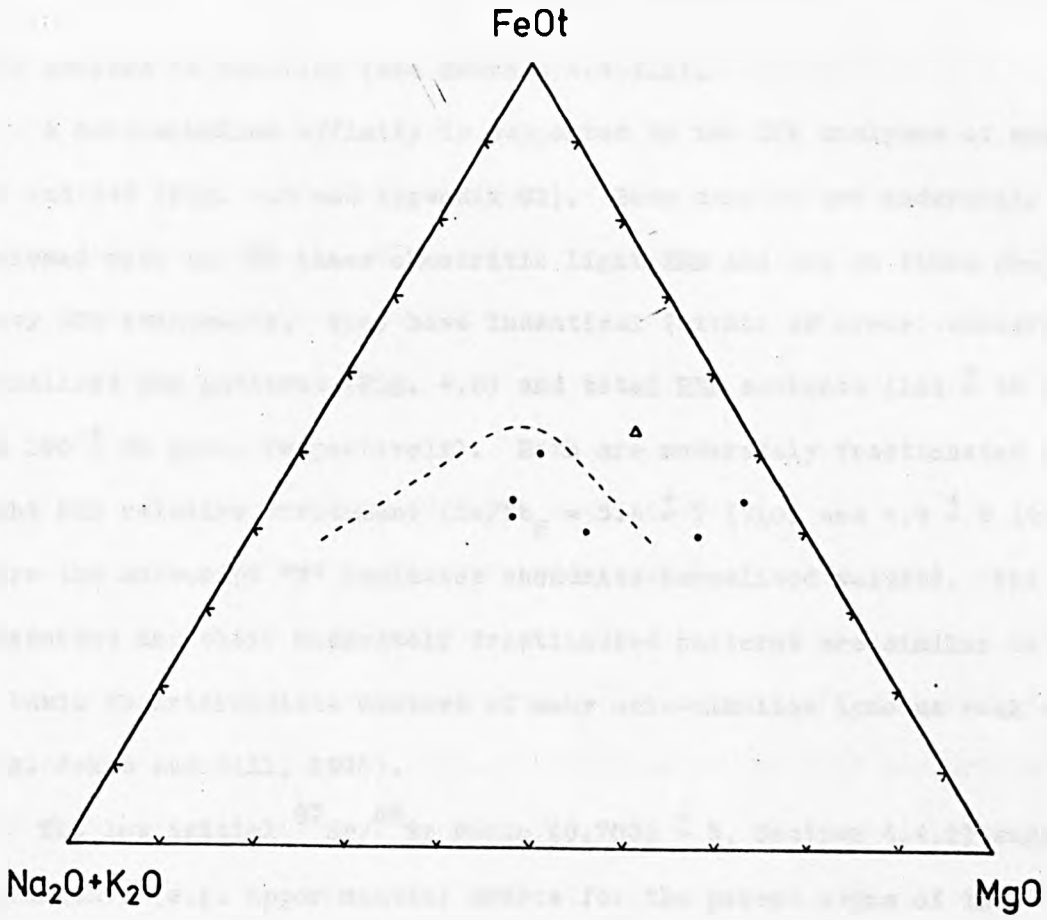
FeOt
Na_2O+K_2O
MgO

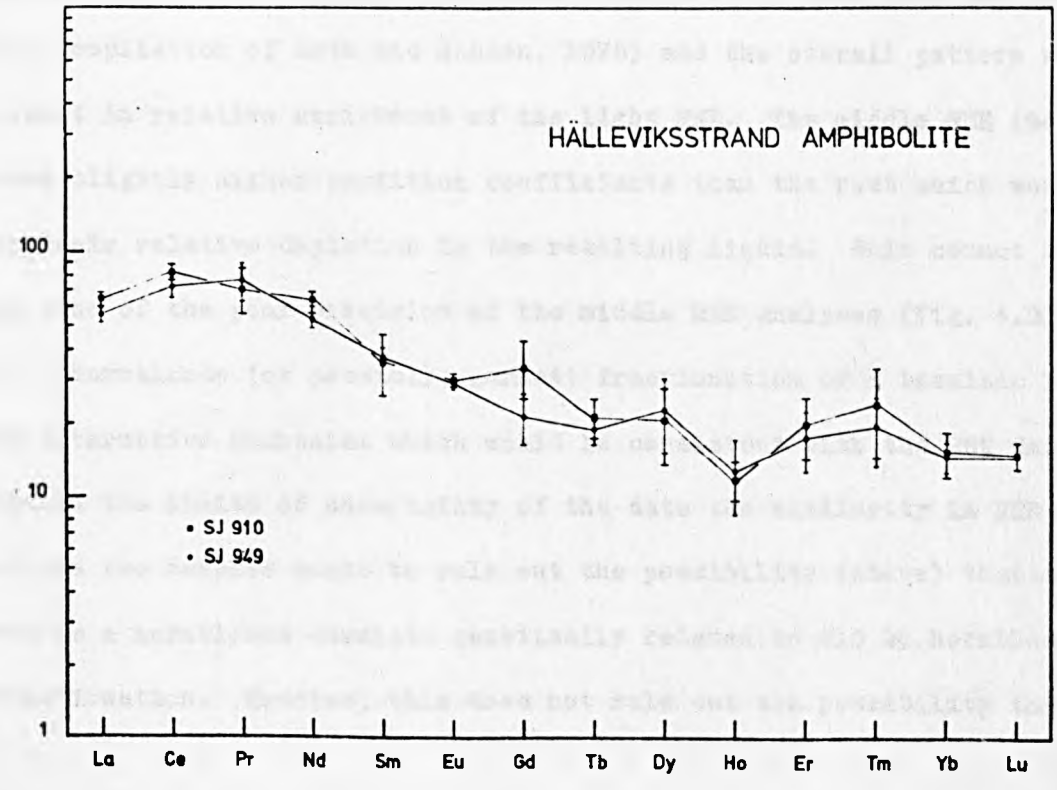
HÄLLEVIKSSTRAND AMPHIBOLITE
100
10
1
• SJ 910
• SJ 949
La
Ce
Pr
Nd
Sm
Eu
Gd
Tb
Dy
Ho
Er
Tm
Yb
Lu

were avoided in sampling (see Section 4.4.2.1).

A calc-alkaline affinity is supported by two REE analyses of samples 910 and 949 (Fig. 4.3 and Appendix C2). Both samples are moderately enriched with ca. 70 times chondritic light REE and ca. 20 times chondritic heavy REE abundances. They have indentical (within 2σ error) chondrite-normalised REE patterns (Fig. 4.3) and total REE contents (182 $\pm$ 46 ppm. and 160 $\pm$ 36 ppm., respectively). Both are moderately fractionated with light REE relative enrichment (Ce/Yb_N = 5.4 $\pm$ 7 (910) and 4.9 $\pm$ 6 (949), where the subscript "N" indicates chondrite-normalised values). The REE abundances and their moderately fractionated patterns are similar to those of basic to intermediate members of many calc-alkaline igneous rock series (e.g. Jakes and Gill, 1970).

The low initial $^{87}Sr/^{86}Sr$ ratio (0.7032 $\pm$ 5, Section 4.4.2) suggests a primitive (e.g. upper mantle) source for the parent magma of the Hällevikstrand amphibolite. Assuming that this source had an unfractionated REE pattern, partial melting in the presence of residual hornblende or possibly small amounts of garnet would account for the observed REE abundances and the light REE relative enrichment. Mean REE crystal/liquid partition coefficients for hornblende in basic rocks are all less than one (e.g. see the compilation of Arth and Hanson, 1975) and the overall pattern would result in relative enrichment of the light REE. The middle REE (Gd, Dy) have slightly higher partition coefficients than the rest which would result in their relative depletion in the resulting liquid. This cannot be tested in view of the poor precision of the middle REE analyses (Fig. 4.3).

Hornblende (or possibly, garnet) fractionation of a basaltic liquid is an alternative mechanism which would be consistent with the REE data. Within the limits of uncertainty of the data the similarity in REE pattern of the two samples seems to rule out the possibility (above) that sample 949 is a hornblende cumulate genetically related to 910 by hornblende fractionation. However, this does not rule out the possibility that all

six samples are related by hornblende/liquid differentiation of a common parent magma.

The data does not allow any distinction to be made between the two mechanisms outlined. In the absence of identifiable igneous phases and in view of the uncertainties in the values of the partition coefficients (particularly their P,T dependence) no quantitative modelling using the REE has been attempted.

4.3.2 The Assmunderöd-Myckleby augen granite.

Eleven samples of the Assmunderöd-Myckleby augen granite, eight of which were collected for geochronology (Section 4.4.3) have been analysed for major and selected trace elements. One fourteen-REE analysis of sample 944 has also been obtained. Ten of the samples came from eastern Orust (see Map), of which five (940, 941, 942, 943 and 944) were collected from the north-western (Assmunderöd) body of augen granite, which is separated from the Myckleby body by a narrow septum of migmatitic gneiss (Fig. 4.15 and Map). One sample (662) is from a hornblende-bearing part of the augen granite (Section 4.2.3). Details of sampling of the eight geochronology samples are given in Section 4.4. The samples are described in Appendix C1 and the geochemistry is summarised in Table 4.2.

4.3.2.1 Summary of the geochemical features.

The augen granite samples vary over a narrow range in SiO_2 (mean 70%, range 68.4-73.4%, Table 4.2). They have high total iron contents (ca. 4.7% as Fe_2O_3) and high total iron/MgO ratios (ca. 4.7 as Fe_2O_3/MgO). K_2O content is also high (4.9%) and the Na_2O/K_2O ratios are low (ca. 0.6). The low Na_2O content (less than 3.2% Na_2O at ca. 5% K_2O) together with the high initial $^{87}Sr/^{86}Sr$ ratio (0.713 $\pm$ 3, Section 4.4.3) indicates an S-type (sedimentary parent) designation of the augen granites according to the classification of Chappell and White (op. cit.). However, the mean molecular $Al_2O_3/(CaO + Na_2O + K_2O)$ ratio (1.06) is lessthan 1.1 and this suggests an I-type (igneous parent) classification (see Section 4.3.3.1). It is not known if this contradiction has any significance other than to

Table 4.2

Summary geochemical data: Assmunderöd-Myckleby augen granite (eleven samples).

	mean	range	
(wt. %)			
SiO_2	70.1	68.4 — 73.4	
TiO_2	0.6	0.3 — 0.8	
Al_2O_3	13.5	12.3 — 13.9	
Fe_2O_3*1	4.7	2.6 — 5.9	
MnO	0.07	0.03 — 0.09	
MgO	0.9	0.5 — 1.3	
CaO	1.7	1.2 — 2.0	
Na_2O	2.7	2.6 — 3.0	
K_2O	4.9	4.6 — 5.2	
P_2O_5	0.17	0.09 — 0.14	
(ppm.)			*2
Cr	41	27 — 53	
Ga	20	16 — 24	
Nb	28	21 — 37	(32)
Ni	21	15 — 33	
Sc	10	5 — 13	
Rb	199	174 — 253	(232)
Sr	119	75 — 167	
Y	72	65 — 101	(80)
Zr	368	232 — 475	
ratios			
K/Rb	204	171 — 208	
Na_2O/K_2O	0.6	0.5 — 0.6	
Fe_2O_3*1/MgO	5.7	2.7 — 8.2	

Notes: *1 total iron as Fe_2O_3

*2 range if different when SJ662 is excluded

question the usefulness of the classification.

One sample (944) has a total REE content of 300 ± 11 ppm. and a moderately fractionated REE pattern (Ce/Yb_N = 6.1 ± 6). The light REE are enriched (ca. 130 times chondritic) relative to the heavy REE (ca. 20 times chondritic) and there is a significant Eu anomaly (Eu/Eu* = 0.45 ± 5) (Fig. 4.4). The restricted variation in composition is illustrated by the small dispersion of the data points parallel to the A-F join on the AFM diagram and the tight cluster on the $CaO-Na_2O-K_2O$ diagram (plotted together on Fig. 4.5). However, over the narrow range in composition sampled, the data show regular variations in a number of components - e.g. relative to SiO_2 (Figs. 4.6 and 4.7). The tendency to a bimodal grouping on this diagram is not related to the geographical position of the samples.

TiO_2, total iron (as Fe_2O_3) and CaO decrease steadily as SiO_2 increases (Fig. 4.6). Sample 944 is the most leucocratic, with the highest SiO_2 content and a marked depletion in Al_2O_3 relative to the other samples. These have a negative correlation of Al_2O_3 with SiO_2 but there is considerable scatter about the trend (Fig. 4.6). MgO (not plotted) shows a general decrease with increasing SiO_2 for most of the samples but there is again a marked scatter of the data. The decrease of CaO with increasing SiO_2 is mirrored by the behaviour of Sr. CaO and Sr are closely correlated with one another (not plotted) with the exception of one sample (662) with an anomalously low Sr content. This sample is also anomalous on plots of P_2O_5 and Zr, both of which decrease with increasing SiO_2 (Fig. 4.7). In addition this sample has the highest Y content. The positive correlation of CaO with Sr and their negative correlation with SiO_2 is in contrast to the positive (but scattered) correlation of K_2O with SiO_2 (Fig. 4.7).

4.3.2.2 Interpretation and petrogenesis.

The observed patterns of variation (above) may be accounted for in terms of the mineralogy - the principal variations being in the proportion of biotite and feldspars. However, due to the coarse grain size, modal

Fig. 4.4 REE data for a single sample (944) of the Assmunderöd-Myckleby augen granite, normalised to the mean of 22 chondrites (Herrmann, 1974).

Fig. 4.5 Combined AFM (■) and CaO-Na_2O-K_2O (●) plots for the Assmunderöd-Myckleby augen granite. Larger dot indicates five coincident points.

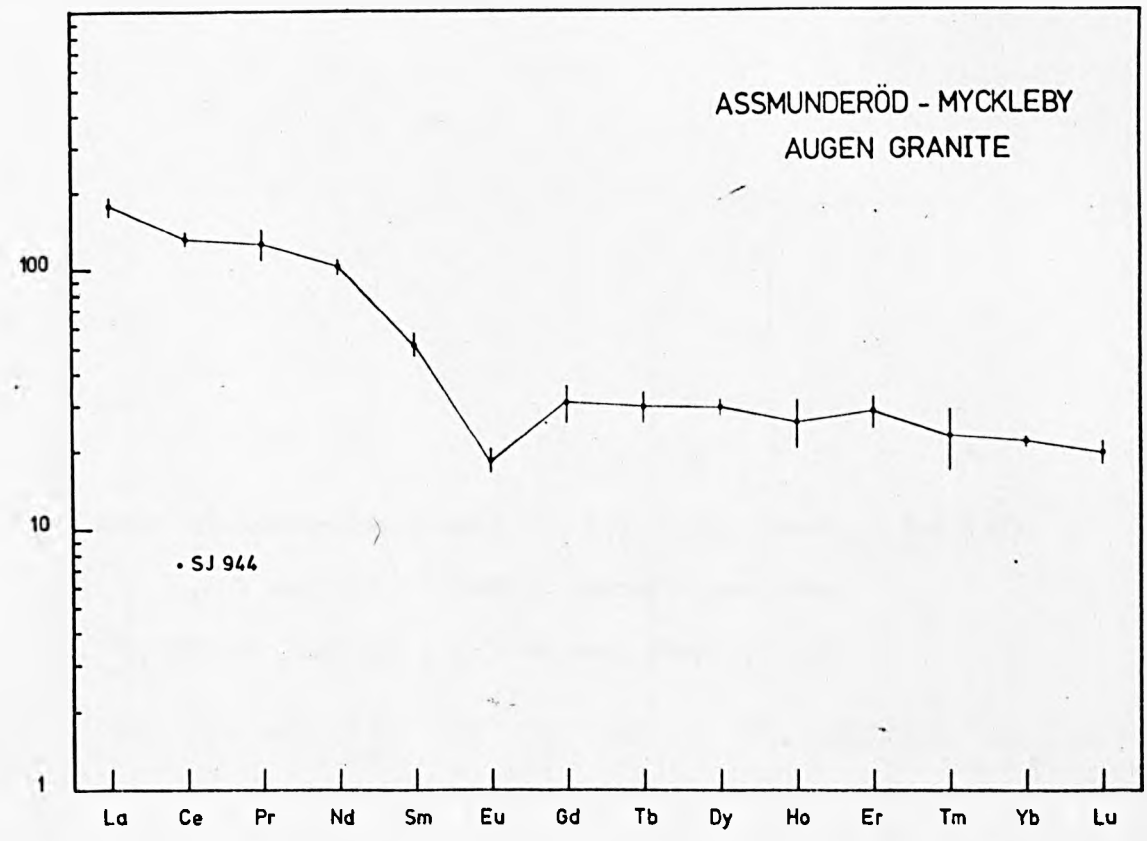
ASSMUNDERÖD - MYCKLEBY
AUGEN GRANITE
100
10
1
• SJ 944
La
Ce
Pr
Nd
Sm
Eu
Gd
Tb
Dy
Ho
Er
Tm
Yb
Lu

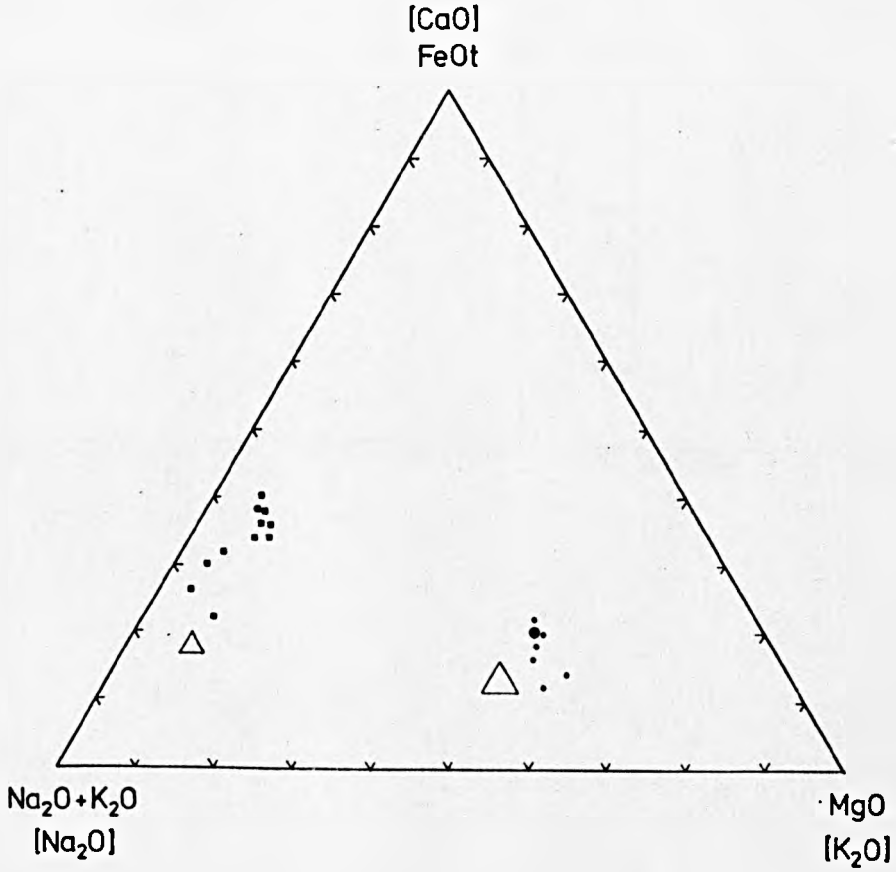
[CaO]
FeOt
Na_2O+K_2O
$[Na_2O]$
MgO
$[K_2O]$

Fig. 4.6 Binary plots for the Assmunderöd-Myckleby augen granite. Clockwise from top right:- CaO, Al_2O_3, total iron as Fe_2O_3 and TiO_2 vs. SiO_2.

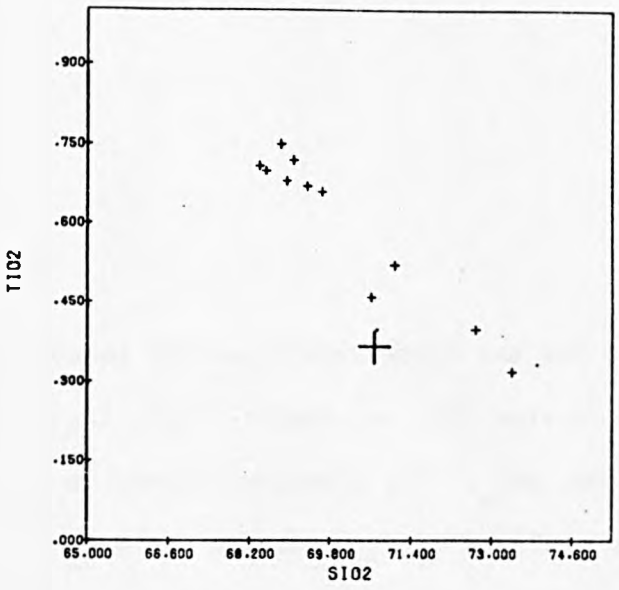
TIO2
.900
.750
.600
.450
.300
.150
.000
65.000
66.600
68.200
69.800
71.400
73.000
74.600
SIO2

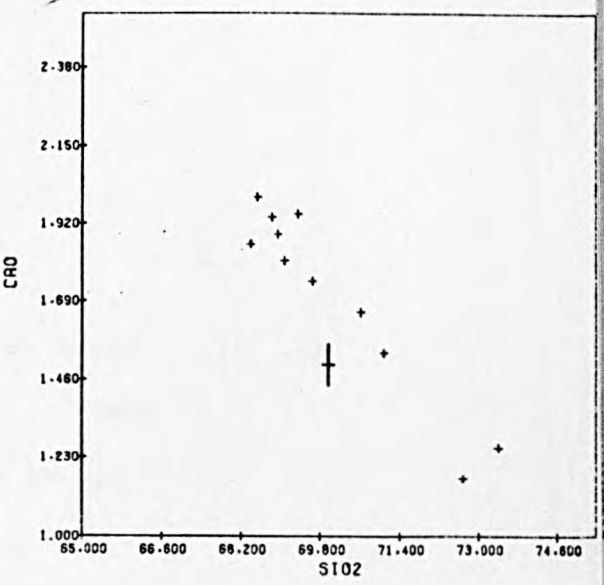
CAO
2.380
2.150
1.920
1.690
1.460
1.230
1.000
65.000
66.600
68.200
69.800
71.400
73.000
74.600
SIO2

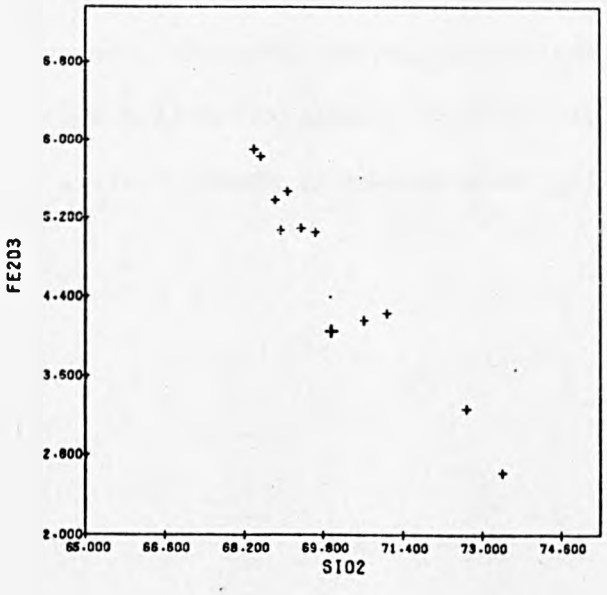
FE203
6.800
6.000
5.200
4.400
3.600
2.800
2.000
65.000
66.600
68.200
69.800
71.400
73.000
74.600
SIO2

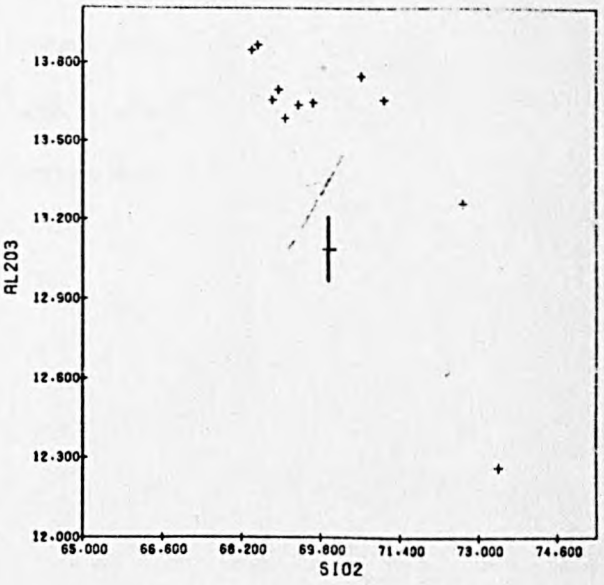
AL203
13.800
13.500
13.200
12.900
12.600
12.300
12.000
65.000
66.600
68.200
69.800
71.400
73.000
74.600
SIO2

Fig. 4.7 Binary plots for the Assmunderod-Myckleby augen granite. Clockwise from top right:- K_2O, Zr, P_2O_5 and Sr vs. SiO_2. The anomalous behaviour of SJ 662 on plots of Sr, P_2O_5 and Zr vs. SiO_2 reflects the mineralogy of this hornblende-bearing granite. It is not known if this facies of the granite is derived from a separate source. The hornblende-bearing granite outcrops over a ca. 3 $Km.^2$ area west of Varekil and grades into the surrounding biotite-bearing augen granite.

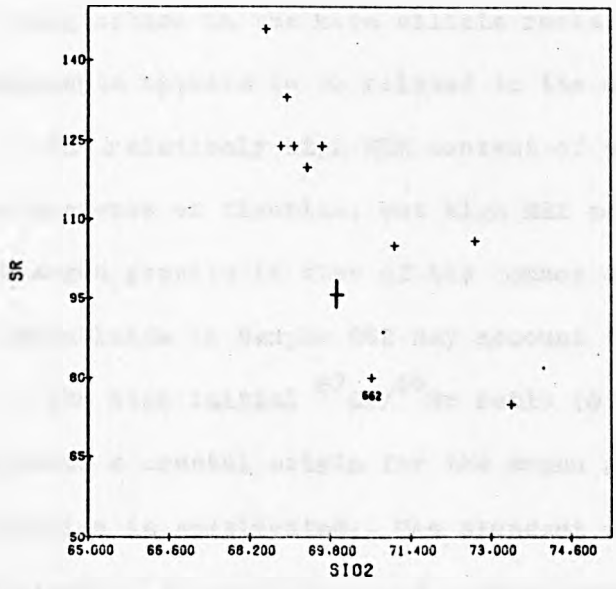
SR
140
125
110
95
80
65
50
65.000
66.600
68.200
69.800
71.400
73.000
74.600
SIO2
662

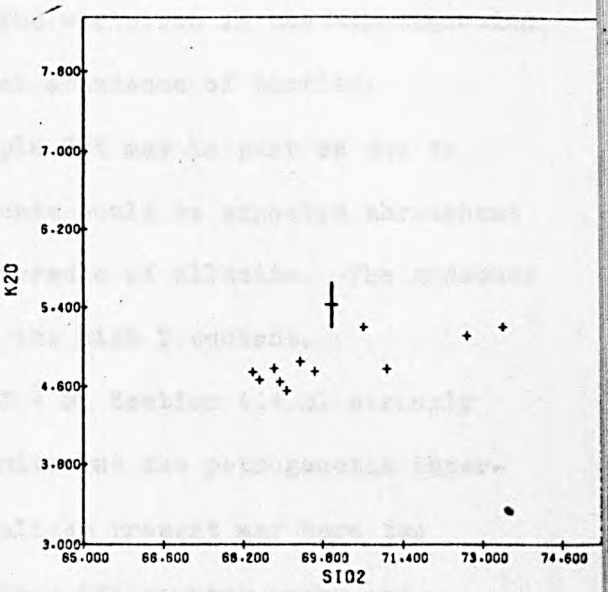
K20
7.800
7.000
6.200
5.400
4.600
3.800
3.000
65.000
66.600
68.200
69.800
71.400
73.000
74.600
SIO2

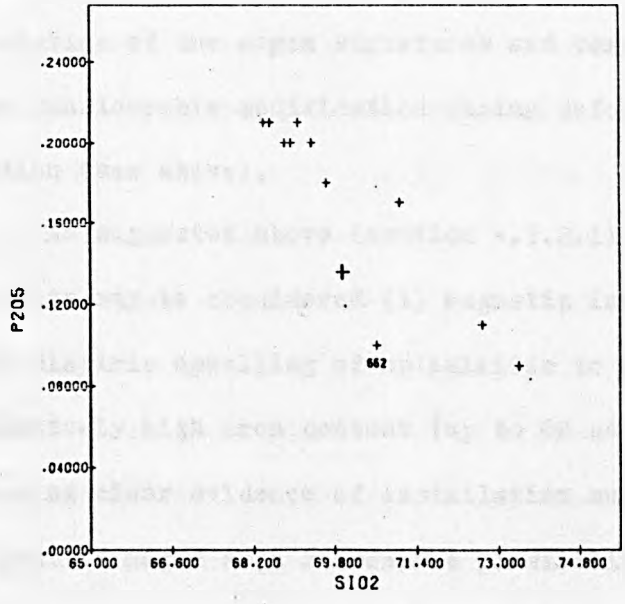
P205
.24000
.20000
.15000
.12000
.08000
.04000
.00000
65.000
66.600
68.200
69.800
71.400
73.000
74.600
SIO2
662

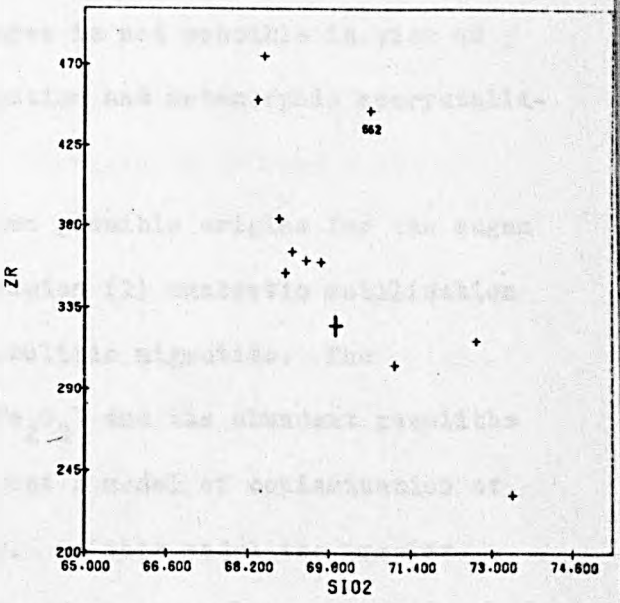
ZR
470
425
380
335
290
245
200
65.000
66.600
68.200
69.800
71.400
73.000
74.600
SIO2
662

abundances are difficult to estimate accurately. The positive correlation of CaO with Sr and their negative correlation with SiO_2 may be related to the modal variation in plagioclase and the irregular positive correlation of K_2O with SiO_2 may reflect the relative increase in K-feldspar relative to plagioclase in the more silicic rocks. The variation in the ferromagnesian components appears to be related to the modal abundance of biotite.

The relatively high REE content of sample 944 may in part be due to the presence of fluorite, but high REE contents would be expected throughout the augen granite in view of the common occurrence of allanite. The presence of hornblende in Sample 662 may account for the high Y content.

The high initial $^{87}Sr/^{86}Sr$ ratio (0.713 $\pm$ 3, Section 4.4.3) strongly suggests a crustal origin for the augen granite but the petrogenetic interpretation is complicated: The abundant xenoliths present may have two origins:- (1) locally derived contaminants from the country rocks and (2) residual material after partial melting carried upwards from the site of derivation of the augen granite. Furthermore, an unequivocal interpretation of the augen structures and textures is not possible in view of the considerable modification during deformation and metamorphic recrystallisation (see above).

As suggested above (Section 4.2.3.1) two possible origins for the augen granite may be considered (1) magmatic intrusion (2) anatectic mobilisation and diapiric upwelling of opthalmitic to nebulitic migmatite. The relatively high iron content (up to 6% as Fe_2O_3) and the abundant xenoliths showing clear evidence of assimilation suggest a model of contamination of a granite magma as a reasonable possibility. On this model the samples with the highest TiO_2, total iron, MgO, CaO and Al_2O_3 content would have the highest proportion of assimilated material. The more leucocratic rocks (e.g. 944) represent those with the least contamination. An additional complication concerns the possible contribution of magmatic differentiation (e.g. crystal fractionation) to the geochemical variation. The importance of this process is not known.

The second model is also consistent with the geological and geochemical evidence. As with the smaller-scale example of the Hällevikstrand granite (Section 3.3.1.4) it is possible to account for the geochemical variation in terms of relative separation of anatectic melt from residual material (cf. White and Chappell, op. cit.). On this model, sample 944 would represent a composition close to that of the melt phase and the samples with the highest TiO_2, total iron, MgO, CaO and Al_2O_3 would represent the highest proportion of residual material. It is possible that the polycrystalline (glomeroblastic) augen, containing recrystallised quartz, plagioclase and K-feldspar, may represent pockets of partial melt. Thus the biotite (and garnet) within the foliation would represent the residuum in equilibrium with the melt. The small ablated xenoliths would represent unequilibrated residue.

It is not possible to test this possibility - the observed variation in augen composition may be partly original (reflecting compositional variation in the parent rocks, cf. Kilinc, op. cit.) and partly the result of metamorphic recrystallisation. A melting origin seems to be less likely for the monocrystalline microcline augen but again, in view of the extent of recrystallisation, it is not possible to distinguish between a purely metamorphic or phenocryst origin for these.

The limited REE data are consistent with both models. It is possible that the Eu anomaly (Fig. 4.4) may be the result of feldspar fractionation under reducing conditions (Eu^{2+} is more readily accommodated in feldspars than the M^{3+} REE). However, the Eu anomaly could equally arise by separation of melt from a residuum which included residual (calcic) plagioclase. The overall fractionation and enrichment in light REE is consistent with residual garnet. Furthermore the REE pattern and the Eu anomaly could be inherited from the source rocks for which no REE data is available.

Given the various possibilities outlined above no firm conclusion as to the petrogenesis of the augen granite may be drawn. The present data constitutes a poorly constrained test for the White and Chappell (op. cit.)

model of granite genesis.

4.3.3 The younger granites.

Twenty-three samples of the younger granites suite have been analysed for major and selected trace elements. The majority of the samples were collected for geochronology and details of sampling are given in Section 4.4. The samples are described in Appendix C1 and the geochemical data together with a Pearson correlation matrix are presented in Appendix C2. The geochemistry is summarised in Table 4.3.

4.3.3.1 Geochemical variation in the younger granites.

From Table 4.3 the wide range in composition is apparent. SiO_2 varies over a range of ca. 15% from the tonalite (GP3) to the alkali granites (e.g. SJ902, GP5). Much of the variance in SiO_2 is due to two samples (GP3 and GP8) and the majority have granodioritic compositions close to 70% SiO_2. The single tonalite sample (GP3) has the highest TiO_2, Al_2O_3, total iron, MnO, MgO, CaO, P_2O_5, Cr, Sc and Sr contents. In addition the data are heavily weighted by three multiple-sampled granodiorite sheets (SJ905-7, 913-6, 917-20) and this tends to over-emphasise the composition of sample GP3. Total alkali content varies very little about a mean value of ca. 7% and the mean Na_2O/K_2O ratio is 2.4. Only one sample (GP5) has K_2O greater than Na_2O with a Na_2O/K_2O ratio of 0.9. The K/Rb ratio varies from 148 to 375 and the mean value is 248, close to the value (ca. 220) for the para-gneisses (Table 3.1).

According to the classification of Chappell and White (op. cit. and Section 3.3) the younger granites are I-types (**e.g. igne**ous parents) with high Na_2O contents and a mean molecular $Al_2O_3/(CaO + Na_2O + K_2O)$ ratio of 1.06.

The younger granites display a regular trend on the AFM diagram (Fig. 4.8), similar to that of many calc-alkaline series (e.g. Irvine and Barager, 1971). The overall variation in $CaO-Na_2O-K_2O$ (Fig. 4.9) also suggests a calc-alkaline affinity (e.g. Nockolds and Allen, 1953) but there

Table 4.3

Summary geochemical data: younger granites (23 samples, except where indicated).

	mean	range	
	(wt. %)		
SiO_2	70.5	58.9 — 75.0	
TiO_2	0.3	0.1 — 1.1	
Al_2O_3	15.8	14.1 — 19.1	
Fe_2O_3*1	2.3	0.4 — 6.0	
MnO	0.03	0.01 — 0.07	
MgO	0.9	0.3 — 2.2	
CaO	2.6	0.6 — 5.3	
Na_2O	4.7	4.0 — 5.6	
K_2O	2.2	1.3 — 4.6	
P_2O_5	0.11	0.05 — 0.44	
	(ppm.)		*3
Cr	34	28 — 49	(13)
Ga	19	13 — 27	
Nb	13	7 — 22	(22)
Ni	22	15 — 28	(13)
Sc	6	BDL*2 — 13	(22)
Rb	77	42 — 169	
Sr	289	20 — 530	
Y	17	9 — 28	
Zr	163	13 — 462	
	ratios		
K/Rb	248	148 — 375	
Na_2O/K_2O	2.4	0.9 — 4.2	
Fe_2O_3*1/MgO	2.5	1.1 — 3.2	

Notes: *1 total iron as Fe_2O_3

*2 BDL = below detection limit

*3 number of samples if less than 23

Fig. 4.8 AFM diagram for the younger granites. The trend in the data is similar to that of many calc-alkaline series.

Fig. 4.9 CaO - Na_2O - K_2O variation diagram for the younger granites.

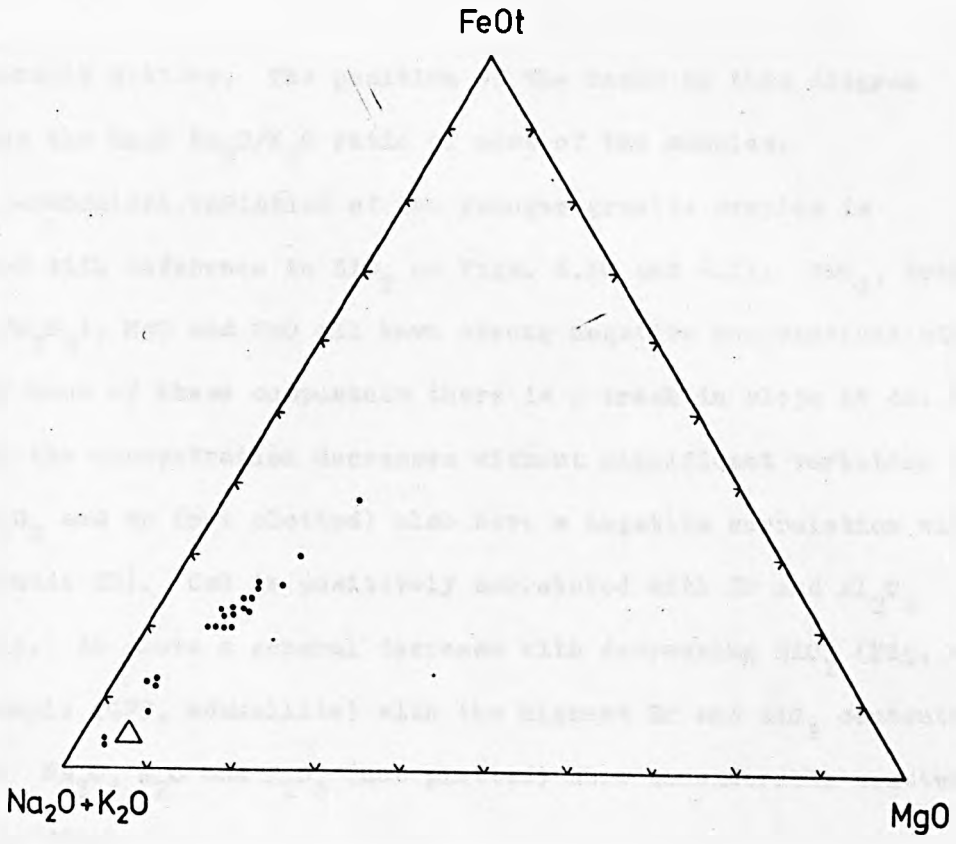
FeOt
Na_2O+K_2O
MgO

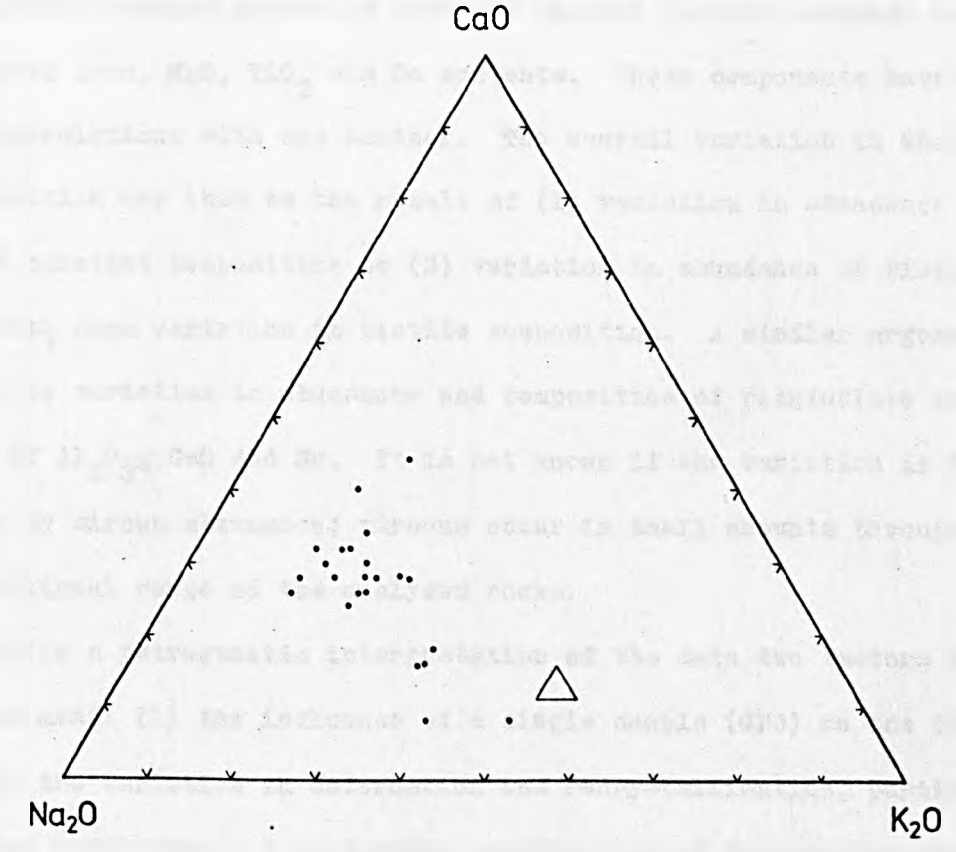
CaO
Na_2O
K_2O

is considerable scatter. The position of the rocks on this diagram illustrates the high Na_2O/K_2O ratio of most of the samples.

The geochemical variation of the younger granite samples is illustrated with reference to SiO_2 on Figs. 4.10 and 4.11. TiO_2, total iron (as Fe_2O_3), MgO and CaO all have strong negative correlations with SiO_2. For each of these components there is a break in slope at ca. 74% SiO_2 where the concentration decreases without significant variation in SiO_2. Al_2O_3 and Sr (not plotted) also have a negative correlation with SiO_2 (Appendix C2). CaO is positively correlated with Sr and Al_2O_3 (Fig. 4.11). Zr shows a general decrease with decreasing SiO_2 (Fig. 4.11) but one sample (GP9, adamellite) with the highest Zr and SiO_2 contents is anomalous. Na_2O, K_2O and P_2O_5 (not plotted) show considerable scatter relative to SiO_2.

4.3.3.2 Interpretation and petrogenesis.

The geochemical variation in the younger granites is probably accounted for by the variation in modal abundance of biotite and feldspars. The least siliceous samples generally have the highest biotite contents and highest total iron, MgO, TiO_2 and Sc contents. These components have strong positive correlations with one another. The overall variation in whole rock composition may thus be the result of (1) variation in abundance of biotite of constant composition or (2) variation in abundance of biotite together with some variation in biotite composition. A similar argument holds for the variation in abundance and composition of plagioclase and the behaviour of Al_2O_3, CaO and Sr. It is not known if the variation in Zr is controlled by zircon abundance; zircons occur in small amounts throughout the compositional range of the analysed rocks.

In making a petrogenetic interpretation of the data two factors must be borne in mind: (1) the influence of a single sample (GP3) on the data set and (2) the variation in deformation and recrystallisation, particularly of micas and K-feldspar. Considerable modification of the geochemistry of

Fig. 4.10 Binary plots for the younger granites, clockwise from top right:- MgO, CaO, total iron as Fe_2O_3 and TiO_2 vs. SiO_2. Sample GP 3 has the lowest SiO_2 content.

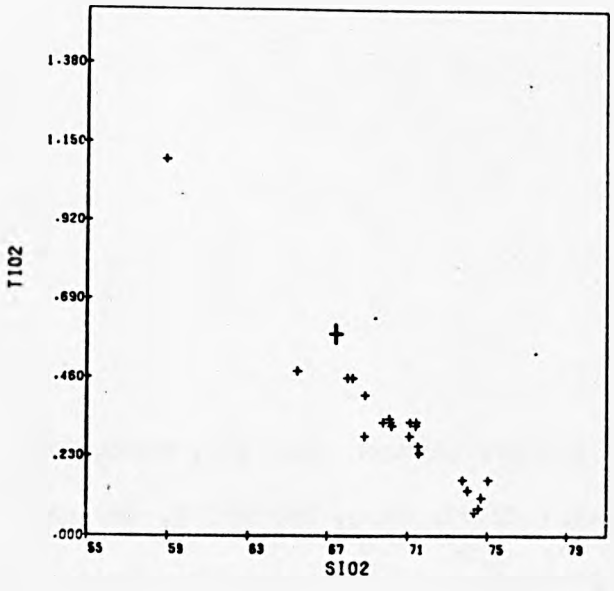
TIO2
1.380
1.150
.920
.690
.460
.230
.000
55
59
63
67
71
75
79
SIO2

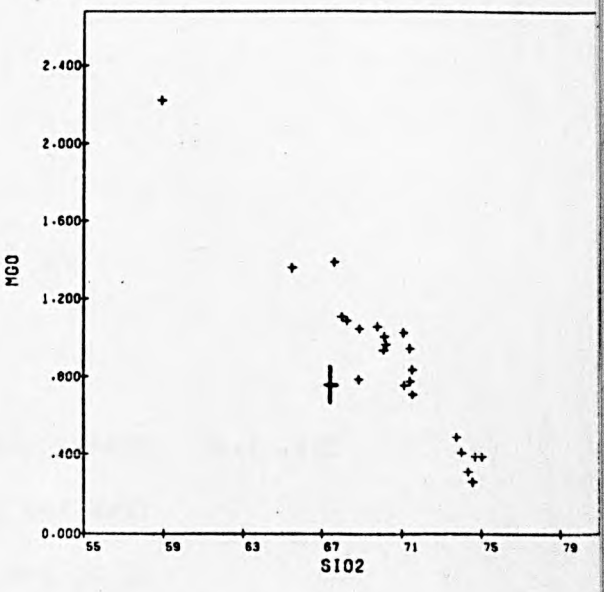
MGO
2.400
2.000
1.600
1.200
.800
.400
0.000
55
59
63
67
71
75
79
SIO2

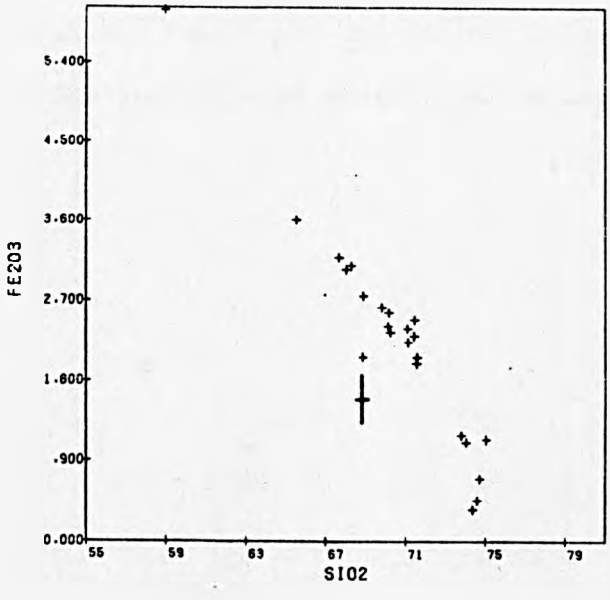
FE203
5.400
4.500
3.600
2.700
1.800
.900
0.000
55
59
63
67
71
75
79
SIO2

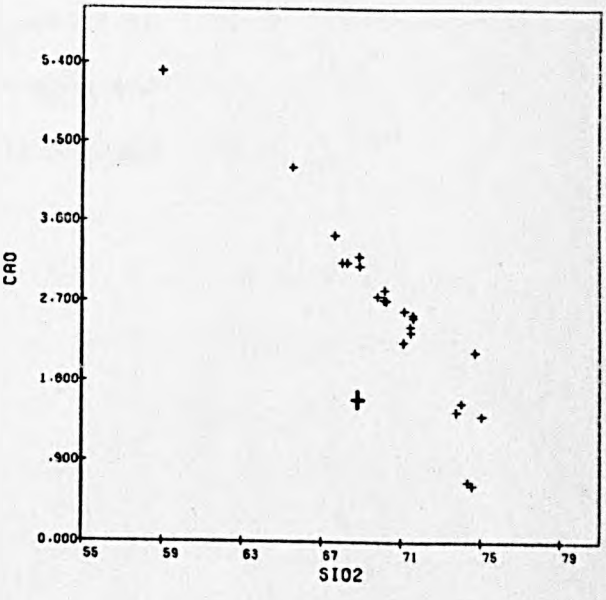
CAO
5.400
4.500
3.600
2.700
1.800
.900
0.000
55
59
63
67
71
75
79
SIO2

Fig. 4.11 Binary plots for the younger granites, clockwise from top right:- Zr vs. SiO_2, CaO vs. Y, CaO vs. Al_2O_3 and CaO vs. Sr.
Sample GP 3 has the highest CaO and SiO_2 contents. On the Zr vs. SiO_2 plot the anomalous sample is GP 9 (see text). On the CaO vs. Y plot C.A.T. is the calc-alkaline trend taken from Lambert and Holland (1974).

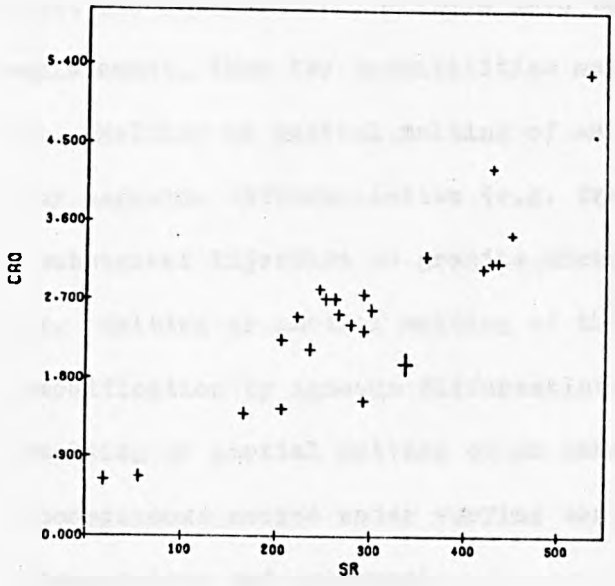
CAO
5.400
4.500
3.600
2.700
1.800
.900
0.000
100
200
300
400
500
SR

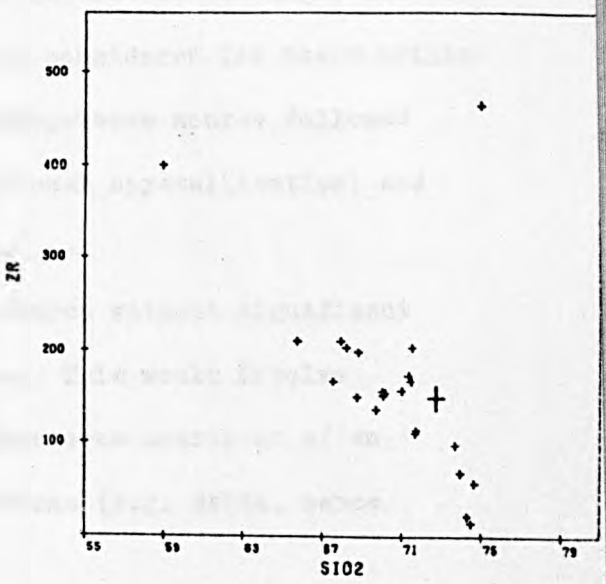
ZR
500
400
300
200
100
55
59
63
67
71
75
79
SIO2

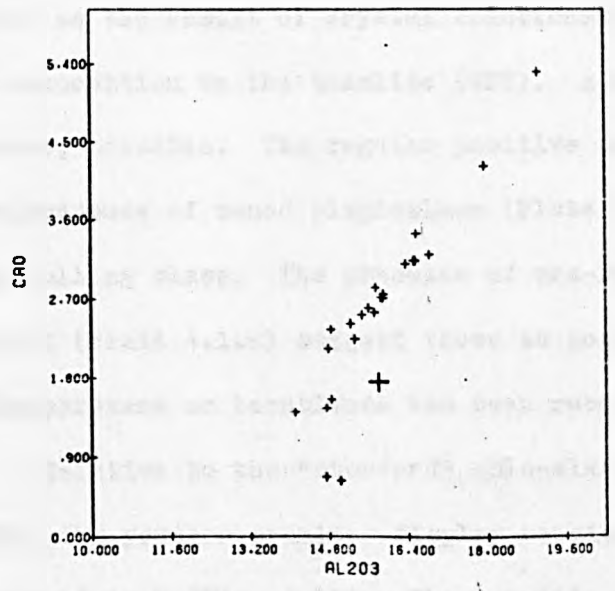
CAO
5.400
4.500
3.600
2.700
1.800
.900
0.000
10.000
11.600
13.200
14.800
16.400
18.000
19.600
AL203

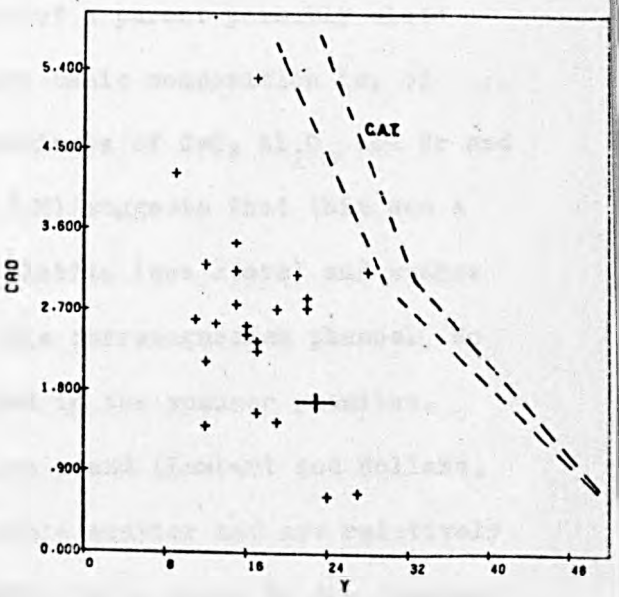
CAO
CAT
5.400
4.500
3.600
2.700
1.800
.900
0.000
0
8
16
24
32
40
48
Y

these narrow (less than 5 m. wide) sheets may have taken place during the syn-D3 metamorphism, particularly involving the alkalis and Sr (see discussion of Sr geochemistry in Section 4.4.4.2).

If it is assumed that the samples of younger granite are cogenetic and that the observed compositions have been little altered since the time of emplacement, then two possibilities may be considered for their origin:

1. Melting or partial melting of an homogeneous source followed by magmatic differentiation (e.g. fractional crystallisation) and subsequent injection as granite sheets.
2. Melting or partial melting of the source without significant modification by igneous differentiation. This would involve melting or partial melting of an inhomogeneous source or of an homogeneous source under varying conditions (e.g. depth, hence temperature and pressure).

Alternative 1.

This would explain the regular inter-element variations (Figs. 4.8-4.11) as the result of crystal fractionation of a parent possibly close in composition to the tonalite (GP3). A more basic composition is, of course, possible. The regular positive covariance of CaO, Al_2O_3 and Sr and the presence of zoned plagioclase (Plate 4.3.M) suggests that this was a controlling phase. The presence of pre-D3 biotite (see above) and sparse garnet (Plate 4.1.M) suggest these as possible ferromagnesian phases. No clinopyroxene or hornblende has been recorded in the younger granites.

Relative to the "standard" calc-alkaline trend (Lambert and Holland, 1974) the younger granites display considerable scatter and are relatively depleted in Y (Fig. 4.11). The tonalite (GP3) falls close to the standard trend and if this rock is the assumed parent in order to fit the crystal fractionation model removal of sphene, apatite or hornblende is required (Lambert and Holland, 1974). Removal of plagioclase would enrich the liquid in Y. This raises an apparent inconsistency which cannot be resolved due to the scatter of the data.

A further difficulty is posed by the behaviour of Zr. The anomalous behaviour of one sample (GP9, see above) cannot be explained. In the absence of geological evidence for it specific contamination from the gneisses is not invoked.

Alternative 2.

For the individual intrusive sheets to represent unmodified separate batches of melt, considerable variation in source composition and/or in the conditions of melting are required in order to produce the range of compositions observed. The development of pegmatitic zones in the more leucocratic sheets and the presence of possibly original biotite and muscovite (pre-D3) suggests that at least some of the melts were hydrous. The small sheet volumes suggest that some may have been water-saturated during emplacement and both imply relatively short distances from the site of melting (e.g. Cann, 1970a, Brown, 1970).

It is possible that the compositional range alkali granite - adamellite - granodiorite - tonalite represents melting at successively greater depths and higher liquidus temperatures (cf. G. C. Brown, 1973).

The first alternative (magmatic differentiation) would seem to explain the data provided a non-crustal (e.g. upper mantle) source is invoked. The parental magma could be similar in composition to the Hälleviksstrand amphibolite (Table 4.1) or close to that of the tonalite (GP3). A lower crustal source for tonalitic liquids is probably ruled out by the high degrees of partial melting and the unreasonably high temperatures required - e.g. up to 1100°C (Wyllie, 1977). An upper mantle-type source would also be consistent with the I-type designation of the younger granites (above).

The second alternative (localised partial melting and direct injection of the resulting liquid) implies a crustal source (e.g. the para-gneisses of the basement complex). It is certainly possible to produce granodioritic and granitic (s.l.) melts from the range of compositions present (Table 3.1 and e.g. Kilinc, op. cit.) but a separate source would seem to be required for the tonalitic rocks for the reasons indicated above.

The data do not allow any definite distinction between these

possibilities and they are not mutually exclusive - introduction of basic or tonalitic magma from below could have initiated melting of the paragneisses. However, given the regular interelement variation a magmatic differentiation model is favoured and plagioclase is suggested as one of the possible fractionating phases.

4.4 Geochronology of the pre-dyke intrusive rocks.

4.4.1 Introduction.

Rb/Sr and $^{87}Sr/^{86}Sr$ analytical data are presented for the Hallevikssstrand amphibolite (Section 4.2.1), the Assmunderöd-Myckleby augen granite (Section 4.2.3) and the younger granite suite (Section 4.2.5). Data for the Hällevikssstrand amphibolite and the Assmunderöd-Myckleby augen granite have also been presented elsewhere (Daly et al., in press).

4.4.2 The Hällevikssstrand amphibolite.

4.4.2.1 Sampling.

Six samples of the Hällevikssstrand amphibolite (Figs. 4.1, 4.13 and Appendix C1) were collected over a distance of ca. 300 m. on the coast south of Hällevikssstrand. Two samples (911 and 912) were collected from a blasted exposure. Samples were selected away from large migmatitic leucosomes. However, minor quartz-plagioclase-clinozoisite veining, generally 1 mm. thick or less, was visible in four samples (908, 910, 911 and 949). 911 also contained a small (3 mm.) folded leucosome vein. In order to assess the effects of any Rb and Sr redistribution during these veining processes, material 1.5 cm. to 2 cm. on either side of the thin veins was removed from each of the samples and the veined portions were treated as separate samples (908V, 910V, 911V and 949V respectively). The six samples comprising vein-free material each weighed ca. 5 kg. The veined samples weighed ca. 3 kg.

Table 4.4

Rb-Sr analytical data: Hälleviksstrand amphibolite

Sample	Rb (ppm)*1	Sr (ppm)*1	Rb/Sr*2	$^{87}Rb/^{86}Sr$*2	$^{87}Sr/^{86}Sr$*3
908	71	688	0.103	0.298	0.70933 ± 11
908v	70	679	0.103	0.298	0.70937 ± 4
909	122	662	0.184	0.531	0.71396 ± 7
910	51	304	0.165	0.479	0.71319 ± 3
910v	50	285	0.174	0.502	0.71339 ± 11
911	107	784	0.136	0.393	0.71138 ± 2
911v	100	836	0.120	0.347	0.71110 ± 7
912	80	684	0.118	0.341	0.71013 ± 4
949	19	114	0.163	0.470	0.71276 ± 2
949v	24	118	0.199	0.576	0.71459 ± 7

*1 Errors in Rb and Sr contents estimated at ± 5% (2σ)

*2 Errors in Rb/Sr and $^{87}Rb/^{86}Sr$ estimated at ± 2% (2σ)

*3 $^{87}Sr/^{86}Sr$ values are normalised to $^{88}Sr/^{86}Sr = 8.37521$

Quoted errors are 2σ based on "in run" statistics.

4.4.2.2 Isotopic data and interpretation.

Isotopic data are presented in Table 4.4 and plotted on a Nicolaysen diagram in Fig. 4.12. Six vein-free samples of the Hälleviksstrand amphibolite define a perfect isochron corresponding to an age of 1432 ± 92 m.y. (MSWD = 1.61) which is interpreted as the age of emplacement of the Hälleviksstrand magma. This is supported by the low initial $^{87}Sr/^{86}Sr$ ratio of 0.7032 ± 5 which lies in the lowest part of the range of values obtained from unmetamorphosed mid-Proterozoic basic intrusive rocks from the Svecofennian terrain of S. Sweden (Patchett, 1976) and is within the range of values for mantle-derived magmas of Faure and Powell (1972). The large uncertainty in the age (± 92 m.y.) is due to the small range in Rb/Sr ratio (and hence

Fig. 4.12 Nicolaysen diagram for the Hällevikstrand amphibolite. Six samples (excluding veins and margins, see text) define a perfect isochron corresponding to an age of 1432 ± 92 m.y. and an initial $^{87}Sr/^{86}Sr$ ratio of 0.7032 ± 5. The age is interpreted as the age of emplacement. Inset shows the veined samples and their vein free relatives. The impersistent quartz-plagioclase-clinozoisite veins do not plot significantly off the isochron. One veined sample (91lv) contains a small folded leucosome and plots significantly off the line. This implies that the leucosome formation and the D2 folding episode post-date the equilibrium recorded by the isochron.

Fig. 4.13 Location of the samples of the Hällevikstrand amphibolite. The area of this figure is shown on Fig. 4.1. Geological boundary after Park et al. (op. cit.)

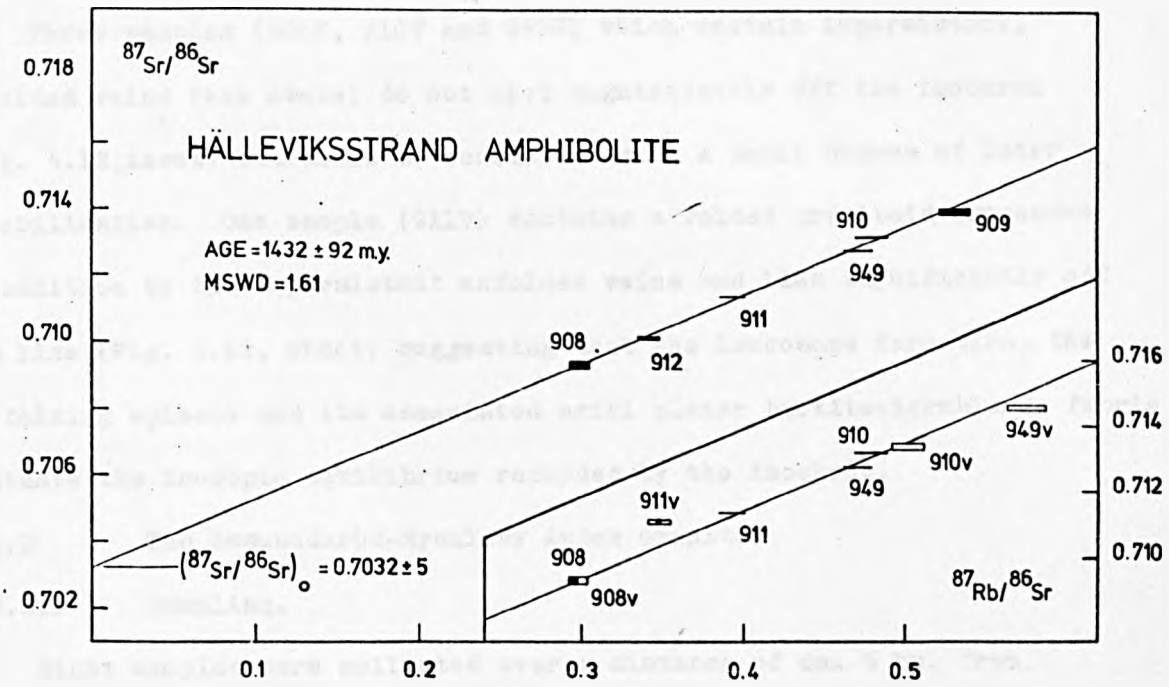
$^{87}Sr/^{86}Sr$
HÄLLEVIKSSTRAND AMPHIBOLITE
AGE = 1432 ± 92 m.y.
MSWD = 1.61
$(^{87}Sr/^{86}Sr)_o$ = 0.7032 ± 5
$^{87}Rb/^{86}Sr$
0.718
0.714
0.710
0.706
0.702
0.716
0.714
0.712
0.710
0.1
0.2
0.3
0.4
0.5
910
909
949
911
908
912
910
949v
910v
949
911v
911
908
908v

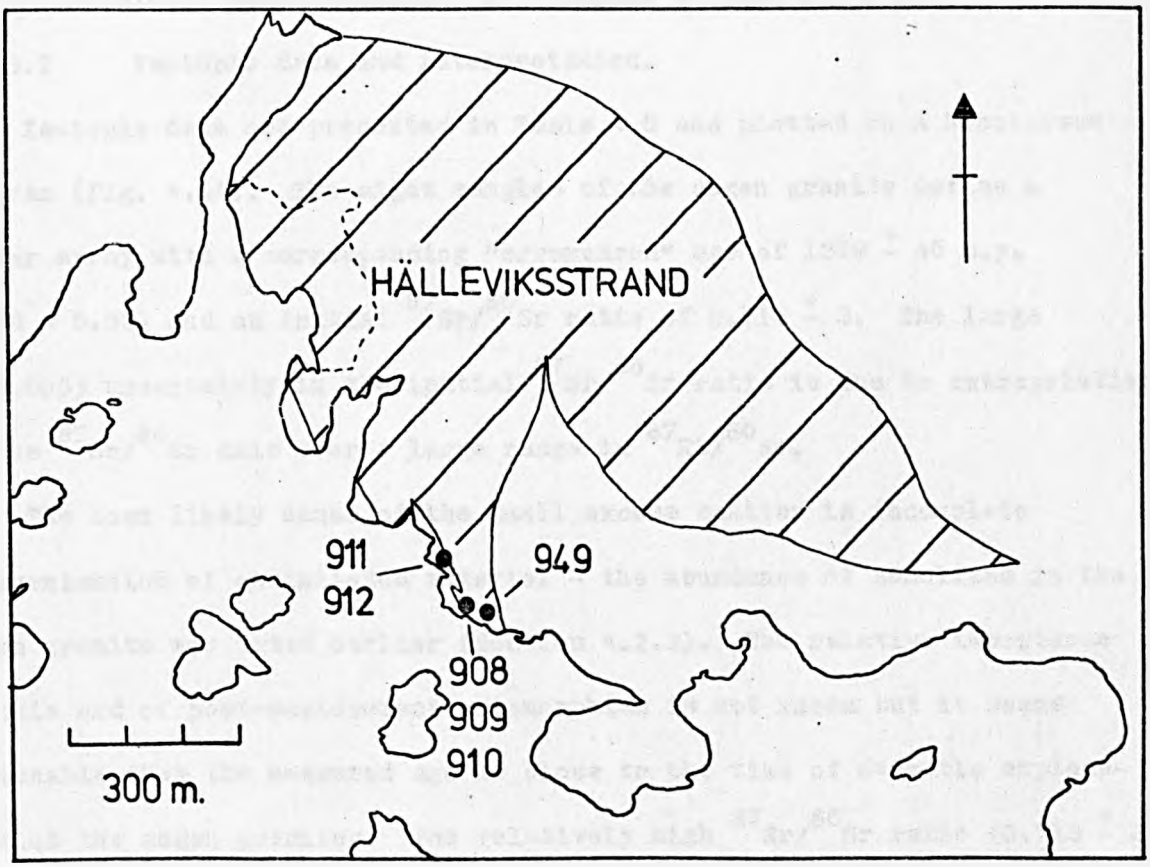
HÄLLEVIKSSTRAND
911
912
949
908
909
910
300 m.

$^{87}Rb/^{86}Sr$) in the samples.

Three samples (908V, 910V and 949V) which contain impersistent, unfolded veins (see above) do not plot significantly off the isochron (Fig. 4.12,inset) but would be consistent with a small degree of later remobilisation. One sample (911V) contains a folded granitoid leucosome in addition to the impersistent unfolded veins and lies significantly off the line (Fig. 4.12, inset) suggesting that the leucosome formation, the F2 folding episode and its associated axial planar biotite-hornblende fabric postdate the isotopic equilibrium recorded by the isochron.

4.4.3 The Assmunderöd-Myckleby Augen Granite.

4.4.3.1 Sampling.

Eight samples were collected over a distance of ca. 5 km. from recently blasted roadside exposures of the Assmunderöd-Myckleby augen granite south of Slussen (Fig. 4.15 and Appendix C1). One sample (954) was obtained by discarding a semipelitic xenolith and its surrounding 2-3 cm. margin of augen granite. All samples weighed ca. 5 kg.

4.4.3.2 Isotopic data and interpretation.

Isotopic data are presented in Table 4.5 and plotted on a Nicolaysen diagram (Fig. 4.14). The eight samples of the augen granite define a linear array with a corresponding "errorchron" age of 1379 $\pm$ 46 m.y. (MSWD = 6.32) and an initial $^{87}Sr/^{86}Sr$ ratio of 0.713 $\pm$ 3. The large ($\pm$ 0.003) uncertainty in the initial $^{87}Sr/^{86}Sr$ ratio is due to extrapolation to the $^{87}Sr/^{86}Sr$ axis over a large range in $^{87}Rb/^{86}Sr$.

The most likely cause of the small excess scatter is incomplete homogenisation of assimilated material - the abundance of xenoliths in the augen granite was noted earlier (Section 4.2.3). The relative importance of this and of post-emplacement metamorphism is not known but it seems reasonable that the measured age is close to the time of magmatic emplacement of the augen granites. The relatively high $^{87}Sr/^{86}Sr$ ratio (0.713 $\pm$ 3) suggests a previous but short lived crustal history for the parent rocks of the augen granites - ca. 150 m.y. if the average $^{87}Rb/^{86}Sr$ of the analysed samples (= 5.51) is taken as typical for the complex.

Fig. 4.14 Nicolaysen diagram for the Assmunderöd-Myckleby augen granite. The "errorchron" age (MSWD = 6.32) is 1379 ± 46 m.y. The high initial $^{87}Sr/^{86}Sr$ ratio (0.713 ± 3) implies a crustal source for the augen granite. Taking the mean $^{87}Rb/^{86}Sr$ ratio of the samples (= 5.51) a crustal residence time of ca. 150 m.y. may be calculated. The likely cause of the small excess scatter in the data is incomplete homogenisation of the assimilated xenoliths.

Fig. 4.15 Location of the samples of the Assmunderöd-Myckleby augen granite. Geological boundary is from Berthelsen and Murthy (1970) and the author's mapping. Samples SJ 940-944 are from the Assmunderöd body, the remainder are from the Myckleby body. The area of the figure is indicated on the Map.

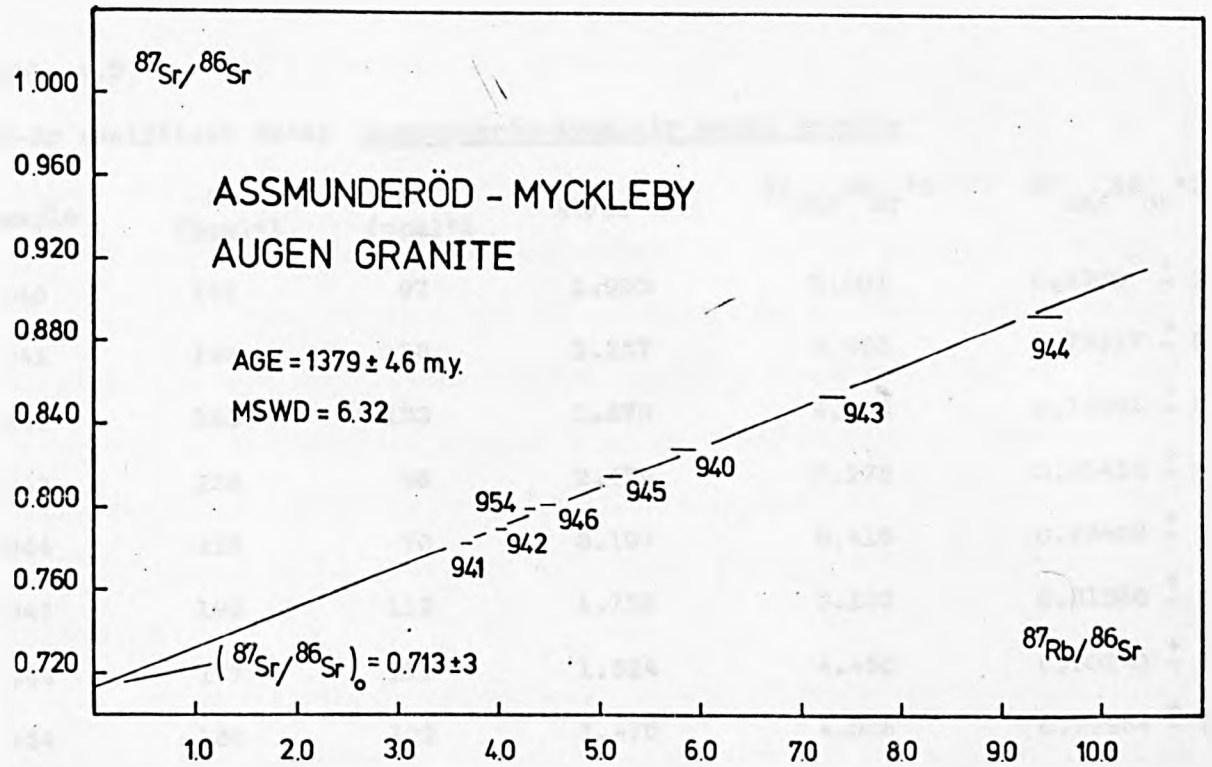
87Sr/86Sr
1.000
0.960
0.920
0.880
0.840
0.800
0.760
0.720
ASSMUNDERÖD - MYCKLEBY
AUGEN GRANITE
AGE = 1379 ± 46 m.y.
MSWD = 6.32
944
943
940
945
954
946
942
941
(87Sr/86Sr)o = 0.713±3
87Rb/86Sr
1.0
2.0
3.0
4.0
5.0
6.0
7.0
8.0
9.0
10.0

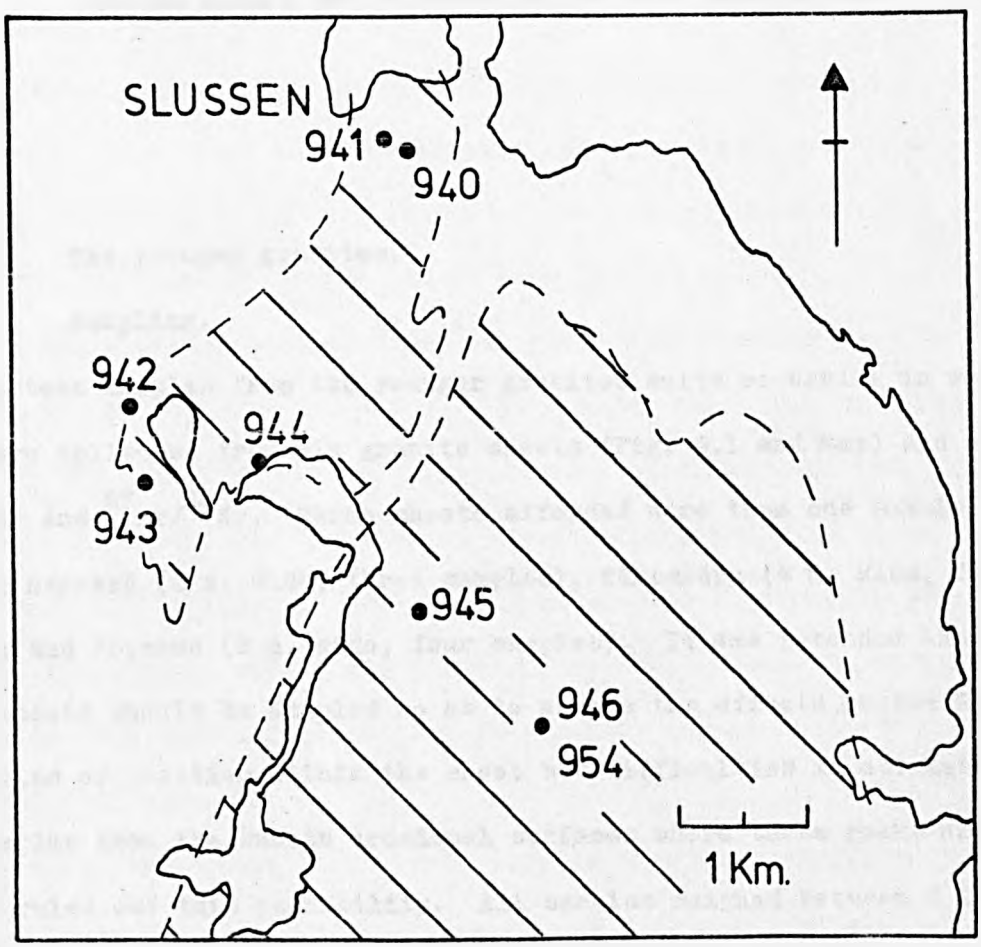
SLUSSEN
941
940
942
944
943
945
946
954
1 Km.

Table 4.5

Rb-Sr analytical data: Assmunderöd-Myckleby augen granite

Sample	Rb (ppm)*1	Sr (ppm)*1	Rb/Sr*2	$^{87}Rb/^{86}Sr$*2	$^{87}Sr/^{86}Sr$*3
940	191	97	1.983	5.805	0.8300 ± 2
941	193	153	1.257	3.663	0.78317 ± 8
942	183	133	1.373	4.005	0.78991 ± 3
943	238	96	2.479	7.275	0.85456 ± 4
944	225	70	3.197	9.416	0.89409 ± 3
945	196	112	1.755	5.132	0.81566 ± 8
946	177	116	1.524	4.450	0.80240 ± 6
954	180	122	1.476	4.308	0.79984 ± 6

*1 Errors in Rb and Sr contents estimated at ± 5% (2σ)

*2 Errors in Rb/Sr and $^{87}Rb/^{86}Sr$ estimated at ± 2% (2σ)

*3 $^{87}Sr/^{86}Sr$ values are normalised to $^{88}Sr/^{86}Sr = 8.37521$

Quoted errors are 2σ based on "in run" statistics.

4.4.4 The younger granites.

4.4.4.1 Sampling.

Fourteen samples from the younger granites suite occurring in western Orust were collected from six granite sheets (Fig. 4.1 and Map) and analysed for Rb/Sr and $^{87}Sr/^{86}Sr$. Three sheets afforded more than one sample: Southern Härmanö (2 m. wide, three samples), Tåkeskärn (4 m. wide, four samples) and Roparen (3 m. wide, four samples). It was intended that the larger sheets should be sampled so as to assess the effects on the Rb-Sr systematics of position within the sheet but difficulties in obtaining suitable samples from the smooth erosional surfaces where these rocks are best exposed ruled out this possibility. All samples weighed between 5 Kg. and 10 Kg. and are described in Appendix C1.

4.4.4.2 Isotopic data and interpretation.

Isotopic data are presented in Table 4.6 and plotted on a Nicolaysen diagram in Fig. 4.16. Thirteen of the samples have Rb/Sr ratios which fall within a narrow range while one sample (902) is greatly enriched in Rb and ^{87}Sr relative to the others. The full data set shows a wild scatter (MSWD = 141.2) and is even worse (MSWD = 153.5) when the "anchoring" effect of 902 is removed and the thirteen samples with low Rb/Sr ratios are considered separately. The respective best-fit lines correspond to "ages" and initial $^{87}Sr/^{86}Sr$ ratios as follows: 1552 $\pm$ 23 m.y., 0.7043 $\pm$ 2 and 1574 $\pm$ 29 m.y., 0.7041 $\pm$ 3.

No geological age significance can be attributed to these grossly aberrant regression lines. The age of emplacement of the granite sheets is known to be younger than ca. 1350 - 1450 m.y., which is the age of emplacement of the Hälleviksstrand amphibolite and the Assmunderöd-Myckleby augen granite. The older apparent "ages" and the scatter of the data may have arisen as follows:

1. Inheritance of the isotopic systematics of the source region. Apparent ages older than the maximum age of ca. 1350 - 1450 m.y. would be consistent with the derivation of the younger granites from an isotopically inhomogeneous source (see Section 4.3.3.2, Alternative 2). Variation of initial $^{87}Sr/^{86}Sr$ ratio might be expected from such a mechanism (cf. Roddick and Compston, 1976, Pankhurst and Pidgeon, 1976) but equilibration on the scale of the individual small granite sheets (as magma) at the time of emplacement would also be expected. In fact only one of the three multiple-sampled sheets (Tåkeskärn, Fig. 4.16) shows sufficient dispersion in Rb/Sr ratio to test this and these samples (913-916) are only poorly correlated on the Nicolaysen diagram.

2. Metamorphic disturbance and interaction with the country rocks. This is a more likely explanation of the data and arises in at least two ways. The first is disturbance of the isotopic systematics during

Table 4.6

Rb-Sr analytical data: Younger granites

Sample	Rb (ppm)*1	Sr (ppm)*1	Rb/Sr*2	$^{87}Rb/^{86}Sr$*2	$^{87}Sr/^{86}Sr$*3
S. Härmanö					
905	86	241	0.357	1.035	0.72653 ± 3
906	88	231	0.379	1.099	0.72736 ± 8
907	84	226	0.372	1.078	0.72863 ± 4
Tåkeskärn					
913	73	191	0.383	1.112	0.72798 ± 4
914	60	243	0.247	0.716	0.71835 ± 9
915	64	243	0.247	0.715	0.71735 ± 4
916	53	205	0.261	0.755	0.72000 ± 5
Roparen					
917	59	387	0.152	0.442	0.71677 ± 2
918	54	382	0.142	0.411	0.71338 ± 2
919	66	395	0.166	0.479	0.71433 ± 5
920	60	403	0.149	0.433	0.71304 ± 3
Other samples (one sample per sheet)					
902	169	19	8.997	27.552	1.3070 ± 2
956	69	194	0.354	1.027	0.72721 ± 3
957	60	270	0.224	0.648	0.72279 ± 8

*1 Errors in Rb and Sr contents estimated at ± 5% (2σ)

*2 Errors in Rb/Sr and $^{87}Rb/^{86}Sr$ estimated at ± 2% (2σ)

*3 $^{87}Sr/^{86}Sr$ values are normalised to $^{88}Sr/^{86}Sr = 8.37521$

Quoted errors are 2σ based on "in run" statistics.

Fig. 4.16 Nicolaysen diagram for the younger granites. Dashed lines enclose the fields of individual granite sheets. The slope of the best-fit line to the full data (including SJ 902, inset) corresponds to an "age" of 1552 $\pm$ 22 m.y. In view of the very large excess scatter (MSWD = 141.2) no geological age significance may be attached to this line. Disturbance of the isotopic systems during the syn-D3 and later metamorphism is a likely explanation for the disequilibrium.

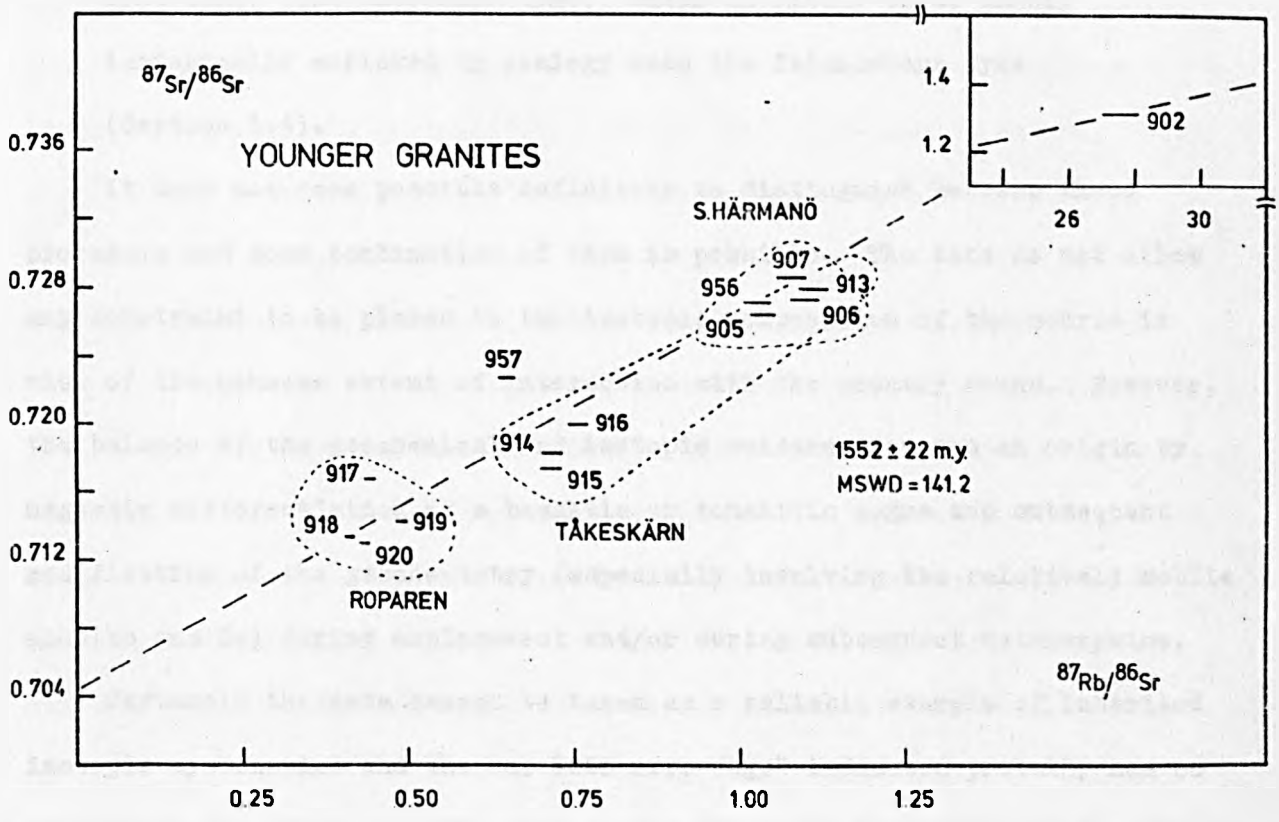
$^{87}Sr/^{86}Sr$
YOUNGER GRANITES
0.736
0.728
0.720
0.712
0.704
0.25
0.50
0.75
1.00
1.25
$^{87}Rb/^{86}Sr$
1.4
1.2
902
26
30
S.HÄRMANÖ
907
956
913
905
906
957
916
914
915
TÅKESKÄRN
917
918
919
920
ROPAREN
1552 ± 22 m.y.
MSWD = 141.2

the syn-D3 (or later) metamorphism due to growth of muscovite and biotite, and due to post-tectonic growth of microcline (Section 4.2.5). Secondly some local interaction with the country rocks has evidently taken place. One of the granite sheets (S. Härmanö) contains angular xenoliths of augen granite (see Appendix B for isotopic data on this contaminant) and these samples (905-907) have among the highest Rb/Sr and $^{87}Sr/^{86}Sr$ ratios. In addition, the Tåkeskärn granite sheet (913-916) is cut by a member of the dyke suite (the Tåkeskärn dyke), which is likely to be highly isotopically enriched by analogy with the Islandsberg dyke (Section 5.4).

It does not seem possible definitely to distinguish between these processes and some combination of them is possible. The data do not allow any constraint to be placed on the isotopic composition of the source in view of the unknown extent of interaction with the country rocks. However, the balance of the geochemical and isotopic evidence favours an origin by magmatic differentiation of a basaltic or tonalitic magma and subsequent modification of the geochemistry (especially involving the relatively mobile alkalis and Sr) during emplacement and/or during subsequent metamorphism.

Certainly the data cannot be taken as a reliable example of inherited isotopic systematics and the ca. 1560 m.y. "age" indicated probably has no geological significance. The data do not allow any refinement on the age of emplacement which is constrained between ca. 1350 - 1450 m.y. (ages of emplacement of the Hälleviksstrand amphibolite and the Assmunderöd-Myckleby augen granite) and ca. 1060 m.y. (age of the post-dyke (Sveconorwegian) metamorphism, Section 5.4).

4.4.5 Conclusions on the geochronology.

The measured ages of the Hällevikstrand amphibolite and the Assmunderöd-Myckleby augen granite fall within 2σ error. An emplacement age ca. 1350 - 1450 m.y. for these rocks is important in providing both a younger limit for the age of the main pre-D1 migmatisation within the

Stora Le - Marstrand belt and an older age limit for the second-generation leucosome and for all subsequent events including the emplacement of the younger granites. Samples of the latter group show considerable scatter of the Rb-Sr data and no age conclusion can be drawn. They could represent an equivalent of the ca. 1220 m.y. Hästefjorden granites of the Åmål belt (Gorbatschev and Welin, 1975 and Welin and Gorbatschev, 1976c).

The ages obtained for the Hälleviksstrand amphibolite and the Assmunderöd-Myckleby augen granite overlap with recently published Rb-Sr whole-rock ages of plutonic intrusives within the Åmål belt to the north-east; the Härserud granites (ca. 1375 m.y.), the Ljungbergen granites (1371 ± 78 m.y.), the post-Ellenö granites (1375 ± 49 m.y.) (Skiöld, 1976), and the Lane granites (1427 ± 27 m.y.) (Welin and Gorbatschev, 1978a).

Of these the post-Ellenö and Lane granites are known to be later than the Åmål(I) complex (Gorbatschev, 1971, Welin and Gorbatschev, 1976b and Chapter 1) but their relationship and that of the other ca. 1400 m.y. granites of the Åmål belt to the Åmål(II) granites (Chapter 1) is not known at present. The presence of plutonic intrusives of similar age within the Stora Le - Marstrand belt confirms that this is an important period of igneous activity and points to a possible correlation of the Stora Le - Marstrand migmatitic gneisses with the early components of the Åmål belt.

CHAPTER 5. The dyke suite and the post-dyke (Sveconorwegian) events.

5.1 Introduction.

The dyke suite is dominated by mafic to ultramafic amphibolites but includes a minor proportion (less than 5%) of intermediate to acidic compositions. Both kinds of dyke cut the younger granites, F2 fold structures and the migmatitic gneisses (Plate 5.1). Mafic and ultramafic dykes also cut the Assmunderöd-Myckleby augen granite and its contacts with the gneisses. The dyke suite is an important chronological marker (Park et al., op. cit. and Berthelsen and Murthy, op. cit.) and it separates at least two phases of regional deformation (D3 and D4) from earlier events.

Members of the dyke suite have been recognised throughout Orust (Map) but there appears to be a greater concentration in the west, especially on the island of Härmanö. Amphibolite dykes are evident in Bergström's (1963) description of the geology of Tjörn but were not separated (ibid.) from the older amphibolites (Section 3.2.3). Berthelsen and Murthy (op. cit.) recorded amphibolite dykes in north-eastern Orust. The dyke suite has been recorded within the Stora Le - Marstrand belt over a distance of ca. 250 Km. from the southern part (Lundegardh, 1958, Magnusson et al., 1960) to the Norwegian continuation in the Ostfold Series (Hageskov, 1978).

5.2 Geology and petrography.

Mafic and ultramafic members of the dyke suite are distinguished from the older amphibolites by the absence of migmatitic leucosome, by their generally straight and regular outcrop and clearly intrusive contacts. Some mafic dykes have sharp chilled margins. The intermediate to acidic members are usually garnetiferous and have a characteristic pale grey colour and spotted appearance. Both kinds of dyke have sharp, generally steeply dipping, contacts with the country rocks and many of the mafic dykes have

Plate 5.1 Photographs to illustrate the age relations of the dyke suite. Locality: south-western Härmanö (38, 47).

Above: A narrow (ca. 30 cm. wide) relatively undeformed, fine-grained, mafic dyke cuts the concordant (first generation) migmatitic banding and (at right) small bodies of second generation leucosome in the para-gneisses. Lens cap measures 4 cm.

Below: A narrow (ca. 20 cm. wide) deformed, coarse-grained, garnet-bearing, mafic dyke has a margin-parallel S3 mineral fabric and cuts a post-D2 zone of shearing in the migmatitic para-gneisses, which affects both generations of migmatitic leucosome. The sheared migmatitic gneisses are cut (at top centre) by a narrow (10 cm. to 15 cm. wide) dyke of leucocratic younger granite (Section 4.2.5), which is in turn cut by the mafic dyke.

Hammer head measures 15 cm.

fine-grained margins.

The dykes vary in width from ca. 60m. to a few cm. but the majority are less than 5m. wide. Several of the wider mafic dykes on Härmanö represent multiple intrusions with coarse-grained central parts and fine-grained margins. Typically the dykes may be followed for several tens of metres but some are at least 4Km. in length.

Within the mafic and ultramafic dykes the extent of metamorphic recrystallisation and the response to deformation are very variable. The majority of the larger (greater than 5m. wide) dykes have suffered little deformation during D3 and D4 and frequently mineral fabrics are restricted to the margins. However, several narrow dykes are similarly undeformed and there is no general rule relating dyke thickness to response to deformation. In western Orust, Park et al. (op. cit.) have identified discrete zones of pre-dyke shearing within which post-dyke deformation has been concentrated. Generally the acid dykes have been intensely deformed and all examples recorded have a strong (D3) biotite fabric.

5.2.1 Mafic and ultramafic dykes.

These rocks exhibit considerable petrographic variation but all contain hornblende as the major phase. The rocks are green to dark grey in colour and the grain size varies from fine-grained, less than 1mm., to very coarse (hornblendes several cm. long). They contain hornblende (50-85%), biotite (1-40%) and quartz + plagioclase (1-30%). The majority of the dykes have a mafic composition with quartz and plagioclase together making up between 10% and 30% and with biotite less than 20%. Garnet occurs in many of the dykes but usually makes up less than 5% of the mode. Chlorite occurs in variable amounts, up to 10% of the mode in some altered samples. Sphene, opaque ores (including both ilmenite and pyrite) epidote group minerals and calcite occur in accessory amounts.

Apart from opaque ores, some of which may represent original igneous minerals, the mafic phases have apparently been entirely recrystallised

during the syn-D3 metamorphism. Hornblendes contain rounded inclusions of quartz and skeletal ore (Plate 5.1.M) which would be consistent with derivation from clinopyroxene. Syn-D3 mineral fabrics are represented by planar alignment of hornblende and biotite (Plate 5.2.M) and are locally overgrown by garnet. Garnets may contain inclusions of sphene, Fe-Ti oxides, quartz and hornblende and syntectonic rotation is evident in some examples (Plate 5.3.M). In many examples opaque ores (probably ilmenite) are mantled by rims of sphene and in some cases these mantled grains are stretched out parallel to the syn-D3 fabric. (Plate 5.4.M).

Plagioclase composition varies from An 20 to An 40 (based mainly on optical determination) but the majority of plagioclase grains are close to An 30 in composition (see Chapter 6). Thus the stable assemblage: hornblende - plagioclase (ca. An 30) - garnet - biotite with quartz and sphene corresponds to the amphibolite facies of Turner (1968) or to the medium grade of metamorphism of Winkler (1974). Epidote group minerals are generally not in equilibrium with this assemblage but occur as inclusions in hornblende and as alteration products.

Alteration effects result from retrogressive metamorphism which is younger than D4 in age. The D3 fabric is deformed in F4 chevron folds which locally have a strong crenulation cleavage. Generally recrystallisation of biotite is not related to this deformation. Post-D4 alteration is common: biotite and chlorite replace garnet, and epidote (s.l.), chlorite and calcite replace biotite.

Relict igneous texture is frequently present. Sericitised or partially recrystallised feldspar laths (Plate 5.5.M) which presumably originated as phenocrysts occur in both the coarse and fine-grained dykes. Pseudo-ophitic or subophitic textures are often discernible in thin section and on weathered surfaces.

5.2.2 Intermediate and acidic dykes

The acidic dykes are medium to fine-grained (1mm. to 2mm. average grain

Plate 5.1.M Photomicrograph to illustrate inclusions of skeletal opaque ore (probably ilmenite) and rounded quartz in a hornblende grain in a basic dyke.
X 80. XN.

Plate 5.2.M Photomicrograph to illustrate the syn-D3 foliation defined by coplanar hornblende and biotite in a basic dyke.
X 55. XN.

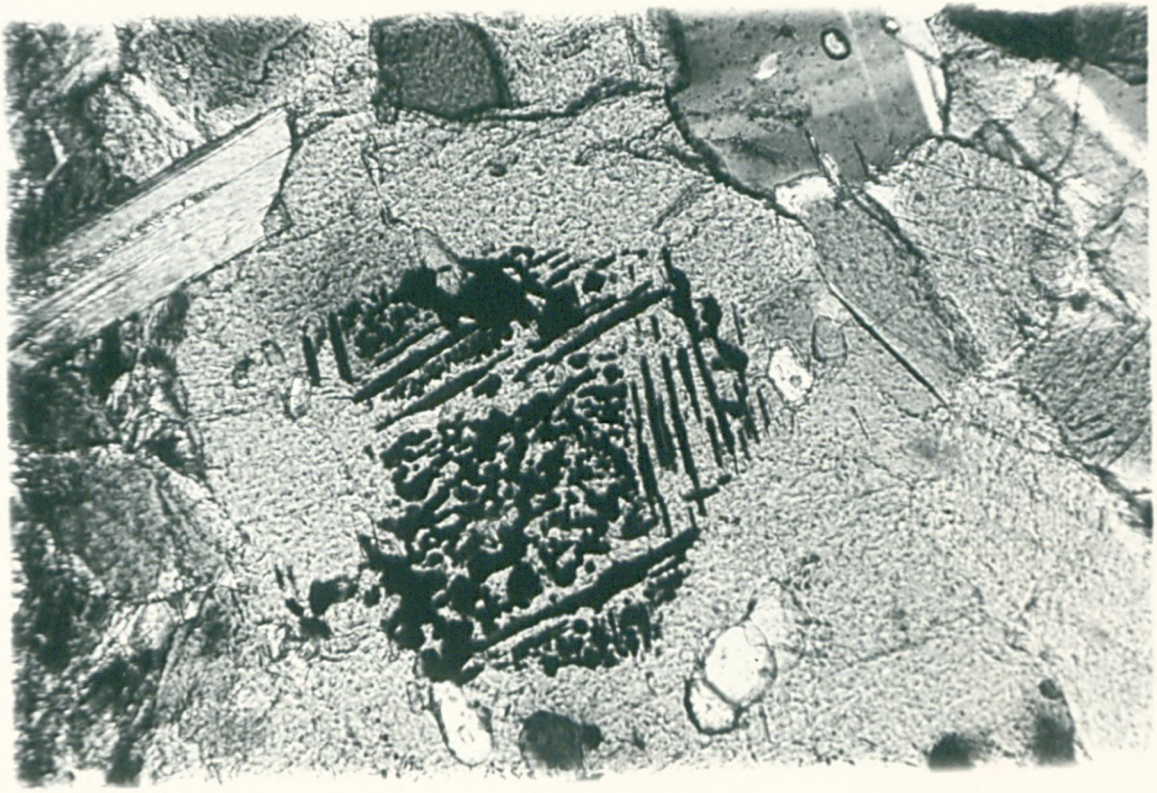

Plate 5.3.M Photomicrograph to illustrate syntectonic rotation in garnet in a basic dyke. Garnet contains inclusions of quartz (clear) and fine-grained sphene (mottled). The grain lies within a strong syn-D3 biotite fabric but biotite crystals at right are aligned at right angles to the fabric in the strain shadow of the garnet.

X 55. XN.

Plate 5.4.M Photomicrograph to illustrate opaque ores (probably ilmenite) mantled by sphene and aligned parallel to the syn-D3 fabric (developed less strongly than that illustrated in Plate 5.2.M) in a basic dyke (sample RCS 17).

X 55. XN.

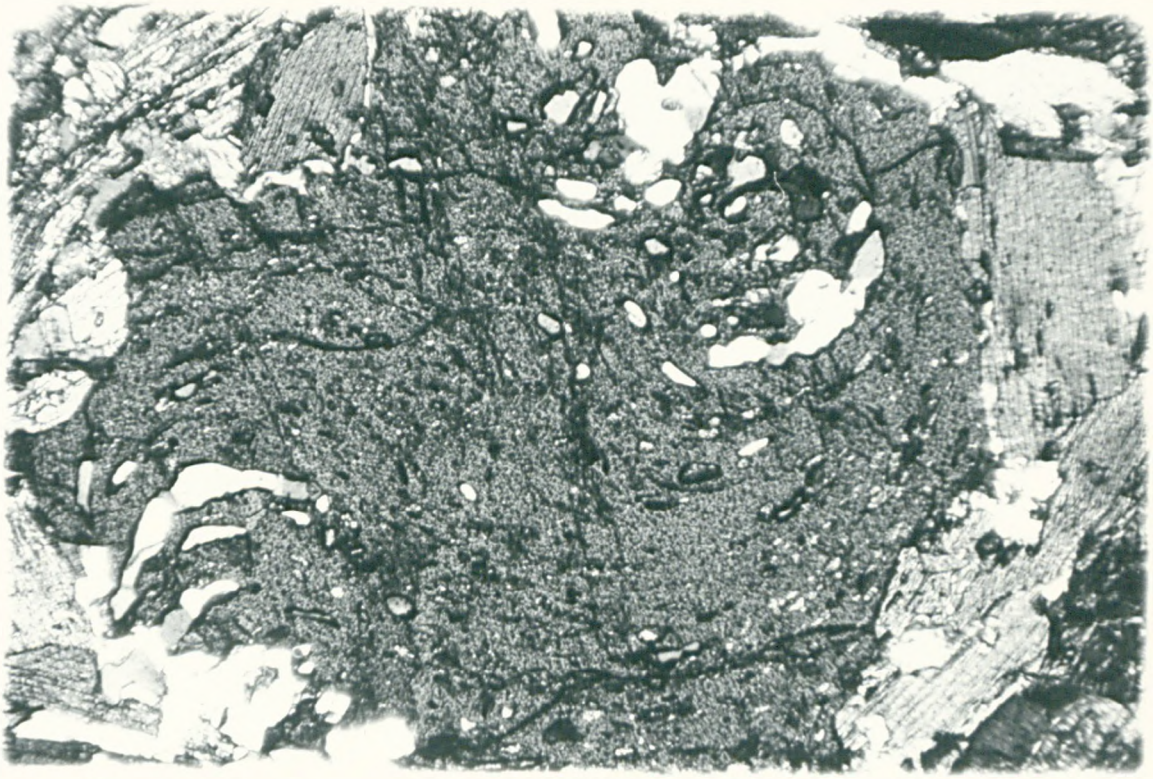

Plate 5.5.M Photomicrograph to illustrate relict igneous plagioclase, a probable phenocryst, in a basic dyke (SJ 638, Härmanö dyke). The plagioclase is partially recrystallised and replaced by decussate hornblende.
X 55. XN.

Plate 5.6.M Photomicrograph to illustrate poikiloblastic garnet and biotite fabric in the intermediate Islandsberg dyke (SJ 626). Garnets contain inclusions of quartz and sphene.
X 55. XN.

size) and contain quartz (20-30%), feldspars (40-50%), garnet (10-30%) and variable amounts of sphene and calcite (up to 5% each). Zircon, apatite, opaque ores, epidote (s.l.) and muscovite occur as accessories. Alteration of biotite to chlorite is much less common than in the mafic and ultramafic dykes. Microcline generally dominates over plagioclase and biotite usually defines a syn-D3 mineral fabric.

The intermediate dykes are generally similar and there is no sharp distinction between these and the acidic variety. They are more coarse-grained, 2 mm. to 3 mm. average grain size and contain up to 15% hornblende with greater amounts of epidote (s.l.) and biotite and lesser amounts of quartz and feldspars than the acidic dykes.

Garnets in both varieties are poikiloblastic (Plate 5.6.M), and up to 5mm. in size with numerous inclusions of quartz, sometimes showing evidence of syn-tectonic rotation. Some examples have inclusion-free cores. Garnet rims are locally post-tectonic in relation to the biotite fabric but many garnets are wrapped around by the foliation. Hornblende, sphene, epidote and muscovite all locally overgrow the biotite fabric.

Evidence of original igneous textures is generally lacking but some recrystallised clots of quartz, plagioclase and plagioclase with microcline may represent original phenocrysts.

5.3 Geochemistry of the dyke suite

5.3.1 Introduction

Seventy-one samples from thirty-nine dykes have been analysed for major and selected trace elements by X.R.F.S. (see Chapter 2). Of these, nine samples were prepared in duplicate and thirty-five prepared samples were analysed twice. One sample (SJ 632) was used in a replicate sampling experiment (see Chapter 2 and Appendix A). In addition twenty-nine of the

samples were analysed for nine major elements, excluding P_2O_5, using A.A.S and F.E.S. techniques (Chapter 2).

Fifty-eight of the samples represent the mafic to ultramafic dykes (Section 5.2.1) and thirteen have an intermediate to acidic composition (Section 5.2.2). Of the fifty-eight mafic to ultramafic dykes, multiple samples were obtained from five dykes as follows: Henån (4), Svineviken (9), Lavö (5), Härmanö (8) and Tvet (3). Thirteen samples were obtained from intermediate to acidic dykes, of which the majority come from two dykes: Islandsberg (8) and Tåkeskärn (2). The latter dyke cuts one of the multiple-sampled younger granite bodies (SJ 913-6, Section 4.3). The dyke samples are located on Fig. 5.1 and on the Map and are briefly described in Appendix D1.

The majority of samples weighed 5Kg.-10Kg. and were collected as single large blocks, primarily for geochronology (Section 5.4). Original sample weights are not known for samples prefixed "RCS", supplied by R. C. Standley, but they were in the range 1Kg.-2Kg.

5.3.2 Geochemical data and general observations.

The data and a Pearson correlation matrix for the mafic to ultramafic dykes are presented in Appendix D2 (see also Chapter 2). Summary data are given in Table 5.1. The mafic to ultramafic dykes have a basaltic composition which varies over a narrow range (Table 5.1) and is similar to an average value for continental tholeiites (Condie et al., 1969), with the exception of lower Na_2O and higher K_2O contents. Summary data for ocean floor tholeiites, calc-alkaline basalts and island arc tholeiites are also given (Table 5.1). Such comparisons are, however, of limited usefulness, especially when dealing with rocks whose average composition may be influenced by crystal fractionation, which may produce strong biases towards compositions either depleted or enriched in various components relative to the parent magma.

The intermediate to acidic rocks are highly enriched relative to the

Fig. 5.1 Geological map of western Orust taken from Park et al. (op. cit.), showing the locations of samples of the dyke suite (▲) and of two pegmatite samples (▽). Whole-rock samples of the Härmanö dyke and the Lavö dyke and muscovite and plagioclase from SJ 921 and 922 (pegmatites) have been analysed for Rb-Sr geochronology.
Inset shows the location of the Orust area and the main tectonic and lithological divisions of part of the Sveconorwegian province. A = Åmål belt, B = Bohus granite, D = Dal Group, SLM = Stora Le - Marstrand belt, P = Pregothian belt.

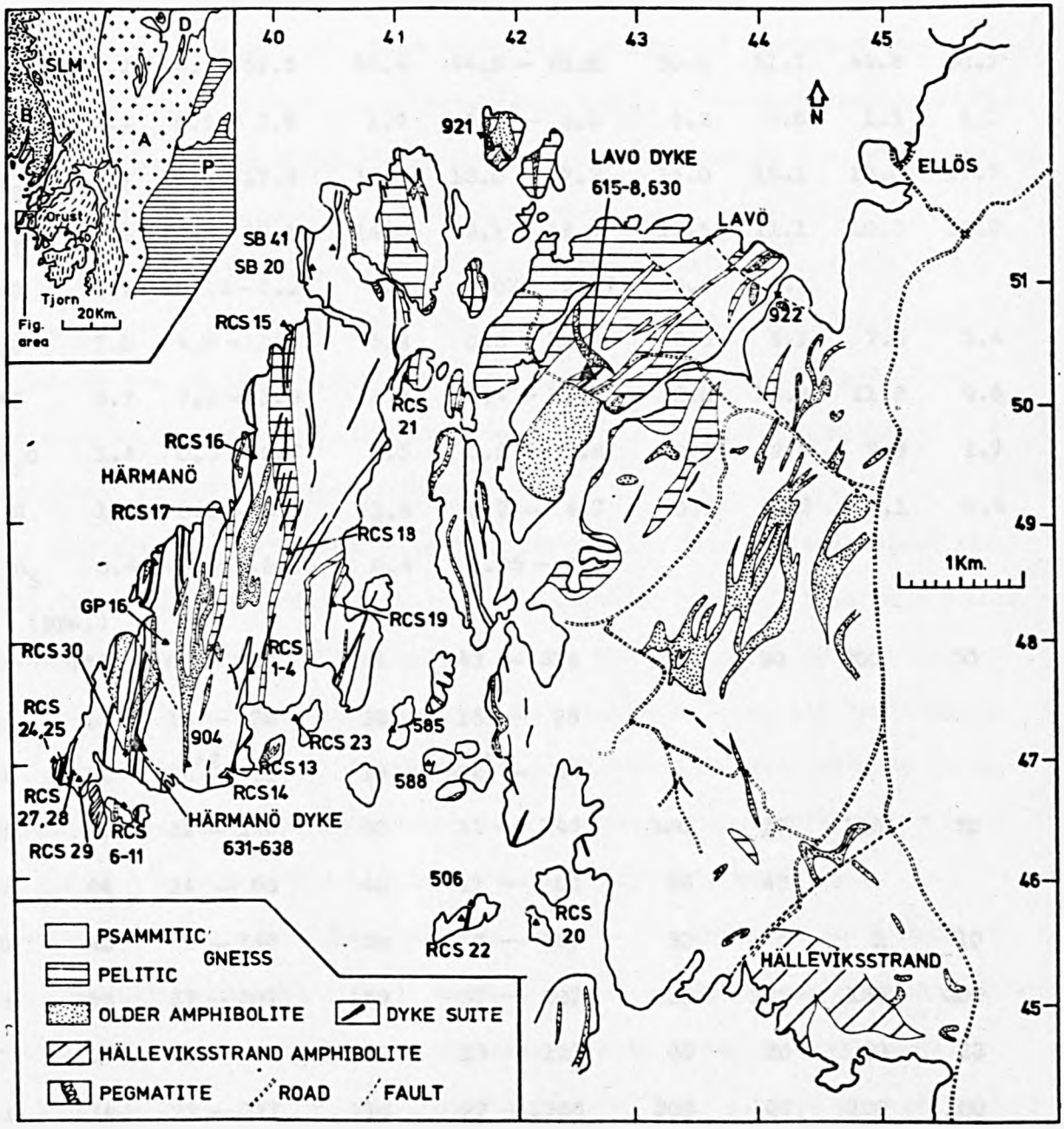
SLM
B
A
P
D
Orust
Tjorn
Fig. area
20Km.
40
41
42
43
44
45
N
921
LAVO DYKE
615-8,630
ELLÖS
LAVÖ
SB 41
SB 20
922
RCS 15
RCS 21
RCS 16
HÄRMANÖ
RCS 17
RCS 18
RCS 19
GP 16
RCS 30
RCS 1-4
RCS 24,25
904
RCS 23
585
RCS 13
588
RCS 14
RCS 27,28
RCS 29
RCS 6-11
HÄRMANÖ DYKE
631-638
506
RCS 22
RCS 20
HÄLLEVIKSSTRAND
1Km.
51
50
49
48
47
46
45
PSAMMITIC GNEISS
PELITIC
OLDER AMPHIBOLITE
DYKE SUITE
HÄLLEVIKSSTRAND AMPHIBOLITE
PEGMATITE
ROAD
FAULT

Table 5.1

Summary geochemical data: dyke suite.

	(a)		(b)					
	mean	range	mean	range	(1)	(2)	(3)	(4)
(Wt. %)								
SiO_2	47.2	44.5 – 52.6	50.4	44.5 – 70.8	50.1	51.1	49.8	50.2
TiO_2	2.2	0.5 – 3.6	1.9	0.5 – 3.6	2.2	0.8	1.5	1.0
Al_2O_3	14.7	13.4 – 17.3	14.4	13.0 – 17.3	14.0	16.1	16.0	17.7
Fe_2O_3*1	14.8	10.4 – 18.1	14.0	5.1 – 18.1	13.5	11.1	10.3	10.9
MnO	0.2	0.16 – 0.27	0.2	0.07 – 0.27	0.2	0.2		
MgO	7.0	4.6 – 10.0	5.8	0.3 – 10.0	6.5	5.1	7.5	5.4
CaO	9.7	7.2 – 11.6	8.6	1.4 – 11.6	9.8	10.8	11.2	9.8
Na_2O	1.4	0.5 – 2.7	1.5	0.5 – 2.8	2.5	2.0	2.8	2.7
K_2O	1.4	0.2 – 3.2	1.8	0.2 – 4.7	0.8	0.3	0.1	0.9
P_2O_5	0.4	0.05 – 0.95	0.4	0.05 – 0.95				
(ppm.)								
Cr	156	103 – 319	136	43 – 319	100	50	300	50
Ga	23	15 – 28	23	15 – 28				
Nb	11	BDL*2 – 21	18	BDL*2 – 54				
Ni	70	32 – 146	60	11 – 146	100	25	100	50
Sc	44	24 – 65	40	11 – 65	36	43		
Rb	49	5 – 146	59	5 – 157	30	5	1	10
Sr	153	57 – 307	159	57 – 307	350	225	135	300
Y	39	15 – 64	52	15 – 128	30	20	30	23
Zr	174	22 – 327	110	22 – 1388	200	60	100	100
ratios								
K/Rb	264	142 – 443	268	142 – 443	300	700	1200	350
Y/Nb	3.7	2.4 – 6.3	3.4	2.1 – 6.3				

Notes *1 total iron as Fe_2O_3 *2 BDL = below detection limit
(a) mafic and ultramafic dykes (n = 58)
(b) all dykes (n = 71)
(1) average continental tholeiite
(2) average island arc tholeiite
(3) average ocean floor tholeiite
(4) average calc-alkaline basalt
Literature compilations from Condie et al. (1969) and Condie (1976)

basic dykes especially in certain incompatible elements, e.g. Zr, Nb, Y and light REE and have an unusually high total iron content (ca. 12% TFe_2O_3 at ca. 63% SiO_2).

Over the narrow compositional range observed the basic rocks display regular inter-element variations on various binary and ternary plots (Figs. 5.2 - 5.6). There is some tendency toward a bimodal grouping of the data and the pattern displayed by one large dyke (Härmanö, 30m. wide) exerts considerable influence on many of the diagrams.

There is a marked compositional gap between the basic and the more siliceous rocks but the apparent bimodality here is due to the weighting effect of the multiple samples of the Islandsberg dyke. If the data for the more siliceous dykes is reduced to four points representing the individual dykes this feature is removed.

The question arises as to whether or not the intermediate-acidic and basic dykes may be derived from a common magmatic parent. This is a common problem in the study of igneous rock suites and is compounded in this case by the amphibolite grade metamorphism (Section 5.2.1) and the variation in deformation (Appendix D1). The spread of the data is considered to be too large and the inter-element variation too consistently regular for a large number of components (Figs. 5.2 - 5.6) to result from metamorphic re-distribution alone. Certainly the pattern of enrichment in certain of the incompatible elements (e.g. Zr, Nb, Y), especially in the intermediate-acidic dykes is too great to be accounted for in terms of contamination from the surrounding gneisses (Section 3.3 and Table 3.1 for average country rock geochemical data).

It is, of course, possible and, indeed, likely that exchange of some components with the gneisses and/or with the ambient fluid has taken place during metamorphism and deformation and that this may account for some of the variation in dyke chemistry. There is abundant petrographic evidence for low range mobility, e.g. sphene rims on Fe-Ti oxides (Ti, Ca), epidote and sericite replacing plagioclase (Ca, Na, K, Sr, Rb) and chlorite replacing

biotite (Ti, K, Rb, ± Fe, Mg) (Section 5.2.1). However it is not generally possible to demonstrate such geochemical mobility from the present data. An important exception is the pattern of alkali variation and the evident exchange of Rb and Sr with the gneisses (Section 5.4.4).

Both highly deformed and undeformed dykes occur at both ends of the compositional spectrum for many components (see Appendices D1 and D2) implying that there has been no general control of the dyke chemistry as a result of deformation. Furthermore, no systematic variation between position in the dyke (e.g. relative to the margins) and composition could be established for any of the multiple sampled dykes. The largest such dyke (Harmano, 30m. wide) is undeformed and has locally developed fine-grained margins. The dyke has a relatively primitive composition and shows a significant (linear) spread on nearly all of the compositional variation diagrams (Fig. 5.2 et seq.). Samples SJ 631 and SJ 635-6 (adjacent) were collected ca.50m. apart close to the western margin. These samples (SJ 635-6 are similar) lie at opposite ends of the compositional range for a number of components (e.g. MgO, P_2O_5, Zr). The observed trend in the data for this dyke may be due instead to repeated injection of small batches of magma or to in situ differentiation as discussed below.

In all of the compositional variation diagrams (Figs. 5.2 et seq.) the data points are shown individually and the fields of each dyke are indicated. The error bars have been determined from one of the replicate sampling experiments (Chapter 2 and Appendix A). Thus from the various diagrams the overall variation of the data set between pairs or terns of components may be compared with the variation within dykes and with the estinated experimental uncertainties.

5.3.3 Inter-element variations and petrogenesis.

5.3.3.1 Major elements.

The entire suite defines a strong iron enrichment trend on an AFM diagram, (Fig. 5.2) which lies very close to that of the Skaergaard

Fig. 5.2 AFM diagram for the dyke suite. A = trend of the Skaergaard intrusion (Wager and Deer, 1939). B = boundary between tholeiitic (above) and calc-alkaline rock types (Irvine and Barager, 1971). Large dots represent coincidence of five or more points. 1 = Härmanö dyke, 2 = Tvet dyke, 3 = Lavö dyke, 4 = Svineviken dyke, 5 = Henån dyke and 6 = Islandsberg dyke.

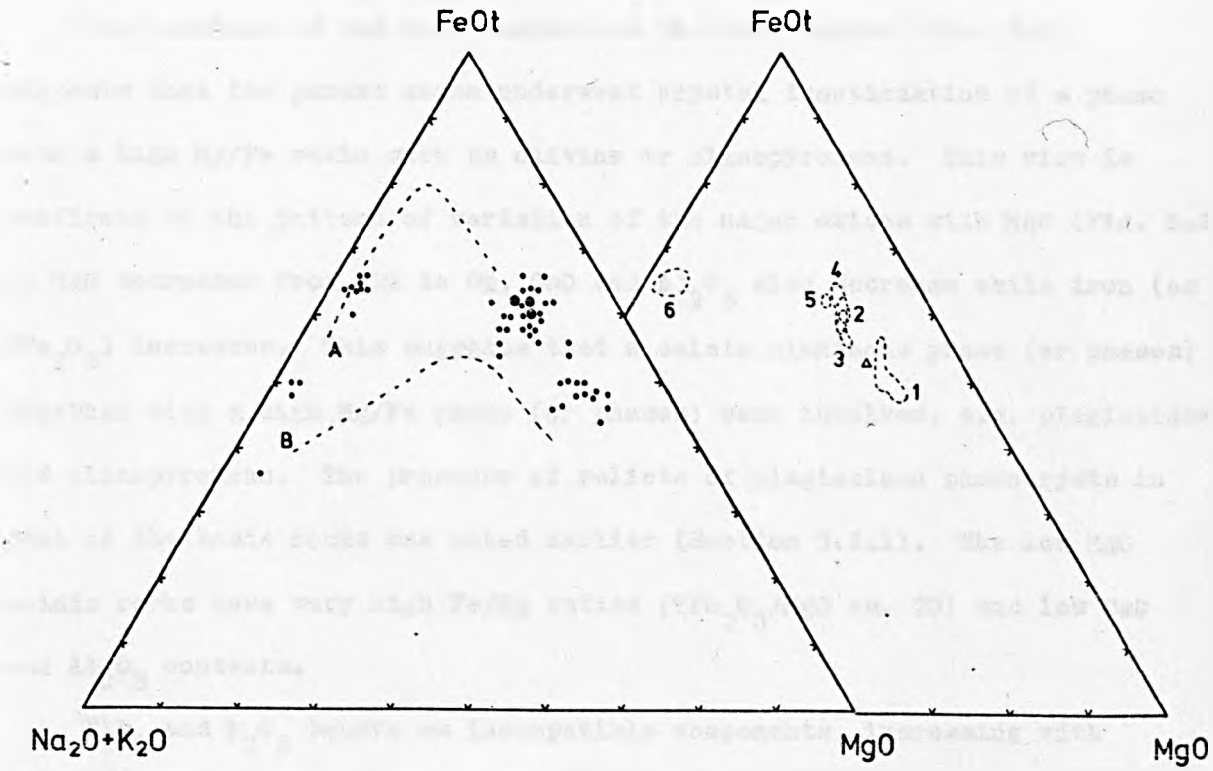
FeOt
FeOt
A
B
6
5
4
2
3
1
Na_2O+K_2O
MgO
MgO

intrusion (Wager and Deer, 1939) and well within the tholeiite field above an arbitrary line which distinguishes between tholeiitic and calc-alkaline rock types (Irvine and Barager, 1971). The intermediate-acidic rocks lie close to the A-F join. The trend of the basic rocks is similar to that of the older amphibolites (Section 3.3) but is quite distinct from that of the Hällevikstrand amphibolite (Section 4.3), which has a calc-alkaline affinity on this basis.

The position of the dyke samples on the AFM diagram (Fig. 5.2) suggests that the parent magma underwent crystal fractionation of a phase with a high Mg/Fe ratio such as olivine or clinopyroxene. This view is confirmed by the pattern of variation of the major oxides with MgO (Fig. 5.3). As MgO decreases from 10% to 6%, CaO and Al_2O_3 also decrease while iron (as TFe_2O_3) increases. This suggests that a calcic aluminous phase (or phases) together with a high Mg/Fe phase (or phases) were involved, e.g. plagioclase and clinopyroxene. The presence of relicts of plagioclase phenocrysts in some of the basic rocks was noted earlier (Section 5.2.1). The low MgO acidic rocks have very high Fe/Mg ratios (TFe_2O_3/MgO ca. 20) and low CaO and Al_2O_3 contents.

TiO_2 and P_2O_5 behave as incompatible components, increasing with decreasing MgO until ca. 6% MgO, below which there is a discontinuous trend to the more evolved acidic rocks. Iron also begins to decrease with MgO at this point and taken together these observations are consistent with loss of Fe-Ti oxides and apatite from the parent magma. Four samples show enrichment in P_2O_5 suggesting accumulation of apatite in these rocks (RCS 3, 7, 28 and SJ 904) but none of the binary plots display definite cross trends and none of the dykes may be regarded as cumulates.

The extreme iron enrichment in the intermediate Islandsberg dyke is unusual but similar chemical compositions are found in late-stage differentiates of the Skaergaard intrusion (Wager and Brown, 1968, table 9: melanogranophyre (4332); ca. 16% TFe_2O_3 at 60% SiO_2, transitional grano-

Fig. 5.3 Binary plots for the dyke suite. Clockwise from top right:- CaO, Al_2O_3, SiO_2, total iron as Fe_2O_3, TiO_2 and P_2O_5 vs. MgO. Fields of individual dykes as for Fig. 5.2. In addition 7 = Tåkeskärn dyke.

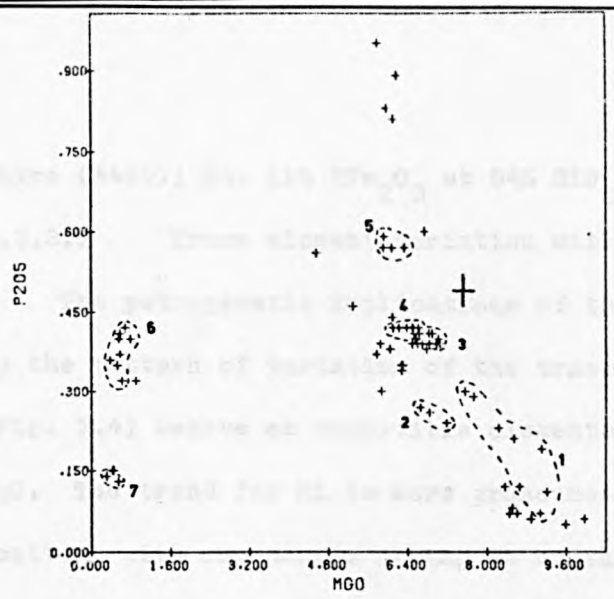
P2O5
MGO
.900
.750
.600
.450
.300
.150
0.000
0.000
1.600
3.200
4.800
6.400
8.000
9.600
1
2
3
4
5
6
7

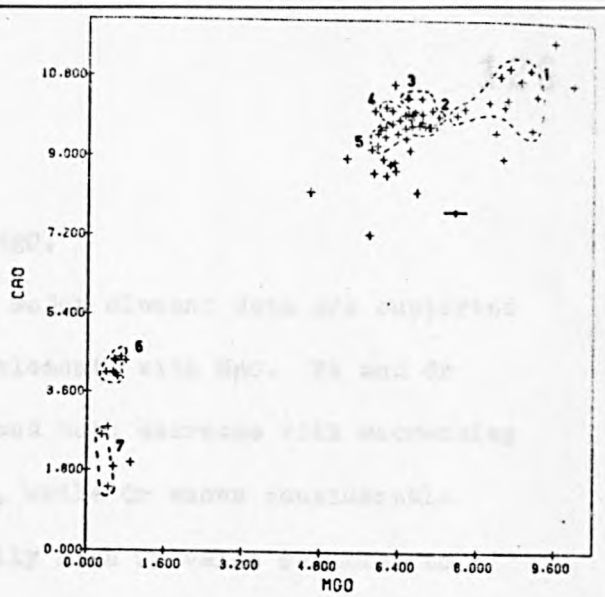
CAO
MGO
10.800
9.000
7.200
5.400
3.600
1.800
0.000
0.000
1.600
3.200
4.800
6.400
8.000
9.600
1
2
3
4
5
6
7

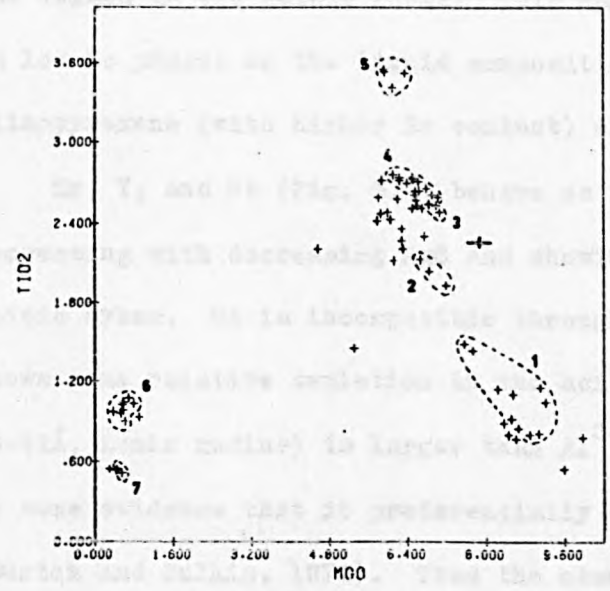
TIO2
MGO
3.600
3.000
2.400
1.800
1.200
.600
0.000
0.000
1.600
3.200
4.800
6.400
8.000
9.600
1
2
3
4
5
6
7

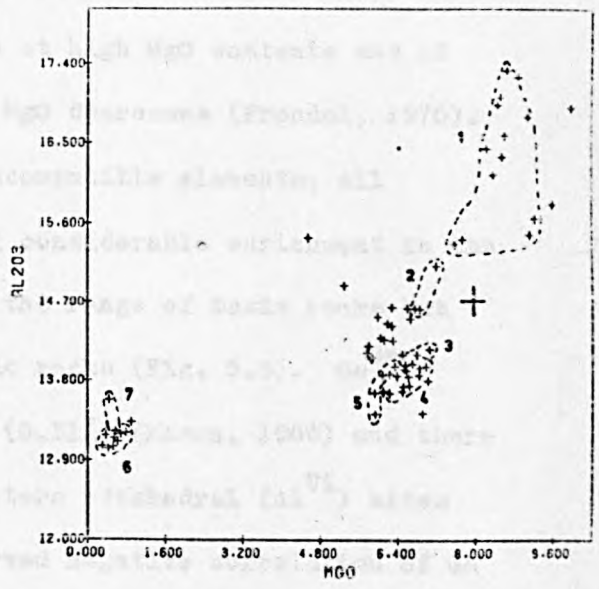
AL2O3
MGO
17.400
16.500
15.600
14.700
13.800
12.900
12.000
0.000
1.600
3.200
4.800
6.400
8.000
9.600
1
2
3
4
5
6
7

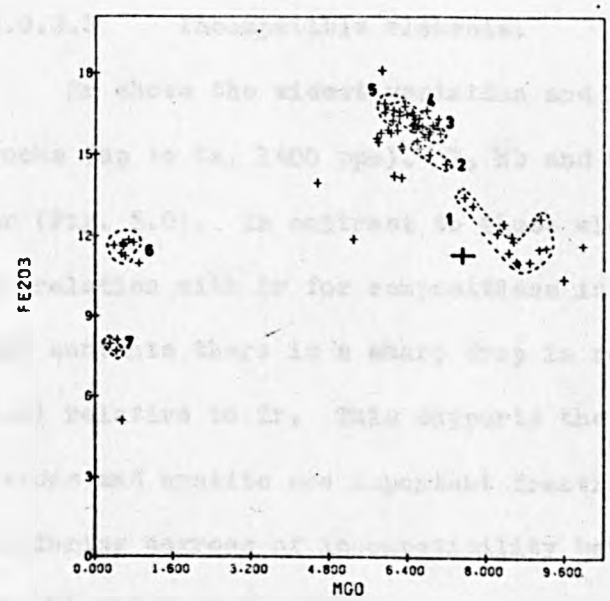
FE2O3
MGO
18
15
12
9
6
3
0
0.000
1.600
3.200
4.800
6.400
8.000
9.600
1
2
3
4
5
6
7

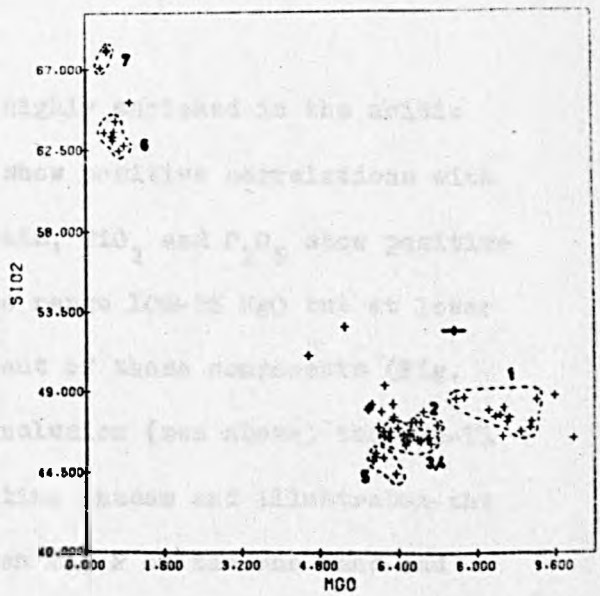
SIO2
MGO
67.000
62.500
58.000
53.500
49.000
44.500
40.000
0.000
1.600
3.200
4.800
6.400
8.000
9.600
1
2
3
4
5
6
7

phyre (4489); ca. 11% TFe_2O_3 at 64% SiO_2)

5.3.3.2 Trace element variation with MgO.

The petrogenetic implications of the major element data are supported by the pattern of variation of the trace elements with MgO. Ni and Cr (Fig. 5.4) behave as compatible elements and both decrease with decreasing MgO. The trend for Ni is more pronounced, while Cr shows considerable scatter, with one sample having an unusually high Cr value relative to the others. Scandium shows an inflection at ca. 7% MgO. At higher values of MgO Sc increases with decreasing MgO and later decreases towards the values in the acidic rocks. This may reflect the influence of olivine (a low Sc phase) on the liquid composition at high MgO contents and of clinopyroxene (with higher Sc content) as MgO decreases (Frondel, 1970).

Zr, Y, and Nb (Fig. 5.4) behave as incompatible elements, all increasing with decreasing MgO and showing considerable enrichment in the acidic dykes. Ga is incompatible through the range of basic rocks but shows some relative depletion in the acidic rocks (Fig. 5.5). Ga^{3+} (0.62Å, ionic radius) is larger than Al^{3+} (0.51Å) (Mason, 1966) and there is some evidence that it preferentially enters octahedral (Al^{VI}) sites (Burton and Culkin, 1972). Thus the observed negative correlation of Ga with Al_2O_3 (Fig. 5.5) may reflect depletion of the magma in phases with high Al^{IV}/Al^{VI} ratios, e.g. clinopyroxene and plagioclase.

5.3.3.3 Incompatible elements.

Zr shows the widest variation and is highly enriched in the acidic rocks (up to ca. 1400 ppm). Y, Nb and Ga show positive correlations with Zr (Fig. 5.6). In contrast to these elements, TiO_2 and P_2O_5 show positive correlation with Zr for compositions in the range 10%-6% MgO but at lower MgO contents there is a sharp drop in content of these components (Fig. 5.6) relative to Zr. This supports the conclusion (see above) that Fe-Ti oxides and apatite are important fractionating phases and illustrates the differing degrees of incompatibility between Ti, P on the one hand and Zr, Nb and Y on the other.

Fig. 5.4 Binary plots for the dyke suite. Clockwise from top right:- Ni, Cr, Sc, Nb, Y and Zr vs. MgO. Fields of individual dykes as for Fig. 5.3. Arrow points to one sample (RCS O) with 319 ppm. Cr, outside the range of the diagram.

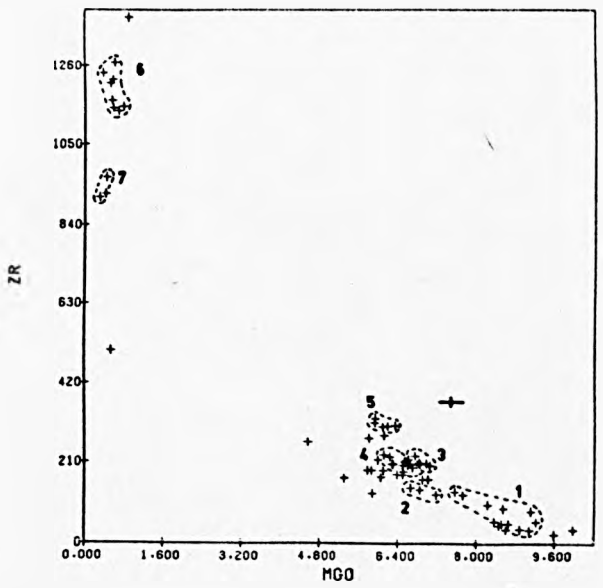
ZR
MGO
0.000
1.600
3.200
4.800
6.400
8.000
9.600
0
210
420
630
840
1050
1260
1
2
3
4
5
6
7

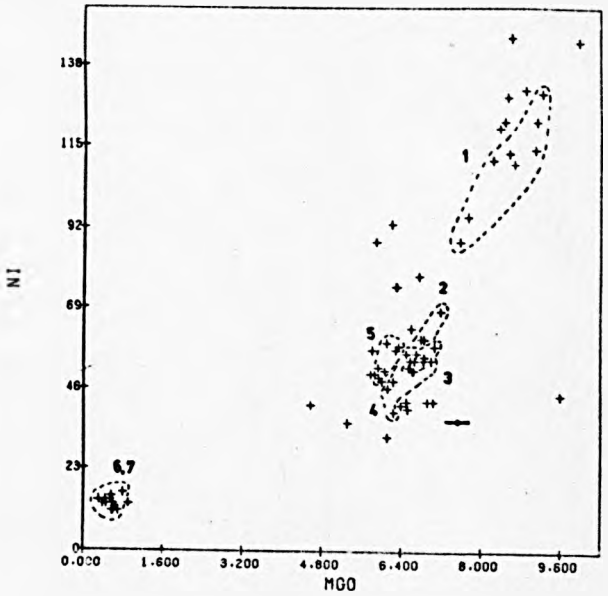
NI
MGO
0.000
1.600
3.200
4.800
6.400
8.000
9.600
0
23
46
69
92
115
138
1
2
3
4
5
6,7

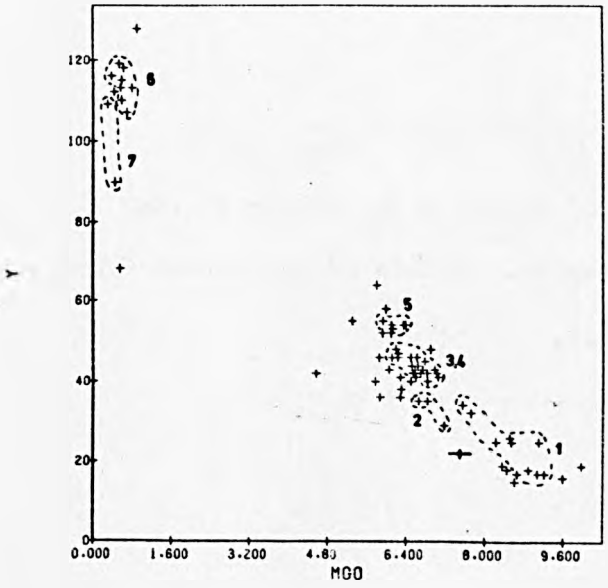
Y
MGO
0.000
1.600
3.200
4.800
6.400
8.000
9.600
0
20
40
60
80
100
120
1
2
3,4
5
6
7

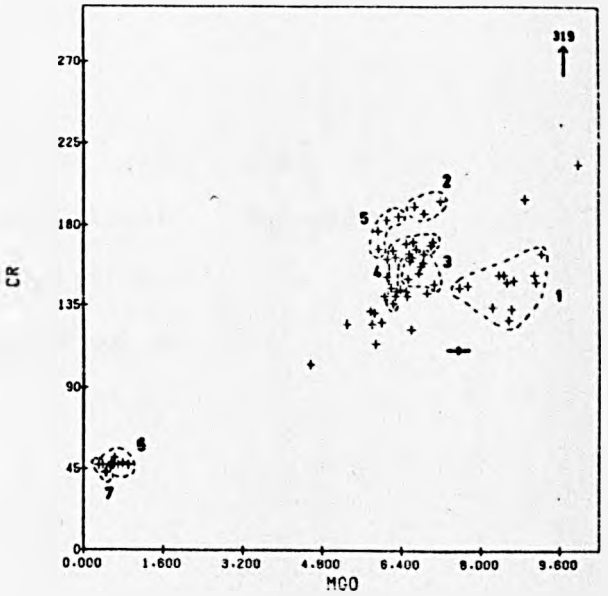
CR
MGO
0.000
1.600
3.200
4.800
6.400
8.000
9.600
0
45
90
135
180
225
270
319
1
2
3
4
5
6
7

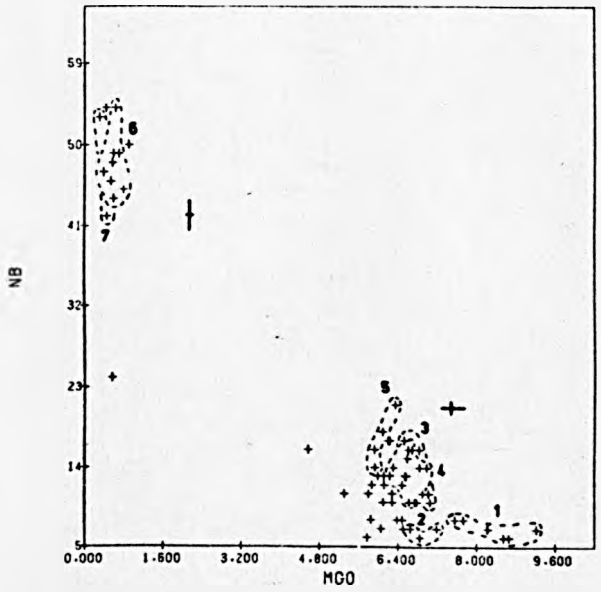
NB
MGO
0.000
1.600
3.200
4.800
6.400
8.000
9.600
5
14
23
32
41
50
59
1
2
3
4
5
6
7

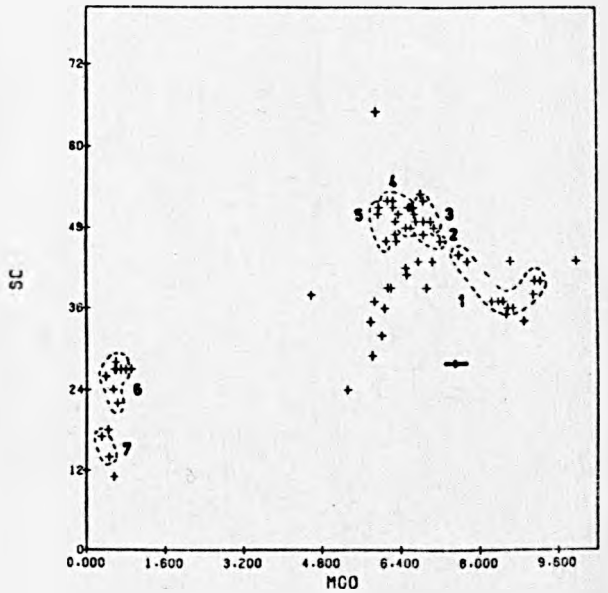
SC
MGO
0.000
1.600
3.200
4.800
6.400
8.000
9.600
0
12
24
36
48
60
72
1
2
3
4
5
6
7

Fig. 5.5 Binary plots of Ga vs. Al_2O_3 and Ga vs. MgO for the dyke suite. Fields of individual dykes as for Fig. 5.2.

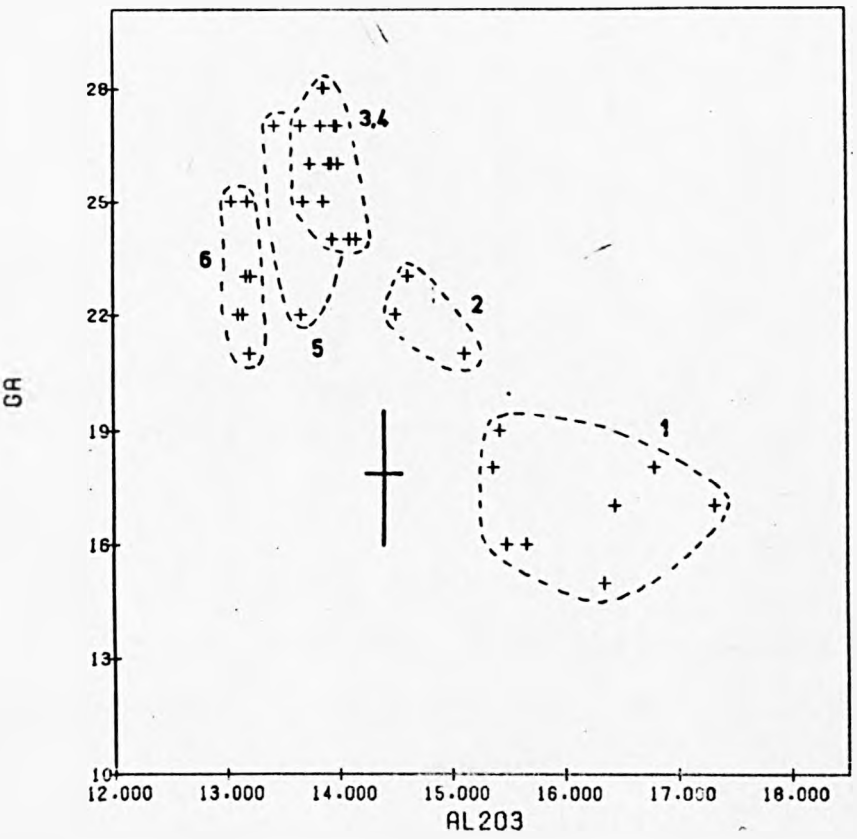
GA
28
25
22
19
16
13
10
12.000
13.000
14.000
15.000
16.000
17.000
18.000
AL203
3,4
6
5
2
1

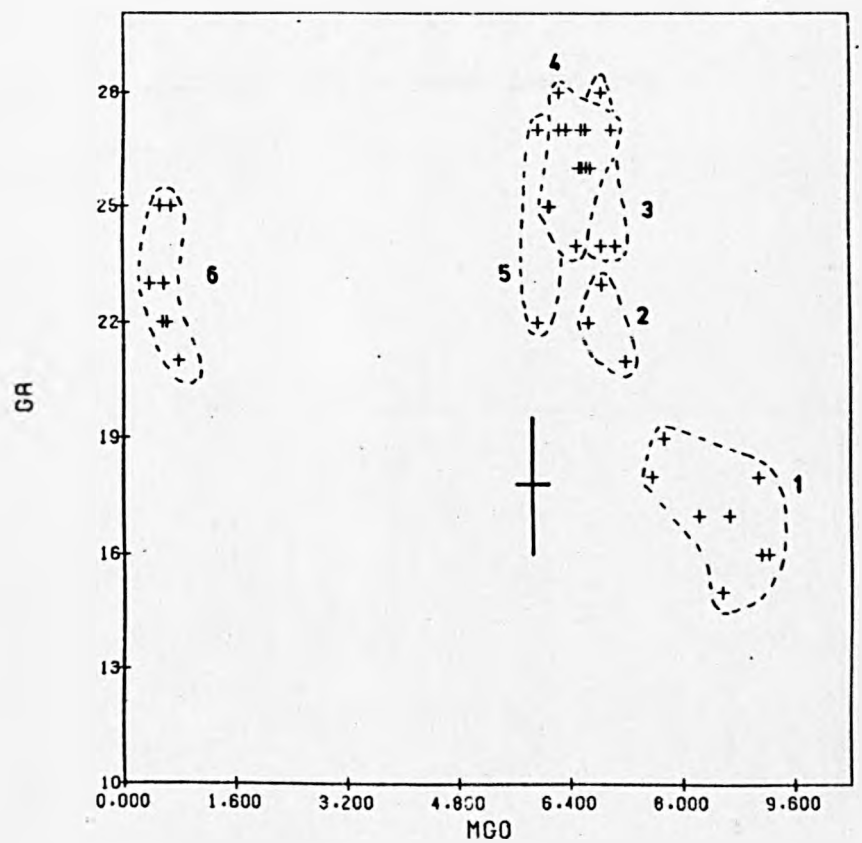
GA
28
25
22
19
16
13
10
0.000
1.600
3.200
4.800
6.400
8.000
9.600
MGO
4
6
5
3
2
1

Fig. 5.6 Binary plots for the dyke suite. Clockwise from top right:- Nb, Y, Ga, P_2O_5, TiO_2 vs. Zr. Fields of individual dykes as for Fig. 5.3.

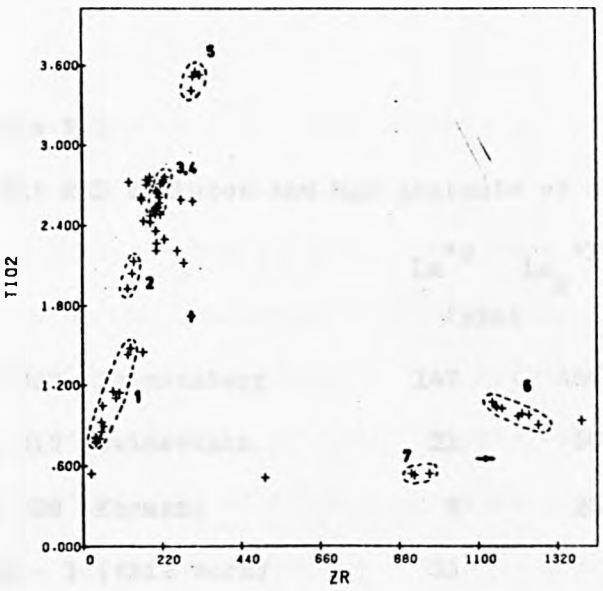
TIO2
ZR
0.000
.600
1.200
1.800
2.400
3.000
3.600
0
220
440
660
880
1100
1320
1
2
3,4
5
6
7

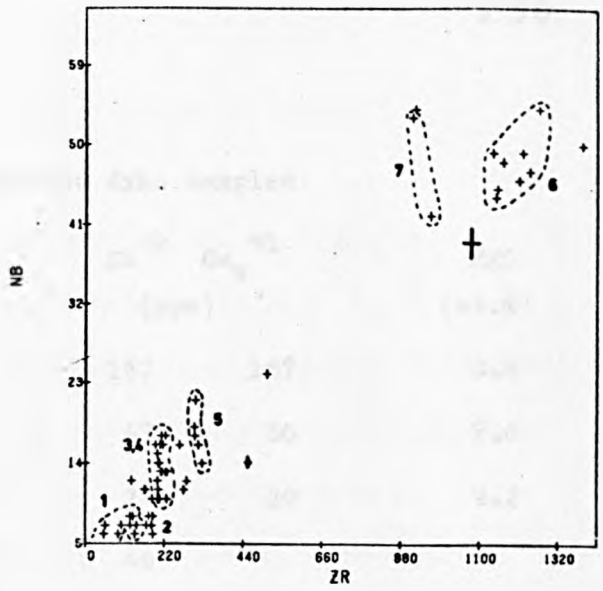
NB
ZR
5
14
23
32
41
50
59
0
220
440
660
880
1100
1320
1
2
3,4
5
6
7

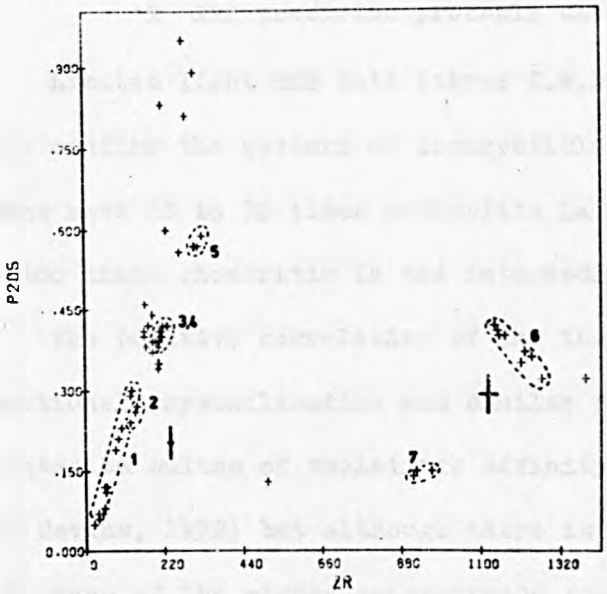
P2O5
ZR
0.000
.150
.300
.450
.600
.750
.900
0
220
440
660
880
1100
1320
1
2
3,4
5
6
7

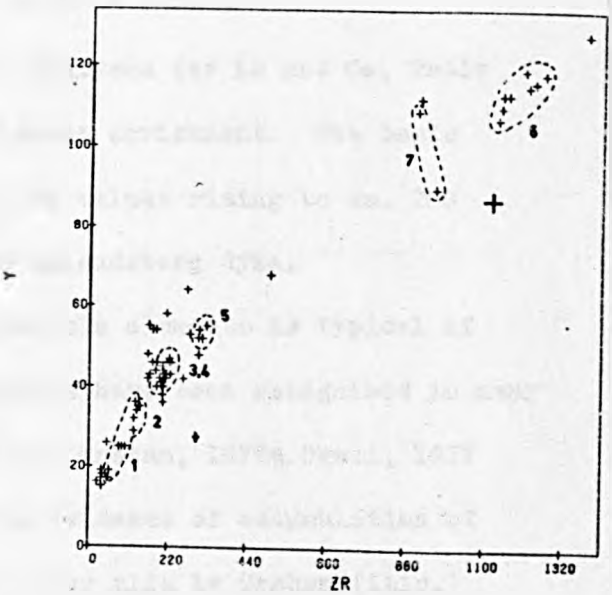
Y
ZR
0
20
40
60
80
100
120
0
220
440
660
880
1100
1320
1
2
3,4
5
6
7

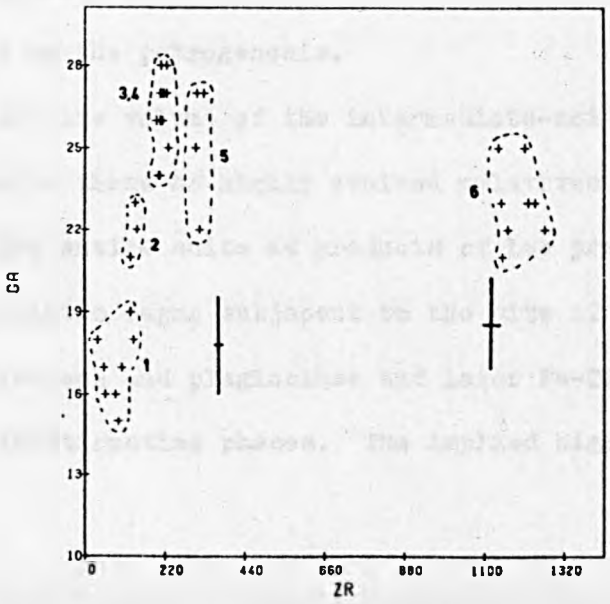
CR
ZR
10
13
16
19
22
25
28
0
220
440
660
880
1100
1320
1
2
3,4
5
6

Table 5.2

Light REE analyses and MgO contents of selected dyke samples

		La^{*2}	$La_N{}^{*1}$	Ce^{*2}	$Ce_N{}^{*1}$	MgO
		(ppm)		(ppm)		(wt.%)
SJ 620	Islandsberg	147	459	157	167	0.8
SJ 612	Svineviken	21	66	47	50	7.0
SJ 638	Härmanö	8	25	27	29	9.2
BCR - 1	(this work)	31		49		
BCR - 1	(Abbey, 1975)	25		54		

*1 Chondrite - normalised data

*2 XRF precision probably close to $\pm$ 5% (2σ)

Limited light REE data (three X.R.F.S. analyses for La and Ce, Table 5.2) confirm the pattern of incompatible element enrichment. The basic rocks have 25 to 70 times chondritic La and Ce values rising to ca. 200 to 400 times chondritic in the intermediate Islandsberg dyke.

The positive correlation of the incompatible elements is typical of fractional crystallisation and similar patterns have been recognised in many metabasite suites of tholeiitic affinity (e.g. Graham, 1976a, Ogezi, 1977 and Bevins, 1979) but although there is some evidence of accumulation of P_2O_5 none of the strong cross-trends found inter alia by Graham (ibid.) is observed. The latter study (of Dalradian metabasites) shows greater enrichments in P_2O_5 and TiO_2 and there is some independent geological evidence that cumulates are present.

5.3.3.4 Conclusions on the petrogenesis.

Given the small relative volume of the intermediate-acidic dykes it seems reasonable to regard these as highly evolved relatives of the basic rocks and to consider the entire suite as products of low pressure crystal fractionation of a tholeiitic magma subjacent to the site of dyke emplacement. Olivine, clinopyroxene and plagioclase and later Fe-Ti oxides and apatite were probable fractionating phases. The implied high level of

dyke intrusion is consistent with the geological evidence (Section 5.2 and Park et al., op. cit.).

In situ differentiation may have contributed to the geochemical variation in the larger dykes but only four examples with high P_2O_5 contents show any indication of crystal accumulation. A mechanism involving repeated injection of small volumes of evolving magma would account both for the intra-dyke variation (e.g. Härmanö dyke) and for the geochemical variation of the suite as a whole. Examples of clear cases of multiple intrusion were noted earlier (Section 5.2) but these have not been sampled.

5.3.4 Geochemical variation in the basic dykes and the use of "immobile" trace element discriminant diagrams.

There is ample evidence for modification of the chemistry of metabasic rocks during metamorphism and deformation (e.g. Beach, 1976, Kerrich et al., 1977). In order to demonstrate such modifications it is necessary to examine cases where heterogeneities due to deformation and/or metamorphism are present and where there is good control on initial variation in composition. Several studies of variation on a small scale between sheared dyke margins and undeformed centres (e.g. Burns 1966, Chapman, 1978) have illustrated the importance of internal redistribution of material as well as exchange with the surroundings. Dostal and Fratta (1977) have studied the variation in composition of a single dyke where it cuts country rocks of contrasted composition. The results of such studies, which involved both major and trace elements, have emphasised the relative mobility of alkali elements and Sr, and contrasted the behaviour of less mobile components. In such studies the concept of "relative mobility" is critical. Tests of bulk changes in composition are difficult to devise (e.g. Kerrich et al., 1977) but a commonly employed test is to make use of constant ratios of so-called immobile elements as criteria of immobility. However, such a test may be misleading and may merely reflect the close chemical coherence of the components involved.

In recent years there have been a number of schemes which have attempted to use inter-relationships between elements regarded as immobile during low grade metamorphism and alteration, e.g. Ti, Zr, Y, P, Nb, to distinguish between magma types and to infer the tectonic setting of metabasites (e.g. Cann, 1970b, Pearce and Cann, 1971, 1973, Pearce, 1975, Floyd and Winchester, 1975, Winchester and Floyd, 1976 etc.). The majority of attempts to use such techniques have been restricted to low grade metamorphic environments. Winchester and Floyd (1976) included rocks at higher grades of metamorphism (up to "amphibolite facies") to illustrate the application of their diagrams.

Detailed critical appraisal of the various methods (e.g. Smith and Smith, 1976 and Morrison, 1978) has been confined to examples at low metamorphic grade. Graham (1976b) and Floyd and Winchester (1976) have pointed out the possible difficulties arising due to igneous differentiation processes. Graham (ibid.) has specifically criticised the use by Winchester and Floyd (1976) of the TiO_2-Zr/P_2O_5 diagram (Floyd and Winchester, 1975) as applied to Dalradian amphibolites.

When plotted on the various discriminant diagrams proposed to distinguish e.g. tholeiitic (or subalkaline) from alkaline magma types the present data may be used as an illustration of the range of variation to be expected in a suite of consanguineous amphibolites. The data for the mafic to ultramafic (all basic) dykes have been plotted (Figs. 5.7-5.11) and the variation in the data set may be compared with the range of values in the individual dykes and with the estimated experimental uncertainties.

Fig. 5.7 illustrates the failure of a conventional alkali-silica variation diagram (Macdonald and Katsura, 1964) to assign a magma type to metamorphosed rocks. The crude negative correlation between total alkalis and SiO_2 is dominated by increase in K_2O from the Härmanö dyke (undeformed) to the biotite-rich Henån dyke.

Fig. 5.8, Fig. 5.9 and 5.10 illustrate the discriminant scheme used

Fig. 5.7 Binary plot of total alkalis (ALKS = $Na_2O + K_2O$) vs. SiO_2 for the mafic to ultramafic dykes after Macdonald and Katsura (1964). The dashed line separates tholeiitic (below) from alkaline (above) basaltic rocks. Fields of individual dykes as for Fig. 5.2.

Fig. 5.8 Binary plot of Ti vs. Zr for the mafic to ultramafic dykes, after Pearce and Cann (1973). Ocean-floor basalts plot in fields D and B, low-potassium tholeiites (island arc tholeiites) plot in fields A and B and calc-alkaline basalts plot in fields C and B. The differentiated nature of the dyke suite results in the majority of samples plotting outside the discriminant fields. Fields of individual dykes as for Fig. 5.2.

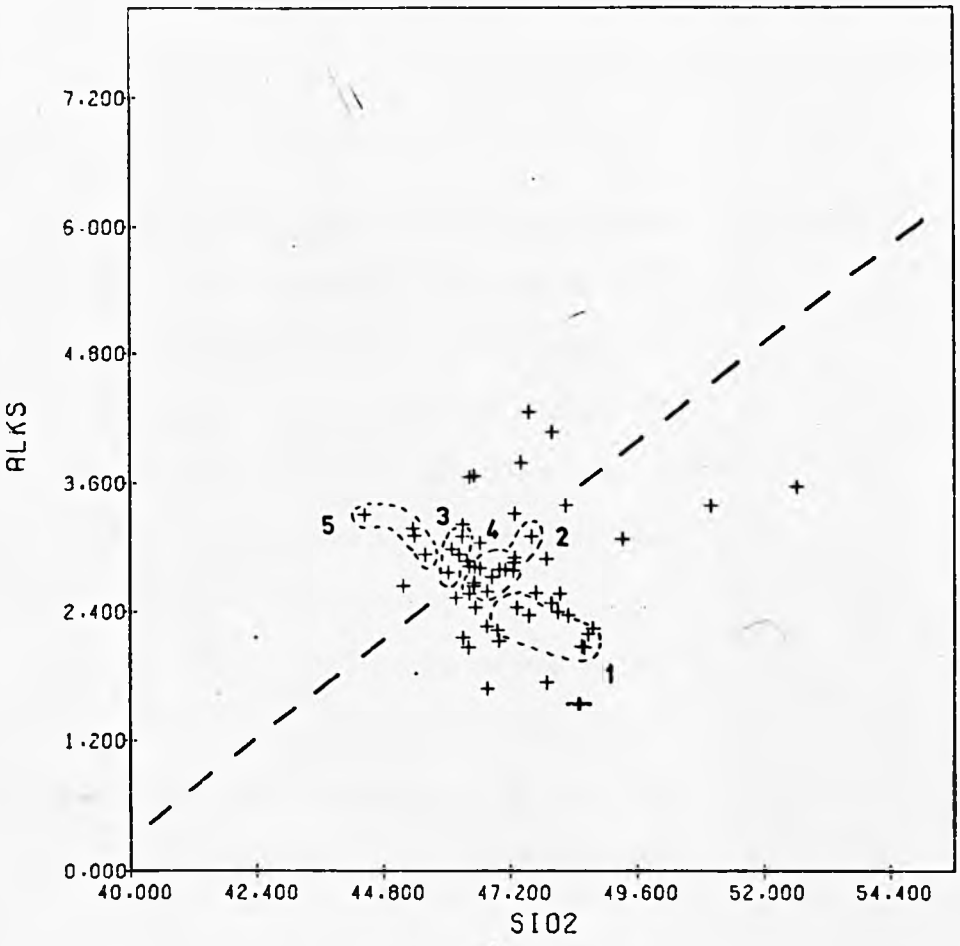
7.200
6.000
4.800
3.600
2.400
1.200
0.000
ALKS
40.000
42.400
44.800
47.200
49.600
52.000
54.400
SIO2
5
3
4
2
1

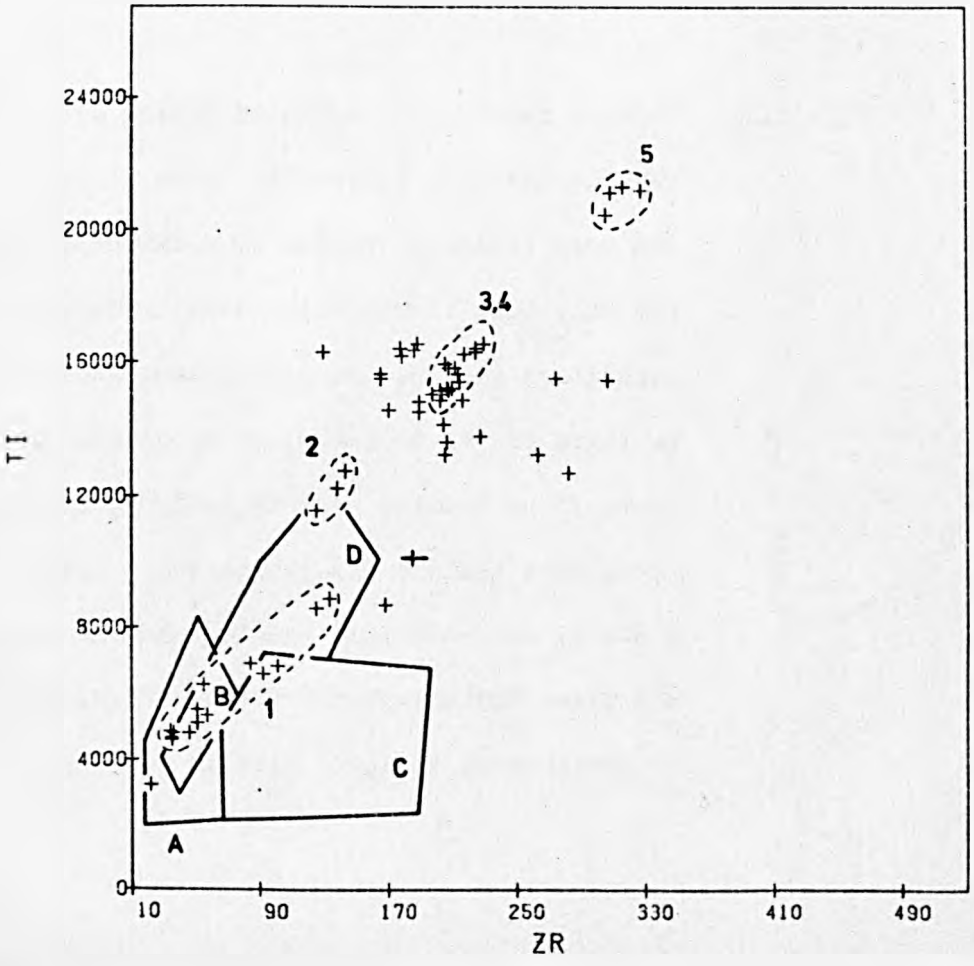
24000
20000
16000
12000
8000
4000
0
TI
10
90
170
250
330
410
490
ZR
5
3,4
2
D
B
1
C
A

Fig. 5.9 Ternary variation diagram of Ti/100 - Zr - Sr/2 for the mafic to ultramafic dykes after Pearce and Cann (1973). Fields of individual dykes as for Fig. 5.2. Ocean-floor basalts plot in field C, low-potassium tholeiites (island arc tholeiites) plot in field A and calc-alkaline basalts plot in field B. The position of the dyke samples illustrates the constant Ti/Zr ratio and relatively larger variation in Sr - the latter probably a function of exchange with the country rocks (see Section 5.4).

Fig. 5.10 Ternary variation diagram of Ti/100 - Zr - Y x 3 for the mafic to ultramafic dykes after Pearce and Cann (ibid.). Fields of individual dykes as for Fig. 5.2. Large dots indicate five or more coincident points. Field E illustrates the position of the intermediate to acidic dykes. Ocean-floor basalts plot in field B, low-potassium tholeiites (island arc tholeiites) plot in fields A and B, calc-alkaline basalts plot in fields C and B and "within-plate" basalts (i.e. ocean island or continental basalts) plot in field D.

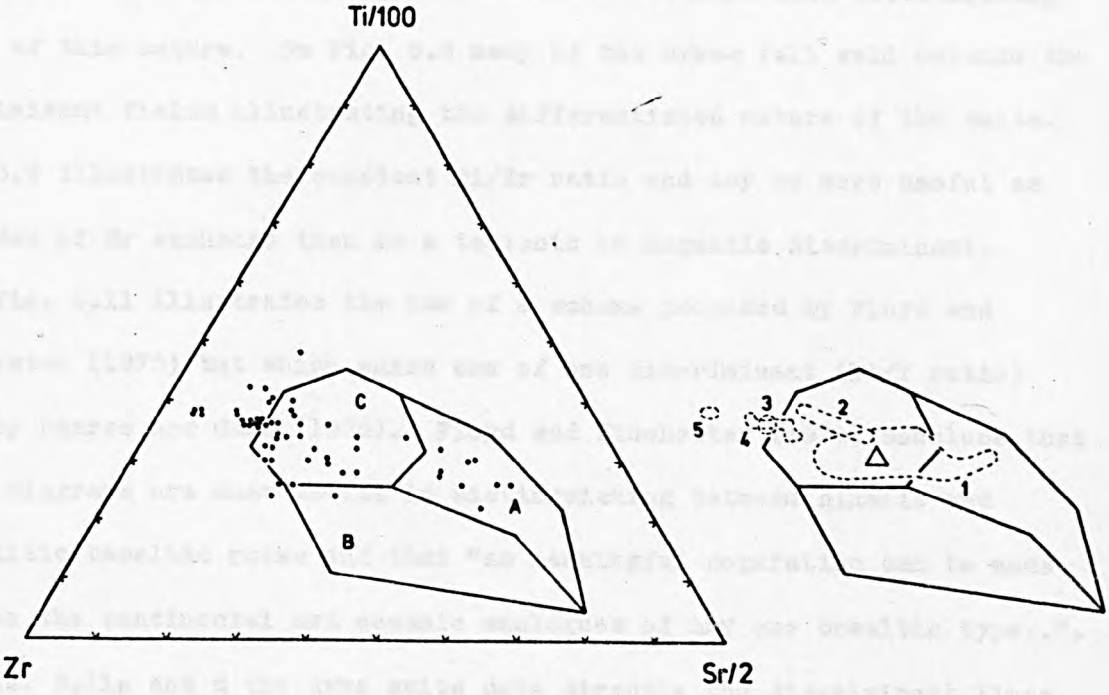
Ti/100
Zr
Sr/2
C
A
B
1
2
3
4
5
Δ

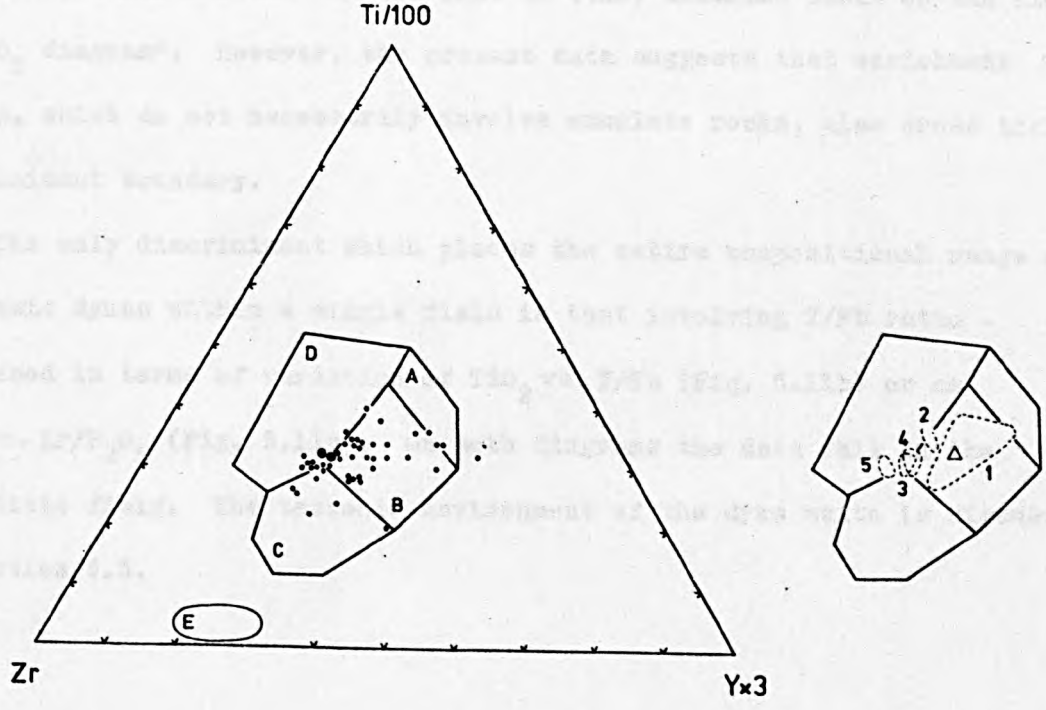
Ti/100
Zr
Y×3
D
A
B
C
E
1
2
3
4
5
Δ

by Pearce and Cann (1973) and Pearce (1975). The behaviour of a single dyke (Härmanö) clearly militates against the use of these diagrams to discriminate between magma types or tectonic settings when investigating rocks of this nature. On Fig. 5.8 many of the dykes fall well outside the discriminant fields illustrating the differentiated nature of the suite. Fig. 5.9 illustrates the constant Ti/Zr ratio and may be more useful as an index of Sr exchange than as a tectonic or magmatic discriminant.

Fig. 5.11 illustrates the use of a scheme proposed by Floyd and Winchester (1975) but which makes use of one discriminant (Nb/Y ratio) used by Pearce and Cann (1973). Floyd and Winchester (1975) conclude that their diagrams are most useful in distinguishing between alkalic and tholeiitic basaltic rocks and that "no meaningful separation can be made between the continental and oceanic analogues of any one basaltic type..". On Figs. 5.11a and d the dyke suite data straddle the discriminant lines. On both diagrams the invasion of the alkaline field is greatest for those samples with the highest enrichment in P_2O_5 (RCS 3, 7, 28 and SJ 904). Floyd and Winchester (1976), in reply to Graham (1976b), agree that "Ti- and P-rich cumulus rocks tend to plot in (the) alkaline field on the TiO_2-Zr/P_2O_5 diagram". However, the present data suggests that enrichment trends, which do not necessarily involve cumulate rocks, also cross their discriminant boundary.

The only discriminant which places the entire compositional range of the basic dykes within a single field is that involving Y/Nb ratio - expressed in terms of variation of TiO_2 vs. Y/Nb (Fig. 5.11b) or as Nb/Y vs. Zr/P_2O_5 (Fig. 5.11c). On both diagrams the data fall in the tholeiitic field. The tectonic environment of the dyke suite is discussed in Section 5.5.

Fig. 5.11 Binary plots for the mafic and ultramafic dykes which illustrate the discriminant scheme of Floyd and Winchester (1975). Fields of individual dykes as for Fig. 5.2. Clockwise from top left:- (a) TiO_2 vs. Zr/P_2O_5, (b) TiO_2 vs. Y/Nb, (d) P_2O_5 vs. Zr and (c) Nb/Y vs. Zr/P_2O_5. Dashed line is the boundary between tholeiite (or subalkaline) basalts (field T) and alkaline basalts (field A). On Figs. 5.11b and 5.11c (both involve Y/Nb ratio or its inverse) the data fall in the tholeiite field. The data straddle the discriminant boundary in Fig. 5.11a (TiO_2 vs. Zr/P_2O_5) and Fig. 5.11d (P_2O_5 vs. Zr.)

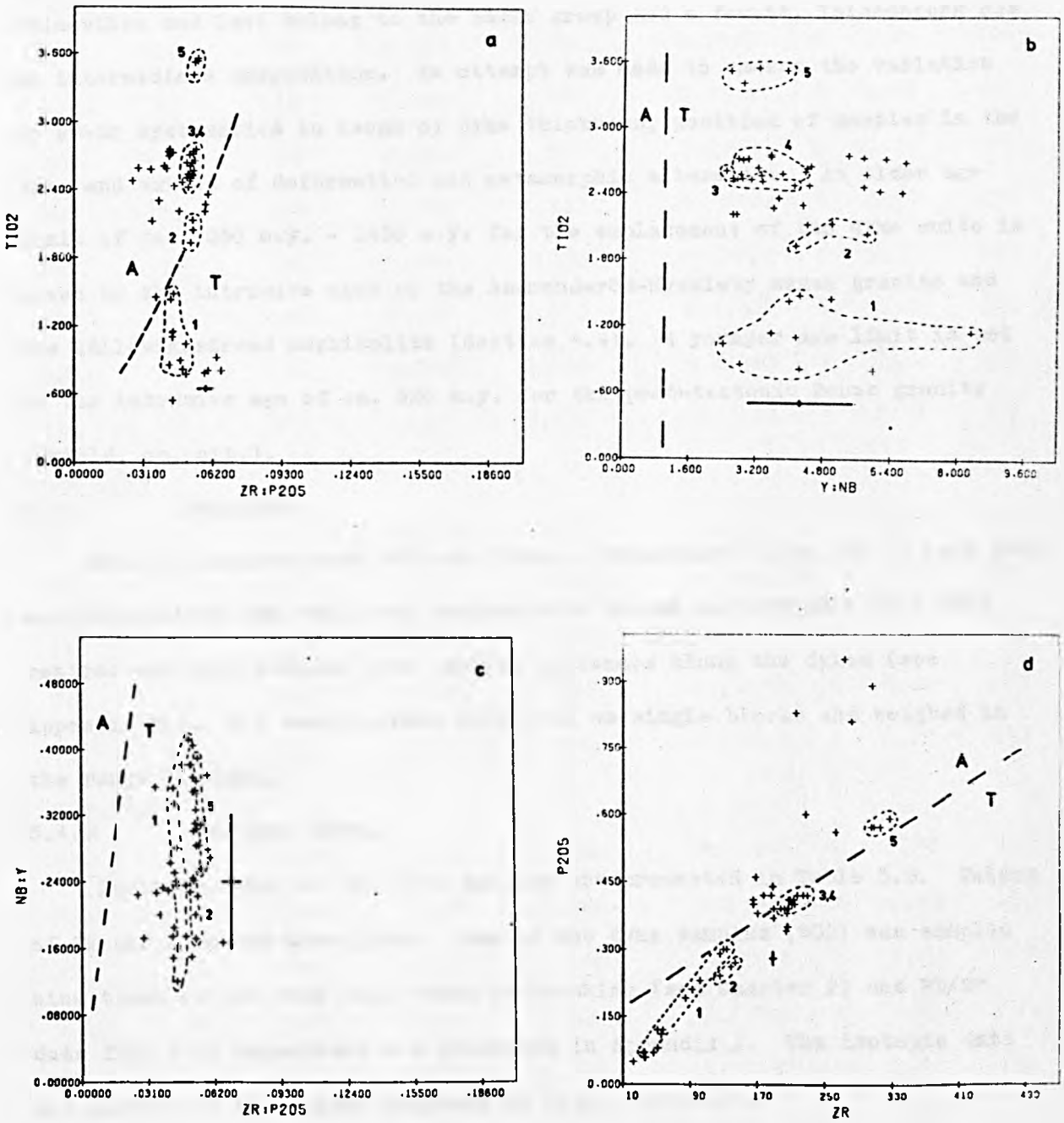
a
TiO2
ZR:P2O5
A
T
1
2
3,4
5
b
TiO2
Y:NB
A
T
c
NB:Y
ZR:P2O5
A
T
d
P2O5
ZR
A
T

5.4 Geochronology of the dyke suite.

5.4.1 Introduction.

Twenty-eight samples from four dykes (Fig. 5.1, Map and Appendix D1) have been analysed for Rb/Sr and $^{87}Sr/^{86}Sr$. Three of these dykes; Härmanö, Svineviken and Lavö belong to the basic group and a fourth, Islandsberg has an intermediate composition. An attempt was made to assess the variation in Rb-Sr systematics in terms of dyke thickness, position of samples in the dyke and extent of deformation and metamorphic alteration. An older age limit of ca. 1350 m.y. - 1450 m.y. for the emplacement of the dyke suite is given by the intrusive ages of the Assmunderöd-Myckleby augen granite and the Hällevikstrand amphibolite (Section 4.4). A younger age limit is set by the intrusive age of ca. 890 m.y. for the post-tectonic Bohus granite (Skiöld, op. cit.).

5.4.2 Sampling.

Dyke thicknesses are: Härmanö (30m.), Svineviken (1.5m.-2m.), Lavö (2m.) and Islandsberg (5m.-8m.) and samples were chosen to represent both dyke centres and dyke margins over varying distances along the dykes (see Appendix D1). All samples were collected as single blocks and weighed in the range 5Kg-10Kg.

5.4.3 Isotopic data.

Isotopic data for the dyke samples are presented in Table 5.3. Values of K% and K/Rb are also given. One of the dyke samples (632) was sampled nine times at the rock chip stage of crushing (see Chapter 2) and Rb/Sr data from this experiment are presented in Appendix A. The isotopic data are plotted on Nicolaysen diagrams in Figs. 5.12-5.15.

The data define linear arrays which are close to perfect isochrons in the case of Lavö and Svineviken dykes (MSWD = 2.46 and 2.73 respectively). These lines correspond to ages of 1062 $\pm$ 93 m.y. and 1106 $\pm$ 39 m.y. with initial $^{87}Sr/^{86}Sr$ ratios of 0.710 $\pm$ 2 and 0.7074 $\pm$ 7 respectively. The Islandsberg dyke gives a similar age (999 $\pm$ 83 m.y.) with an initial

Table 5.3

Rb-Sr and K/Rb analytical data: dyke suite

Sample	Rb (ppm)*1	Sr (ppm)*1	Rb/Sr*2	$^{87}Rb/^{86}Sr$*2	$^{87}Sr/^{86}Sr$*3	K%*4	K/Rb*4
Svineviken Dyke							
607	53	157	0.340	0.986	0.72259 ± 4	1.34	274
608	57	98	0.576	1.670	0.73394 ± 6	1.35	271
609	54	96	0.564	1.637	0.73343 ± 6	1.34	269
610	65	109	0.595	1.725	0.73443 ± 8	1.51	252
611	55	128	0.432	1.251	0.72711 ± 4	1.31	252
612	59	156	0.376	1.090	0.72431 ± 8	1.33	251
613	49	124	0.396	1.148	0.72586 ± 4	1.11	247
614	47	164	0.286	0.828	0.72071 ± 6	1.11	253
Lavö Dyke							
615	62	117	0.534	1.549	0.73325 ± 6	1.43	250
616	65	117	0.552	1.600	0.73485 ± 4	1.49	252
617	77	114	0.672	1.949	0.73947 ± 6	1.64	227
618	55	124	0.444	1.286	0.72943 ± 8	1.31	262
630	79	115	0.689	1.999	0.74013 ± 4	1.70	240
Islandsberg Dyke							
619	114	189	0.606	1.758	0.73892 ± 4	2.37	222
620	122	204	0.600	1.742	0.73837 ± 6	2.62	234
621	92	196	0.469	1.362	0.73368 ± 4	2.76	328
622	114	205	0.555	1.610	0.73630 ± 8	2.64	254
623	115	200	0.574	1.664	0.73668 ± 4	2.56	240
624	92	195	0.470	1.362	0.73317 ± 4	2.81	326
625	97	206	0.471	1.365	0.73241 ± 5	2.69	296
626	100	201	0.495	1.435	0.73396 ± 4	2.76	304

Table 5.3 (continued)

Rb-Sr and K/Rb analytical data: dyke suite

Sample	Rb (ppm)*1	Sr (ppm)*1	Rb/Sr*2	$^{87}Rb/^{86}Sr$*2	$^{87}Sr/^{86}Sr$*3	K%*4	K/Rb*4
Härmanö Dyke							
631	6	147	0.041	0.117	0.70513 ± 4	0.20	398
632	15	151	0.098	0.283	0.70987 ± 6	0.37	281
633	29	132	0.225	0.647	0.71364 ± 17	0.51	198
634	13	152	0.089	0.257	0.70862 ± 8	0.36	275
635	11	138	0.080	0.229	0.70939 ± 6	0.32	324
637	5	164	0.031	0.091	0.70533 ± 6	0.22	432
638	8	134	0.062	0.179	0.70751 ± 6	0.25	311

*1 Errors in Rb and Sr contents estimated at ± 5% (2σ)

*2 Errors in Rb/Sr and $^{87}Rb/^{86}Sr$ estimated at ± 2% (2σ)

*3 $^{87}Sr/^{86}Sr$ values are normalised to $^{88}Sr/^{86}Sr = 8.37521$

Quoted errors are 2σ based on "in run" statistics.

*4 K% calculated from K_2O in Appendix D, K/Rb calculated using Rb values measured at Keele (Appendix D, values are within ± 5% of Leeds values).

Fig. 5.12 Nicolaysen diagram for five samples of the narrow (ca. 2 m. wide), deformed Lavö basic dyke. The data define a perfect isochron (MSWD = 246) corresponding to an age of 1062 $\pm$ 93 m.y. and an initial $^{87}Sr/^{86}Sr$ ratio of 0.710 $\pm$ 2.

Fig. 5.13 Nicolaysen diagram for eight samples of the narrow (ca. 2 m. wide), deformed Svineviken basic dyke. The data define a near perfect isochron (MSWD = 2.73) corresponding to an age of 1106 $\pm$ 39 m.y. and an initial $^{87}Sr/^{86}Sr$ ratio of 0.7074 $\pm$ 7.

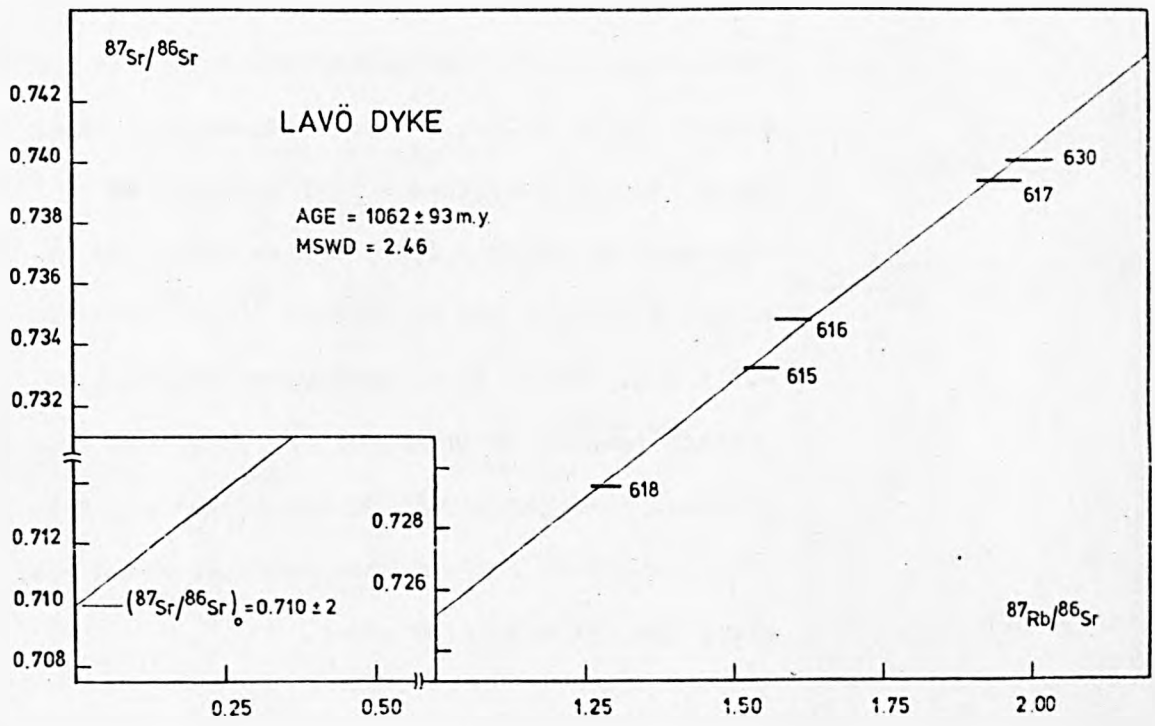
$^{87}Sr/^{86}Sr$
LAVÖ DYKE
AGE = 1062 ± 93 m.y.
MSWD = 2.46
0.742
0.740
0.738
0.736
0.734
0.732
0.712
0.710
0.708
0.728
0.726
$(^{87}Sr/^{86}Sr)_o = 0.710 \pm 2$
630
617
616
615
618
$^{87}Rb/^{86}Sr$
0.25
0.50
1.25
1.50
1.75
2.00

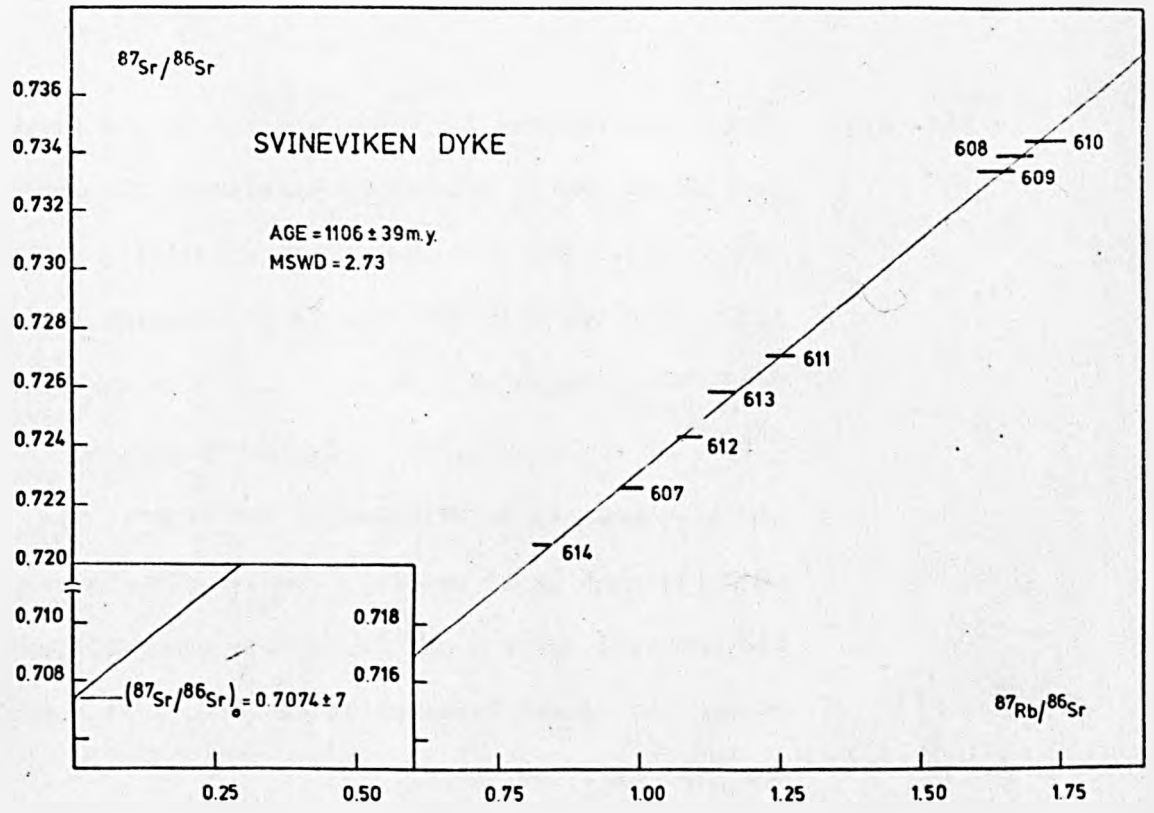
$^{87}Sr/^{86}Sr$
SVINEVIKEN DYKE
AGE = 1106 ± 39 m.y.
MSWD = 2.73
0.736
0.734
0.732
0.730
0.728
0.726
0.724
0.722
0.720
0.710
0.708
0.718
0.716
$(^{87}Sr/^{86}Sr)_o = 0.7074 \pm 7$
608
610
609
611
613
612
607
614
$^{87}Rb/^{86}Sr$
0.25
0.50
0.75
1.00
1.25
1.50
1.75

Fig. 5.14 Nicolaysen diagram for eight samples of the intermediate (8 m. wide), deformed Islandsberg basic dyke. The data defines a well constrained "errorchron" (MSWD = 5.23) corresponding to an age of 999 ± 83 m.y. and an initial $^{87}Sr/^{86}Sr$ ratio of 0.714 ± 2. There is no geological evidence to justify removal of either SJ 621 or SJ 625 from the diagram. Removal of either one of these points would result in perfect isochrons but would not alter the age within 2σ error.

Fig. 5.15 Nicolaysen diagram for seven samples of the large (ca. 30 m. wide), relatively undeformed Härmanö basic dyke. The data are poorly correlated (MSWD = 153.4) and the best fit line (shown dashed) corresponds to an "age" of 1169 ± 39 m.y. with an initial $^{87}Sr/^{86}Sr$ ratio of 0.7044 ± 1. No geological significance may be attached to the "age". The observed scatter is probably due to disturbance of the isotopic systems and incomplete re-equilibration during the syn-D3 Sveconorwegian metamorphism at ca. 1060 m.y. (see text).

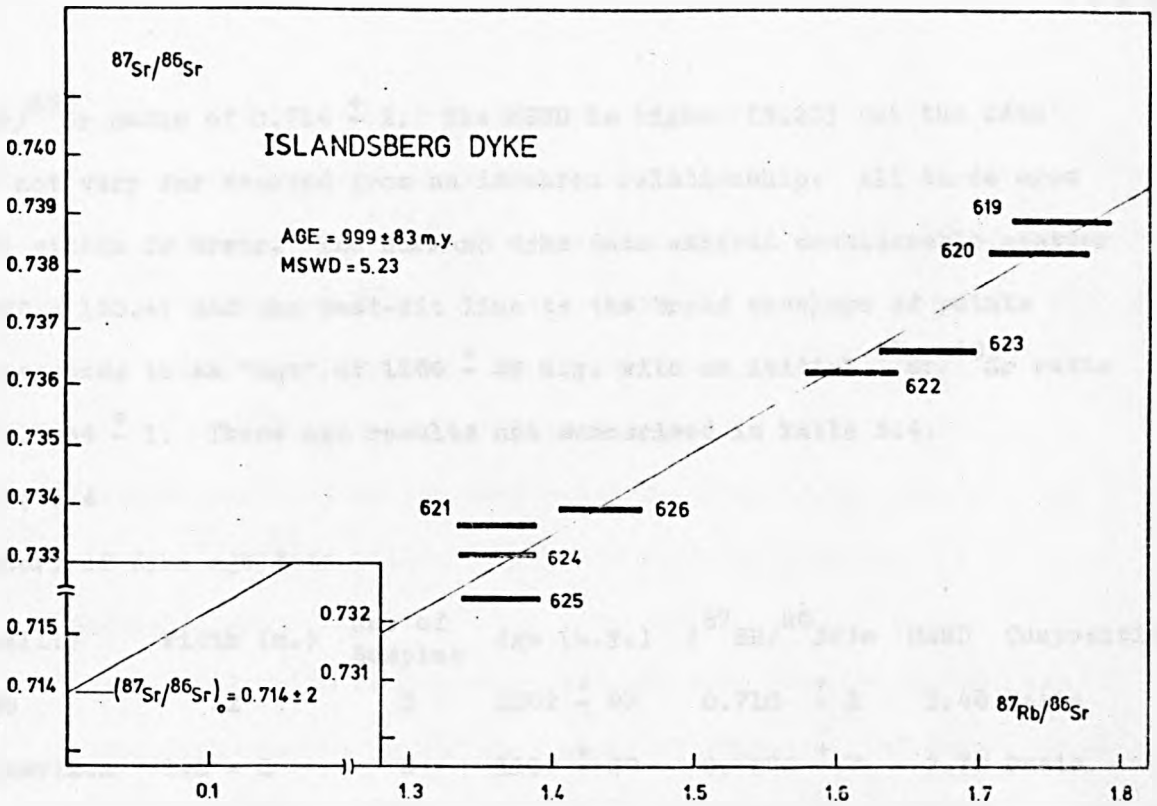
87Sr/86Sr
ISLANDSBERG DYKE
AGE = 999 ± 83 m.y.
MSWD = 5.23
619
620
623
622
621
626
624
625
(87Sr/86Sr)o = 0.714 ± 2
87Rb/86Sr
0.740
0.739
0.738
0.737
0.736
0.735
0.734
0.733
0.732
0.731
0.715
0.714
0.1
1.3
1.4
1.5
1.6
1.7
1.8

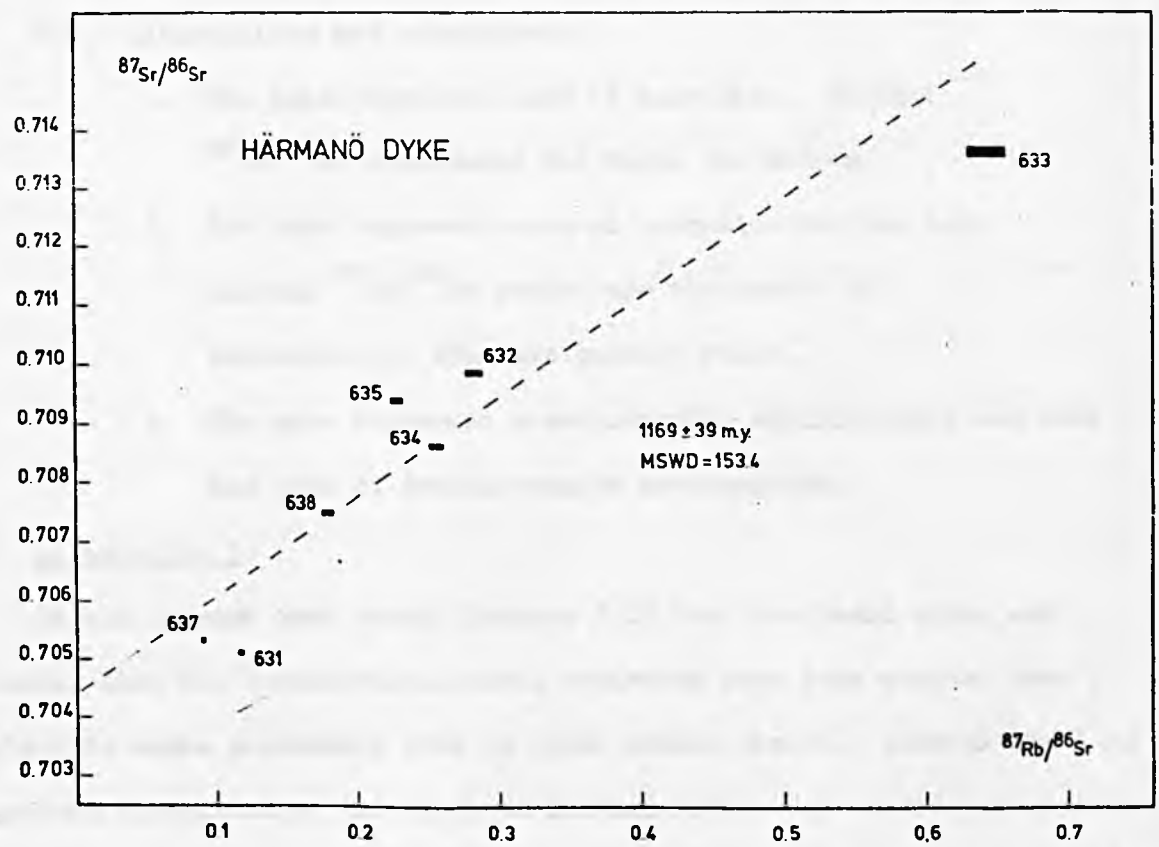
87Sr/86Sr
HÄRMANÖ DYKE
633
632
635
634
1169 ± 39 m.y.
MSWD = 153.4
638
637
631
87Rb/86Sr
0.714
0.713
0.712
0.711
0.710
0.709
0.708
0.707
0.706
0.705
0.704
0.703
0.1
0.2
0.3
0.4
0.5
0.6
0.7

$^{87}Sr/^{86}Sr$ ratio of 0.714 ± 2. The MSWD is higher (5.23) but the data are not very far removed from an isochron relationship. All three ages fall within 2σ error. The Härmanö dyke data exhibit considerable scatter (MSWD = 153.4) and the best-fit line to the broad envelope of points corresponds to an "age" of 1169 ± 39 m.y. with an initial $^{87}Sr/^{86}Sr$ ratio of 0.7044 ± 1. These age results are summarised in Table 5.4.

Table 5.4

Summary of dyke age data

Locality	Width (m.)	No. of Samples	Age (m.y.)	$(^{87}SR/^{86}Sr)o$	MSWD	Composition
Lavö	2	5	1062 ± 93	0.710 ± 2	2.46	Basic
Svineviken	1.5 - 2	8	1106 ± 39	0.7074 ± 7	2.73	Basic
Islandsberg	5 - 8	8	999 ± 83	0.714 ± 2	5.23	Intermediate
Härmanö	30	7	1169 ± 39	0.7044 ± 1	153.4	Basic

5.4.4 Interpretation of dyke ages

5.4.4.1 Svineviken, Lavö and Islandsberg dykes

Three alternatives are considered:-

1. The ages represent ages of intrusion. Initial $^{87}Sr/^{86}Sr$ represents the value for source.
2. The ages represent ages of intrusion but the high initial $^{87}Sr/^{86}Sr$ ratios are the result of contamination from the country rocks.
3. The ages represent post-intrusion equilibration and date the peak of Sveconorwegian metamorphism.

Alternative 1.

It has already been shown (Section 5.3) that the basic dykes and probably also the intermediate-acidic varieties have been derived from a tholeiitic magma presumably from an upper mantle source. Alternative 1 is therefore discounted as the observed initial ratios are outside reasonable upper mantle values (Faure and Powell, 1972). The lowest value (0.7074 ± 7, Svineviken dyke) overlaps the uppermost part of Patchett's (1976) range for

unmetamorphosed mid- and late- Proterozoic (post Svecofennian) dykes in eastern and central Sweden. However, these high initial ratios were interpreted (ibid.) in terms of contamination from the surrounding gneisses and were not regarded as indicating the $^{87}Sr/^{86}Sr$ ratio of the upper mantle beneath the Svecofennian terrain. A further constraint on Scandinavian upper mantle $^{87}Sr/^{86}Sr$ ratios in the Proterozoic is given by the Hällevikstrand amphibolite (Section 4.4.2 and Daly et al., op.cit.) which has an initial $^{87}Sr/^{86}Sr$ ratio of 0.7032 $\pm$ 5 at ca. 1430 m.y.

Alternative 2.

No rhemorphic melts of the country rocks have been recognised and the rare xenoliths present do not show signs of ablation. At first sight the extremely enriched character of the Islandsberg dyke (Section 5.3), especially the high Zr content, suggests contamination from the gneisses as a strong possibility but this has already been shown to be unreasonable (see above). It was concluded from the geochemical data (Section 5.3) that the basic and intermediate-acidic dykes were derived from a common magmatic parent. Moreover, the largest analysed dyke (Härmanö) which might be expected to have had the greatest thermal effects on the country rocks shows least isotopic equilibration.

It is, of course, possible that considerable chemical interaction and isotopic exchange took place between the dyke magma and the wall rocks during ascent to the present position. However, any contamination which pre-dated the metamorphism of the dykes, whether acting on the magma or under sub-solidus conditions, would be virtually impossible to distinguish from metamorphic effects.

Alternative 3.

It is suggested that the measured ages of the Svineviken, Lavö and Islandsberg dykes (mean age ca. 1060 m.y.) represent equilibration of the Rb-Sr systematics during Sveconorwegian amphibolite facies metamorphism when the D3 biotite-hornblende fabric developed in the dykes (Plate 5.2.M)

and was locally overprinted by growth of garnet.

The narrow (ca. 2m. wide) Lavö and Svineviken dykes, which have a strong mineral fabric and no trace of igneous textures, define the closest-fitting isochrons. The 5m. - 8m. wide Islandsberg dyke has a strong biotite fabric but has equilibrated to a lesser extent. This could either be due to incomplete equilibration during the metamorphism or to subsequent disturbance of the isotopic systems. The possibility of contamination of this dyke has been discussed above. All three dykes have high initial $^{87}Sr/^{86}Sr$ ratios presumably as a result of exchange of Sr with the surrounding gneisses which probably had $^{87}Sr/^{86}Sr$ ratios close to 0.72 - 0.74 at ca. 1060 m.y. (calculated from Hällevikstrand granite data (Section 3.4.3) and other data on the basement complex (Appendix B).

5.4.4.2 Härmanö dyke.

The Härmanö dyke, which is much less deformed and less thoroughly recrystallised than many of the other dykes (Plate 5.5.M), shows a scatter of the data points (Fig. 5.15). It is doubtful if any geological significance can be attached to the "age" (1169 $\pm$ 39 m.y.) given by the best fit line but the general disposition of the data points and the low initial $^{87}Sr/^{86}Sr$ ratio indicated (close to 0.704) is consistent with mantle derivation at some time before the isotopic equilibrium recorded by the other dykes (at ca. 1060 m.y.). There is some geological and geochemical evidence for multiple intrusion in this dyke (Section 5.3) but this is not likely to have contributed to any significant variation in initial $^{87}Sr/^{86}Sr$ ratio. Recrystallisation during the Sveconorwegian metamorphism (ca. 1060 m.y.) has disturbed the isotopic systematics but re-equilibration apparently was not achieved and this probably accounts for most of the observed scatter.

5.4.4.3 K and Rb geochemistry of the dykes.

Metamorphic equilibration as an explanation for the dyke ages and high initial $^{87}Sr/^{86}Sr$ ratios is supported by the pattern of K and Rb variation. K and Rb contents (Table 5.3 and Fig. 5.16) vary over a narrow

Fig. 5.16 Binary plot of K/Rb vs. K for the dyke suite. Fields of individual dykes as for Fig. 5.3. The isotopically equilibrated dykes (3, 4 = Lavö and Svineviken) and the incompletely equilibrated dyke (7 = Islandsberg) group tightly together and the mean K/Rb ratio is close to the average value of the country rocks. The Härmanö dyke (1) shows a significant range in K/Rb ratio and a steep decrease in this relative to increasing K (see text).

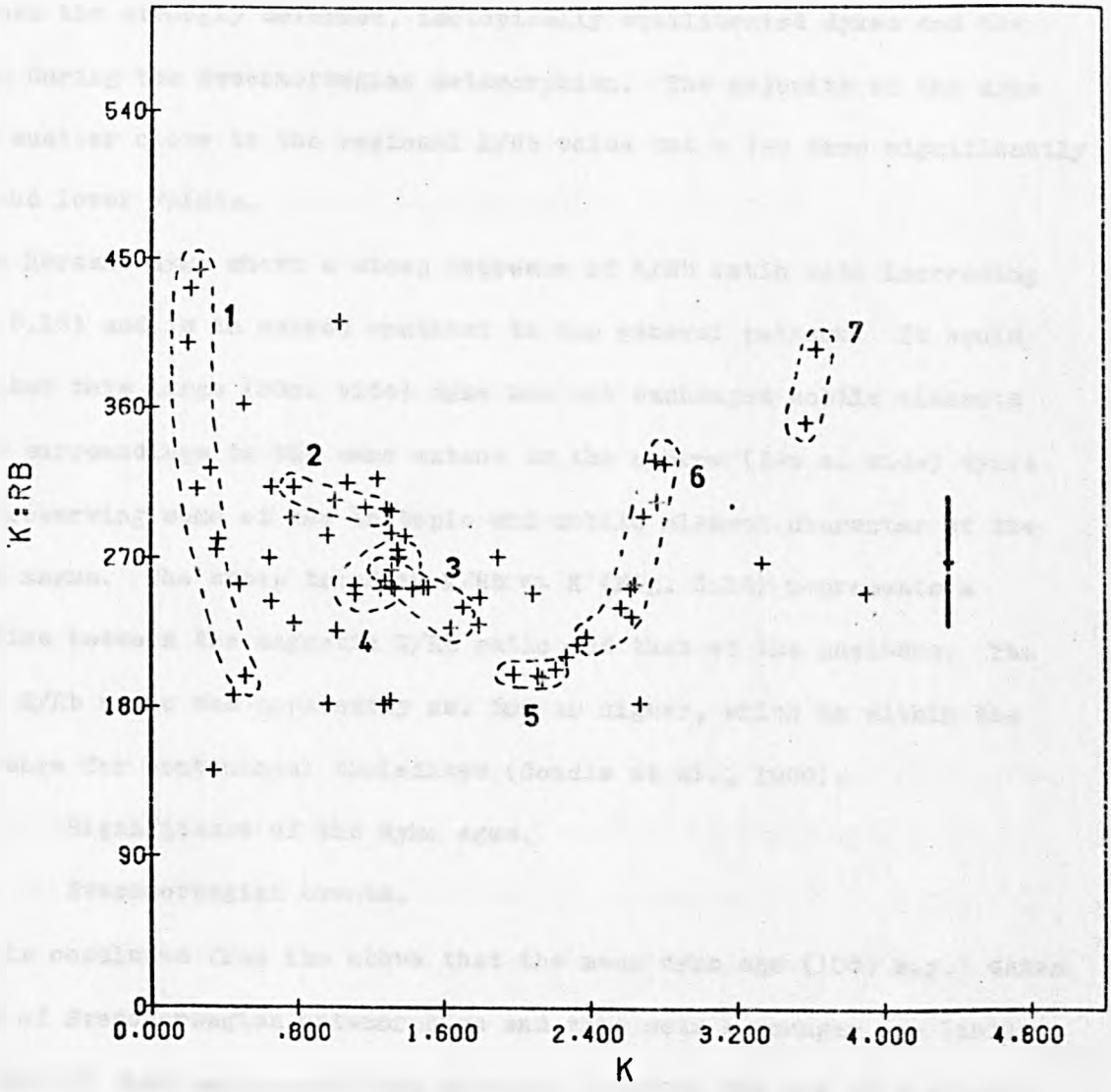
540
450
360
270
180
90
0
K:RB
0.000
.800
1.600
2.400
3.200
4.000
4.800
K
1
2
3
4
5
6
7

range in the isotopically equilibrated dykes and the K/Rb ratio (ca. 260) falls close to the average value for virtually all of the country rocks. K/Rb ratios for the gneisses, migmatitic leucosomes, younger granites, augen granites and the Hällevikstrand granite fall in the range 180 to 300. It seems, therefore, that there has been considerable exchange of alkalis and Sr between the strongly deformed, isotopically equilibrated dykes and the gneisses during the Sveconorwegian metamorphism. The majority of the dyke samples scatter close to the regional K/Rb value but a few show significantly higher and lower values.

The Härmanö dyke shows a steep decrease of K/Rb ratio with increasing K (Fig. 5.16) and is in marked contrast to the general pattern. It would appear that this large (30m. wide) dyke has not exchanged mobile elements with its surroundings to the same extent as the narrow (few m. wide) dykes and is preserving some of the isotopic and mobile element character of the original magma. The steep trend in K/Rb vs. K (Fig. 5.16) represents a mixing line between the magmatic K/Rb ratio and that of the gneisses. The original K/Rb ratio was apparently ca. 500 or higher, which is within the normal range for continental tholeiites (Condie et al., 1969).

5.4.5 Significance of the dyke ages.

5.4.5.1 Sveconorwegian events.

It is concluded from the above that the mean dyke age (1060 m.y.) dates the peak of Sveconorwegian metamorphism and this sets a younger age limit on the time of dyke emplacement and an older limit on the age of the last major deformation in the area (D4 of Park et al.,op. cit. and Table 1.1). A younger age limit for the D4 deformation is given by the emplacement age of the post-tectonic Bohus granite (ca. 890 m.y., Skiöld, op. cit.).

Previous evidence for Magnusson's (1960) "Sveconorwegian regeneration" is derived from: 1. the age of the Bohus granite; 2. whole rock and mineral K-Ar ages (Magnusson, 1960, Skiöld, op. cit.); 3. pegmatite U-Pb mineral ages (Welin and Blomqvist, 1964) and 4. a Rb-Sr whole rock isochron

(1028 ± 39 m.y.) on the Dal slate (Skiöld, op. cit.), the deformation of which has not been correlated with events in the Amal basement it unconformably overlies. Sveconorwegian deformation (D3 and D4) has not previously been recognised as such in the Stora Le - Marstrand belt.

The ca. 1060 m.y. age for the Sveconorwegian metamorphism and deformation is in good agreement with Rb-Sr whole rock ages and U-Pb zircon ages obtained, mainly on gneisses, elsewhere in the Sveconorwegian province (inter alia O'Nions and Baadsgaard, 1971, Versteeve, 1975).

5.4.5.2 Scale of Sr isotopic equilibration.

An understanding of the scale of isotopic equilibration during metamorphism is critical to the interpretation of geochronological studies of metamorphic rocks. Few "natural experiments" which make a reliable contribution to the subject have been documented. Krogh and Davis (1973) have shown that isotopic equilibration does not necessarily take place even over small distances (few cm.) during high grade metamorphism.

At first sight the isotopic results from the Orust dykes might be taken as evidence of isotopic equilibration on a relatively large scale - a volume of equilibration of at least ca. $2m.^3$ is implied by the near perfect isochron (Fig. 5.12) for the Lavö dyke. Attainment of isotopic equilibrium in the Lavö and Svineviken (2m. wide, sampled over a distance of 8m.) dykes and to a lesser extent in the wider (5m. - 8m.) Islandsberg dyke (sampled over 240m.) is in marked contrast to the lack of equilibration in the Härmanö dyke (30m. wide, sampled over 200m). In addition to dyke width and the volume over which samples were collected the degree of deformation seems to be important; the least deformed dyke (Härmanö) shows least equilibration.

Two points illustrate some of the difficulty in interpreting this data as a natural experiment on the scale of isotopic equilibration. Firstly, as Roddick and Compston (1976) have argued, the scale of apparent isotopic homogenisation depends critically on the scale of variation of Rb/Sr ratio (and thus $^{87}Sr/^{86}Sr$) within the body of rock concerned. They reasoned that

a volume of rock could be considered in terms of small subvolumes such that each subvolume has the same mean Rb/Sr ratio (and $^{87}Sr/^{86}Sr$) as the mean Rb/Sr ratio (and $^{87}Sr/^{86}Sr$) of the entire body. If the domain over which isotopic equilibration can take place during metamorphism is larger than or similar in size to these subvolumes then complete isotopic equilibration over the entire body may appear to have taken place. Thus isotopic homogenisation (and congruent metamorphic ages) might be obtained from the metamorphism of gneiss terrains which have only small scale variations in Rb/Sr ratio. Larger-scale variations in Rb/Sr ratio (e.g. a geographical variation imposed by crystal fractionation or accumulation in a large igneous intrusion) might be expected to prevent large-scale equilibration and yield an age closer to that of emplacement than of metamorphism.

Secondly, it has been argued (above) that there may have been considerable exchange of Sr and alkalis between the Orust dykes and the country rocks during the syn-D3 metamorphism. Since neither the relative volumes of gneiss and dyke involved nor the dominant transport direction (i.e. along or across the dykes) are known it is not possible to evaluate the contribution which this process has made to the observed isotopic homogenisation. Neither may the relative importance of internal homogenisation and exchange with the surrounding gneisses be assessed.

Clearly it is unreasonable to draw any firm conclusion on the scale of isotopic equilibration during amphibolite-grade metamorphism from the present data. All that can be said, in summary is (1) the mechanism of isotopic equilibration is intimately bound up with the process of metamorphic recrystallisation during the D3 deformation and (2) isotopic equilibrium has been achieved in the relatively narrow strongly deformed dykes but only disturbance of the isotopic systematics has taken place in the large relatively undeformed (Härmanö) dyke.

5.4.5.3 Age of dyke emplacement.

The time gap between the emplacement of the dyke suite and the post-dyke (Sveconorwegian) metamorphism at ca. 1060 m.y. cannot be ascertained from the present evidence. In view of the evidence for exchange of mobile elements with the surrounding gneisses (Section 5.4.4) it does not seem appropriate to use the Rb-Sr data to calculate model "maximum ages" of derivation assuming a mantle initial $^{87}Sr/^{86}Sr$ ratio. Clearly, however, in view of the older age limit set by the emplacement ages of the Hälleviksstrand amphibolite and the Assmunderöd-Myckleby augen granite (Chapter 4), the age of dyke emplacement must lie between ca. 1350 m.y. - 1450 m.y. and ca. 1060 m.y.

5.5 Tectonic environment of the dyke suite.

It was suggested above (Section 5.3.3.4) that the dyke suite was the product of crystal fractionation and a tholeiitic parent magma is indicated by the strong iron enrichment trend (Figs. 5.2 and 5.3) and the high Y/Nb ratio (Fig. 5.11). The field evidence (Section 5.2 and Park et al., op. cit.) suggests emplacement into brittle crust associated with tensional stresses acting along a possible strike length of 250 Km. (Section 5.1).

It is possible that the dyke suite represents early Sveconorwegian continental rifting prior to the Sveconorwegian orogeny and correlates with ca. 1260 m.y. to 1190 m.y. old dolerite swarms in Canada (Sudbury and Mackenzie), south west Greenland (middle Gardar) (Patchett et al., 1978) and central Sweden (Patchett, 1976). It has been suggested (e.g. Baer, 1976, Emslie, 1978) that widespread continental rifting took place along the Grenville belt prior to the Grenville orogeny. Assuming a correlation between the Grenville and Sveconorwegian belts (Wynne-Edwards and Hasan, 1972) the evidence so far available from the Orust dyke suite is consistent

with this idea. However, much more information is required on the large scale tectonics of the Sveconorwegian belt and on the lateral as well as the longitudinal extent of the dyke suite before this possibility can be properly evaluated.

5.6 Pegmatite mineral ages.

5.6.1 Introduction.

Several large pegmatite sheets occur in the area. They range in width from a few m. to 20 m. and some may be followed for 500 m. The majority are granitic in composition and contain quartz, plagioclase, K-feldspar, muscovite, biotite (minor) and garnet. A small number of pegmatitic quartz-feldspar bodies also occur. Brotzen (1961) has catalogued the mineralogy of the Orust pegmatites.

The pegmatites cut the migmatitic banding in the gneisses, the F2 folds and some post-D2 shears. At least one body (not sampled), near Tvet in southern Orust, cuts a basic dyke. The pegmatites show varying degrees of deformation; kinking of muscovite plates and plagioclase twin lamellae and development of mortar textures are common. Some muscovite has a secondary origin and appears to be later than the cataclasis. Some pegmatite bodies e.g. at Timmerhult in eastern Orust have margins folded by F4 folds.

Three muscovite-plagioclase pairs from two pegmatite bodies (Högholmen, 921 and Lavö, 922, see Map) have been analysed for $^{87}Sr/^{86}Sr$, $^{87}Rb/^{86}Sr$ and Rb and Sr contents by isotope dilution. One muscovite book (921/1, 4 cm. across) was divided, using a pair of scissors, into core and rim to investigate the effects of post-emplacement deformation and to assess the degree of attainment of isotopic equilibrium.

Table 5.5

Rb-Sr analytical data and measured ages: Pegmatite minerals

Sample	Rb*3 (ppm)	Sr*4 (ppm)	$^{87}Sr/^{86}Sr$*4	$^{87}Rb/^{86}Sr$	Age
921/1 plag.	13	122	0.7309 ± 12	0.315 ± 2	
921/1 plag.*1		124	0.7305 ± 2	0.311 ± 2	
921/1 musc. core	871	11	5.1583 ± 80	327 ± 1	948 ± 5 m.y.
921/1 musc. core		11	5.0504 ± 10	316 ± 1	957 ± 4 m.y.
921/1 musc. rim	900	10	6.3827 ± 21	390.6 ± 9	1012 ± 3 m.y.
921/3 plag.	57	188	0.7358 ± 3	0.873 ± 3	
921/3 musc.	863	10	5.63 ± 2	364.7 ± 6	941 ± 5 m.y.
921/3 musc.*1		10	5.654 ± 15	364.3 ± 7	947 ± 5 m.y.
922/1 plag.	33	64	0.7271 ± 9	1.450 ± 8	
922/1 musc.	1238	8	14.46 ± 34*2	1000 ± 3	962 ± 2 m.y.
922/1 musc.*1		8	13.741 ± 6	964 ± 3	946 ± 4 m.y.

Quoted errors are 2σ based on "in run" statistics.

*1 Reload and re-run for Sr content and $^{87}Sr/^{86}Sr$.

*2 Very poor mass spectrometer run; only two sets of data recovered (others ca. 10 sets).

*3 Rb content by isotope dilution (2σ error ca. 1%), using $^{87}Rb/^{85}Rb = 0.3907 \pm 9$, measured on three natural Rb samples. MS5 mass spectrometer.

*4 Error in Sr content ca. 1.5-2% (2σ). $^{87}Rb/^{85}Rb$ from spike run used to correct for ^{87}Rb if detected in Sr run. MM30 mass spectrometer.

5.6.2 Isotopic data and interpretation.

Isotopic data and calculated ages are presented in Table 5.5. The analytical errors, quoted at 2σ level, are based on "in run" statistics and are thus minimum values. Some data (marked *1 in Table 5.5) have been obtained by duplicate loading of the original sample. Repeated decompositions have not been made. Calculated ages for adjacent muscovite-plagioclase pairs are given opposite the muscovite samples. The uncertainties in these ages take account of the experimental errors and the repeated plagioclase analyses in the case of 921/1.

Most of the ages cluster tightly around ca. 948 m.y. The 962 ± 2 m.y. age for one run of 922/1 is not considered to be reliable since a very poor Sr run was obtained in the mass spectrometer. An age of 1012 ± 3 m.y. was obtained from the rim of muscovite 921/1. This shows that the core and rim of this muscovite are not in isotopic equilibrium. It is not possible to attach any geological significance to the older (rim) age nor to ascribe the observed disequilibrium to any particular geological event (e.g. the D4 or any other phase of deformation).

The complication introduced by this single sample casts some doubt on the validity of any age conclusion based on the limited amount of data presented. However, it seems likely that an age close to 948 m.y., seen in three mineral pairs from two pegmatite bodies, is a reasonable estimate of the age of emplacement. The age is close to a U-Pb concordia intercept age (930 m.y.) for pegmatite minerals from south west Sweden (Welin and Blomqvist, 1964). Both ages are significantly older than the emplacement age of the Bohus granite (ca. 890 m.y., Skiöld, op. cit.). It is not known if the pegmatites are related to the Bohus granite and the observed age difference does not rule out this possibility.

CHAPTER 6. Mineral compositions and geothermometry of the dyke suite.

6.1 Introduction.

Compositions of garnet, biotite and plagioclase in samples of four basic dykes have been determined using EDS (energy-dispersive spectrometry) electron-microprobe analysis (see Chapter 2). The data and sample descriptions and locations are presented in Appendix E. The microprobe technique used cannot discriminate between Fe^{2+} and Fe^{3+} and no separate determination of ferrous iron has been attempted.

Index minerals and low variance assemblages which may be used to define the P,T conditions of metamorphism are rare in the Orust area. The mineral pair garnet-biotite, present in many of the rock types, affords a potentially useful geothermometer which depends on equilibrium partitioning of Mg and Fe between the two phases. Three recently published calibrations are discussed and the results of temperature calculations based upon them are presented in Section 6.3.

6.2 Mineral compositions.

6.2.1 Garnet.

Twenty-four microprobe analyses (EDS) of seven garnet grains in four basic dykes are presented in Appendix E. Fe_2O_3 has not been determined and total iron is presented as FeO (for all mineral analyses). However, when the analyses are recalculated (as cations per 12 oxygens, Appendix E) no cation deficiency is detectable and within analytical uncertainty there are two Al atoms per formula unit and Σ Fe + Ca + Mn + Mg has a value of three. Thus the amount of the andradite (Fe^{3+}) component present must be very small.

Assuming all iron to be present as Fe^{2+} the garnets are grossular-almandine solid solutions with minor amounts of spessartine and pyrope.

Almandine is the major component (ca. 46-60 mol. %) together with grossular (ca. 25-43 mol. %), spessartine (ca. 5-8 mol. %) and pyrope (ca. 4-9 mol. %).

Chemical zoning was detected in all of the analysed garnets and this is illustrated in Fig. 6.1. In garnets from two rocks (SB20 and SB72, not plotted) the amount of intra-grain variation is very close to analytical uncertainty for each element. Garnets from two rocks (SB41 and SBR25) (Fig. 6.1) have rims depleted in Mn relative to the rest of the grain. Considering the mean analyses at each spot the pattern of variation of Fe, Ca and Mg in sample SB41 is complicated with relative depletion in Mn and relative enrichment in Fe and Mg in both the core and rims compared with the remainder of the grain. However, the variation in Ca and Fe is probably within the analytical uncertainty. Sample SBR25 has a symmetrical variation in Fe, Mg and Mn while Ca is skewed. Fe is enriched at the rims relative to the core and the Mg variation is within analytical uncertainty. The overall pattern of variation (dominantly Mn depletion in the rims) may be the result of fractionation during growth (cf. Hollister, 1966 and Atherton, 1968).

6.2.2 Biotite.

Fourteen microprobe analyses of twelve biotite grains in three basic dykes (SB41, SB72 and SBR25) are presented in Appendix E. The recalculated analyses (as cations per 22 oxygens) group closely together on a plot of Si vs. Mg/(Mg + Fe + Mn) (Fig. 6.2). The composition lies towards the magnesian end of the biotite field, midway between annite and siderophyllite.

6.2.3 Plagioclase.

Twelve microprobe analyses of five plagioclase grains in three basic dykes (SB20, SB72 and SBR25) are presented in Appendix E. Recalculated analyses (as cations per 8 oxygens, and as molecular components) are also given. K_2O was detected in only two of the analyses presented. Plagioclases from two rocks (SB20 and SB72) have mean An values of 32 and 29 respectively. A single analysis of the core of a partially recrystallised plagioclase, in

Fig. 6.1 Variation of (from top) total iron as FeO, CaO, MnO, MgO across two garnet grains (SB41, left and SBR 25, right). Numbers below points refer to analysis numbers in Appendix D, Table 1. Distances between points and across the grains are approximate.

Fig. 6.2 Biotite compositions plotted in terms of Mg/Mg + Fe + Mn vs. Si. Large dot indicates six coincident points. Et = Eastonite, Ph = Phlogopite, An = Annite, Sd = Siderophyllite.

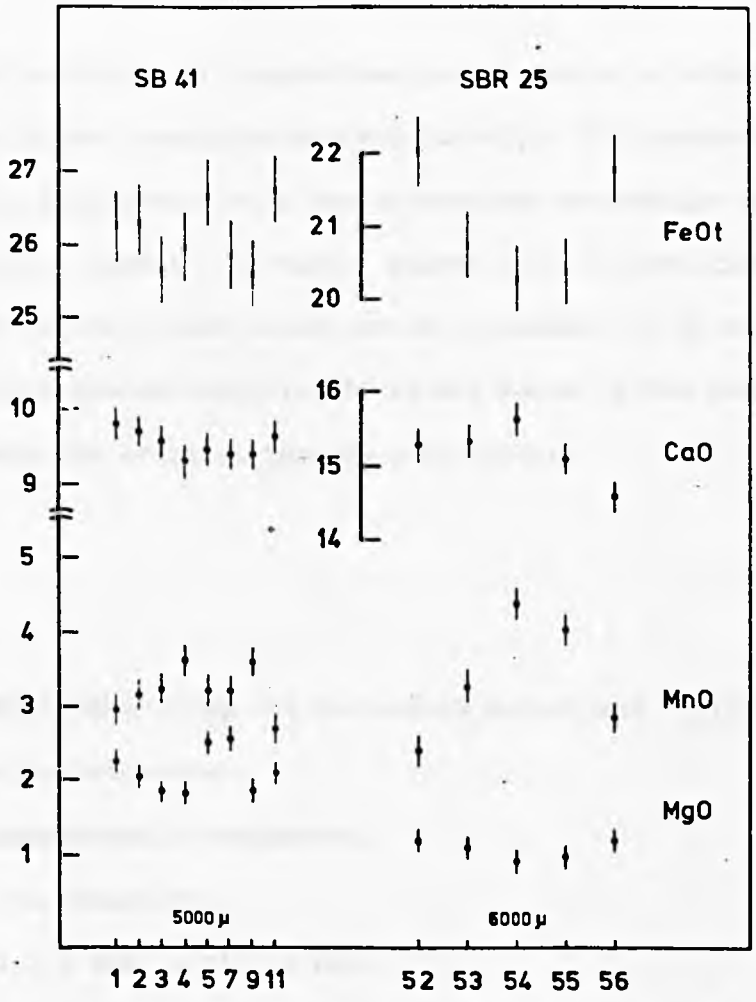
SB 41
SBR 25
27
26
25
10
9
5
4
3
2
1
22
21
20
16
15
14
FeOt
CaO
MnO
MgO
5000 µ
6000 µ
1 2 3 4 5 7 9 11
52 53 54 55 56

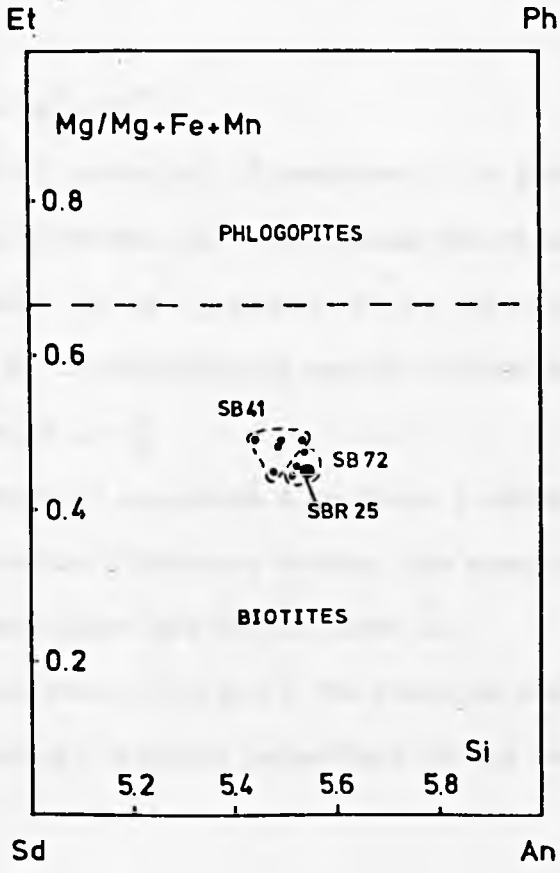
Et
Ph
Mg/Mg+Fe+Mn
0.8
PHLOGOPITES
0.6
SB41
SB 72
SBR 25
0.4
BIOTITES
0.2
Si
5.2
5.4
5.6
5.8
Sd
An

a rock (SBR25) in which the plagioclase grains define a relict igneous texture, has a higher anorthite content (An 42). This composition is probably not in equilibrium with the metamorphic assemblage present in the rock (hornblende - garnet - biotite - quartz and recrystallised plagioclase). The An content of the latter is not known precisely but appears to be close to An 30 (optical determination). It is not known if the plagioclase with An 42 represents the original igneous composition.

6.3 Partitioning of Mg and Fe between garnet and biotite - a geothermometer.

6.3.1 Thermodynamic background.

Consider the reaction:

$$A(p) + B(q) = C(r) + D(s) \qquad (1)$$

where A, B, C and D are components of the phases p, q, r and s. At equilibrium the difference in chemical potential between the reactants and products is zero, i.e.

$$\mu_A^p + \mu_B^q = \mu_C^r + \mu_D^s \qquad (2)$$

where μ_i^j is the chemical potential of component i in phase j. Relative to the standard chemical potential (μ^o) and taking the standard state as the pure phase at the temperature (T) and pressure (P) of interest each term (e.g. component A in phase p) in equation (2) may be written as:

$$\mu_A^p = \mu_A^o + RT \ln a_A^p \qquad (3)$$

where a_A^p is the activity of component A in phase p and R is the gas constant. Equation (3) expresses the difference between the chemical potential of component A in the pure phase and in the phase p.

The standard free energy charge of the reaction (ΔG^o) may be written as the difference in standard chemical potentials of the reactants and products:

$$\Delta G^\circ = \mu_C^\circ + \mu_D^\circ - \mu_A^\circ - \mu_B^\circ \qquad (4)$$

Rearranging and substituting each term in (4) by its analogue of equation (3), gives:

$$\Delta G^\circ = -RT \ln\left(\frac{a_C^r \cdot a_D^s}{a_A^p \cdot a_B^q}\right) \qquad (5)$$

The term in brackets in equation (5) is the activity product or the equilibrium constant (K).

Consider now the garnet-biotite Mg-Fe exchange reaction which may be written in terms of the end members as follows:

$$Fe_3Al_2Si_3O_{12} + KMg_3AlSi_3O_{10}(OH)_2 = KFe_3AlSi_3O_{10}(OH)_2 + Mg_3Al_2SI_3O_{12} \qquad (6)$$

almandine phlogopite annite pyrope

Substituting into equation (5):

$$\Delta G^\circ = -RT \ln\left(\frac{a^G_{Mg\text{-}G} \cdot a^B_{Fe\text{-}B}}{a^G_{Fe\text{-}G} \cdot a^B_{Mg\text{-}B}}\right) \qquad (7)$$

where G and B refer to garnet and biotite and Mg-G refers to the pyrope component etc. Each activity term in equation (7) may be expressed in terms of composition (e.g. for the pyrope term):

$$a^G_{Mg\text{-}G} = \left(\gamma^G_{Mg\text{-}G} \cdot X^G_{Mg\text{-}G}\right)^3 \qquad (8)$$

where γ is the activity coefficient, X is the mole fraction of the pyrope component in the garnet and the exponent (= 3) is the same for garnet and biotite and arises from the three exchangeable cations in each end-member. For ideal solid solution (zero free energy of mixing) each of the γ terms is equal to one and substitution of equation (8) into equation (7) gives:

$$\Delta G^\circ = -3RT \ln\left(\frac{X^G_{Mg\text{-}G} \cdot X^B_{Fe\text{-}B}}{X^G_{Fe\text{-}G} \cdot X^B_{Mg\text{-}B}}\right) \qquad (9)$$

The term in brackets in equation (9) is the empirical distribution coefficient (K_D) which may be written as:

$$K_D = (Mg/Fe)_G \; / \; (Mg/Fe)_B \; . \qquad (10)$$

Substituting the enthalpy (H), entropy (S) and volume (V) terms for ΔG°, rearrangement of equations (9) and (10) gives:

$$\Delta H_{1\ bar,\ T} - T\Delta S^\circ_T + (P - 1)\Delta V^\circ = -RT \ln K_D \; . \qquad (11)$$

Thus if the one-bar enthalpy, and standard entropy and volume changes are known the distribution coefficient (K_D) may be expressed in terms of P and T. For solid-solid equilibria ΔS values are small and so, depending on the relative contributions of the enthalpy and volume terms, K_D may vary dominantly as a function of either T or P. Large values of ΔH relative to ΔV or small values of ΔV alone imply a large variation of K_D with T in which case the reaction may be useful as a geothermometer. ΔV for the garnet-biotite Mg-Fe exchange reaction is in fact small (inter alia Albee, 1965 and Robie et al., 1967) and K_D varies with temperature and composition. The pressure dependence of K_D has been calculated to be significant only at extremely high pressures (Perchuk, 1970).

6.3.2 Calibration of the garnet-biotite Mg-Fe exchange geothermometer.

In the absence of sufficient thermodynamic data (the various ΔH, ΔS, ΔV terms are poorly known) there are two approaches to the problem of calibration: (1) experimental (from which the thermodynamic data may be derived) and (2) empirical. Both approaches will be illustrated and three methods will be considered here.

(1) Experimental calibration.

Method (a)

Ferry and Spear (1978) have investigated the partitioning of Mg and Fe between garnet and biotite in the temperature range 500°C to 800°C using synthetic almandine-pyrope and annite-phlogopite mixtures. Their work represents the first successful determination of Mg-Fe partitioning at geologically useful (less than 800°C) temperatures.

Garnet reacts much more slowly than biotite and to overcome this

kinetic problem a high molar garnet/biotite ratio (98:2) was used. Thus attainment of equilibrium required only a small change in the garnet composition for a relatively large change in the biotite. Equilibrium was demonstrated at each temperature by simultaneously reacting two experimental charges: one containing garnet and a biotite more magnesian than the equilibrium composition and another containing garnet and a biotite more iron-rich than the equilibrium composition at a given temperature.

The experimental results were expressed (ibid, from equation (1) as a linear equation:

$$\ln K_D = -2109/T(^{\circ}K) + 0.782 \qquad (12)$$

in which the coefficients were determined by linear regression of ln K vs. 1/T at a pressure of 2.07 Kb. ($\ln K_D$ as above, (10)). The experiments did not include any attempt to estimate the effects of other components on K_D but comparison with other calibrations ((b) and (c) below) led Ferry and Spear (ibid.) to suggest that the calibration (12) was applicable as a geothermometer "without correction for components (up to ca. 0.2 = (Ca + Mn)/(Ca + Mn + Fe + Mg) in garnet and up to ca. 0.15 = $(Al^{VI} + Ti)/(Al^{VI} + Ti + Fe + Mg)$ in biotite) other than Fe and Mg". Their calibration (12) has a minimum uncertainty of $\pm$ 50°C arising from the experimental uncertainties. Practical applications to natural rocks will have additional contributions to uncertainty from analytical errors. In view of the small pressure dependence of the reaction no correction for pressure is necessary up to ca. 10 Kb.

(2) Empirical calibrations.

Method (b)

Thompson (1976) obtained an inverse linear relationship between $\ln K_D'$ (K_D' is the inverse of K_D i.e. $K_D' = (Fe/Mg)_G/(Fe/Mg)_B$) of natural garnet-biotite pairs in New England pelites and temperature in the range 500°C - 700°C. The latter was estimated from phase assemblages in a variety of coexisting rocks which were assumed to have equilibrated at the same

temperature as the garnet-biotite pairs.

From Thompson (ibid., Fig. 1B and cited references therein) the following expression has been calculated:

$$\ln K_D' = -0.0033\ T\ (^\circ C) + 3.6667. \qquad (13)$$

In the temperature range 450°C to 600°C temperature estimates which use equation (13) will be subject to uncertainty of at least ± 50°C and perhaps as much as ± 80°C at the lower temperature end. This method does not take into account compositional parameters other than Mg and Fe.

Method (c)

Goldman and Albee (1977) have attempted to correlate partitioning of Mg and Fe between natural garnet and biotite in pelitic rocks (also from New England) with temperature estimated from $^{18}O / ^{16}O$ fractionation between coexisting quartz-magnetite and quartz-ilmenite pairs in the same rocks. In addition, their correlation technique (multivariate least squares analysis) has taken account of a variety of compositional parameters (X^G_{Mn}, X^G_{Ca}, X^B_{Fe}, X^B_{Ti}, $X^B_{Al}{}^{VI}$, where

$$X^G_{Mn} = Mn/\ (Fe + Mg + Mn + Ca)$$

$$X^G_{Ca} = Ca/\ (Fe + Mg + Mn + Ca)$$

$$X^B_{Fe} = Fe/\ (Fe + Mg)$$

$$X^B_{Ti} = Ti/\ (Fe + Mg + Mn + Ti + Al^{VI})$$

$$X^B_{Al}{}^{VI} = Al^{VI}/\ (Fe + Mg + Mn + Ti + Al^{VI})).$$

The method relies on the assumption that the garnet-biotite pairs analysed have equilibrated at the same temperature as the quartz-magnetite and quartz-ilmenite oxygen isotope systems. Garnet zoning was detected in many of the samples and only garnet rims and adjacent biotites were used. Additional data for garnet-biotite pairs in rocks, whose equilibrium temperatures were measured independently, were incorporated to refine the compositional parameters. In particular this procedure produced a significant shift in the X^G_{Ca} term (see below).

The following relationship was obtained (ibid., equation (9)):

$$\ln K_D = -0.177(\pm 0.010)1000 \ln\alpha^{Q}_{M} - 1.22(\pm 0.14)X^{G}_{Mn}$$
$$- 2.14(\pm 0.013)X^{G}_{Ca} + 1.40(\pm 0.09)X^{B}_{Fe} + 0.942(\pm 0.019)X^{B}_{Ti}$$
$$- 1.59(\pm 0.021)X^{B}_{Al}VI - 0.492(\pm 0.068) \qquad (14)$$

where $1000 \ln\alpha^{Q}_{M}$ is the oxygen isotopic fractionation between quartz (Q) and magnetite (M) and is related to temperature by Bottinga and Javoy (1973):

$$1000 \ln\alpha^{Q}_{M} = 5.57\ (10^6/T^2). \qquad (15)$$

From equation (14) it is clear (from their relatively large coefficients) that X^{B}_{Fe} and X^{G}_{Ca} are important compositional parameters. That these parameters are large indicates non-ideality of mixing in both garnet and biotite. In particular the influence of X^{G}_{Ca} corroborates the conclusions of Hensen et al. (1975) who found large departures from ideality in the system pyrope-grossular garnet. Furthermore the negative coefficients in the X^{G}_{Ca} and X^{G}_{Mn} terms (14) (i.e. an inverse relationship of these with $\ln K_D$) agree with the findings of Sen and Chakraborty (1968) for Ca and of, inter alia, Kretz (1959) and Saxena (1968) for Mn.

6.3.3 Application of the calibrations to the garnet-biotite data for the dyke suite.

Compositional data for six garnet-biotite pairs from three dykes (SB41, SB72 and SBR25) are summarised in Table 6.1 and include values of X^{B}_{Fe}, X^{G}_{Ca}, K_D and $\ln K_D$. From Table 6.1 a negative correlation of K_D with X^{G}_{Ca} may be deduced, similar to that found by Sen and Chakraborty (op. cit.). Equilibrium temperatures were calculated using the methods (a, b, c) outlined above. As indicated above the minimum uncertainty for each of the temperature methods is $\pm$ 50°C. Taking into account the errors in microprobe analyses, realistic (2σ) uncertainties at the ca. 500°C level are $\pm$ 80°C. Thus there is good agreement between the pairs in each rock and between all three rocks for any one method. Methods (a) (Ferry and Spear, op. cit.) and (b) (Thompson, op. cit.) agree closely with one another while temperatures from method (c) are probably (i.e. taking account of uncertainties) significantly higher than the others. The results for sample SB41 are within $\pm$ 50°C of one another for all three methods.

Table 6.1

Compositional data for garnet (G) - biotite (B) contact pairs, Mg-Fe distribution coefficients (K_D) and equilibrium temperatures calculated using the methods of (a) Ferry and Spear (1978), (b) Thompson (1976) and (c) Goldman and Albee (1977). For explanation see text.

Sample and analysis No.	(G, B)	Mg/Fe_G	Mg/Fe_B	X^G_{Ca}	X^B_{Fe}	K_D	ln K_D	Temperature (°C) (a)	(b)	(c)
SB41	1,17	0.149	0.991	0.275	0.502	0.151	-1.894	515	537	607
	11,25	0.142	0.899	0.270	0.527	0.158	-1.846	529	546	581
SB72	31,32	0.103	0.868	0.342	0.535	0.119	-2.125	452	463	566
	37,38	0.105	0.933	0.332	0.517	0.113	-2.185	438	445	555
SBR25	52,60	0.096	0.823	0.424	0.548	0.116	-2.153	446	454	593
	56,57	0.098	0.848	0.410	0.541	0.116	-2.155	446	454	567

From Table 6.1 the values of X^G_{Ca} are high relative to those of any of the garnets used in the calibrations. The mean values of (Ca + Mn)/(Ca + Mn + Fe + Mg) for SB41, SB72 and SBR25 (0.3, 0.4, 0.5 respectively) are higher than the recommended maximum value (0.2) for application of the uncorrected Ferry and Spear method. These high values imply considerable departures from ideal mixing in the Orust dyke garnets. In the absence of the appropriate thermodynamic data, the ideal mixing model is all that is available. Thus the best approximation to the equilibrium temperature may be that calculated from the Goldman and Albee method (c), which takes account of components other than Mg and Fe in the garnet and biotite. However, as indicated above the X^G_{Ca} term is itself compositionally dependent and the X^G_{Ca} values (less than 0.2) in the garnets used are lower than the corresponding values for the garnets in the Orust dykes (Table 6.1). In order to minimise the unknown effect of the large X^G_{Ca}, the data for SB41 (with the

lowest X^{G}_{Ca} value ca. 0.3) is considered to provide the best estimate of the equilibrium temperature i.e. 594°C ± ca. 80°C (mean) using the Goldman and Albee calibration (method (c)). That the effect of Ca on the equilibrium temperature estimate is minimised at an X^{G}_{Ca} value of ca. 0.3 is suggested by the agreement between the three methods for SB41.

6.3.4 Significance of the estimated temperature.

It is not known if the estimated equilibrium temperature records the thermal peak of metamorphism or if it corresponds to the temperature of equilibration of the Rb-Sr isotopic systematics at ca. 1060 m.y. (Section 4.4). It is possible that the estimated temperature represents equilibration below the temperature of the thermal maximum since the blocking temperature for diffusion of Mg and Fe between garnet and biotite is not known. It is unlikely that the post-D4 alteration and retrogression (Section 5.2) has affected the garnet composition in view of the low rates of diffusion in garnet (cf. Ferry and Spear, op. cit.). However, relatively large changes in biotite composition (with respect to Fe, Mg) may be achieved more rapidly and it is not known to what extent the biotites have been modified since the time of equilibration. Chloritisation of biotite is a common feature in these rocks but great care was taken to avoid such altered biotites and in addition biotites in close proximity to Fe, Mg-bearing phases (other than garnet i.e. hornblende, epidote, chlorite) were not used.

The temperature estimate (ca. 594 ± 80°C) is within the range (ca. 450°C to 650°C), estimated by Turner (1968) for the amphibolite facies of metamorphism of which the assemblage:

hornblende-plagioclase (ca. An 30) - garnet-biotite

is a typical representative. The corresponding pressure range is 2 Kb. to 10 Kb. Neither the garnet-biotite data for the dykes nor the phase assemblages in the surrounding rocks allow any constrained estimate of the equilibrium load pressure.

CHAPTER 7. Conclusions.

7.1 The basement complex.

The rock types and sequence of events identified in western Orust by Park et al. (op. cit.) can be recognised over the area discussed in this thesis.

Geochemical data on the migmatitic gneisses is consistent with the geological evidence of a sedimentary origin. The older amphibolites may have an intrusive or volcanic origin and the geochemical evidence suggests a tholeiitic magma type.

Two generations of migmatitic leucosome have been recognised throughout the Orust area. The first (pre-D1) is volumetrically more significant and grades into localised areas of nebulitic migmatite.

The geochemistry of the gneisses and the nebulitic migmatites (the Hälleviksstrand granite) is consistent with closed-system anatexis and localised collection of the resulting melt. The geochemical variation is probably the result of varying degrees of separation of melt and residuum. Some of the variation in the alkalis may be the result of the second migmatisation and of later alteration. Both processes appear to have contributed to the open system behaviour of the Rb-Sr isotopes in the Hälleviksstrand granite, but incomplete equilibration during the first migmatisation cannot be ruled out as an alternative explanation. The data do not allow any precise constraint to be placed on the age of either migmatisation.

7.2 The pre-dyke intrusive rocks.

The Hälleviksstrand amphibolite, of probable calc-alkaline affinity, was emplaced after the first migmatisation and D1 deformation in the paragneisses. The body is affected by the second migmatisation and deformed during D2. The age of emplacement is 1432 $\pm$ 92 m.y. and the low initial

$^{87}Sr/^{86}Sr$ ratio (0.7032 ± 5) implies a primitive source, possibly in the upper mantle.

The Assmunderöd-Myckleby augen granite post-dates the first generation leucosome but is locally cut by the second. The geochemical variation within the body arises either from contamination by the country rocks or from varying degrees of separation of melt from residuum. An "errorchron" age of 1379 ± 46 m.y. is interpreted as the age of intrusion. The high initial $^{87}Sr/^{86}Sr$ ratio (0.713 ± 3) indicates a crustal source for the magma and a probable maximum period of crustal residence of the source rocks of ca. 150 m.y. The imperfect isotopic equilibration is probably the result of xenolith contamination.

The younger granites cut both generations of migmatitic leucosome in the gneisses, the Hällevikstrand amphibolite, the Assmunderöd-Myckleby augen granite and the F2 folds. According to the preferred interpretation of the geochemical data the younger granites are igneous differentiates of a basaltic or tonalitic magma. A primitive (non-crustal) source is preferred, at least for the tonalites. The disequilibrium of the isotopic systems is due either to variation in initial $^{87}Sr/^{86}Sr$ ratio or to subsequent metamorphic disturbance.

7.3 The dyke suite and the post-dyke (Sveconorwegian) events.

Basic and minor acidic dykes cut both generations of migmatitic leucosome in the para-gneisses, the younger granites and the D2 structures and also post-date the pre-dyke intrusive rocks. The geochemical data are consistent with fractional crystallisation of a tholeiite magma possibly involving the separation of plagioclase, clinopyroxene and, later, Fe-Ti oxides and apatite. It is possible that the small volumes of acidic dykes are derived from the same source.

The patterns of variation of the "immobile" incompatible trace elements in the basic dykes, both on the scale of individual dykes and regionally, suggests caution in the application of magma type discriminant diagrams to rocks metamorphosed at amphibolite grade.

Isotopic equilibration in narrow, deformed basic and intermediate dykes during the syn-D3 metamorphism is dated at ca. 1060 m.y. The high initial $^{87}Sr/^{86}Sr$ ratios (0.707 - 0.714 are interpreted as the result of exchange of Rb and Sr between the dykes and the country rocks. The measured age places an older age limit on the D4 deformation and a younger limit on the age of dyke emplacement. Sheets of pegmatite, at least some of which were emplaced later than the dyke suite, have Rb-Sr mineral ages close to 950 m.y., interpreted as the age of emplacement. Evidence of disequilibrium was seen in one muscovite sample and is probably caused by post-emplacement deformation.

The equilibrium temperature of Mg-Fe partitioning between garnet and biotite in the basic dykes is estimated at ca. 590°C. This is consistent with the amphibolite facies assemblage: hornblende - plagioclase (An 30) - garnet - biotite, developed during the D3 deformation. No precise constraint on the pressure of metamorphism is possible.

7.4 Synthesis and significance of the geochronological results.

The isotopic data for the Hällevikstrand granite affords no definite information on its age but is not in conflict with previous estimates of a Svecofennian age for the early components of the Stora Le - Marstrand belt.

The emplacement ages (ca. 1350-1450 m.y.) of the Hällevikstrand amphibolite and the Assmunderöd-Myckleby augen granite are within 2σ error and they place a younger age limit on the first migmatisation and the D1 deformation and an older age limit on subsequent events. Since the migmatitic

para-gneisses form the bulk of the Stora Le - Marstrand belt the addition of significant volumes of new crustal material after ca. 1400 m.y., apart from the Bohus granites, seems to be ruled out. Thus subsequent deformation and metamorphism, including the Sveconorwegian events, essentially involved reworking of pre-existing crust over at least this segment of the Stora Le - Marstrand belt.

The igneous activity in the Orust area at ca. 1350-1450 m.y. correlates with the intrusion of a variety of (post-Åmål (I)) granites in the Åmål belt to the east and this points to a possible correlation of the first generation migmatisation in the Stora Le - Marstrand belt with the early components of the Åmål belt.

The dating of the D3 metamorphism (at 1060 m.y.) in the dykes places a younger limit on their age of emplacement, and on that of the younger granites, and an older age limit on subsequent events. The measured age lies within the range of the Sveconorwegian - Grenville orogeny (inter alia Kratz et al., op. cit.). Thus the regional D4 deformation, with a younger age limit of ca. 890 m.y. (defined by the age of the post-tectonic Bohus granite) is identified as a Sveconorwegian event.

The dyke suite was emplaced between ca. 1400 m.y. and ca. 1060 m.y. but no precise estimate of the age may be made. It is possible that the dyke suite may be correlated with the widespread dolerite dykes in North America, south Greenland and central Sweden emplaced at ca. 1260 m.y. to 1190 m.y.

APPENDIX A

Appendix A Table 1 Results of replicate sampling of sample SJ632 (1-9).

(a) Uncorrected X.R.F.S. data, major elements

Na_2O on pressed powder, L.O.I. at 1000 °C

SiO_2 to P_2O_5 on $LiBO_2$ glass.

(wt. %)

	SiO_2	TiO_2	Al_2O_3	$Fe_2O_3^*$	MnO	MgO	CaO	K_2O	P_2O_5	L.O.I.	Na_2O
SJ632/1	48.31	1.16	16.54	12.23	.18	8.31	10.37	.44	.23	.88	2.01
SJ632/2	48.21	1.15	16.57	12.20	.18	8.29	10.40	.45	.24	.97	2.03
SJ632/3	48.01	1.17	16.67	12.21	.18	8.39	10.35	.44	.23	.88	2.04
SJ632/4	48.51	1.15	16.75	12.25	.18	8.20	10.37	.45	.23	.99	2.04
SJ632/5	48.43	1.15	16.59	12.28	.18	8.35	10.39	.44	.23	1.01	2.02
SJ632/6	48.72	1.15	16.67	12.27	.18	8.13	10.39	.44	.23	.89	2.03
SJ632/7	48.36	1.16	16.52	12.14	.18	8.26	10.33	.45	.23	.96	2.07
SJ632/8	48.77	1.14	16.57	12.24	.18	8.47	10.35	.45	.23	1.01	2.06
SJ632/9	48.79	1.17	16.53	12.24	.18	8.37	10.40	.45	.23	1.00	2.05

* = total iron as Fe_2O_3

Appendix A Table 1 (continued)

(b) Normalised major element geochemical data (Uncorrected X.R.F.S. data recalculated to 100% , including L.O.I. as a component.

(wt. %)

	SiO_2	TiO_2	Al_2O_3	$Fe_2O_3^*$	MnO	MgO	CaO	Na_2O	K_2O	P_2O_5
SJ632/1	47.99	1.15	16.43	12.15	.18	8.25	10.30	2.01	.44	.23
SJ632/2	47.87	1.14	16.45	12.11	.18	8.24	10.33	2.03	.44	.24
SJ632/3	47.74	1.16	16.57	12.14	.18	8.34	10.29	2.04	.44	.23
SJ632/4	47.96	1.14	16.55	12.11	.17	8.10	10.26	2.04	.44	.23
SJ632/5	47.90	1.13	16.41	12.15	.18	8.26	10.28	2.02	.44	.23
SJ632/6	48.18	1.14	16.48	12.13	.17	8.04	10.28	2.03	.44	.23
SJ632/7	48.04	1.15	16.41	12.06	.17	8.21	10.26	2.07	.45	.22
SJ632/8	48.04	1.12	16.32	12.06	.18	8.36	10.20	2.06	.44	.22
SJ632/9	48.08	1.16	16.29	12.06	.18	8.25	10.25	2.05	.45	.23
mean	47.98	1.14	16.43	12.11	.18	8.23	10.27	2.04	.44	.23
s.dev. ‡	.26	.03	.18	.08	.01	.21	.07	.04	.01	.01
c.of v. (%)	.54	2.28	1.13	.64	5.65	2.50	.70	1.86	1.81	5.24

* = total iron as Fe_2O_3

‡ both at 2σ level

Appendix A Table 1 (continued)

(c) Trace element geochemical data.

(ppm.)

	Cr	Ga	Nb	Ni	Sc	Rb	Sr	Y	Zr
SJ632/1	133	16	BDL	109	37	13	156	24	102
SJ632/2	135	17	BDL	111	36	14	156	25	101
SJ632/3	133	14	BDL	110	37	12	158	25	104
SJ632/4	135	18	BDL	111	36	13	158	25	102
SJ632/5	137	18	7	111	37	13	155	24	102
SJ632/6	133	17	8	109	37	14	158	25	101
SJ632/7	132	18	8	109	37	14	161	25	99
SJ632/8	136	17	8	112	37	13	158	24	99
SJ632/9	133	16	BDL	111	37	12	156	25	101

BDL = below detection limit

mean	134	17		110	37	13	157	25	101
s.dev. *	3.4	2.6		1.2	.9	1.6	3.6	1.0	3.1
c.of v. * (%)	2.5	15.5		2.0	2.4	11.9	2.3	4.1	1.6

* both at 2σ level

Appendix A Table 2 Results of replicate sampling of sample SJ522 (1-9)

(a) Uncorrected X.R.F.S. data, major elements
Na_2O on pressed powders. L.O.I. at 1000 °C
SiO_2 to P_2O_5 on $LiBO_2$ glass.
(wt. %)

	SiO_2	TiO_2	Al_2O_3	$Fe_2O_3^*$	MnO	MgO	CaO	K_2O	P_2O_5	L.O.I.	Na_2O
SJ522/1	74.26	.08	15.18	.36	.006	.45	1.31	5.09	.13	.87	3.39
SJ522/2	73.90	.07	14.97	.28	.004	.31	1.25	5.08	.14	.94	3.53
SJ522/3	74.16	.08	15.24	.30	.005	.57	1.26	5.36	.13	.90	3.38
SJ522/4	74.19	.08	15.44	.36	.009	.41	1.37	5.07	.13	.94	3.54
SJ522/5	74.47	.06	15.33	.20	.003	.33	1.30	5.36	.13	.90	3.55
SJ522/6	74.57	.06	15.37	.19	.004	.47	1.34	5.24	.13	.88	3.63
SJ522/7	74.40	.08	15.35	.35	.006	.43	1.38	5.19	.13	.89	3.50
SJ522/8	74.69	.09	15.30	.31	.006	.61	1.36	5.34	.13	.88	3.43
SJ522/9	75.12	.08	15.40	.32	.006	.46	1.32	5.46	.13	.94	3.36

* = total iron as Fe_2O_3

Appendix A Table 2 (continued)

(b) Normalised major element geochemical data (Uncorrected X.R.F.S. data recalculated to 100% , including L.O.I. as a component.

(wt. %)

	SiO_2	TiO_2	Al_2O_3	$Fe_2O_3^*$	MnO	MgO	CaO	Na_2O	K_2O	P_2O_5
SJ522/1	73.40	.08	15.01	.35	.01	.44	1.29	3.39	5.03	.13
SJ522/2	73.54	.07	14.90	.28	BDL	.31	1.24	3.53	5.05	.13
SJ522/3	73.11	.07	15.04	.29	BDL	.56	1.24	3.38	5.28	.13
SJ522/4	73.02	.08	15.20	.36	.01	.40	1.35	3.54	4.99	.12
SJ522/5	73.22	.06	15.07	.20	BDL	.33	1.28	3.55	5.26	.13
SJ522/6	73.12	.06	15.07	.18	BDL	.46	1.32	3.63	5.14	.13
SJ522/7	73.10	.08	15.08	.34	.01	.43	1.35	3.50	5.10	.13
SJ522/8	73.06	.08	14.96	.30	.01	.59	1.33	3.43	5.22	.13
SJ522/9	73.14	.08	15.00	.31	.01	.45	1.28	3.36	5.31	.13
mean	73.19	.07	15.04	.29		.44	1.30	3.48	5.15	.13
s.dev. *	.34	.02	.17	.13		.18	.08	.19	.24	.01
c.of v. * (%)	.47	24.7	1.13	43.4		41.7	6.5	5.4	4.6	4.7

* = total iron as Fe_2O_3

* both at 2σ level

Appendix A Table 2 (continued)

(c) Trace element geochemical data.

(ppm.)

	Ga	Nb	Rb	Sr	Y	Zr
SJ522/1	13	7	123	190	16	38
SJ522/2	14	9	124	184	16	39
SJ522/3	13	10	129	191	16	34
SJ522/4	12	8	126	189	14	36
SJ522/5	10	7	130	191	15	35
SJ522/6	11	9	128	191	15	36
SJ522/7	12	8	130	188	16	37
SJ522/8	11	8	130	189	15	34
SJ522/9	11	7	134	187	14	34
	(Cr,Ni and Sc not determined)					
mean	12	8	128	189	15	36
s.dev. ⁂	2.5	2.1	6.8	4.6	1.7	3.7
c.of v. ⁂	21.3	25.9	5.3	2.5	10.9	10.2

⁂ both at 2σ level

Appendix A. Table 3

Element	K	Ti	Si	Ca	Al	Mg	Na	P	Fe	Mn
Radiation line used	Kα	Kα	Kα	Kα	Kα	Kα	Kα	Kα	Kα	Kα
Tube	Cr	Cr	Cr	Cr	Cr	Cr	Cr	Cr	W	W
Kv	40	40	40	40	60	40	40	60	60	60
mA	8	8	16	8	24	35	40	24	8	32
Crystal	PET	LiF 200	PET	LiF 200	PET	KAP	TlAP	GE	LiF 220	LiF 220
Collimator	C	F	C	F	C	C	C	C	FINE	FINE
Counter	F	F	F	F	F	F	F	F	FLOW	FLOW
Vacuum/air path	VAC.	VAC.	VAC.	VAC.	VAC.	VAC.	VAC.	VAC.	VAC.	VAC.
Method	ABS. RAT.	ABS. RAT.	ABS. RAT.	ABS. RAT.	ABS. RAT.	ABS. RAT.	ABS. RAT.	ABS. RAT.	ABS. RAT.	ABS. RAT.
Time	FC	FC	FC	FC	FC	FC	FC	FC	FC	FC
Counts	3×10^4	3×10^4	3×10^4	3×10^4	3×10^4	3×10^4	3×10^4	3×10^4	10^4	3×10^4

Appendix A. Table 4

Element	Ce	Cr	Ga	Nb	Ni	Sc	Rb	Sr	Y	Zr
Radiation line used	$L\beta_1$	K∝	K∝	K∝	K∝	K∝	K∝	K∝	K∝	K∝
Tube	W	W	Mo	W	W	Cr	Mo	Mo	Mo	Mo
Kv	60	60	90	60	60	60	90	90	90	90
mA	32	32	20	32	32	24	20	20	20	20
Crystal	LiF 220	LiF 220	LiF 220	LiF 220	LiF 220	LiF 200	LiF 220	LiF 220	LiF 220	LiF 220
Collimator	FINE	FINE	FINE	FINE	FINE	F	FINE	FINE	FINE	FINE
Counter	FLOW	FLOW	FLOW	SCINT.	FLOW	F	SCINT.	SCINT.	SCINT.	SCINT.
Vacuum/air path	VAC.	VAC.	VAC.	VAC.	VAC.	VAC.	VAC.	VAC.	VAC.	VAC.
Method	ABS. RAT.	ABS. RAT.	ABS. RAT.	ABS. RAT.	ABS. RAT.	ABS.	ABS.	ABS.	ABS.	ABS.
Time	FC	FC	FC	FC	FC	40 sec.	40 sec.	40 sec.	40 sec.	40 sec.
Detection limit (ppm.)	-	12	5	6-8	15	4	2	3	2-3	6

Appendix A. Table 5.

$^{87}Sr/^{86}Sr$ ratio measurements on NBS standard SRM987

$^{87}Sr/^{86}Sr$ uncorrected	tailing (%) *1	$^{87}Sr/^{86}Sr$ corrected	sets *2
0.710398 ± 54	0.010	0.71037 ± 6	24
0.710281 ± 44	0.010	0.71026 ± 4	16
0.710355 ± 16	0.012	0.71033 ± 2	64
0.710301 ± 28	0.000	0.71030 ± 3	31
0.710304 ± 26	0.006	0.71029 ± 3	43
0.710313 ± 100	0.010	0.71031 ± 10	23

Comparative results

$^{87}Sr/^{86}Sr$	source	laboratory
0.71031 ± 4	This work (mean)	Leeds
0.71029 ± 3	Higgins et al. (1978)	Leeds
0.71023 ± 5	Patchett et al. (1978)	East Kilbride
0.71004 ± 8	Patchett et al. (1978)	Münster
0.71035 ± 16	Hansen (1976)	Zurich

Notes: *1 "tailing" is the interference of the ^{88}Sr peak on the ^{87}Sr peak, measured at mass number 87.5 and expressed as a percentage of the ^{87}Sr peak. It is assumed that the tail under the ^{87}Sr peak is one third of that in the 87.5 position. The correction for tailing is usually not significant and is made by reducing the ^{87}Sr counts (hence $^{87}Sr/^{86}Sr$ ratio) by one third of the counts measured in the 87.5 position.

*2 Each set is the mean of ten cycles through the measured mass number positions i.e. 88, 87.5, 87, 86, 85 (to check if any Rb contaminant is present) and 84.5 (zero, i.e. baseline).

Appendix A. Table 6.

Rb-Sr analytical data: X.R.F.S. analyses for Rb, Sr contents and Rb/Sr ratios for nine replicate samples of SJ 632 (Härmanö dyke, see Chapter 5). Philips PW 1212 X-ray fluorescence spectrometer, University of Leeds.

Sample	Rb (ppm.)	Sr (ppm.)	Rb/Sr
632/1	15.0	150	0.0998
632/1	15.1	151	0.0998
632/1	14.4	150	0.0960
632/2	15.4	152	0.1015
632/3	14.6	151	0.0971
632/4	14.6	152	0.0964
632/5	14.8	149	0.0991
632/6	14.7	151	0.0975
632/7	14.8	154	0.0960
632/8	14.5	152	0.0950
632/9	14.5	150	0.0970
Mean	14.8	151	0.0977
S.D	0.296	1.307	0.002
C. of V.(%)	2.0	0.9	2.1

Quoted errors are 1σ

Note: Calibration based on internal standard Rh-75-67, Rb (179.2 $\pm$ 5 ppm.), Sr (245.6 $\pm$ 4 ppm.) and Rb/Sr (0.7299 $\pm$ 210):- Analyst A. R. Gledhill (Leeds).

Appendix A. Table 7.

Rb-Sr analytical data: U.S.G.S. standards, comparison with published results.

Standard	Elements and Ratios	Results			
		1	2	3	4
BCR-1	Rb	48	47.3 ± 2	46	47
	Sr	335	332.1 ± 6	319.5	330
	Rb/Sr	0.1426	0.1424 ± 7	0.1442 ± 10	
AVG-1	Rb	68	67.1 ± 5	67	67
	Sr	667	662 ± 1	653.5	660
	Rb/Sr	0.1023	0.1014 ± 7	0.1021 ± 6	
GSP-1	Rb	251	254.7 ± 7	250	250
	Sr	232	233.1 ± 4	230	230
	Rb/Sr	1.0809	1.093 ± 4	1.089 ± 4	
G-2	Rb	168	169.3 ± 7	171	170
	Sr	475	476.3 ± 1.3	483	480
	Rb/Sr	0.3538	0.355 ± 2	0.354 ± 2	

Notes 1 This work, X.R.F.S. PW 1212 Leeds.
Realistic errors in Rb and Sr contents estimated at ± 5% (2σ); errors in Rb/Sr ratios estimated at ± 2% (2σ).

2 Pankhurst and O'Nions (1973), isotope dilution.

3 Pankhurst and O'Nions (1973), X.R.F.S.

4 Abbey (1975).

Appendix A.

Table 8.

REE data - average of 22 chondrite (from Herrmann, 1974), used to normalise REE analyses for the Hällevikstrand amphibolite, the Assmunderöd-Myckleby augen granite and the dyke suite. See text and Figs. 4.3, 4.4 and Table 5.2.

La	0.32
Ce	0.94
Pr	0.12
Nd	0.6
Sm	0.2
Eu	0.073
Gd	0.31
Tb	0.05
Dy	0.31
Ho	0.073
Er	0.21
Tm	0.033
Yb	0.19
Lu	0.031

APPENDIX B

Appendix B1.

Sample descriptions:- Basement complex.

Abbreviations:

Ap - apatite	Mi - microcline
Bt - biotite	Mu - muscovite
Chl - chlorite	Pl - plagioclase
Ep - epidote	Sp - sphene
Gt - garnet	Qz - quartz
Hb - hornblende	Zr - zircon

Gneisses. A total of thirty samples were analysed. Seventeen of these are migmatised para-gneisses and thirteen are nebulitic migmatites (the Hallevikssstrand granite). Twenty five of the samples are located within the area mapped by Park et al. Samples prefixed "SJ" (16), "SB" (10) and "GP" (1) were collected by the author, A. I. Bailey and R. G. Park. B. S. P. Moorlock supplied three samples (prefixed "S"), collected in the vicinity of the Källviken augen granite. One sample (SJ 953) was collected at Slussen in north-eastern Orust.

Migmatitic gneisses (n = 17). All but two of these (GP 19 and SJ 521) contain more than ten per cent by volume of migmatitic leucosome.

SB 26 (40, 51).

Migmatised coarse-grained semi-pelitic gneiss contains Qz (30), Pl (20), Mu (20%), Bt (10%), Gt (10%). Bt partially chloritised. Accessory Ap, Zr, opaque ores. Leucosomes impersistent, 2-5 mm wide, trondhjemitic to granodioritic in composition. Strong D1 Bt fabric parallel to leucosomes. Ca. 25% leucosome.

SB 82 (41, 51).

Strongly foliated dark grey psammite. Inhomogenous development of impersistent flecks of granodioritic leucosome which makes up ca. 15% of rock. Larger (up to 3 mm. wide) leucosomes have 1-2 mm. wide Bt selvedges.

SB 90 (40, 50).

Coarse-grained migmatised gneiss. Granodioritic leucosomes make up ca. 50% of the rock. In places palaeosomes breached by adjacent leucosomes. Bt in palaeosome largely replaced by Chl.

SB 95 (40, 50).

Coarse-grained portions of this rock up to 5 cm. across are heavily migmatised and opthalmitic structure is developed. Palaeosome surrounding these areas is Bt-rich psammite containing Qz (45%), Pl ca. An 30 (35%), Bt + Mu (20%) with accessory Ap and Sp. Strong Bt fabric developed in the palaeosome.

SB 118 (39, 50).

Lighter in colour and has pink Mi (minor) in the leucosome. Otherwise similar to SB 82.

SB 136 (42, 46).

Medium to fine-grained dark grey Bt-rich palaeosome. Minor development (10-15%) of narrow Qz-rich leucosomes (2-4 mm. across) and parallel small Qz veins (1 mm.).

SBH 31 (43, 46).

Medium to fine-grained Bt-rich migmatised pelite. Stromatic leucosome makes up ca. 30% of the rock.

SBH 52 (44, 46).

Coarse-grained granodioritic gneiss. Incipient development of opthalmitic structure. Contains Qz (35%), Pl (40%), Bt (15%), Gt (10%). Some chloritisation of Bt.

SJ 512 (42, 50).

Medium to coarse-grained migmatised semi-pelite. Mu (15%) overgrows Bt selvedges to leucosomes (see Plate 3.1.M).

SJ 521 (43, 50).

Relatively unmigmatised Bt-rich medium to fine-grained psammite. Less than 5% laterally persistent (2-4 mm. wide) leucosomes.

SJ 530 (43, 47).

Migmatised semipelitic pod (few m. long and ca. 20 cm. across) within nebulitic migmatite. Leucosome makes up ca. 25% of the rock.

SJ 552 (45, 51).

Heavily migmatised semipelite with stromatic structure. Leucosome makes up ca. 30% of the rock. Small amounts of (heavily sericitised) probably anti-perthitic Pl in granodioritic leucosome.

SJ 953 (62, 61). Slussen, north-eastern Orust.

Mu-rich migmatised semi-pelite with stromatic structure. Mu overgrows and replaces Bt along selvedges between 0.5 cm. - 4 cm. wide coarse-grained granodioritic to adamellitic leucosomes and medium to fine-grained more Bt-rich palaeosome.

S 40 (47, 63).

Mu-rich strongly-foliated medium-grained grey psammitic gneiss. Approx. 10-15% of impersistent leucosome.

S41 (47, 63).

Coarse-grained pink cataclastic gneiss. Chl and Mu rich with local preservation of original stromatic migmatite structure.

S10 (46, 60).

Medium-grained grey Bt-rich psammite. Ca. 10-15% granodioritic leucosome.

GP 19 (41, 47).

Grey medium-grained psammitic gneiss. Less than 10% leucosome which is developed sporadically as impersistent blebs and bands (up to 5 mm. across) which grade into the post rock.

The Hälleviksstrand granite. Thirteen samples of nebulitic migmatite in which the degree of homogeneity varies considerably.

SJ 923 (43, 47).

Homogeneous coarse-grained nebulitic gneiss. Granodioritic composition: Qz (35%), Pl (35%+), micas (20%). Microcline encloses plag with development of myrmekite. Bt replaced by fine grained Mu, some of which is in turn surrounded by pyrite. Pl locally heavily sericitised and some replacement of Bt by Chl.

SJ 924 (43, 47).

Homogeneous nebulitic gneiss with 2-3 cm. wide Bt schlieren which persist for ca. 10-15 cm. Similar to 923.

SJ 925 (43, 46).

Inhomogeneous medium to coarse-grained nebulite containing small (less than 1 cm. across) xenoliths of psammite. Contains small amount of chloritised Gt and is cut by ca. 10% of pegmatitic leucosome, locally stictolithic (Bt flecks).

SJ 926 (43, 47).

Inhomogeneous nebulite similar to 925.

SJ 927 (43, 47).

Inhomogeneous nebulite with fine-grained psammitic xenoliths and similar development of stictolithic leucosome as 925. Contains Qz (40%), Pl (30%), Mu + Bt (25%) and Mi largely replacing Pl (5%). Bt chloritised and large (ca. 2-3%) amount of Sp present. Cataclastic texture developed around Pl porphyroblastics.

SJ 928 (43, 47).

Homogeneous Gt rich (5%) coarse-grained nebulite. Contains Qz (35%), Pl (25%), Bt (20%), Mu (10%), Mi (5%). Cut by large patches (several cm. across) of stictolithic leucosome. Locally mortar texture developed around Pl porphyroclasts.

SJ 929 (43, 47).

Homogeneous nebulite similar to 928. Smaller amounts of small (less than 1 cm.) blebs of leucosome.

SJ 930 (43, 47).

Similar to 928 but considerable proportion (ca. 30%) of fine-grained Mu, which replaces Pl and Bt.

SJ 948 (43, 47).

Homogeneous nebulite contains Qz (40%), Pl (35%), micas (25%) and Mi (ca. 2%). Euhedral Bt mantled by Qz and enclosed in Pl.

SJ 955 (43, 46).

Similar to 948, but in addition has a strong Mu fabric.

SB 148 (43, 46).

Coarse-grained homogeneous nebulite contains Qz (40%), Pl (35%), Bt (15%), Mu (10%) and small amount of tourmaline.

SBH 2 (43, 47).

Coarse-grained leucocratic homogeneous nebulite containing less than 15% micas, most of which is Bt. Small amount of Gt breaking down to Chl.

Older amphibolites (total of seven samples analysed).

SB 125 (41, 50).

Coarse-grained ultramafic amphibolite contains Hb (80%), Bt (6%), Qz (5%), Pl An 40 (less than 5%) and minor amounts of zoisite and Ap.

SB 133 (41, 51).

Medium to coarse-grained Bt-rich amphibolite contains Hb (55%), Pl ca. An 35-40 (20%), Qz (5%), Bt (20%). Large Hb poikiloblasts up to 0.5 cm. across.

SBH 17 (44, 47).

Medium-grained amphibolite pod in nebulitic migmatite. Hb, Bt, Pl, minor Qz.

SA2/1 (locality not known).

Sheared margin to older amphibolite body several m. across. Hb, Bt, Gt, Pl, Qz. Strong Bt fabric parallel to sheared and recrystallised Qz rich leucosomes.

SJ 532 (43, 47).

Small (1 m. across) pod in inhomogeneous nebulite.

Discordant pegmatitic leucosomes

GP 11 (41, 47).

Coarse-grained Pl-Mi-Qz rock cuts migmatic para-gneisses with small veinlets of zoisite and Mu. Mu also occurs as medium to coarse-grained aggregates up to 0.5 mm. across. Pl contains numerous small Mu inclusions. Mi contains fine-grained rounded Qz. Locally a cataclastic texture develops around the l ger Mi and Pl grains.

GP 26 (41, 47).

Similar to GP 11. In addition accessory Ep and Zr. Zoisite veinlets less common.

GP 12 (41, 47).

Coarse-grained trondhjemitic (Qz + Pl) rock with small amount of Mu.

SJ 582 (41, 47).

Similar to GP 26.

GP 13, Edshultshall

Mu rich alkali-granitic pegmatite. Small amount of chloritised Bt. Mu concentrated in narrow (1 mm.) wide stringers surrounding porphyroblastic Qz and Mi.

Appendix B2 Table 1 Basement complex gneisses.
Uncorrected X.R.F.S. data . Na_2O on pressed powder, L.O.I. at 1000 °C. SiO_2 to P_2O_5 on $LiBO_2$ glass

(wt. %)

	SiO_2	TiO_2	Al_2O_3	$Fe_2O_3^*$	MnO	MgO	CaO	K_2O	P_2O_5	L.O.I.	Na_2O
GP19	66.60	.49	18.46	3.60	.03	1.35	4.28	1.60	.14	.86	3.14
SB26	68.41	.66	16.31	5.79	.11	2.18	1.65	3.38	.07	1.74	1.17
SB82	76.05	.65	11.35	3.58	.05	1.38	1.33	3.31	.06	.83	2.23
SB90	69.50	.43	16.05	4.46	.09	1.73	1.09	3.15	.07	2.71	2.19
SB95	68.25	.84	15.86	5.75	.06	2.61	1.88	3.38	.10	1.22	2.67
SB118	78.26	.52	10.72	2.43	.02	.67	1.23	2.82	.09	.60	2.66
SB136	73.86	.58	12.65	3.97	.05	1.48	1.46	2.39	.07	.97	3.00
SBH31	71.26	.68	14.06	4.28	.04	1.65	.87	4.15	.09	1.16	1.98
SBH52	70.00	.45	14.74	5.21	.11	1.81	1.72	2.06	.10	1.29	3.54
SJ512	75.40	.64	13.49	4.01	.05	1.73	1.00	3.92	.13	1.31	1.54
SJ521	76.61	.51	11.84	5.15	.20	1.60	3.72	.98	.11	.32	1.66
SJ530	72.64	.29	14.95	4.08	.07	2.03	1.22	3.44	.07	1.36	2.60
SJ552	69.26	.67	15.27	4.81	.05	2.43	2.24	2.58	.07	.82	3.54
S40	69.75	.60	15.37	4.41	.06	1.64	1.75	2.42	.15	1.99	3.98
S41	72.44	.44	15.15	3.06	.04	1.45	1.26	2.60	.05	1.67	4.13
S10	70.18	.79	13.72	5.38	.08	1.13	1.90	4.84	.26	1.39	2.76

* = total iron as Fe_2O_3

Appendix B2 Table 2 Basement complex gneisses.
Normalised major element geochemical data. (Uncorrected X.R.F.S. data recalculated to 100%, including L.O.I. as a component).

(wt. %)	SiO_2	TiO_2	Al_2O_3	$Fe_2O_3^*$	MnO	MgO	CaO	Na_2O	K_2O	P_2O_5
GP19	66.22	.49	18.35	3.58	.03	1.34	4.25	3.14	1.59	.14
SB26	67.39	.65	16.07	5.70	.11	2.15	1.62	1.17	3.33	.07
SB82	75.40	.65	11.25	3.56	.05	1.37	1.32	2.23	3.29	.06
SB90	68.44	.43	15.81	4.39	.09	1.70	1.08	2.19	3.10	.06
SB95	66.44	.82	15.44	5.60	.06	2.54	1.83	2.67	3.29	.09
SB118	78.23	.52	10.72	2.43	.02	.67	1.22	2.66	2.83	.09
SB136	73.48	.58	12.59	3.95	.05	1.47	1.45	3.00	2.38	.07
SBH31	71.09	.68	14.03	4.27	.04	1.63	.87	1.98	4.14	.09
SBH52	69.25	.45	14.58	5.15	.11	1.79	1.70	3.54	2.04	.10
SJ512	73.00	.62	13.06	3.88	.04	1.67	.97	1.54	3,79	.12
SJ521	74.56	.50	11.52	5.01	.19	1.56	3.62	1.66	.95	.11
SJ530	70.62	.28	14.54	3.97	.06	1.97	1.19	2.60	3.35	.07
SJ552	68.03	.66	15.00	4.72	.05	2.39	2.20	3.54	2.53	.07
S40	68.22	.58	15.03	4.32	.06	1.60	1.71	3.98	2.36	.15
S41	70.72	.43	14.79	2.99	.04	1.41	1.23	4.13	2.54	.05
S10	68.44	.77	13.38	5.24	.08	1.10	1.85	2.76	4.72	.26

* = total iron as Fe_2O_3

Appendix B2 Table 3 Basement complex gneisses.
Trace element geochemical data.
(ppm.)

	Cr	Ga	Nb	Ni	Sc	Rb	Sr	Y	Zr
GP19	46	28	50	47	-	82	163	40	319
SB26	83	20	16	37	20	100	202	37	247
SB82	62	27	54	59	27	109	175	28	464
SB90	47	16	17	24	11	89	209	28	214
SB95	119	40	50	142	50	122	220	37	307
SB118	57	23	58	53	16	71	184	21	423
SB136	80	31	51	87	24	105	142	30	279
SBH31	64	40	55	78	25	139	150	21	345
SBH52	99	39	44	81	51	102	219	78	199
SJ512	117	16	25	37	12	149	119	36	241
SJ521	78	10	18	27	10	69	275	35	223
SJ552	121	20	19	42	10	124	263	40	239
SJ953	65	12	29	20	7	164	129	40	261
S40	-	33	-	-	-	124	175	43	264
S41	-	30	-	-	-	127	142	36	160
S10	28	33	-	-	-	182	146	67	464

- = not determined

Appendix B2 Table 4 Nebulitic migmatites (the Hälleviksstrand granite)
Uncorrected X.R.F.S. data. Na_2O on pressed powders, L.O.I. at
1000 °C. SiO_2 to P_2O_5 on $LiBO_2$ glass.

(wt. %)

	SiO_2	TiO_2	Al_2O_3	$Fe_2O_3^*$	MnO	MgO	CaO	K_2O	P_2O_5	L.O.I.	Na_2O
SJ923	72.98	.70	13.78	4.66	.05	1.94	1.44	3.15	.09	1.03	2.82
SJ924	71.08	.83	13.98	5.44	.07	2.41	1.14	3.66	.08	1.48	1.95
SJ925	70.50	.70	14.57	5.55	.11	3.18	1.18	3.85	.08	1.41	2.12
SJ926	76.39	.59	11.62	3.46	.08	2.42	.69	4.09	.08	.82	1.82
SJ927	75.62	.46	13.38	3.71	.06	1.42	1.42	2.27	.09	1.49	2.85
SJ928	72.48	.61	13.92	4.78	.12	1.67	2.28	2.05	.08	.80	3.51
SJ929	79.01	.39	11.87	3.44	.05	1.75	.77	2.83	.08	1.42	1.73
SJ930	68.74	.62	16.14	5.50	.07	1.98	.94	4.67	.09	1.57	2.17
SJ955	69.07	.92	14.46	5.44	.05	2.65	1.26	3.80	.07	1.38	2.07
SJ955	74.66	.31	14.46	3.80	.18	1.36	1.06	3.78	.10	1.15	2.41
SB148	66.15	1.49	14.60	7.73	.08	2.57	1.44	3.44	.12	1.23	2.65
SBH2	74.05	.19	14.04	1.39	.03	.52	.77	4.73	.09	1.00	3.42
SJ531	75.68	.48	13.57	3.26	.05	1.52	1.22	3.20	.08	1.14	2.84

* = total iron as Fe_2O_3

Appendix B2 Table 5 Nebulitic migmatites.

Normalised major element geochemical data.(Uncorrected X.R.F.S. data recalculated to 100%, including L.O.I. as a component).

(wt. %)

	SiO_2	TiO_2	Al_2O_3	$Fe_2O_3^*$	MnO	MgO	CaO	Na_2O	K_2O	P_2O_5
SJ923	71.05	.69	13.41	4.53	.05	1.89	1.40	2.82	3.06	.08
SJ924	69.56	.81	13.68	5.33	.07	2.36	1.11	1.95	3.58	.08
SJ925	68.20	.68	14.10	5.37	.10	3.07	1.14	2.12	3.73	.08
SJ926	74.83	.57	11.38	3.38	.08	2.37	.68	1.82	4.01	.07
SJ927	73.49	.45	13.00	3.60	.06	1.38	1.38	2.85	2.21	.09
SJ928	70.78	.59	13.60	4.67	.12	1.63	2.22	3.51	2.00	.08
SJ929	76.38	.38	11.47	3.33	.05	1.69	.75	1.73	2.74	.08
SJ930	67.01	.60	15.73	5.36	.07	1.94	.92	2.17	4.55	.09
SJ948	68.25	.90	14.29	5.38	.05	2.62	1.24	2.07	3.76	.07
SJ955	72.21	.30	13.99	3.68	.13	1.32	1.02	2.41	3.66	.09
SB148	65.14	1.47	14.38	7.61	.08	2.53	1.41	2.65	3.39	11
SBH2	73.87	.19	14.02	1.39	.03	.52	.76	3.42	4.72	.09
SJ531	73.35	.46	13.16	3.16	.05	1.48	1.18	2.84	3.11	.07

* = total iron as Fe_2O_3

Appendix B2 Table 6 Nebulitic migmatites.
Trace element geochemical data.(the Hällevikstrand granite)
(ppm.)

	Cr	Ga	Nb	Ni	Sc	Rb	Sr	Y	Zr
SJ923	93	16	22	83	14	130	167	38	285
SJ924	113	18	22	38	13	152	125	35	322
SJ925	103	16	17	40	22	152	148	58	326
SJ926	70	12	18	22	11	117	136	37	334
SJ927	83	13	14	51	13	88	184	39	380
SJ928	141	15	18	35	21	111	215	64	435
SJ929	80	10	12	22	8	86	128	35	395
SJ930	83	20	19	29	13	184	138	51	288
SJ948	133	21	24	41	12	164	136	30	288
SJ955	81	11	11	26	27	103	155	63	310
SB148	163	25	44	47	27	251	114	41	354
SBH2	28	29	-	54	13	117	149	39	144
SJ531	67	15	20	23	10	115	186	39	238

- = not determined

Appendix B2 Table 7 Older amphibolites.

Uncorrected X.R.F.S. data. Na_2O on pressed powder, L.O.I. at 1000 °C. SiO_2 to P_2O_5 on $LiBO_2$ glass.

(wt. %)

	SiO_2	TiO_2	Al_2O_3	$Fe_2O_3^*$	MnO	MgO	CaO	K_2O	P_2O_5	L.O.I.	Na_2O
SB125	49.66	.43	15.82	9.47	.17	8.45	10.01	2.23	.05	1.06	1.15
SB133	54.28	.62	16.16	10.31	.16	7.52	7.50	1.78	.08	1.69	2.09
SBH17	51.51	.82	14.88	11.63	.20	8.33	10.23	1.35	.11	1.05	.93
SA2/1	58.76	1.66	13.53	13.31	.31	4.84	4.90	3.48	.11	1.33	.24
SJ528	49.48	.81	16.23	10.89	.18	7.68	12.75	.39	.06	.63	2.38
SJ532	49.96	.49	17.30	8.43	.14	10.78	12.33	.61	.05	1.04	1.20
S24	47.42	2.08	14.45	15.86	.26	7.03	8.12	.78	.27	1.37	2.57

* = total iron as Fe_2O_3

Appendix B2 Table 8 Older amphibolites.
Normalised major element data. (Uncorrected X.R.F.S. data recalculated to 100%, including L.O.I. as a component).
(wt. %)

	SiO_2	TiO_2	Al_2O_3	Fe_2O_3*	MnO	MgO	CaO	Na_2O	K_2O	P_2O_5
SB125	50.44	.44	16.06	9.62	.17	8.58	10.17	1.15	2.27	.05
SB133	53.08	.60	15.80	10.08	.15	7.35	7.35	2.09	1.74	.07
SBH17	50.99	.80	14.73	11.50	.20	8.24	10.12	.93	1.34	.11
SA2/1	57.32	1.62	13.20	12.98	.30	4.73	4.78	.24	3.40	.11
SJ528	48.74	.80	15.98	10.73	.18	7.56	12.56	2.38	.39	.06
SJ532	48.80	.47	16.90	8.23	.13	10.53	12.04	1.20	.59	.05
S24	47.32	2.07	14.42	15.83	.25	7.02	8.10	2.57	.78	.27

Appendix D2 Table 9 Older amphibolites.
Trace element geochemical data.
(ppm.)

	Cr	Ga	Nb	Ni	Sc	Rb	Sr	Y	Zr
SB125	69	15	BDL	18	43	92	167	21	33
SB133	69	-	7	27	47	87	136	19	55
SBH17	361	-	8	120	54	84	123	25	50
SA2/1	12	17	13	59	32	127	195	52	341
SJ528	274	13	BDL	100	50	9	131	18	33
SJ532	463	15	BDL	73	37	28	115	17	45
S24	156	22	BDL	58	49	45	134	35	147

* = total iron as Fe_2O_3, - = not determined, BDL = below detection limit

APPENDIX B2, TABLE 10
UNCORRECTED X.R.F.S.DATA FOR PEGMATITIC LEUCOSOMES
NA2O ON PRESSED POWDER, L.O.I. AT 1000 DEG C
SIO2 TO P2O5 ON LIBO2 GLASS

SAMPLE	SIO2	TIO2	AL2O3	FE2O3	MNO	MGO	CAO	K2O	P2O5	L.O.I.	NA2O
GP11	74.36	.09	16.24	.16	.01	.47	1.14	5.07	.08	.72	4.30
GP13	77.87	.27	14.16	1.63	.02	.73	.59	4.69	.09	.94	3.49
GP26	70.14	.09	17.12	.10	.00	.26	.65	8.40	.12	.77	2.85
SJ582	71.74	.06	16.95	.12	.01	.30	1.06	7.61	.07	.49	3.02
SJ522	74.42	.08	15.29	.30	.01	.45	1.32	5.24	.13	.90	3.48
GP12	77.49	.10	14.73	.22	.00	.30	1.74	1.21	.05	.62	5.13
SJ562	83.52	.05	11.30	.38	.01	1.06	2.54	.65	.02	.46	3.22

Appendix B_2 Table 11 Discordant pegmatitic leucosomes.
Normalised major element geochemical data. (Uncorrected X.R.F.S. data recalculated to 100%, including L.O.I. as a component). *= total iron as Fe_2O_3
(wt. %)

	SiO_2	TiO_2	Al_2O_3	$Fe_2O_3^*$	MnO	MgO	CaO	Na_2O	K_2O	P_2O_5
GP11	72.37	.09	15.80	.15	.01	.45	1.10	4.30	4.93	.08
GP13	74.38	.26	13.53	1.56	.02	.70	.56	3.49	4.48	.09
GP26	69.78	.09	17.03	.09	BDL	.26	.65	2.85	8.36	.12
SJ582	70.68	.06	16.70	.12	.01	.30	1.04	3.02	7.50	.07
SJ522	73.19	.07	15.04	.29	.01	.44	1.30	3.48	5.16	.13
GP12	76.21	.10	14.48	.22	BDL	.29	1.71	5.13	1.19	.05
SJ562	80.83	.04	10.94	.37	.01	1.03	2.46	3.22	.63	.02

Appendix B2 Table 12 Discordant pegmatitic leucosomes.
Trace element geochemical data.
(ppm.)

	Cr	Ga	Nb	Ni	Sc	Rb	Sr	Y	Zr
GP11	23	10	10	BDL	BDL	106	148	22	27
GP12	34	8	14	22	BDL	157	99	39	167
GP26	16	11	9	20	-	121	276	31	BDL
SJ582	-	10	BDL	-	-	45	207	20	113
SJ522	-	12	8	-	-	128	189	15	36
GP12	29	9	10	17	BDL	22	261	BDL	12
SJ562	-	6	13	-	BDL	49	306	3	18

- = not determined, BDL = below detection limit (ca. .002 for MnO)

Appendix B

Additional isotopic data on the basement complex and the Källviken augen granite (936). Errors as for Table 3.4.

	$^{87}Sr/^{86}Sr$	Rb/Sr	$^{87}Rb/^{86}Sr$
951	0.76720 ± 3	1.004	2.902
952	0.82280 ± 7	1.854	5.43
953	0.78665 ± 6	1.380	4.03
936	0.79070 ± 4	1.391	4.06

Assuming a minimum age of ca. 1350-1450 m.y. (age range of the Hälleviksstrand amphibolite and the Assmunderöd-Myckleby augen granite) the mean $^{87}Sr/^{86}Sr$ ratio at ca. 1060 m.y. (the syn-D3 metamorphism, see Section 5.4) may be calculated at close to 0.72 - 0.73. This is similar to a value (0.72) obtained from the Hällevikstrand granite data, assuming the same age constraints.

APPENDIX C

Appendix C1 (see Appendix B for abbreviations).

Sample descriptions:- pre-dyke intrusive rocks.

Hälleviksstrand amphibolite. Six samples from west coast of Crust, south of Hälleviksstrand. Grid square (PK 44, 44). All samples collected from western arm of the intrusion. 908-910 and 949 collected from outcrop making use of joint surfaces. 911 and 912 collected from blasted face of boatyard (Fig. 4.13).

SJ 908.

Med. to coarse-grained (generally 2 mm. but Hb up to 1 cm.) mesocratic amphibolite, grey-green. Syn-D2 mineral fabric defined by Hb-Bt. Hb (ca. 40%), Qz + Pl (45%), Bt (10%); accessory Ep (s.l.), opaque ore 1-2 mm. veinlets of Qz + Pl + Ep (s.l.) removed together with adjacent 3 cm. of amphibolite.

SJ 909

Med. grained, some poikiloblastic Hb up to 0.5 cm. which contain rounded inclusions of Qz, opaque ore and Ep. Hb overgrows Bt. No veins present. Darker than 908 with Hb (ca. 50%).

SJ 910

Med. to coarse grained (mean grain size 3 mm.) green amphibolite. Hb lineation and alignment of Bt (5%). Hb (60%), Qz + Pl (35%). Pl mildly sericitised. Veinlets of Qz + Pl and minor Py, removed with ca. 2 cm. of the marginal amphibolite.

SJ 911

Inhomogeneous medium to fine-grained Ep-amphibolite. Locally patches of to 3 cm. across consist of Ep, Qz and Minor Bt. Elsewhere normal amphibolite similar in composition to 909. In addition to small veinlets of Qz + Pl + Ep this sample contained

a small (2 cm. x 3 mm.) folded bleb of trondhjemitic leucosome. This and the smaller unfolded veinlets removed together with ca. 3 cm. margin of amphibolite.

SJ 912

Similar to SJ 908 but significant alteration of Pl to Ep and Bt to Chl. No veinlets. Mild sericitisation of Pl.

SJ 949

Hornblendite with polygonal texture and less than 5% of sericitised Pl, Cc and Chl occurring interstitially. Hb overgrows opaque ores. Small veinlets of Qz, Pl and Ep removed with the 2 cm. margin of amphibolite.

Assmunderöd-Myckleby augen granite. Eleven samples, of which eight (numbers starting SJ 9) were collected for geochronology. All samples collected from blasted (roadside) exposures.

SJ 940, Assmunderöd body, (62, 61).

Strongly foliated pink to grey augen granite, augen less than 0.5 cm. across, local developments of Bt schlieren a few cm. wide, up to 50 cm. in length. Augen composition adamellitic containing Qz (35%), mildly sericitised Pl (25%), Mi (some of which replaces Pl, 35%) and green Bt (10%). Small amounts of allanite, sphene, zircon and apatite.

SJ 941, Assmunderöd body, (62, 61).

Similar to 940, augen less than 1 cm., strong foliation. Contains small patch (2 cm. x 5 cm. x 0.5 cm.) of second generation leucosome with diffuse margins which is locally discordant to the biotite foliation. This leucocratic patch was incorporated in crushing ca. 8 Kg. of the sample.

SJ 942, Assmunderöd body, (60, 59).
Similar to 940 but more strongly foliated. Some sericitised Pl grains have clear rims of Ab. Locally, sericitisation is heavy and small amounts of Mu overgrow the Bt fabric.

SJ 943, Assmunderöd body, (60, 58).
Similar to 942. In addition to small amounts of Mu there is some chloritisation of Bt.

SJ 944, Assmunderöd body, (61, 58).
Fluorite-bearing grey augen granite. Augen up to 1 cm. across, strongly foliated. Augen composition alkali granite with Mi making up just over two-thirds of total feldspar. Fluorite interstitial to Qz and feldspars. Some chloritisation of Bt.

SJ 945, Myckleby body, (62, 57).
Very coarse-grained augen granite, much less strongly flattened than the above. Augen up to 1 cm. across, approx. 50% are Mi with cataclastic margins and abundant myrmekite developed in contact with Pl. Mi augen have sericitised (sometimes myrmekitised) Pl inclusions. Small amount Gt with inclusions of Sp and Qz occurs with Bt in the matrix.

SJ 946, Myckleby body (63, 56).
Strongly lineated pink augen granite with numerous xenoliths lineated parallel to fabric. Augen less than 0.5 cm. across but up to 5 cm. along the lineation. Many are Mi-cored with cataclastic margins of Qz-Mi-Pl. Small amount of skeletal Bt present. Large amounts of Sp in patches associated with Bt. Accessory Mu.

SJ 954, Myckleby body (63, 56).

Strongly foliated pink augen granite with mortar texture. Xenolith of fine-grained semi-pelite (Qz-Pl-Bt-Mi) and the surrounding 2-3 cm. margin of augen granite removed from this sample before crushing. Glomeroblastic or glomeroclastic augen is centred on large Mi (up to 1 cm. across). Granoblastic Pl (heavily sericitised), Mi and Qz surround the Mi core and an outer cataclastic zone contains fine-grained Qz, myrmekite, Mi and Pl.

SJ 639, Myckleby body (59, 50).

Weakly-foliated grey Gt-bearing augen granite. Augen generally ca. 1 cm. but up to ca. 3 cm. across.

SJ 649, Myckleby body (60, 48).

Strongly foliated garnet-bearing grey augen granite. Contains small (few cm. long, less than one cm. across) biotite schlieren. Augen up to 2 cm. across.

SJ 662, west of Varekil (56, 46).

Coarse-grained Hb-bearing adamellite. Foliation defined by planar arrangement of Hb and locally by lepidoblastic Bt. This rock grades into Bt-bearing augen granite. Contains Qz (ca. 30%), Mi (ca. 25%), Pl (ca. 20%), Hb (15%) and Bt (5%). Significant amounts of Ep associated with Hb. Accessory Sp, Zr and allanite.

The younger granites. Twenty three samples, twenty two of which were collected in western Orust in the area mapped by Park et al. (op. cit.). One sample (SJ 572) was collected in eastern Orust. Samples prefixed "SJ" were collected by the author of which fourteen with numbers beginning "SJ 9" were collected for geochronology. These samples weighed between 5 Kg. and 10 Kg. Multiple samples were obtained from three granite sheets: Southern Härmanö (2 m. wide, three samples), Tåkeskärn (4 m. wide, four samples) and Roparen (3 m. wide, four samples). An attempt was made to sample the sheets systematically to assess the geochemical and isotopic variation in terms of position in the sheet but was not successful. The younger granites are best exposed on smooth erosion surfaces in low-lying coastal areas, and samples could only be obtained by exploiting intersecting joints. One sample only (916) was obtained within 0.5 m. of a sheet margin. The rest were close to the sheet centres. Samples prefixed "GP" were collected by R. G. Park in western Orust. Samples other than SJ 572 are located on Fig. 4.1.

SJ 902, South Härmanö (39, 46).
Coarse-grained, locally pegmatitic, 2 m. wide leucogranite dyke, cut by 1 - 2 m. wide basic dyke (see SJ 904, Appendix D. Mu-adamellite, cataclastic texture. Mildly sericitised Pl (An 25) in fine-grained Qz-Pl matrix. Cataclasis is post-D3 Mu fabric. V. little Bt present.

SJ 905-907, Southern Härmanö (39, 47).
Medium to coarse-grained 1 m. to 2m. wide sill with 10 cm. to 20 cm. wide central pegmatitic portion. Cuts (and contains stoped xenoliths of) "porphyritic augen granite" dyke (see Park et al. op. cit. for description and Appendix B for isotopic data). No sign of assimilation of xenoliths. Bt - granodiorite with granular texture locally modified by weak Bt (S3) foliation, locally overgrown by Mu. SJ 906 is coarse-grained and has heaviest sericitisation of Pl.

SJ 913-916, Tåkeskärn (41, 45).

Coarse-grained 4 m. wide dyke of Bt - Mu granodiorite. Inequigranular. Porphyroblasts of Pl in a granular matrix of Qz and feldspar. Locally heavy sericitisation of Pl. Mi replaces Pl and in SJ 915 a 2 cm. long Mi megacryst, with marginal cataclasis, overgrows a weak (S3) mica foliation. This megacryst was removed from sample together with ca. 1 Kg. of surrounding rock, before crushing. Resulting sample weighed ca. 6 Kg.

SJ 917-920, Roparen (40, 47).

Medium-grained granodiorite sheet (3 m. wide) cuts F2 folds in gneisses. Mu and sericite replace Pl, some of which is zoned and possibly igneous (see Plate 4.3.M) and forms nuclei to growth of unzoned porphyroblastic Pl.

SJ 956 (41, 52) small island off north coast of Harmano.

Medium-grained granodiorite dyke (ca. 1 m. wide) cuts F2 folds and itself crenulated by D4. Weak foliation defined by micas and elongated Qz grains. Small amount (less than 1%) of inclusion-free garnet present. Considerable cataclasis, Mi and Pl porphyroclasts in a mortar texture.

SJ 957, (42, 50) blasted roadside exposure.

Medium-grained granodiorite dyke containing Qz (30%), mildly to heavily sericitised Pl An 25 (50%), Mi (largely replacing Pl, ca. 10%), Bt and minor Mu (together ca. 10%). Weak foliation defined by micas. Incipient chloritisation of Bt. Accessory Ap.

GP 2, (38, 47).

Medium to coarse-grained granodiorite. Heavily sericitised Pl porphyroblasts up to 5 mm. across with inclusions of Mu, Qu

and Bt. Bt heavily chloritised resulting in preservation of weak (S3) Bt foliation. Several 0.5 mm. Qz-Ep (s.l.) veins present.

GP 3, (38, 47).

Medium-grained tonalite contains Qz (25%), Pl An 22 (45%), Bt (20%) and small amounts of Gt, Ep (s.l.), opaque ore and sphene. Garnet has a euhedral habit but is typically corroded with three faces preserved and the remainder of the grain in skeletal intergrowth with Qz and Pl. See Plate 4.1.M.

GP 5, (41, 47).

Medium to coarse-grained leucocratic adamellite containing Qz (30%), Pl An 20 (25%), Mi (27%) and Mu (18%). Small amount of anhedral Gt (with Qz inclusions) and accessory zircon and apatite. S3 Mu fabric and narrow (2 mm.) parallel zones of cataclasis. Qz and feldspar inequigranular. Both Mi and Pl occur as porphyroblasts up to 5 mm. across, which locally form augen in the S3 Mu fabric. See Plate 4.2.M.

GP 7, (41, 47).

Medium-grained Mu-granodiorite. Heavy sericitisation of Pl. Bt absent.

GP 8, (38, 47).

Medium to coarse-grained granodiorite contains Qz (30%), mildly sericitised Pl (45%), Mi (10%), Bt and minor Mu (ca. 15%). Inequigranular. Porphyroblasts of Pl sometimes as augen in strong Bt fabric. Accessory Sp.

GP 9, (38, 47).

Medium-grained leucocratic adamellite. Mu and minor Bt define strong S3 fabric. Narrow (few mm. wide) zones of cataclasis parallel to fabric (similar to GP 5).

GP 17, (39, 47).

Medium to fine-grained granodiorite with Bt ca. 20% defining a strong fabric. Small amount of Mu, Ep, Ap.

SJ 572, (59, 58) nr. Torp in northeastern Orust.

Grey colour-banded (3 m. wide) dyke. Gt-bearing adamellite. Strong foliation defined by small amount of Mu present (ca. 5%) and parallel zones of partially recrystallised ribbon quartz - the latter apparently responsible for the colour banding.

SJ 589, (41, 47).

Coarse-grained Bt-granodiorite from a ca. 3 m. wide dyke, ca. 50% of which is pegmatitic.

Appendix C2 Table 1 Hälleviksstrand amphibolite.
Uncorrected X.R.F.S. data . Na_2O on pressed powder, L.O.I. at 1000 °C. SiO_2 to P_2O_5 on $LiBO_2$ glass.

(wt. %)

	SiO_2	TiO_2	Al_2O_3	$Fe_2O_3^*$	MnO	MgO	CaO	K_2O	P_2O_5	L.O.I.	Na_2O
SJ908	55.77	.92	16.50	8.05	.12	4.29	5.97	2.11	.30	.82	3.07
SJ909	50.62	1.71	16.96	10.97	.15	5.24	7.78	2.46	.74	.97	2.23
SJ910	54.89	.78	11.57	9.79	.17	10.72	8.65	1.27	.21	1.02	1.38
SJ911	53.00	1.19	17.34	9.30	.12	5.27	6.74	2.88	.29	.96	3.01
SJ912	51.90	1.25	16.38	9.13	.13	7.48	8.38	2.23	.19	1.04	2.89
SJ949	47.53	1.40	9.56	13.33	.19	13.97	11.96	.53	.11	1.00	.74

* = total iron as Fe_2O_3

Appendix C2 Table 2 Hällevikssstrand amphibolite.

Normalised major element geochemical data. (Uncorrected X.R.F.S. data recalculated to 100%, including L.O.I. as a component

(wt. %)	SiO_2	TiO_2	Al_2O_3	$Fe_2O_3^*$	MnO	MgO	CaO	Na_2	K_2O	P_2O_5
SJ908	57.00	.94	16.86	8.23	.13	4.38	6.11	3.07	2.16	.30
SJ909	50.71	1.72	16.99	10.99	.15	5.25	7.79	2.23	2.46	.74
SJ910	54.63	.78	11.52	9.74	.17	10.67	8.61	1.38	1.27	.21
SJ911	52.95	1.18	17.32	9.29	.12	5.27	6.74	3.01	2.88	.29
SJ912	51.36	1.24	16.21	9.04	.12	7.40	8.30	2.89	2.21	.18
SJ949	47.38	1.38	9.53	13.29	.19	13.92	11.92	.74	.52	.11

Appendix C2 Table 3 Hallevikssstrand amphibolite.

Trace element geochemical data.

(ppm.)	Cr	Ga	Nb	Ni	Sc	Rb	Sr	Y	Zr
SJ908	96	18	15	56	17	67	710	37	207
SJ909	146	22	18	71	29	114	679	49	392
SJ910	612	15	BDL	238	35	47	317	30	76
SJ911	127	20	10	87	20	97	820	14	148
SJ912	199	18	BDL	140	31	73	712	18	83
SJ949	670	18	9	258	76	17	120	29	75

* = total iron as Fe_2O_3, BDL = below detection limit

Appendix C2.

Table 3 (continued). Geochemical data for the Hällevikstrand amphibolite.

14 REE analyses, obtained on a commercial basis from the Universities Research Reactor, Risley. The analytical technique (radiochemical group separation and thermal-neutron activation) is a modification of the method of Graber et al. (1970). Data (*) of Abbey (1975) for BCR-1 is given for comparison. Errors are reported at one sigma level.

	SJ 910	SJ 949	BCR-1	BCR-1*
La	20.6 ± 0.7	17.9 ± 0.6	27.4 ± 0.9	25
Ce	78 ± 3	68 ± 3	54.9 ± 6.2	54
Pr	8.5 ± 0.9	9.2 ± 0.8	6.3 ± 0.8	
Nd	38.2 ± 2.1	31.6 ± 1.1	28.4 ± 1.8	29
Sm	7.2 ± 1.0	7.5 ± 0.3	6.5 ± 0.5	6.6
Eu	2.21 ± 0.07	2.14 ± 0.06	2.08 ± 0.07	1.9
Gd	10.5 ± 1.3	6.7 ± 0.8	8.4 ± 0.8	6.6
Tb	1.07 ± 0.10	0.96 ± 0.07	1.02 ± 0.05	1.0
Dy	6.5 ± 1.1	7.1 ± 1.2	5.9 ± 1.0	6.3
Ho	0.87 ± 0.08	0.94 ± 0.16	1.19 ± 0.14	
Er	4.2 ± 0.6	3.7 ± 0.5	4.1 ± 0.5	3.6
Tm	0.80 ± 0.16	0.64 ± 0.10	0.88 ± 0.12	0.6
Yb	2.9 ± 0.3	2.8 ± 0.2	3.6 ± 0.3	3.8
Lu	0.46 ± 0.03	0.46 ± 0.03	0.52 ± 0.03	0.55

APPENDIX C2, TABLE 4
UNCORRECTED X.R.F.S. DATA FOR THE ASSMUNDERÖD-MYCKLEBY AUGEN GRANITE
NA2O ON PRESSED POWDER, L.O.I. AT 1000 DEG C
SIO2 TO P2O5 ON LIBO2 GLASS

SAMPLE	SIO2	TIO2	AL2O3	FE2O3	MNO	MGO	CAO	K2O	P2O5	L.O.I.	NA2O
SJ940	74.15	.41	13.52	3.33	.05	.48	1.19	5.22	.11	.50	2.97
SJ941	69.66	.72	14.08	6.00	.09	.88	1.89	4.83	.22	.63	2.74
SJ942	69.76	.72	14.12	5.93	.09	.86	2.04	4.75	.22	.57	2.68
SJ943	70.79	.51	13.60	4.22	.06	.65	1.53	4.77	.17	.59	2.72
SJ944	75.32	.33	12.58	2.69	.04	1.01	1.29	5.34	.10	1.25	2.56
SJ945	68.54	.67	13.49	5.03	.06	.97	1.92	4.81	.20	.51	2.68
SJ946	68.57	.72	13.49	5.43	.08	.96	1.80	4.52	.21	.90	2.61
SJ954	70.25	.70	13.96	5.17	.07	1.29	1.93	4.74	.20	.84	2.69
SJ639	70.96	.67	13.91	5.14	.07	1.06	1.78	4.85	.19	.66	2.55
SJ649	70.18	.76	13.93	5.49	.07	1.21	1.98	4.89	.21	.54	2.66
SJ662	71.71	.47	13.96	4.22	.06	.52	1.69	5.29	.10	.48	2.99

Appendix C2 Table 5 Assmunderöd-Myckleby augen granite.
Normalised major element geochemical data. Uncorrected X.R.F.S. data recalculated to 100%, including L.O.I. as a component).

(wt. %)	SiO_2	TiO_2	Al_2O_3	$Fe_2O_3^*$	MnO	MgO	CaO	Na_2O	K_2O	P_2O_5
SJ940	72.69	.40	13.26	3.27	.05	.47	1.17	2.97	5.12	.11
SJ941	68.40	.71	13.85	5.90	.09	.86	1.86	2.74	4.75	.21
SJ942	68.53	.70	13.87	5.83	.09	.85	2.00	2.68	4.67	.21
SJ943	71.08	.52	13.66	4.23	.06	.65	1.54	2.72	4.79	.17
SJ944	73.41	.32	12.26	2.62	.03	.99	1.26	2.56	5.21	.09
SJ945	69.35	.67	13.64	5.09	.06	.98	1.95	2.68	4.86	.20
SJ946	69.08	.72	13.59	5.47	.08	.97	1.81	2.61	4.56	.21
SJ954	68.94	.68	13.70	5.07	.07	1.27	1.89	2.69	4.65	.20
SJ639	69.64	.66	13.65	5.05	.07	1.04	1.75	2.55	4.76	.18
SJ649	68.82	.75	13.66	5.38	.07	1.19	1.94	2.66	4.79	.20
SJ662	70.62	.46	13.75	4.16	.06	.52	1.66	2.99	5.21	.10

* = total iron as Fe_2O_3

Appendix C2 Table 6 Assmunderöd-Myckleby augen granite.
Trace element geochemical data.

(ppm.)

	Cr	Ga	Nb	Ni	Sc	Rb	Sr	Y	Zr
SJ940	27	19	21	21	7	195	106	80	317
SJ941	30	24	25	28	13	190	167	74	451
SJ942	29	23	28	31	13	181	146	75	475
SJ943	36	19	26	33	10	232	105	66	304
SJ944	31	16	23	19	5	223	75	65	232
SJ945	50	19	27	18	11	194	120	67	361
SJ946	51	19	29	19	12	174	124	67	366
SJ954	53	20	27	17	-	177	133	66	354
SJ639	53	20	30	17	-	184	124	67	360
SJ649	50	20	32	18	-	189	124	68	384
SJ662	45	21	37	15	-	253	80	101	445

- = not determined

Appendix C2.

Table 6 (continued). Geochemical data for the Assmunderöd-Myckleby augen granite. 14 REE analyses, for explanation see Table 3 . Quoted errors are one sigma.

	SJ 944
La	55.7 ± 2.4
Ce	123 ± 3
Pr	15.0 ± 1.0
Nd	61.1 ± 1.7
Sm	10.4 ± 0.5
Eu	1.35 ± 0.07
Gd	9.6 ± 0.8
Tb	1.5 ± 0.1
Dy	9.2 ± 0.3
Ho	1.9 ± 0.2
Er	6.0 ± 0.4
Tm	0.76 ± 0.10
Yb	4.1 ± 0.1
Lu	0.61 ± 0.03

APPENDIX C2, TABLE 7
UNCORRECTED X.R.F.S. DATA FOR THE YOUNGER GRANITES
NA2O ON PRESSED POWDER, L.O.I. AT 1000 DEG C
SIO2 TO P2O5 ON LIBO2 GLASS

SAMPLE	SIO2	TIO2	AL2O3	FE2O3	MNO	MGO	CAO	K2O	P2O5	L.O.I.	NA2O
GP2	73.07	.34	16.03	2.29	.03	.78	2.67	1.29	.12	.72	5.23
GP3	58.84	1.10	19.02	5.99	.07	2.22	5.30	2.15	.44	.34	4.39
GP5	73.87	.07	14.64	.35	.03	.31	.67	4.60	.13	.65	4.08
GP7	74.98	.11	14.83	.70	.02	.39	2.14	1.91	.11	.76	4.40
GP8	66.27	.49	18.17	3.65	.03	1.37	4.27	1.52	.14	.55	4.66
GP9	75.45	.16	14.18	1.14	.03	.39	1.40	3.03	.06	.48	4.21
GP17	72.52	.32	15.47	2.33	.04	.96	2.46	2.14	.07	.75	4.39
SJ902	74.90	.08	15.09	.45	.02	.26	.64	3.47	.16	.72	4.63
SJ905	71.66	.33	16.23	2.39	.04	.99	2.77	2.67	.11	.47	4.31
SJ906	70.05	.34	15.84	2.40	.04	.94	2.72	2.60	.10	.45	4.46
SJ907	70.79	.33	15.90	2.59	.03	1.02	2.85	1.51	.07	.62	5.16
SJ913	71.52	.30	15.41	2.40	.04	1.04	2.25	2.06	.06	.44	5.08
SJ914	71.61	.26	15.73	1.99	.03	.85	2.55	1.97	.09	.47	4.53
SJ915	71.10	.33	16.21	2.67	.05	1.08	2.81	1.81	.11	.40	5.20
SJ916	71.07	.24	15.37	2.04	.04	.70	2.51	1.32	.06	.38	5.62
SJ917	67.99	.46	16.49	3.07	.04	1.09	3.12	1.86	.06	.52	4.96
SJ918	68.83	.41	16.35	2.75	.03	1.05	3.08	1.67	.06	.61	5.11
SJ919	68.88	.46	16.73	3.08	.04	1.12	3.17	2.13	.15	.55	4.91
SJ920	68.61	.49	15.81	3.23	.04	1.41	3.49	1.92	.14	.54	4.70
SJ956	73.93	.17	14.77	1.18	.02	.49	1.45	2.98	.06	.67	4.47
SJ957	62.32	.29	12.94	2.17	.04	.68	2.05	1.89	.10	.61	4.84
SJ572	74.17	.13	14.87	1.11	.03	.41	1.55	3.03	.09	.75	4.04
SJ589	70.32	.30	17.20	2.10	.04	.81	3.27	1.52	.10	.91	5.46

Appendix C2 Table 8 younger granites.

Normalised major element geochemical data. (Uncorrected X.R.F.S. data recalculated to 100% , including L.O.I. as a component.

(wt. %)	SiO_2	TiO_2	Al_2O_3	$Fe_2O_3^*$	MnO	MgO	CaO	Na_2O	K_2O	P_2O_5
GP2	71.12	.33	15.60	2.23	.03	.76	2.60	5.23	1.26	.11
GP3	58.93	1.10	19.05	6.00	.07	2.22	5.31	4.39	2.15	.44
GP5	74.35	.07	14.73	.35	.03	.31	.67	4.08	4.63	.13
GP7	74.70	.11	14.78	.69	.02	.39	2.13	4.40	1.90	.11
GP8	65.50	.48	17.95	3.60	.03	1.36	4.22	4.66	1.50	.14
GP9	75.04	.16	14.10	1.13	.03	.39	1.40	4.21	3.01	.06
GP17	71.42	.32	15.24	2.30	.03	.95	2.42	4.39	2.11	.07
SJ902	74.57	.08	15.03	.45	.01	.26	.63	4.63	3.46	.16
SJ905	70.21	.32	15.90	2.34	.04	.97	2.71	4.31	2.61	.11
SJ906	70.10	.34	15.85	2.41	.04	.94	2.72	4.46	2.60	.10
SJ907	70.14	.33	15.75	2.56	.03	1.01	2.83	5.16	1.50	.07
SJ913	71.08	.29	15.32	2.38	.04	1.03	2.24	5.08	2.05	.05
SJ914	71.55	.26	15.72	1.99	.03	.84	2.55	4.53	1.97	.09
SJ915	69.79	.33	15.91	2.62	.05	1.06	2.76	5.20	1.77	.11
SJ916	71.57	.24	15.47	2.06	.04	.71	2.52	5.62	1.33	.06

* = total iron as Fe_2O_3

Appendix C2 Table 8 (continued).

(wt. %)

	SiO_2	TiO_2	Al_2O_3	Fe_2O_3*	MnO	MgO	CaO	Na_2O	K_2O	P_2O_5
SJ917	68.25	.46	16.55	3.08	.04	1.09	3.13	4.96	1.87	.06
SJ918	68.87	.41	16.36	2.75	.03	1.05	3.09	5.11	1.67	.06
SJ919	68.00	.46	16.52	3.04	.04	1.11	3.13	4.91	2.10	.15
SJ920	67.63	.49	16.57	3.18	.04	1.39	3.44	4.70	1.89	.14
SJ956	73.78	.16	14.74	1.18	.02	.49	1.45	4.47	2.97	.06
SJ957	71.44	.33	14.84	2.48	.04	.78	2.35	4.84	2.16	.11
SJ572	74.03	.13	14.84	1.10	.03	.41	1.55	4.04	3.02	.09
SJ589	68.85	.29	16.84	2.06	.03	.79	3.20	5.46	1.48	.09

* = total iron as Fe_2O_3

Appendix C2 Table 9 younger granites.
Trace element geochemical data.
(ppm.)

	Cr	Ga	Nb	Ni	Sc	Rb	Sr	Y	Zr
GP2	33	-	-	-	-	53	302	11	171
GP3	49	26	15	20	13	84	530	17	400
GP5	28	13	13	15	BDL	107	55	27	19
GP7	30	21	20	20	5	42	237	12	52
GP8	34	27	13	24	11	60	427	9	208
GP9	31	20	15	21	BDL	149	166	12	462
GP17	33	22	16	21	6	64	279	16	163
SJ902	31	18	22	27	BDL	169	20	24	13
SJ905	-	21	12	-	5	87	262	19	154
SJ906	32	19	12	21	5	91	254	22	155
SJ907	-	18	11	-	6	84	245	22	150
SJ913	-	19	15	-	6	73	208	17	156
SJ914	-	17	9	-	BDL	61	265	13	111
SJ915	34	21	10	28	5	65	294	15	136
SJ916	-	18	11	-	BDL	53	223	16	113

- = not determined, BDL = below detection limit

Appendix C2 Table 9 (continued).

(ppm.)

	Cr	Ga	Nb	Ni	Sc	Rb	Sr	Y	Zr
SJ917	33	20	10	21	9	59	427	28	203
SJ918	34	19	13	24	8	54	420	21	197
SJ919	34	20	7	22	6	66	437	15	209
SJ920	39	22	11	23	7	62	445	15	165
SJ956	-	15	10	-	BDL	69	206	19	98
SJ957	-	16	13	-	6	61	294	17	204
SJ572	-	14	14	-	5	85	293	17	68
SJ589	-	17	12	-	5	68	356	12	145

- = not determined, BDL = below detection limit.

APPENDIX C2 TABLE 10 PEARSON CORRELATION COEFFICIENTS FOR THE YOUNGER GRANITES

	SIO2	TIO2	AL2O3	FE2O3	MNO	MGO	CAO	NA2O	K2O	P2O5	CR	GA	NB	NI	SC	RB	SR	Y	ZR
SIO2	1.0																		
TIO2	-.96	1.0																	
AL2O3	-.96	.88	1.0																
FE2O3	-.97	.97	.88	1.0															
MNO	-.75	.80	.61	.81	1.0														
MGO	-.97	.96	.89	.98	.79	1.0													
CAO	-.95	.90	.92	.94	.70	.93	1.0												
NA2O	-.22	.12	.23	.23	.12	.18	.30	1.0											
K2O	.46	-.40	-.45	-.53	-.26	-.48	-.67	-.73	1.0										
P2O5	-.68	.75	.66	.61	.57	.62	.53	-.24	.08	1.0									
CR	-.39	.44	.39	.35	.23	.38	.31	-.18	.03	.48	1.0								
GA	-.47	.43	.47	.45	.34	.51	.47	-.17	-.10	.31	.26	1.0							
NB	.20	-.17	-.16	-.25	-.24	-.19	-.26	-.40	.38	.14	.07	.54	1.0						
NI	-.24	.24	.27	.18	.08	.23	.16	-.19	.12	.29	.88	.52	.34	1.0					
SC	-.81	.79	.78	.80	.57	.81	.79	-.02	-.33	.51	.34	.77	.24	.38	1.0				
RB	.32	-.26	-.30	-.36	-.26	-.35	-.51	-.41	.69	.13	.11	.03	.46	.23	-.23	1.0			
SR	-.83	.81	.80	.84	.60	.81	.90	.23	-.62	.39	.33	.35	-.34	.19	.74	-.59	1.0		
Y	.11	-.09	-.14	-.15	-.03	-.13	-.31	-.14	.51	-.05	.02	-.04	.18	.12	-.02	.33	-.29	1.0	
ZR	-.50	.62	.38	.60	.55	.53	.51	-.04	-.22	.35	.35	.32	-.11	.21	.50	.11	.48	-.29	1.0

APPENDIX D

Appendix D1 (see Appendix B for abbreviations).

Sample descriptions:- The dyke suite.

Seventy-one samples from thirty-nine dykes were analysed, of which 58 are from mafic to ultramafic dykes. The remainder (13) are from intermediate to acidic dykes. The majority of samples are from western Orust. Samples prefixed "RCS", "SB" and "GP" were collected by R. C. Standley, A. I. Bailey and R. G. Park. Samples prefixed "SJ" were collected by the author.

Mafic to ultramafic dykes (n = 58).

SJ 603-606, Henån dyke (57, 58).

Coarse-grained Bt-rich amphibolite, with strong S3 fabric. Contains large (2-3 cm.) Gt with oriented inclusions of Qz, Sp and opaque ores. At margins Gt overgrows the Bt fabric. Samples in order 603-606 represent adjacent 4 cm. wide blocks to within 1 cm. of dyke edge.

607-614 and 627. Svineviken dyke (1.5-2 m. wide). (53, 59).

Medium to coarse-grained amphibolite dyke with S3 Bt fabric. Hb-Bt-Gt-Pl-Qz present. Gt has numerous inclusions of Sp. Accessory opaque ore. Dyke strikes E. - W. and outcrops on blasted face (10 m. in extent) in Boatyard (on western side). Samples disposed within the dyke as follows:-

607 Reference point (A) at lower edge

608 Upper edge, 8 m. N. of A.

609 Close to 608

610 Below 608, 609, 8 cm. below upper edge

611 7 m. N. of A, 15 cm. - 20 cm. below upper edge

612 below 611

613 7.5 m. N. of A, 5 cm. above lower edge

614 7.75 m. N. of A, at dyke centre

627 5 m. N. of A at dyke centre.

615-618, 630. Lavö dyke (2 m. wide) (42, 50). Dyke strikes E. - W. at right angles to blasted roadside face.
Medium to coarse-grained. Similar to Svineviken dyke.
Gt. less common. Pl composition is An 30. Samples disposed within the dyke as follows:-

615 20 cm. from contact, N. side
616 dyke centre
617 dyke centre
618 30 cm. from contact, N. edge
630 dyke centre

631-638 Härmanö dyke (30 m. wide) (38, 47).
Coarse-grained amphibolite contains Hb (ca. 60%), Pl (ca. 35% together with small amount of Qz), Bt and opaque ores. Randomly oriented Hb with bimodal grain size distribution. Larger Hb porphyroblasts (up to 5 mm. long) some of which are twinned, have inclusions of rounded Qz and less commonly, opaque ores. Patches (several cm. across) of fine-grained Hb with minor Qz and Pl interstitially define a relict ophitic texture with large (up to 4 cm. long) relict Pl phenocrysts. The latter are recrystallised to fine-grained aggregates of Pl, Hb and Qz. Commonly decussate texture is defined by prisms of Hb which overgrow the Pl phenocrysts. Skeletal grains of ilmenite (up to 1 cm. in length) are intergrown with fine-grained Hb.
Dyke strikes ca. N. - S. and samples are disposed as follows. Reference point (B) is at summit of hill (above 25 m. contour) at ca. (387, 472)

631 2 m. from eastern edge, 50 m. S. of B.
632 6 m. from eastern edge, 4 m. S. of B.
633 9 m. from western edge, 50 m. N. of B.
634 nr. centre, 10 m. N. of B.

635 3 m. from western edge, 15 m. S.W. of B.

636 close to 635

637 4 m. from western edge, 150 m. N. of B (across fault).

638 4 m. from eastern edge, 35 m. N. of B.

SJ 904 (39, 46).

Fine-grained amphibolite dyke (few m. wide) cuts younger granite sheet from which sample SJ 902 was obtained. Relict igneous texture defined by randomly-oriented partially recrystallised Pl laths.

SB 20 (40, 51).

Coarse-grained amphibolite contains Hb (70%), Pl (15%), Qz (5%), Bt, opaque ore and small amounts of Gt. Bt heavily chloritised.

SB 41 (40, 51).

Coarse-grained amphibolite with locally developed polygonal texture of Hb, Pl, Bt (minor) and Gt (minor) Gt and Bt in textural equilibrium. Hb has rounded solid inclusions of opaque ore rimmed by Sp.

RCS 2 (39, 47).

Fine-grained garnet-amphibolite with syn-D3 Bt fabric. Gt grains aligned parallel to foliation. Some Bt chloritised.

RCS 3 (39, 47).

Relict ophitic texture in coarse-grained amphibolite. Hb up to 0.5 cm. long, with numerous round Qz inclusions.

RCS 7 (38, 46).

Flattened ilmenite (?) grains rimmed by Sp, parallel to Bt fabric in coarse-grained amphibolite.

RCS 9 (38, 46).

Large (up to 1 cm. long) sericitised Pl phenocrysts in fine-grained matrix of Hb, Pl, Qz. V. little Bt present and largely replaced by Chl.

RCS 10 (38, 46).

Coarse-grained amphibolite. Hb-Bt-Sp-opaque ores (ilmenite). Ilmenites have Sp rims and are also almost totally replaced by Sp.

RCS 15 (40, 50).

Coarse-grained Hb-Gt-Qz rock. Hb long axes aligned parallel to foliation. V. little Bt present. Gt porphyroblasts heavily chloritised.

RCS 17 (39, 49).

Flattened ilmenite grains have Sp rims. See Plate 5.4.M. Similar to RCS 7.

RCS 19

Relict ophitic texture in Hb-Bt-Sp amphibolite, defined by areas (1 cm. across) of recrystallised Pl, Qz and minor Hb set in foliated Hb-Bt matrix. Sp makes up ca. 5-10% of the mode.

Intermediate to acidic dykes (n = 13).

SJ 619-626, Islandsberg dyke (5 m. to 8 m. wide)

Medium to fine-grained Qz-Pl-Mi-Gt-Hb rock with a strong biotite fabric in which poikiloblastic garnets are enclosed (see Plate 5.6.M). Proportion of Hb varies from ca. 10% (in most samples) to ca. 15% in SJ 625. Dyke runs N. - S. and the samples are disposed as follows (relative to E. - W. fault):

SJ 619 1.5 m. from western edge, 110 m. N. of fault.

SJ 620 2 m. from western edge, near 619.

SJ 621 1 m. from western edge, 5 m. N. of fault.

SJ 622 1 m. from western edge, 30 m. S. of fault.

SJ 623 2 m. from western edge, 210 m. N. of fault.

SJ 624 3 m. from eastern edge, near 621.

SJ 625 2 m. from eastern edge, 70 m. N. of fault.

SJ 626 2 m. from eastern edge, 35 m. N. of fault.

APPENDIX D2, TABLE 1
UNCORRECTED X.R.F.S. DATA FOR THE DYKE SUITE
NA2O ON PRESSED POWDER, L.O.I. AT 1000 DEG C
SIO2 TO P2O5 ON LIBO2 GLASS

SAMPLE	SIO2	TIO2	AL2O3	FE2O3	MNO	MGO	CAO	K2O	P2O5	L.O.I.	NA2O
GP16	47.93	.78	16.81	11.20	.18	8.73	10.47	1.60	.07	1.81	1.74
SJ904	49.45	2.12	14.29	14.25	.21	6.14	8.61	2.17	.81	1.25	.92
SB20	47.30	2.57	14.83	15.72	.24	6.68	9.29	1.22	.40	1.32	1.83
SB41	45.39	2.74	14.12	18.20	.25	5.90	10.10	1.59	.30	.81	1.06
SJ585	47.89	2.22	14.34	15.32	.21	6.34	8.76	2.53	.36	.93	1.75
SJ603	44.75	3.55	14.06	16.89	.23	6.39	9.60	2.68	.58	1.32	.64
SJ604	46.11	3.57	13.57	16.74	.25	6.00	9.64	2.41	.60	1.64	.55
SJ605	45.76	3.58	13.77	17.02	.27	5.96	9.32	2.56	.57	1.40	.57
SJ606	45.79	3.44	13.99	16.40	.23	6.14	9.55	2.60	.57	1.61	.60
SJ607	46.71	2.52	14.12	16.12	.22	6.50	9.98	1.62	.39	.83	1.18
SJ608	47.08	2.74	13.75	16.55	.23	6.27	10.13	1.64	.43	.87	.96
SJ609	46.81	2.78	13.77	16.72	.23	6.15	10.19	1.63	.42	.92	1.02
SJ610	46.56	2.75	13.91	16.63	.23	6.25	9.78	1.82	.42	.92	1.00
SJ611	46.81	2.72	13.93	16.19	.23	6.65	9.93	1.59	.42	.89	1.23
SJ612	46.99	2.56	14.14	16.26	.22	7.07	9.83	1.62	.40	.92	1.27
SJ613	46.86	2.68	14.19	16.56	.23	6.65	10.15	1.36	.41	1.18	1.19
SJ614	47.32	2.55	14.23	16.32	.22	6.81	10.22	1.37	.39	.92	1.33
SJ627	47.48	2.67	13.93	16.58	.23	6.72	9.85	1.56	.41	.70	1.18
SJ615	46.41	2.55	13.91	15.81	.22	6.86	10.39	1.73	.41	.86	1.20
SJ616	46.84	2.61	14.09	16.17	.24	6.66	10.48	1.82	.41	.82	1.14
SJ617	46.88	2.57	14.11	16.06	.22	6.93	10.11	1.99	.40	.85	1.13
SJ618	46.48	2.63	14.07	16.31	.24	6.60	10.45	1.60	.41	1.00	1.18
SJ630	46.47	2.50	14.27	15.89	.22	7.10	10.15	2.07	.39	.79	.93
SJ631	47.71	.82	17.04	11.70	.18	9.22	11.17	.24	.07	1.44	1.89
SJ632	48.46	1.16	16.60	12.23	.18	8.31	10.37	.45	.23	.95	2.04
SJ633	48.32	1.18	15.81	12.91	.19	9.30	9.88	.63	.19	1.78	1.82
SJ634	48.93	1.12	16.63	12.03	.18	8.70	10.36	.44	.21	1.11	1.97
SJ635	49.31	1.50	15.59	13.63	.20	7.67	10.12	.40	.30	1.04	1.68
SJ636	49.28	1.45	15.61	13.29	.20	7.83	10.25	.33	.29	.83	1.87
SJ637	48.15	.86	17.53	11.11	.17	8.77	11.18	.27	.12	.94	2.11
SJ638	49.14	1.05	15.85	11.70	.18	9.33	10.56	.30	.11	1.17	1.78

APPENDIX D2, TABLE 1 (CONTINUED)
UNCORRECTED X.R.F.S. DATA FOR THE DYKE SUITE
NA2O ON PRESSED POWDER, L.O.I. AT 1000 DEG C
SIO2 TO P2O5 ON LIBO2 GLASS

SAMPLE	SIO2	TIO2	AL2O3	FE2O3	MNO	MGO	CAO	K2O	P2O5	L.O.I.	NA2O
SJ641	47.49	2.05	14.67	15.07	.21	6.86	9.84	1.58	.26	1.06	1.32
SJ642	47.40	2.14	14.55	15.28	.22	6.67	10.01	1.42	.27	.96	1.37
SJ643	46.55	1.91	14.93	14.50	.20	7.10	9.81	.93	.23	.85	1.85
RCS0	48.98	.54	15.90	10.46	.17	9.64	11.70	.62	.05	.75	1.64
RCS1	47.21	2.72	13.92	16.58	.23	6.42	9.90	1.30	.43	.88	.94
RCS2	47.20	2.79	13.80	16.80	.26	6.16	9.78	1.69	.44	1.41	.60
RCS3	46.95	2.48	14.51	15.91	.22	5.98	9.63	.79	.83	.62	2.00
RCS4	52.78	1.46	14.93	11.93	.17	5.31	8.99	1.52	.46	.67	2.06
RCS6	47.67	.80	16.92	11.38	.17	8.46	10.86	.58	.07	1.06	2.00
RCS7	48.38	2.60	14.26	15.54	.21	5.83	9.22	1.22	.96	.92	1.35
RCS8	48.08	2.44	14.34	15.87	.21	6.08	8.99	1.54	.39	1.10	1.36
RCS9	48.14	.91	16.33	12.59	.18	8.46	9.69	.78	.12	1.56	2.32
RCS10	48.37	2.48	14.09	15.82	.20	5.86	8.66	2.16	.39	.95	1.24
RCS11	48.74	2.46	14.32	15.83	.20	5.86	7.34	3.26	.38	2.23	.87
RCS13	46.79	2.76	13.87	16.64	.23	6.58	9.53	2.76	.43	.96	.48
RCS14	46.96	2.76	13.80	16.71	.23	6.55	9.76	1.51	.43	1.23	.95
RCS15	48.52	2.65	13.62	16.31	.22	6.99	9.84	.93	.42	.96	.83
RCS16	46.83	2.61	13.92	16.47	.22	7.08	9.78	1.17	.40	.95	1.41
RCS17	46.65	2.68	14.20	16.75	.23	6.83	9.82	.80	.38	1.03	1.37
RCS19	47.94	2.29	14.57	15.47	.21	6.35	8.99	2.30	.36	1.06	1.52
RCS21	47.58	.94	17.41	12.26	.19	8.72	9.22	2.87	.09	2.08	.87
RCS23	48.63	2.38	14.74	14.27	.23	6.33	10.71	1.25	.35	.67	1.13
RCS24	47.11	.79	17.15	11.84	.18	10.13	10.86	.55	.07	1.26	1.53
RCS25	47.99	.82	17.70	11.33	.17	9.12	11.05	.42	.07	2.56	1.28
RCS27	47.81	2.33	14.79	15.83	.22	6.81	8.30	1.17	.60	1.52	1.70
RCS28	46.71	2.60	14.53	15.99	.21	6.22	8.88	.95	.90	.85	2.72
RCS29	51.38	2.22	15.55	14.07	.19	4.59	8.25	1.56	.56	.49	1.84
RCS20	66.37	.95	13.59	11.16	.19	.92	2.00	3.21	.33	.54	2.58
RCS22	68.67	.55	13.69	8.15	.11	.45	1.42	4.42	.15	.40	2.80
RCS30	72.49	.52	13.47	5.20	.08	.56	1.91	4.81	.13	.53	2.62
SJ506	68.53	.55	13.34	8.10	.11	.31	2.67	4.41	.14	1.21	2.72
SJ588	69.45	.54	13.31	7.83	.10	.44	2.83	4.11	.15	.88	2.42
SJ619	64.17	.99	13.35	11.72	.16	.59	4.06	2.89	.37	.74	1.96
SJ620	63.33	1.04	13.34	11.86	.16	.80	4.36	3.19	.40	.34	2.10
SJ621	65.25	.91	13.35	11.43	.15	.63	4.02	3.38	.33	.58	1.74
SJ622	63.41	1.03	13.23	11.80	.16	.56	4.38	3.20	.40	.32	2.10
SJ623	63.75	1.05	13.34	11.78	.16	.58	4.34	3.12	.42	.33	1.95
SJ624	63.55	.97	13.20	11.66	.15	.38	4.05	3.39	.36	.26	2.14
SJ625	62.93	1.08	13.30	11.94	.16	.70	4.45	3.27	.42	.48	2.07
SJ626	64.15	.97	13.23	11.48	.15	.54	4.12	3.38	.35	1.07	1.95

Appendix D2 Table 2 Basic dykes.

Normalised major element geochemical data. (Uncorrected X.R.F.S. data recalculated to 100%, including L.O.I. as a component)

(wt. %)

	SiO_2	TiO_2	Al_2C_3	$Fe_2O_3^*$	MnO	MgO	CaO	Na_2O	K_2O	P_2O_5
GP16	47.29	.77	16.58	11.05	.17	8.61	10.33	1.74	1.57	.07
SJ904	49.34	2.12	14.26	14.22	.21	6.12	8.59	.92	2.16	.81
SB20	46.63	2.53	14.62	15.50	.23	6.59	9.16	1.83	1.21	.39
SB41	45.18	2.72	14.06	18.11	.25	5.87	10.05	1.06	1.58	.30
SJ585	47.57	2.21	14.25	15.22	.21	6.30	8.70	1.75	2.51	.35
SJ603	44.45	3.52	13.96	16.78	.23	6.34	9.54	.64	2.66	.57
SJ604	45.60	3.53	13.43	16.56	.25	5.93	9.53	.55	2.38	.57
SJ605	45.40	3.55	13.66	16.88	.27	5.92	9.25	.57	2.54	.57
SJ606	45.37	3.41	13.86	16.25	.22	6.09	9.46	.60	2.57	.57
SJ607	46.63	2.51	14.09	16.09	.22	6.49	9.96	1.18	1.62	.39
SJ608	46.77	2.72	13.66	16.44	.22	6.33	10.06	.96	1.63	.42
SJ609	46.51	2.76	13.68	16.62	.22	6.11	10.13	1.02	1.62	.42
SJ610	46.43	2.74	13.87	16.58	.23	6.23	9.76	1.00	1.83	.42
SJ611	46.53	2.71	13.84	16.10	.23	6.61	9.87	1.23	1.58	.42
SJ612	46.39	2.53	13.96	16.05	.22	6.98	9.70	1.27	1.60	.39
SJ613	46.18	2.64	13.98	16.32	.23	6.55	10.00	1.19	1.34	.40
SJ614	46.52	2.51	13.99	16.05	.21	6.69	10.05	1.33	1.34	.39
SJ627	46.86	2.64	13.74	16.36	.2	6.63	9.72	1.18	1.54	.41

* = total iron as Fe_2O_3

Appendix D2 Table 2 (continued)

(wt. %)

	SiO_2	TiO_2	Al_2O_3	$Fe_2O_3^*$	MnO	MgO	CaO	Na_2O	K_2O	P_2O_5
SJ615	46.25	2.54	13.86	15.55	.22	6.83	10.35	1.20	1.72	.41
SJ616	46.24	2.57	13.91	15.96	.24	6.57	10.35	1.14	1.79	.40
SJ617	46.30	2.54	13.94	15.86	.21	6.84	9.99	1.13	1.97	.39
SJ618	46.03	2.61	13.93	16.15	.24	6.53	10.35	1.18	1.58	.41
SJ630	46.10	2.48	14.15	15.77	.22	7.05	10.07	.93	2.05	.39
SJ631	46.99	.81	16.79	11.52	.17	9.08	11.00	1.89	.24	.07
SJ632	47.98	1.14	16.44	12.11	.18	8.23	10.27	2.04	.44	.22
SJ633	47.33	1.15	15.48	12.65	.19	9.11	9.68	1.82	.63	.19
SJ634	48.10	1.10	16.35	11.83	.18	8.55	10.18	1.97	.43	.21
SJ635	48.60	1.48	15.36	13.43	.19	7.56	9.97	1.68	.39	.30
SJ636	48.67	1.43	15.42	13.12	.19	7.73	10.12	1.87	.32	.29
SJ637	47.56	.85	17.32	10.98	.17	8.66	11.04	2.11	.26	.12
SJ638	48.5	1.04	15.66	11.56	.17	9.22	10.44	.30	.30	.11
SJ641	47.29	2.04	14.61	15.00	.21	6.84	9.80	1.32	1.58	.26
SJ642	47.26	2.13	14.50	15.24	.22	6.65	9.98	1.37	1.41	.27
SJ643	47.11	1.93	15.11	14.67	.21	7.18	99.93	1.85	.94	.24
RCS0	48.76	.54	15.83	10.41	.17	9.59	11.64	1.64	.61	.05
RCS1	46.96	2;70	13.85	16.49	.23	6.38	9.85	.94	1.29	.42
RCS2	46.76	2.76	13.67	16.64	.26	6.10	9.69	.60	1.67	.44
RCS3	47.00	3.48	14.52	15.92	.22	5.99	9.63	2.00	.79	.83
RCS4	52.63	1.45	14.89	11.89	.17	5.30	8.96	2.06	1.51	.46

* = total iron as Fe_2O_3

Appendix D2 Table 2 (continued)

(wt. %)

	SiO_2	TiO_2	Al_2O_3	$Fe_2O_3^*$	MnO	MgO	CaO	Na_2O	K_2O	P_2O_5
RCS6	47.69	.80	16.93	11.38	.17	8.46	10.86	2.00	.58	.07
RCS7	48.14	2.59	14.19	15.46	.21	5.80	9.17	1.35	1.22	.95
RCS8	47.89	2.43	14.28	15.80	.21	6.05	8.96	1.36	1.53	.38
RCS9	47.61	.89	16.15	12.45	.18	8.36	9.59	2.32	.78	.12
RCS10	48.26	2.47	14.05	15.79	.20	5.85	8.64	1.24	2.15	.39
RCS11	48.00	2.42	14.11	15.59	.20	5.77	7.23	.87	3.21	.37
RCS13	46.31	2.73	13.73	16.47	.23	6.51	9.43	.48	2.73	.42
RCS14	46.54	2.74	13.68	16.56	.23	6.49	9.67	.95	1.49	.42
RCS15	47.89	2.61	13.44	16.10	.22	6.90	9.71	.83	.92	.41
RCS16	46.43	2.59	13.80	16.33	.22	7.02	9.70	1.41	1.16	.40
RCS17	46.31	2.66	14.09	16.63	23	6.78	9.74	1.37	.79	.38
RCS19	47.42	2.27	14.42	15.30	.21	6.28	8.89	1.52	2.28	.35
RCS21	46.52	.92	17.02	11.99	.18	8.52	9.01	.87	2.80	.08
RCS23	48.30	2.36	14.63	14.17	.23	6.28	10.64	1.13	1.24	.34
RCS24	46.41	.78	16.90	11.66	.18	9.97	10.70	1.53	.54	.,6
RCS25	46.77	.80	17.25	11.04	.16	8.89	10.77	1.28	.41	.06
RCS27	47.28	2.30	14.62	15.65	.22	6.74	8.21	1.70	1.16	.60
RCS28	46.44	2.58	14.45	15.90	.21	6.19	8.83	2.72	.94	.89
RCS29	51.01	2.21	15.44	13.96	.19	4.56	8.19	1.84	1.56	.56

* = total iron as Fe_2O_3

Appendix D2 Table 2 (continued) Intermediate and acidic dykes.

(wt. %)

	SiO_2	TiO_2	Al_2O_3	$Fe_2O_3^*$	MnO	MgO	CaO	Na_2O	K_2O	P_2O_5
RCS20	65.13	.93	13.33	10.95	.19	.90	1.96	2.58	3.15	.32
RCS22	68.10	.54	13.58	8.08	.11	.45	1.41	2.80	4.38	.15
RCS30	70.80	.51	13.15	5.08	.07	.55	1.86	2.62	4.72	.13
SJ506	67.08	.54	13.06	7.93	.10	.30	2.61	2.72	4.31	.14
SJ588	68.01	.53	13.03	7.67	.10	.43	2.77	2.42	4.02	.15
SJ619	63.52	.98	13.22	11.60	.16	.58	4.02	1.96	2.86	.37
SJ620	62.74	1.03	13.21	11.75	.16	.79	4.32	2.10	3.16	.40
SJ621	64.09	.90	13.11	11.23	.15	.63	3.95	1.74	3.32	.32
SJ622	63.03	1.02	13.15	11.73	.16	.56	4.35	2.10	3.18	.40
SJ623	63.23	1.04	13.23	11.68	.16	.58	4.31	1.95	3.09	.41
SJ624	63.48	.97	13.18	11.64	.15	.38	4.05	2.14	3.38	.36
SJ625	62.44	1.07	13.19	11.85	.16	.69	4.41	2.07	3.24	.42
SJ626	63.25	.96	13.05	11.32	.15	.53	4.06	1.95	3.33	.35

* = total iron as Fe_2O_3

Appendix D2 Table 3 Basic dykes.
Trace element geochemical data.
(ppm.)

	Cr	Ga	Nb	Ni	Sc	Rb	Sr	Y	Zr
GP16	133	-	-	146	43	71	193	15	35
SJ904	-	-	12	-	39	73	247	53	282
SB20	122	-	15	63	48	33	242	41	202
SB41	114	-	12	88	65	.46	106	36	129
SJ585	143	-	14	75	46	84	158	38	205
SJ603	185	27	21	58	50	109	67	54	308
SJ604	167	27	14	49	51	99	57	55	327
SJ605	177	22	16	52	50	106	60	53	316
SJ606	184	25	18	59	46	108	74	52	305
SJ607	170	24	12	56	48	49	166	40	203
SJ608	166	27	17	48	52	50	101	47	224
SJ609	161	25	13	46	52	50	102	46	229
SJ610	136	28	13	39	51	60	113	46	224
SJ611	162	27	16	51	51	52	136	46	317
SJ612	169	27	14	54	49	53	162	43	207
SJ613	164	27	13	52	52	45	130	42	211
SJ614	167	26	16	56	49	44	171	42	197
SJ627	171	26	10	51	51	50	147	44	207

- = not determined

Appendix D2 Table 3 (continued), BDL = below detection limit
- = not determined

(ppm.)

	Cr	Ga	Nb	Ni	Sc	Rb	Sr	Y	Zr
SJ615	159	28	16	54	52	57	120	42	209
SJ616	160	26	13	54	51	59	122	43	214
SJ617	164	24	14	55	49	72	117	40	206
SJ618	150	26	17	52	51	50	128	42	213
SJ630	147	24	10	58	48	71	120	41	202
SJ631	152	18	BDL	114	38	5	151	17	34
SJ632	134	17	7	111	37	13	157	25	101
SJ633	148	16	BDL	122	40	26	138	25	84
SJ634	127	15	BDL	113	36	13	159	25	92
SJ635	145	18	8	88	44	10	144	34	133
SJ636	146	19	8	95	43	6	164	32	125
SJ637	149	17	BDL	110	36	5	174	17	51
SJ638	164	16	7	130	40	8	141	17	55
SJ641	187	23	BDL	60	47	44	120	35	138
SJ642	191	22	7	54	50	39	130	35	143
SJ643	194	21	7	68	46	25	209	29	125
RCS0	319	-	-	44	-	14	136	16	22
RCS1	144	-	8	41	-	34	121	54	178
RCS2	151	-	10	32	-	49	122	54	188
RCS3	126	-	13	48	32	27	294	58	216
RCS4	125	-	11	366	24	50	239	55	168

Appendix D2 Table 3 (continued)

(ppm.)

	Cr	Ga	Nb	Ni	Sc	Rb	Sr	Y	Zr
RCS6	152	-	BDL	122	37	19	157	18	46
RCS7	125	-	11	57	29	45	202	64	274
RCS8	140	-	7	51	36	70	161	43	170
RCS9	152	-	-	120	37	24	256	19	57
RCS10	131	-	8	50	37	78	152	46	189
RCS11	132	-	BDL	50	34	146	119	40	119
RCS13	140	-	7	40	41	108	88	44	186
RCS14	143	-	8	42	42	39	154	46	177
RCS15	142	-	11	42	39	26	92	48	165
RCS16	171	-	11	42	43	34	216	42	165
RCS17	157	-	10	60	53	21	206	45	205
RCS19	140	-	10	75	47	70	142	36	206
RCS21	148	-	-	129	35	107	206	26	51
RCS23	162	-	11	57	49	25	106	41	204
RCS24	214	-	-	145	43	24	121	19	35
RCS25	195	-	-	131	34	24	162	18	36
RCS27	153	-	10	78	43	53	177	43	227
RCS28	145	-	17	93	39	34	307	48	306
RCS29	103	-	16	41	38	43	230	42	263

- = not determined, BDL = below detection limit

Appendix D2 Table 3 (continued) Intermediate and acidic dykes.

(ppm.)

	Cr	Ga	Nb	Ni	Sc	Rb	Sr	Y	Zr
RCS20	47	-	50	BDL	27	104	150	128	1388
RCS22	43	-	42	BDL	14	92	149	90	964
RCS30	48	-	24	BDL	11	157	107	68	506
SJ506	47	-	53	BDL	17	103	150	109	913
SJ588	43	-	54	BDL	18	125	160	112	921
SJ619	47	23	49	BDL	27	107	198	115	1221
SJ620	48	21	45	16	27	112	213	113	1150
SJ621	51	22	54	BDL	22	84	207	118	1268
SJ622	47	22	48	BDL	27	104	216	113	1166
SJ623	47	23	44	BDL	28	107	209	110	1146
SJ624	477	23	47	BDL	26	86	207	116	1240
SJ625	47	25	49	BDL	27	91	218	107	1138
SJ626	46	25	46	BDL	24	91	214	119	1211

- = not determined, BDL = below detection limit

APPENDIX D2 PEARSON CORRELATION COEFFICIENTS FOR THE MAFIC AND ULTRAMAFIC DYKES

	SIO2	TIO2	AL2O3	FE2O3	MNO	MGO	CAO	NA2O	K2O	P2O5	CR	GA	NB	NI	SC	RB	SR	Y	ZR
SIO2	1.0																		
TIO2	-.47	1.0																	
AL2O3	.32	-.92	1.0																
FE2O3	-.52	.95	-.93	1.0															
MNO	-.56	.90	-.85	.91	1.0														
MGO	-.01	-.82	.78	-.78	-.67	1.0													
CAO	-.20	-.41	.38	-.39	-.23	.63	1.0												
NA2O	.47	-.64	.60	-.59	-.63	.39	.12	1.0											
K2O	-.28	.62	-.57	.55	.50	-.60	-.58	-.69	1.0										
P2O5	-.06	.72	-.66	.64	.56	-.77	-.55	-.22	.37	1.0									
CR	-.28	-.13	.11	-.14	-.08	.40	.51	-.04	-.17	-.41	1.0								
GA	-.40	.28	-.26	.24	.25	-.02	.32	-.24	.09	-.01	.25	1.0							
NB	-.28	.82	-.73	.73	.67	-.73	-.28	-.31	.41	.71	-.20	.42	1.0						
NI	-.02	-.74	.83	-.70	-.65	.78	.35	.52	-.49	-.64	.15	-.13	-.61	1.0					
SC	-.42	.34	-.25	.37	.31	-.19	-.02	-.13	.21	.07	-.12	.49	.41	.03	1.0				
RB	-.30	.54	-.45	.45	.39	-.49	-.60	-.64	.96	.33	-.14	.07	.31	-.35	.18	1.0			
SR	.43	-.34	.31	-.28	-.37	.02	-.25	.70	-.34	.18	-.35	-.47	-.14	.14	-.21	-.35	1.0		
Y	-.13	.87	-.84	.80	.73	-.87	-.52	-.50	.52	.89	-.31	.08	.74	-.80	.05	.44	-.07	1.0	
ZR	-.24	.90	-.80	.79	.74	-.85	-.54	-.44	.59	.88	-.27	.25	.87	-.71	.29	.53	-.13	.89	1.0

Appendix D2 Table 5 dyke suite

Major element geochemical data , TiO_2 photometrically, Na_2O and K_2O by F.E.S. , others by A.A.S.

SAMPLE	SIO2	TIO2	AL203	FE203	MNO	MGO	CAO	NA2O	K2O
SJ609	47.40	2.79	12.75	17.20	.26	5.76	9.85	1.32	1.62
SJ610	48.07	2.73	13.27	17.18	.24	5.84	9.35	1.32	1.62
SJ611	48.59	2.74	13.60	17.08	.24	5.68	9.85	1.36	1.47
SJ612	49.93	2.58	13.72	16.54	.25	5.73	9.40	1.41	1.47
SJ613	47.05	2.69	14.28	16.73	.27	5.93	9.69	1.35	1.26
SJ614	48.04	2.57	14.63	16.54	.26	6.39	9.71	1.47	1.31
SJ615	47.29	2.63	13.68	16.47	.26	5.85	9.87	1.34	1.50
SJ616	48.20	2.64	14.02	16.35	.27	5.90	10.08	1.34	1.64
SJ617	46.60	2.61	13.68	16.22	.22	6.20	9.63	1.29	1.75
SJ618	47.85	2.74	14.17	16.49	.24	5.73	9.87	1.41	1.45
SJ630	45.55	2.54	14.30	16.11	.23	6.33	9.63	1.26	1.85
SJ631	47.66	.82	17.21	11.55	.17	8.65	10.43	1.91	.27
SJ632	48.51	1.17	16.98	11.87	.18	7.68	9.78	2.01	.48
SJ633	49.01	1.15	15.54	12.51	.19	9.05	9.41	1.87	.62
SJ634	49.72	.64	16.51	11.93	.17	7.86	9.63	1.96	.46
SJ635	48.56	1.58	15.67	13.33	.19	6.42	9.41	1.74	.44
SJ636	49.39	1.09	15.62	13.34	.20	6.53	9.83	1.86	.37
SJ637	49.88	.85	17.93	11.05	.17	7.96	10.50	2.05	.31
SJ638	51.01	1.18	18.89	11.56	.18	9.01	9.84	1.84	.34
SJ619	62.85	.60	10.70	11.56	.16	.42	4.02	1.79	2.41
SJ620	62.73	1.05	10.88	11.56	.16	.44	4.36	1.93	2.64
SJ621	61.82	.91	10.54	11.27	.15	.33	3.98	1.61	2.78
SJ622	63.25	1.02	10.92	11.56	.17	.39	4.42	1.92	2.69
SJ623	62.44	1.01	10.60	11.79	.15	.43	4.23	1.78	2.59
SJ624	62.44	.97	10.63	11.41	.16	.34	3.96	1.92	2.79
SJ625	64.32	1.07	11.33	11.68	.15	.46	4.37	1.88	2.71
SJ626	66.41	.97	11.36	11.27	.15	.35	4.13	1.83	2.74

APPENDIX E

Appendix E1. Four dyke samples (SB 20, SB 41, SB 72, SBR 25) have been analysed for some combination of garnet, biotite and plagioclase. SB 20, SB 41 analysed as whole rock samples (see Appendix D).

SB 72

Coarse-grained foliated amphibolite contains Hb (70%), Bt (10%), Pl (10%) and small amounts of Sp, Gt and opaque ore. Fabric defined by co-planar alignment of Hb prisms.

SBR 25

Medium to coarse-grained amphibolite contains high proportion of Bt which varies considerably between hand specimens. Bt has inclusions of Ep (s.l.). Some Pl defines a relict igneous texture.

Appendix E Table 1 Garnet analyses

	SB72				SBR 25					SB20			
	28	29	31	37	52	53	54	55	56	12	13	22	23
SiO_2	38.14	37.77	37.58	37.68	37.75	37.79	37.91	37.84	37.90	37.58	38.56	31.17	38.45
Al_2O_3	21.51	21.54	21.44	21.71	21.55	21.42	21.29	21.68	21.42	21.55	21.87	21.88	21.69
* FeO	24.29	23.65	23.96	24.42	22.05	20.75	20.30	20.43	21.83	26.88	26.49	26.46	26.67
MnO	3.58	3.67	3.38	3.66	2.40	3.28	4.42	4.05	2.86	3.60	3.82	4.07	4.04
MgO	1.40	1.48	1.39	1.44	1.18	1.10	.92	.97	1.20	2.23	2.50	2.39	2.55
CaO	12.17	11.98	12.13	11.92	15.28	15.35	15.65	15.09	14.59	8.80	9.04	8.77	8.83

Cation proportions (on the basis of 12 oxygens)

Si	3.00	2.99	2.99	2.97	2.98	2.99	2.99	2.98	3.00	2.98	2.99	2.98	2.99
Al	1.99	2.01	2.01	2.02	2.00	2.00	1.98	2.02	2.00	2.01	2.00	2.02	1.99
Fe	1.60	1.57	1.59	1.61	1.45	1.37	1.34	1.35	1.44	1.78	1.72	1.73	1.74
Mn	.24	.25	.23	.25	.16	.22	.30	.27	.19	.24	.25	.27	.27
Mg	.16	.17	.17	.17	.14	.13	.11	.11	.14	.26	.29	.28	.30
Ca	1.03	1.02	1.03	1.01	1.29	1.30	1.32	1.28	1.24	.75	.75	.73	.74

* total iron as FeO

Appendix E Table 1 Garnet analyses (continued)

SB41

	1	2	3	4	6	7	9	11	12	13	14	15	16
SiO_2	38.36	37.94	37.76	37.35	37.72	37.90	37.71	37.83	37.90	37.86	37.83	37.36	37.68
Al_2O_3	21.48	21.73	21.74	21.22	21.73	22.01	21.23	21.56	21.87	21.63	21.66	21.40	21.72
* FeO	26. 5	26.36	25.67	26.02	26.73	25.88	25.64	26.79	26.03	26.56	26.69	26.47	26.45
MnO	2.89	3.12	3.18	3.64	3.20	3.22	3.56	2.73	3.82	2.85	3.22	2.81	3.03
MgO	2.19	2.03	1.83	1.81	2.51	2.55	1.87	2.13	1.88	2.21	2.12	2.09	2.19
CaO	9.80	9.68	9.56	9.28	9.46	9.42	9.38	9.65	9.28	9.76	9.41	9.67	9.36

Cation proportions (on the basis of 12 oxygens)

Si	3.01	2.99	3.00	2.99	2.96	2.97	3.01	2.99	2.99	2.98	2.98	2.98	2.98
Al	1.99	2.02	2.04	2.00	2.01	2.04	2.00	2.01	2.03	2.01	2.01	2.01	2.02
Fe	1.72	1.74	1.71	1.74	1.76	1.70	1.71	1.77	1.72	1.75	1.75	1.70	1.75
Mn	.19	.21	.21	.25	.21	.21	.24	.18	.26	.19	.22	.19	.21
Mg	.26	.24	.22	.22	.29	.30	.22	.25	.22	.26	.25	.25	.26
Ca	.83	.82	.81	.80	.80	.79	.80	.82	.78	.82	.79	.83	.79

* total iron as FeO

Appendix E Table 2 Biotite analyses

	SB72						SBR 25			SB41				
	32	34	36	38	42	50	57	60	70	17	18	19	23	25
SiO_2	36.06	35.65	35.22	35.92	35.86	36.05	35.31	35.48	36.13	34.86	35.43	35.33	37.01	36.16
TiO_2	1.38	1.52	.96	1.42	1.46	1.58	1.73	1.73	1.70	.88	1.58	1.63	2.13	2.02
Al_2O_3	17.30	17.27	17.13	17.49	16.93	17.16	17.04	1 .03	17.30	17.55	16.87	16.22	17.10	16.76
* FeO	20.56	20.00	21.78	19.71	20.89	20.58	20.99	20.90	20.96	19.75	19.66	19.61	21.00	21.87
MnO	.23	.23	BDL	BDL	BDL	.26	BDL	BDL	BDL	BDL	BDL	BDL	BDL	BDL
MgO	10.01	9.71	10.31	10.32	9.99	9.87	9.99	9.65	10.06	10.98	10.86	10.87	11.42	11.03
CaO	BDL	.15	.16	BDL	BDL	.14	BDL	BDL	BDL	.27	.23	.22	BDL	BDL
Na_2O	BDL	BDL	BDL	BDL	BDL	BDL	BDL	BDL	BDL	BDL	.30	BDL	.29	BDL
K_2O	9.54	9.34	8.62	9.18	9.41	9.29	9.31	9.31	9.23	8.81	8.79	8.95	9.29	8.77
	Cation proportions (on the basis of 22 oxygens)													
Si	5.54	5.54	5.48	5.54	5.55	5.54	5.48	5.52	5.53	5.44	5.50	5.54	5.49	5.47
Al^{IV}	2.46	2.46	2.52	2.46	2.45	2.46	2.52	2.48	2.47	2.56	2.50	2.46	2.51	2.53
Al^{VI}	.67	.60	.62	.72	.63	.66	.60	.64	.65	.68	.57	.54	.48	.47
Ti	.16	.18	.11	.17	.17	.18	.20	.20	.20	.10	.19	.19	.24	.23
Fe	2.64	2.60	2.83	2.54	2.70	2.65	2.73	2.72	2.68	2.58	2.55	2.57	2.63	2.77
Mn	.03	.03				.03								
Mg	2.29	2.25	2.39	2.37	2.30	2.26	2.31	2.24	2.30	2.56	2.51	2.54	2.53	2.49
Ca		.03	.03			.02				.05	.04	.04		
Na											.09		.08	
K	1.87	1.85	1.71	1.81	1.86	1.82	1.84	1.85	1.80	1.76	1.74	1.79	1.76	1.69

* total iron as FeO, BDL = below detection limit (Dunham and Wilkinson, 1978)

APPENDIX E TABLE 3

PLAGIOCLASE ANALYSES BASIC DYKES

	SB20					
	4	6	15	17	19	* 62
SIO2	61.15	59.77	60.26	59.23	60.18	60.64
AL2O3	24.40	25.62	25.59	25.78	25.41	25.40
CAO	5.71	6.74	6.98	7.15	6.97	6.41
NA2O	8.50	7.89	7.78	7.70	7.84	8.19
K2O	0	0	0	0	0	0
TOTAL	99.77	100.01	100.6	99.9	100.4	100.64
CATIONS PER 8 OXYGENS						
SI	2.72	2.66	2.67	2.65	2.67	2.68
AL	1.28	1.34	1.34	1.36	1.33	1.32
CA	0.27	0.32	0.33	0.34	0.33	0.30
NA	0.73	0.68	0.67	0.67	0.67	0.70
K	0	0	0	0	0	0
MOLECULAR COMPONENTS MEAN AN=31.6						
AB	72.9	67.9	66.8	66.1	67.1	69.8
OR	0	0	0	0	0	0
AN	27.1	32.1	33.2	33.9	32.9	30.2

	SB72					SBR25
	27	67	* 43	46	47	* 65
SIO2	60.63	59.32	60.17	61.44	61.71	57.13
AL2O3	24.84	25.45	24.78	24.11	24.03	26.59
CAO	6.21	6.91	6.22	5.60	5.16	8.85
NA2O	8.13	7.66	7.90	8.49	8.54	6.74
K2O	0	0	0.27	0	0.11	0
TOTAL	99.81	99.34	99.33	99.64	99.56	99.31
CATIONS PER 8 OXYGENS						
SI	2.70	2.66	2.70	2.74	2.75	2.58
AL	1.30	1.35	1.31	1.27	1.26	1.41
CA	0.30	0.33	0.30	0.27	0.25	0.43
NA	0.70	0.67	0.69	0.73	0.74	0.59
K	0	0	0.02	0	0.01	0
MOLECULAR COMPONENTS MEAN AN=28.9 (OF SB72)						
AB	70.3	66.7	68.7	73.3	75.0	58.0
OR	0	0	1.5	0	0	0
AN	29.7	33.3	29.8	26.7	25.0	42.0

REFERENCES

Abbey, S., 1975. Studies in "standard samples" of silicate rocks and minerals. Part 4. 1974 edition of "usable values". Geological Survey of Canada Paper 74-41.

Albee, A. L., 1965. Distribution of Fe, Mg and Mn between garnet and biotite in natural mineral assemblages. J. Geol., 73, pp. 155-164.

Arth, J. G. and Hanson, G. N., 1975. Geochemistry and origin of the early Precambrian crust of northeastern Minnesota. Geochim. Cosmochim. Acta, 39, pp. 325-362.

Asklund, B., 1947. Gatsen och kantsten. Sver. Geol. Unders. C479.

Atherton, M. P., 1968. The variation in garnet biotite and chlorite composition in medium grade pelitic rocks from the Dalradian, Scotland, with particular reference to the zonation in garnet. Contrib. Mineral. Petrol., 18, pp. 347-371.

Baer, A. J., 1976. The Grenville Province in Helikian times: a possible model of evolution. Phil. Trans. R. Soc. Lond. A., 280, pp. 499-515.

Beach, A., 1976. The interrelations of fluid transport, deformation, geochemistry and heat flow in early Proterozoic shear zones in the Lewisian complex. Phil. Trans. R. Soc. Lond. A., 280, pp. 569-604.

Bergstrom, A., 1963. Petrology of the Tjörn area in western Sweden. Sveriges geol. Unders., Ser. C, Nr. 593. Årsbok 57, Nr. 4.

Berthelsen, A. and Murthy, T. N. N., 1970. Structural relations between supracrustal and granitoid rocks in north-eastern Orust, western-most Sweden. Sveriges geol. Unders., Ser. C. Nr. 649. Årsbok 64, Nr. 6.

Bevins, R. E., 1979. The geology of the Strumble Head - Fishguard region, Dyfed, Wales. Ph. D. thesis, Univ. Keele (unpubl.).

Bjorlykke, K., 1971. Petrology of Ordovician sediments from Wales. Norsk. Geol. Tidsskr., 51, pp. 123-140.

Bottinga, Y. and Javoy, M., 1973. Comments on oxygen isotope thermometry. Earth Planet. Sci.Lett., 20, pp. 250-265.

Brooks, C., Hart, S. R. and Wendt, I., 1972. Realistic use of two-error regression treatments as applied to Rubidium-Strontium data. Rev. Geophys., 10, pp. 551-577.

Brotzen, O., 1961. On some age relations in the Precambrian of south-western Sweden. Geol. Fören. Stockh. Förh., 83, pp. 227-252.

Brown, G. C., 1970. A comment on the role of water in the partial fusion of crustal rocks. Earth Planet. Sci. Lett., 9, pp. 355-358.

Brown, G. C., 1973. Evolution of granite magmas at destructive plate margins. Nature Phys. Sci., 241, pp. 26-28.

Brown, M., 1973. The definition of Metatexis, Diatexis and Migmatite. Proc. Geol. Ass., 84, pp. 371-382.

Brueckner, H. K., 1972. Interpretation of Rb-Sr ages from the Precambrian and Palaeozoic rocks of southern Norway. Am. J. Sci. 272, pp. 334-358.

Burns, D. J., 1966. Chemical and mineralogical changes associated with the Laxfordian metamorphism of dolerite dykes in the Scourie-Laxford region, Sutherland. Geol. Mag., 103, pp. 19-35.

Burton, J. D. and Culkin, F., 1972. Gallium. In Wedepohl, K. H. (Ed). Handbook of geochemistry, II/3.

Butler, B. C. M., 1965. A chemical study of the Moine Series of Scotland. Quart. J. geol. Soc. Lond., 121, pp. 163-208.

Cann, J. R., 1970a. Upward movement of granitic magma. Geol. Mag., 107, pp. 335-40.

Cann, J. R., 1970b. Rb, Sr, Y, Zr and Nb in some ocean floor basaltic rocks. Earth Planet. Sci. Lett., 10, pp. 7-11.

Chapman, J. H., 1978. Geochronology and isotope geochemistry of Precambrian rocks from northwest Scotland. Ph. D. thesis, Univ. Oxford (unpubl.).

Chappell, B. W. and White, A. J. R., 1974. Two contrasting granite types. Pac. Geol., 8, pp. 173-174.

Condie, K. C., 1976. Trace-element geochemistry of Archean greenstone belts. Earth-Sci. Rev., 12, pp. 393-417.

Condie, K. C., Barsky, C. K., Mueller, P. A., 1969. Geochemistry of Precambrian diabase dikes from Wyoming. Geochim. Cosmochim. Acta., 33, pp. 1371-1388.

Daly, J. S., Park, R. G., Cliff, R. A., in press. Rb-Sr ages of intrusive plutonic rocks from the Stora Le - Marstrand belt in Orust, S. W. Sweden. Precambrian Res.

De la Roche, H., 1965. Sur l'existence de plusieurs facies geochimiques dans les schistes paleozoiques des Pyrenée luchonaises. Geol. Rundsch., 55, pp. 274-301.

Dostal, J. and Fratta, M., 1977. Trace element geochemistry of a Precambrian diabase dike from western Ontario. Can. J. Earth Sci., 14, pp. 2941-2944.

Dunham, F. C. and Wilkinson, F. C. F., 1978. Accuracy, precision and detection limits of energy-dispersive electron-microprobe analyses of silicates. X-ray Spectrom., 7, pp. 50-56.

Emslie, R. F., 1978. Anorthosite massifs, rapakavi granites and late Proterozoic rifting of North America. Precambrian Res., 7, pp. 61-98.

Faure, G. and Powell, J. L., 1972. Strontium Isotope Geology. Springer-Verlay, New York. 188 pp.

Ferry, J. M. and Spear, F. S., 1978. Experimental calibration of the partitioning of Fe and Mg between biotite and garnet. Contrib. Mineral. Petrol., 66, pp. 113-117.

Flanagan, F. J., 1973. 1972 values for international geochemical reference samples. Geochim. Cosmochim. Acta, 37, pp. 1189-1200.

Flood, R. H. and Shaw, S. E., 1977. Two "S-type" granite suites with low initial $^{87}Sr/^{86}Sr$ ratios from the New England Batholith, Australia. Contrib. Mineral. Petrol., 61, pp. 163-173.

Floyd, P. A. and Winchester, J. A., 1975. Magma type and tectonic setting discrimination using immobile elements. Earth Planet. Sci. Lett., 27, pp. 211-218.

Floyd, P. A. and Winchester, J. A., 1976. Petrochemical affinities of Dalradian metabasaltic rocks: a reply to C. M. Graham. Earth Planet. Sci. Lett., 32, pp. 213-214.

Frondel, C., 1970. Scandium. In Wedepohl, K. H. (Ed.) Handbook of geochemistry, II/2.

Goldman, D. S. and Albee, A. L., 1977. Correlation of Mg/Fe partitioning between garnet and biotite with $^{18}O/^{16}O$ partitioning between quartz and magnetite. Am. Jour. Sci., 277, pp. 750-767.

Gorbatschev, R., 1971. Aspects and problems of Precambrian geology in western Sweden. Sver. Geol. Unders. C 650.

Gorbatschev, R., 1975. Fundamental subdivisions of Precambrian granitoids in the Åmål mega-unit and the evolution of the south-western Baltic Shield, Sweden. Geol. Fören. Stockh. Förh., 97, pp. 107-114.

Gorbatschev, R., 1977. Correlation of Precambrian supracrustal complexes in south-western Sweden and the sequence of regional deformation events in the Amal tectonic mega-unit. Geol. Fören., Stockh. Förh., 99, pp. 336-346.

Gorbatschev, R. and Welin, E., 1975. The Rb-Sr age of the Ursand granite on the boundary between the Åmål and "Pregothian" mega-units of south-western Sweden. Geol. Fören. Stockh. Förh., 97, pp. 379-381.

Graber, F. M., Lukens, H. R. and MacKenzie, J. K., 1970. Neutron activation analysis determination of all 14 stable rare-earth elements with group separation and Ge (Li) spectrometry. J. Radioanal. Chem., 4, pp. 229-239.

Graham, C. M., 1976a. Petrochemistry and tectonic significance of Dalradian metabasaltic rocks of the SW. Scottish Highlands. Jl. geol. Soc. Lond., 132, pp. 61-84.

Graham, C. M., 1976b. Petrochemical affinities of Dalradian metabasaltic rocks: discussion of paper by J. A. Winchester and P. A. Floyd. Earth Planet. Sci. Lett., 32, pp. 210-212.

Hageskov, B., 1978. On the Precambrian structures of the Sandbukta-Molen inlier in the Oslo graben, SE Norway. Nor. Geol. Tidsskr., 58, pp. 69-80.

Hansen, B. T., 1976. A geochronological study of polymetamorphism within the Caledonian mountain belt of Central E.Greenland. Ph. D. thesis (Dissertation no. 5761), Swiss Federal Institute of Technology, Zurich (unpubl.).

Harper, C. T., 1967. On the interpretation of potassium-argon ages from the Precambrian Shield and Phanerozoic orogens. Earth Planet. Sci. Lett., 3, pp. 128-132.

Hensen, B. J., Schmid, R. and Wood, B. J., 1975. Activity-composition relationships for pyrope-grossular garnet. Contrib. Mineral. Petrol., 51, pp. 161-166.

Herrmann, A. G., 1974. Yttrium and Lanthanises. In Wedepohl, K. G. (Ed.) Handbook of Geochemistry, II/4.

Higgins, A. K. Friderichsen, J. D., Rex, D. C., Gledhill, A. R., 1978. Early Proterozoic isotopic ages in the East Greenland Caledonian fold belt. Contrib. Mineral. Petrol., 67, pp. 87-94.

Hollister, L. S., 1966. Garnet zoning: An interpretation based on the Rayleigh fractionation model. Science, 154, pp. 1647-1651.

Irvine, T. N. and Barager, W. R. A., 1971. A guide to the chemical classification of the common volcanic rocks. Can. J. Earth Sci., 8, pp. 523-548.

Jakes, P. and Gill, J., 1970. Rare earth elements and the island arc tholeiitic series. Earth Planet. Sci. Lett., 9, pp. 17-28.

Kerrich, R., Fyfe, W. S., Gorman, B. E. and Allison, I., 1977. Local modification of rock chemistry by deformation. Contrib. Mineral. Petrol. 65, pp. 183-190.

Kilinc, I. A., 1972. Experimental study of partial melting of crustal rocks and formation of migmatites. 24th. Int. geol. Congress, Section 2, Petrology, pp. 109-121.

Killeen, P. G. and Heier, K. S., 1975. A uranium and thorium enriched province of the Fennoscandian shield in southern Norway. Geochim. Cosmochim. Acta, 39, pp. 1515-1524.

Klingspor, I.,1976. Radiometric age-determination of basalts, dolerites and related syenite in Skåne, southern Sweden. Geol. Fören. Stockh. Förh., 98, pp. 3-29.

Kratz, K. O., Gerling, E. K. and Lobach-Zuchenko, S. B., 1968. The isotope geology of the Precambrian of the Baltic Shield. Can. J. Earth Sci., 5, pp. 657-660.

Kretz, R., 1959. Chemical study of garnet, biotite and hornblende from gneisses of southwestern Quebec, with emphasis on distribution of elements in coexisting minerals. J. Geol., 67, pp. 371-402.

Krogh, T. E. and Davis, G. L., 1973. The effect of regional metamorphism on U-Pb systems in zircon and a comparison with Rb-Sr systems in the same whole rock and its constituent minerals. Carnegie Inst. Washington Yearb., 72, pp. 601-610.

Lambert, R. St. J. and Holland, J. G., 1974. Yttrium geochemistry applied to petrogenesis utilizing calcium-yttrium relationships in minerals and rocks. Geochim. Cosmochim. Acta, 38, pp. 1393-1414.

Larsson, W., 1947. Nagra resultat ov berggrundsgeologiska studier inom Dalformationens norra gransomrade. Geol. Fören. Stockh. Förh, 69, pp. 321-326.

Larsson, W., 1956. Beskrivning till kartbladet Varvik. Berggrunden. Sver. Geol. Unders. Aa 187.

Leake, B. E., Hendry, G. L., Kemp, A., Plant, A. G., Harvey, P. K., Wilson, J. R., Coats, J. S., Aucott, J. W., Lunel, T. and Howarth, R. J., 1969. The chemical analysis of rock powders by automatic X-ray fluorescence. Chem. Geol., 5, pp. 7-86.

Lindstrom, A., 1902. Beskrivning till Kartbladet Uddevalla. Sveriges geol. Unders. Ser. Ac, Nr. 3.

Lundberg, B., 1973. Granite intrusions in the Dal Group, Central Sweden. Geol. Fören. Stockh. Förh, 95, pp. 113-119.

Lundegårdh, P. H., 1951. Petrology of the Onsala peninsula south of Gothenburg in western Sweden. Geol. Fören. Stockh. Förh., 95, pp. 113-119.

Lundegårdh, P. H., 1953. Petrology of the Molndal-Styrso-Vallda region in the vicinity of Gothenburg. Sver. Geol. Unders., Ser. C, Nr. 531.

Lundegårdh, P. H., 1958. Göteborgstraktens berggrund. Sver. Geol. Unders., Ser. C, Nr. 553.

Lundegårdh, P. H., 1974. Det svenska urberget. In Lundegårdh-Lundqvist-Lindström: Berg och jord i Sverige. Almqvist and Wiksell, Stockholm, 4th edition.

Macdonald, G. A. and Katsura, T., 1964. Chemical composition of Hawaiian lavas. J. Petrol., 5, pp. 82-133.

Magnusson, N. H., 1960. Age determinations of Swedish Precambrian rocks. Geol. Fören. Stockh. Förh., 82, pp. 407-432.

Magnusson, N. H., Thorslund, P., Brotzen, F., Asklund, B. and Kulling, O., 1960. Description to accompany the map of the pre-Quaternary rocks of Sweden. Sver. Geol. Unders., Ba 16, pp. 5-68.

Magnusson, N. H., 1965. The Pre-Cambrian history of Sweden. Quart. J. geol. Soc. Lond., 121, pp. 1-30.

Mason, B., 1966. Principles of Geochemistry. (3rd Ed.). Wiley, New York and London. 329 pp.

McIntyre, G. A., Brooks, C., Compston, W. and Turek, A., 1966. The statistical assessment of Rb-Sr isochrons. J. Geophys. Res., 71, pp. 5459-5468.

Mehnert, K. R., 1968. Migmatites and the origin of granitic rocks. Elsevier, Amsterdam. 403 pp.

Morrison, M. A., 1978. The use of "immobile" trace elements to distinguish the palaeotectonic affinities of metabasalts: Application to the Palaeocene basalts of Mull and Skye, northwest Scotland. Earth Planet. Sci. Lett., 39, pp. 407-416.

Neumann, H., 1960. Apparent ages of Norwegian minerals and rocks. Norsk geol. Tidsskr., 40, pp. 173-191.

Nockolds, S. R., 1954. Average chemical compositions of some igneous rocks. Bull. Geol. Soc. Am., 65, pp. 1007-1032.

Nockolds, S. R. and Allen, R., 1953. The geochemistry of some igneous rock series. Geochim. Cosmochim. Acta, 4, pp. 105-142.

Norrish, K., and Hutton, J. T., 1969. An accurate X-ray spectrographic method for the analysis of a wide range of geological samples. Geochim. Cosmochim. Acta, 33, pp. 431-453.

Ogezi, A. E. O., 1977. Geochemistry and geochronology of basement rocks from northwestern Nigeria. Ph. D. thesis, Univ. Leeds (unpubl.).

O'Nions, R. K. and Baadsgaard, H., 1971. A radiometric study of polymetamorphism in the Bamble Region, Norway. Contrib. Mineral. Petrol., 34, pp. 1-21.

O'Nions, R. K. and Heier, K. S., 1972. A reconnaissance Rb-Sr geochronological study of the Kongsberg area, South Norway. Norsk geol. Tidsskr., 52, pp. 143-150.

Pankhurst, R. J. and O'Nions, R. K., 1973. Determination of Rb/Sr and $^{87}Sr/^{86}Sr$ ratios of some standard rocks and evaluation of X-ray fluorescence spectrometry in Rb-Sr geochemistry. Chem. Geol., 12, pp. 127-136.

Pankhurst, R. J. and Pidgeon, R. T., 1976. Inherited isotope systems and the source region pre-history of early Caledonian granites in the Dalradian Series of Scotland. Earth Planet. Sci. Lett., 31, pp. 55-68.

Park, R. G., Bailey, A. I., Crane, A., Cresswell, D., Standley, R. C., in press. Structure and geological history of the Stora Le - Marstrand rocks of western Orust, S.W. Sweden. Sver. Geol. Unders., C 763.

Patchett, P. J., 1976. Rb-Sr geochronology and geochemistry of Proterozoic basic intrusions in Sweden and South Greenland. Ph. D. thesis, Univ. Edinburgh (unpubl.).

Patchett, P. J., Bylund, G. and Upton, B. G. J., 1978. Palaeomagnetism and the Grenville orogeny: new Rb-Sr ages from dolerites in Canada and Greenland. Earth Planet. Sci. Lett., 40, pp. 349-364.

Pearce, J. A., 1975. Basalt geochemistry used to investigate past tectonic environments on Cyprus. Tectonophysics, 25, pp. 41-67.

Pearce, J. A. and Cann, J. R., 1971. Ophiolite origin investigated by discriminant analysis using Ti, Zr and Y. Earth Planet. Sci. Lett., 12, pp. 339-349.

Pearce, J. A. and Cann, J. R., 1973. Tectonic setting of basic volcanic rocks determined using trace element analyses. Earth Planet. Sci. Lett., 19, pp. 290-300.

Pedersen, S. and Falkum, T., 1975. Rb-Sr isochrons for the granitic plutons around Farsund, southern Norway. Chem. Geol., 15, pp. 97-101.

Perchuk, L. L., 1970. Equilibrium of biotite with garnet in metamorphic rocks. Geochem. Int., pp. 157-179.

Priem, H. N. A., Verschure, R. H., Verdurmen, E. A. T., Hebeda, E. H. and Boelrijk, N. A. I. M., 1973. Rb-Sr investigations on Precambrian granites, granitic gneisses and acidic metavolcanics in central Telemark, Norway: Metamorphic resetting of Rb-Sr whole-rock systems. Nor. Geol. Unders., 289, pp. 37-53.

Ramberg, H., 1955. Natural and experimental boudinage and pinch-and-swell structures. J. Geol., 63, pp. 512-526.

Reynolds, R. C., Jr., 1963. Matrix corrections in trace element analysis by X-ray fluorescence: estimation of the mass absorption coefficient by compton scattering. Am. Mineral., 48, pp. 1133-1143.

Robie, R. A., Bethke, P. M., Beardsley, K. M., 1967. Selected X-ray crystallographic data, molar volumes, and densities of minerals and related substances. U. S. Geol. Surv. Bull., 1248.

Robinson, D. and Leake, B. E., 1975. Sedimentary and igneous trends on AFM diagrams. Geol. Mag., 112, pp. 305-307.

Roddick, J. C. and Compston, W., 1976. Strontium isotopic equilibration: a solution to a paradox. Earth Planet. Sci. Lett., 34, pp. 238-246.

Saxena, S. K., 1968. Distribution of elements between coexisting minerals and the nature of the solid solution in garnet. Am. Mineral., 53, pp. 994-1014.

Sen, S. K. and Chakraborty, K. R., 1968. Magnesium-iron exchange equilibria in garnet-biotite and metamorphic grade. Neues Jahrb. Mineralogie Abh., 108, pp. 181-207.

Shand, S. J., 1950. Eruptive Rocks. Wiley, New York, 4th edition.

Shaw, D. M., 1972. The origin of the Apsley Gneiss, Ontario. Can. J. Earth Sci., 9, pp. 18-35.

Sighinolfi, G. P. and Gorgoni, C., 1978. Chemical evolution of high-grade metamorphic rocks - Anatexis and remotion of material from granulite terrains. Chem. Geol., 22, pp. 157-176.

Skiold, T., 1976. The interpretation of the Rb-Sr and K-Ar ages of late Precambrian rocks in south-western Sweden. Geol. Fören. Stockh. Förh., 98, pp. 3-29.

Smith, R. E. and Smith, S. E., 1976. Comments on the use of Ti, Zr, Y, Sr, K, P and Nb in classification of basaltic magmas. Earth Planet. Sci. Lett., 32, pp. 114-120.

Steiger, R. H. and Jager, E., 1977. Subcommission on Geochronology: convention on the use of decay constants in geo - and cosmochronology. Earth Planet. Sci. Lett., 36, pp. 359-362.

Taylor, S. R., 1965. The application of trace element data to problems in petrology. Phys. Chem. Earth, 6, pp. 133-213.

Thompson, A. B., 1976. Mineral reactions in pelitic rocks: II Calculation of some P - T - X (Fe-Mg) phase relations. Am. Jour. Sci., 276, pp. 425-454.

Turner, F. J., 1968. Metamorphic Petrology. McGraw-Hill, New York. 403 pp.

Van de Kamp, P. C., Leake, B. E. and Senior, A., 1976. The petrography and geochemistry of some Californian arkoses with application to identifying gneisses of metasedimentary origin. J. Geol., 84, pp. 195-212.

Versteeve, A. J., 1975. Isotope geochronology in the high-grade metamorphic Precambrian of South western Norway. Norges geol. Unders., 318, pp. 1-50.

Wager, L. R. and Brown, G. M., 1968. Layered igneous rocks. Freeman, San Francisco.

Wager, L. R. and Deer, W. A., 1939. Geological investigations in East Greenland: pt. III, The petrology of the Skaergaard Intrusion, Kangerdlugssuaq, East Greenland. Geochim. Cosmochim. Acta, 1, pp. 129-208.

Wedepohl, K. H., 1968. Composition and abundance of common sedimentary rocks. In Wedepohl, K. H. (Ed.). Handbook of Geochemistry, I, pp. 250-271.

Welin, E. and Blomqvist, G., 1964. Age measurements on radioactive minerals from Sweden. Geol. Fören. Stockh. Förh., 86, pp. 33-50.

Welin, E. and Gorbatschev, R., 1976a. Rb-Sr age of granitoid gneisses in the "Pregothian" area of south-western Sweden. Geol. Fören. Stockh. Förh, 98, pp. 378-381.

Welin, E. and Gorbatschev, R., 1976b. A Rb-Sr geochronological study of the older granitoids in the Åmål tectonic mega-unit, south-western Sweden. Geol. Fören. Stockh. Förh., 98, pp. 374-377.

Welin, E. and Gorbatschev, R., 1976c. The Rb-Sr age of the Hästefjorden granite and its bearing on the Precambrian evolution of south-western Sweden. Precambrian Res., 3, pp. 187-195.

Welin, E. and Gorbatschev, R., 1978a (in press). Rb-Sr age of the Lane granites in south-western Sweden. Geol. Fören, Stockh. Förh.

Welin, E. and Gorbatschev, R., 1978b (in press). Rb-Sr isotopic relations of a tonalitic intrusion on Tjörn island: A clue to Precambrian events in south-western Sweden. Geol. Fören. Stockh. Förh.

White, A. J. R. and Chappell, B. W., 1977. Ultrametamorphism and granitoid genesis. In: D. H. Green (editor), Experimental Petrology Related to Extreme Metamorphism. Tectonophysics, 43, pp. 7-22.

Winchester, J. A. and Floyd, P. A., 1976. Geochemical magma type discrimination: application to altered and metamorphosed basic igneous rocks. Earth Planet. Sci. Lett., 28, pp. 459-469.

Winkler, H. G., 1974. Petrogenesis of metamorphic rocks. Third edition. Springer-Verlag, New York.

Wyllie, P. J., 1977. Crustal anatexis: an experimental review. In: D. H. Green (editor), Experimental Petrology Related to Extreme Metamorphism. Tectonophysics, 43, pp. 41-71.

Wynne-Edwards, H. R., 1972. The Grenville province. In Price, R. A. and Douglas, R. J. W., (Eds.), Variations in tectonic styles in Canada. Geol. Assoc. Canada Spec. Paper 11, pp. 263-334.

Wynne-Edwards, H. R. and Hasan, Z., 1970. Intersecting orogenic belts across the North Atlantic. Am. Jour. Sci. 268, pp. 289-308.

York, D., 1969. Least squares fitting of a straight line with correlated errors. Earth Planet. Sci. Lett., 5, pp. 320-324.

Yule, J. W. and Swanson, G. A., 1969. A rapid method for decomposition and the analysis of silicates and carbonates by atomic absorption spectroscopy. Atomic Absorption Newsletter, 8, pp. 30-33.

BOHUS GRANITE

Moorlock (pers.comm.) & the author

Bokenäs

S 40.1

S10

KÄLLVIKEN

Dragsmark

Kristineberg

S 24

Flatön

Skaftölandet

SVINEVIKEN DYKE 607-614, 627

HENÅN DYKE 603-606

Timmerhult

Kungsviken

Malö

ISLANDSBERG DYKE 619-626

Högh. 921

956

552

LAVÖ DYKE 615-8, 630

Harmanö

Fig. 3.10

Stocken

HÄRMANÖ DYKE 631-638

P

R

SH

913-6

TAKESKÄRN

Fig. 4.13

HÄLLEVIKSSTRAND

Edshultshall

ORUST

Figs. 3.1, 4.1, 5.1

Berthelsen and Murthy (1970)

Slussen

953

941

940

Torp

Kleya

ASSMUNDERÖD

572

942

944

Ödsmål

943

945

946

954

MYCKLEBY

Fig. 4.15

639

649

Harlycke

641-3

TVET DYKE

Lagmansh.

Svanvik

662

Varekil

Rössön

△ Leucosomes (2nd.)
▽ Pegmatites (post-dyke)
• Gneisses
○ Nebulites
▪ Older amphibolites
● Younger granites
◆ Augen "
▫ Hälleviksstrand amphibolite
▲ Dyke suite
▼ Dyke occurrences (not sampled)
Geol. bdy.
Lithological banding
Fault
Shear zone
Road

P=Pilgrimmen
R=ROPAREN 917-20
SH=S.HÄRMANÖ 905-7

5 Km.

38 40 42 44 46 48 50 52 56 60 62 64 66

64 62 60 58 56 54 52 50 48 46 44 42